Exon, N.F., Kennett, J.P., Malone, M.J., et al., 2001
Proceedings of the Ocean Drilling Program, Initial Reports Volume 189

7. Site 1172[1]

Shipboard Scientific Party[2]

PRINCIPAL RESULTS

Site 1172 is located in a water depth of ~2620 m on the flat western side of the East Tasman Plateau (ETP), ~170 km southeast of Tasmania. At 44°S, the site lies in cool subtropical waters just north of the Subtropical Front in an area where both the Subtropical Front and the East Australian Current have had variable influence through time. The primary objectives of coring and logging at Site 1172 were to obtain in the far southwest Pacific (1) an Oligocene to Holocene pelagic carbonate section under long-term influence of the East Australian Current to construct moderate to high-resolution paleoceanographic and biostratigraphic records, (2) an Eocene siliciclastic sediment sequence for better understanding of paleoceanographic and paleoclimatic conditions before Antarctic Circumpolar Current development, and (3) an Eocene–Oligocene transitional sequence to determine the effects of the initial opening of the Tasmanian Gateway on the paleoceanography of the Pacific Tasmanian margin and to compare and contrast (4) changing paleoenvironmental and paleoceanographic conditions on each side of Tasmania as the Tasmanian Seaway opened and the Antarctic Circumpolar Current developed. This site was also expected to provide valuable information about the tectonic history of the ETP, including evolution of an inferred volcanic hot spot in the Eocene.

Site 1172 is on thinned continental crust on the western side of the ETP. The plateau is roughly circular (200 km across), lies in water depths of 2200–2800 m, has Late Cretaceous oceanic crust to the east and probably to the southwest and south, and is attached to Tasmania to the northwest. During the middle Eocene, the ETP was at ~65°S when its fast northward movement (55 km/m.y.) with Australia commenced. Continental basement rocks form its margins, and seismic profiles and other evidence suggest that at Site 1172 basement is overlain by gently dipping Cretaceous sediments and flat-lying Cenozoic sediments. The

[1]Examples of how to reference the whole or part of this volume.
[2]Shipboard Scientific Party addresses.

Ms 189IR-107

late Eocene Cascade Seamount is a guyot consisting of basaltic volcanics and volcaniclastics in the middle of the plateau.

At Site 1172 we cored two advanced hydraulic piston corer (APC) holes, one APC/XCB (extended core barrel) hole, and a rotary cored hole. Because weather conditions were good during the APC drilling, construction of a composite section of the total triple-cored portion of the sedimentary sequence was possible to 146 m composite depth (mcd) (late Miocene) (Table **T2,** p. 94, in the "Leg 189 Summary" chapter). Beyond that, there are limited gaps, but core recovery averaged 92%. Hole 1172A was APC/XCB cored to 522.6 mbsf with 92.6% recovery. Hole 1172B was APC cored to 206.7 mbsf with 102.1% recovery. Hole 1171C was APC cored to 171 mbsf with 100.9% recovery. Hole 1172D was rotary cored from 344 to 373 mbsf, drilled to 497 mbsf, and cored to 766 mbsf with 80% recovery. Despite heave of up to 10 m, wireline logging was conducted over most of Hole 1172D with successful runs of the triple-combination (triple combo) tool string and the geological high-sensitivity magnetic tool (GHMT)-sonic tool string. However, the heave was too great to run the Formation MicroScanner (FMS) tool string.

The results significantly changed our precruise understanding of the history of the ETP, with much older sequences being cored at the site than expected. Site 1172 penetrated ~65 m of black shallow-marine mudstones of latest Cretaceous (Maastrichtian) age (Fig. **F1**). This sequence was overlain by 335 m of Paleocene and Eocene brown, green, and gray shallow-marine mudstones and 364 m of Oligocene and Neogene pelagic carbonates. The pelagic carbonates were deposited in ever-increasing depths after rapid Oligocene subsidence, and much of the Oligocene and lower Miocene sections are missing because of current action. A series of volcanic ash horizons of late Eocene to Oligocene age suggests that volcanism on Cascade Seamount continued for at least 5 m.y. The lithostratigraphic sequence has been divided into four units, with three subunits in Unit I and two subunits in Units III and IV.

Lithostratigraphic Unit I (0–355.8 mbsf), of early Miocene to Pleistocene age, is divided into three subunits: Subunit IA to 70 mbsf, Subunit IB to 271.2 mbsf, and Subunit IC to 355.8 mbsf. Subunit IA is a white foraminifer nannofossil ooze and foraminifer-bearing nannofossil ooze, whereas Subunit IB is a white and light greenish gray nannofossil ooze. The two subunits are distinguished mainly by a decrease in foraminiferal content in Subunit IB. Subunit IC is a white, pale yellow, and light gray foraminifer-bearing nannofossil chalk marked by an increase in the foraminiferal content and increasing minor components of clay and volcanic glass. Calcium carbonate content increases from 80 wt% in Subunit IA to 97 wt% in Subunit IB and decreases in Subunit IC to 90 wt%.

Lithostratigraphic Unit II (355.8–361.12 mbsf) is a thin uppermost Eocene to Oligocene transitional unit. The sediments are mainly characterized by increased glauconite and a decrease in nannofossil content and consist of variations of greenish gray glauconite-bearing silty diatomaceous claystone and dark greenish gray glauconitic diatomaceous clayey siltstone. A distinct surface at 357.27 mbsf is marked by abundant glauconite and rip-up clasts above and by angular clasts below. This transition may be a highly condensed section or a hiatus. Carbonate content decreases from 69 wt% at the top to 0.3 wt% at the base.

Lithostratigraphic Unit III (361.12–503.4 mbsf), of late to middle Eocene age, has been divided into two subunits: Subunit IIIA to 433.89 mbsf and Subunit IIIB to 503.4 mbsf. Subunit IIIA is a greenish gray and

F1. Postdrilling interpretation for local seismic profile AGSO 125-4, across Site 1172, p. 53.

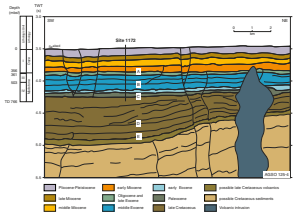

dark brownish gray diatom- and nannofossil-bearing claystone and a very dark grayish brown diatomaceous claystone. Subunit IIIB is a dark gray to dark olive-gray diatomaceous silty claystone. The two subunits are distinguished by calcium carbonate content averaging 10 wt% in Subunit IIIA and very low values, approaching zero, in Subunit IIIB.

Lithostratigraphic Unit IV (503.4–766.5 mbsf) is Late Cretaceous to early Eocene in age and is divided into two subunits: Subunit IVA to 695.99 mbsf and Subunit IVB to 766.5 mbsf. Subunit IVA is a middle Eocene to Paleocene olive-gray claystone with minor amounts of silty claystone, nannofossil-bearing claystone, and clayey siltstone. The subunit is distinguished from Unit III above by a lack of siliceous microfossils and an increase in opaque and accessory minerals, which reach a maximum of 15% at 542 mbsf. Subunit IVB is a Cretaceous (Maastrichtian) very dark olive-gray, very dark gray, and black claystone and silty claystone. It is distinguished from Subunit IVA by its darker color, lesser bioturbation, lesser glauconite content, and greater organic matter content. Sedimentological studies suggest that the Cretaceous/Tertiary (K/T) boundary is at ~696.1 mbsf, where a distinct lithologic change occurs at the subunit boundary, from brown and highly bioturbated silty claystone above to black massive claystone below. Detailed biostratigraphic postcruise studies indicate that the K/T boundary is at ~696.4 mbsf. Carbonate is generally very low with a maximum of 6.5 wt% at 762.9 mbsf.

Microfossils are present throughout the entire Cenozoic and upper Cretaceous sequence at Site 1172 with dominance of different groups drastically changing with depositional environments. Siliceous microfossils are rare to absent in the Quaternary to Pliocene interval but are common to abundant and well preserved in the Miocene. The thin Oligocene succession yielded few radiolarians, whereas diatoms remained abundant downhole. Both groups are common to locally abundant and well preserved in the Eocene. The upper Paleocene to upper Maastrichtian interval is virtually barren of siliceous microfossils, although pyritized biogenic silica is present. Planktonic foraminifers and calcareous nannofossils are generally abundant in the Neogene and Oligocene, with preservation ranging from moderate to good. Although less abundant, calcareous nannofossils remain consistently present until the middle Eocene, when abundance and preservation decrease dramatically. Below the middle Eocene, the Cenozoic succession is barren of calcareous nannofossils. Planktonic foraminifers are virtually absent below the middle/upper Eocene boundary.

Well-preserved and reasonably diversified calcareous microfossils are present in the upper Maastrichtian. Calcareous benthic foraminifers are consistently present throughout the Neogene–Oligocene carbonate succession. The middle Eocene sequence yields only rare agglutinated species. However, calcareous and agglutinated taxa are present in the Paleocene to upper Maastrichtian succession. Well-preserved organic walled dinoflagellate cysts and few sporomorphs are present in the Quaternary. The remaining Neogene to lower Oligocene strata are devoid of acid-resistant organic matter. Moderate to well-preserved dinocysts are the dominant constituent of upper Paleocene to lowermost Oligocene palynological associations and are persistent below this interval. Well-preserved terrestrial palynomorphs dominate upper Maastrichtian to middle Paleocene sediments.

Sedimentation rates at Site 1172 form three distinct phases. In contrast to other Leg 189 sites, sedimentation rates were relatively low (between 2.6 and 1.04 cm/k.y.) in the Maastrichtian through late Eocene. From the late Eocene through the middle Miocene (15 Ma), sedimenta-

tion rates decreased (0.16 to 3.2 cm/k.y) and then have increased again until the present day. These three intervals coincide with, and are probably related to, the succession in global climate change from "Greenhouse" to "Doubthouse" to "Icehouse" states. Site 1172, like Site 1168, appears to have been strategically located to sensitively record these overall shifts in global climate associated with development of the antarctic cryosphere. The higher early Paleogene and late Neogene sedimentation rates resulted from more stable climatic conditions. These were associated with the lack of any significant early Paleogene antarctic cryosphere in the "Greenhouse" world and a late Neogene "Icehouse" world marked by a permanent antarctic ice sheet. Reduced sedimentation rates during the middle Cenozoic at Site 1172 were associated with more highly variable climatic conditions leading to higher rates of deep-sea erosion. The lower-than-normal regional rates of sedimentation during most of the Paleogene at Site 1172 may have resulted from pervasive but gentle shallow-water sediment winnowing by the East Australian Current. Relatively higher rates of late Neogene sedimentation probably resulted from higher marine productivity caused by stimulation of surface-water circulation upon middle Miocene expansion of the antarctic cryosphere.

The geothermal gradient is lower at this site than at the other Leg 189 sites. Despite TOC contents that are similar to those of other Paleogene sequences at the other Leg 189 sites (0.5–1.0 wt%), complete sulfate reduction is not observed and only traces of methane are present. Organic matter is less mature thermally and more labile; however, there is evidence of bitumen in the older siliciclastic sediments, which may indicate the migration of hydrocarbons from below the drilled section. As at other sites, the presence of fresher pore waters was observed on the ETP, which indicates the regional extent of these low-chloride fluids.

The sedimentary succession of Site 1172 is similar to that in the other Leg 189 sites in recording three major phases of paleoenvironmental development:

1. Maastrichtian to early late Eocene deposition of shallow-water siliciclastic sediments during rifting between Antarctica and the STR, a time of minimal or no connection between the Pacific Ocean and the southern Indian Ocean.
2. A transitional interval of slow sedimentation, with shallow-water late Eocene glauconitic siliciclastic sediments giving way suddenly to earliest Oligocene deep-water clayey pelagic carbonates representing the activation of bottom currents as the Tasmanian Gateway opened and deepened during early drifting.
3. Oligocene through Quaternary deposition of pelagic carbonate sediments in increasingly deep waters and more open ocean conditions as the Southern Ocean developed and expanded with the northward flight of the ETP and the Australian continent.

The sediment succession at Site 1172 generally reflects an upward increase in ocean ventilation. Like the other sites drilled during Leg 189, increased ventilation resulted from a fundamental change in paleogeography associated with increasing dispersal of the southern continents and the opening of the ocean basins at high latitudes in the Southern Hemisphere. Thus, the sluggish ocean circulation and restricted environments of sedimentation of the Late Cretaceous and early Paleogene were

eventually replaced by well-ventilated open-ocean conditions of the later Cenozoic.

The Paleocene to middle Eocene was relatively warm based on the character of dinocyst assemblages similar to the middle Eocene record at Site 1171. Terrestrial palynomorphs, also indicative of warm conditions, are especially abundant in the lower Paleogene (Paleocene–early Eocene) sediments and suggest very shallow water–restricted conditions with marked runoff at this time. An absence of foraminifers, and even of nannofossils, in most parts of the Paleocene to middle Eocene confirms the marginal marine interpretation. Maastrichtian sediments were deposited in more open ocean conditions based on higher abundances of calcareous microfossils, more offshore dinocyst assemblages, and few pyritized diatoms.

The middle/late Eocene boundary is marked by a change from an inner neritic setting with marked freshwater influence and sluggish circulation to more offshore, deeper marine environments with increased ventilation and bottom-water current activity. Concomitant cooling is indicated by the increased numbers of endemic antarctic dinocyst species, whereas warmer episodes are also recognized. The Eocene–Oligocene transition (~34.0–33.3 Ma) is marked by a series of distinct stepwise environmental changes reflecting cooling and coeval rapid deepening of the basin. Sediments and biota indicate increasing bottom-water ventilation and the appearance of highly productive surface waters, in outer neritic to bathyal depositional settings, associated with the cooling. This trend culminated in the early Oligocene (33–30 Ma) when rigorous ventilation, and generally oxygen-rich waters, precluded sedimentation of organic matter despite overall high surface-water productivity. The condensed calcareous sequence contains abundant siliceous microfossils and was deposited in an oceanic bathyal environment. Oligocene to present-day pelagic carbonates were deposited in well-ventilated open-ocean conditions.

Although Site 1172 reflects the broad patterns of Cenozoic sedimentation for the Tasmanian region, differences from other sites are almost certainly related to the site's position astride the East Australian Current, and relatively isolated on the ETP, away from major sources of detrital sediments. A distinct increase in neritic diatoms during much of the middle Eocene appears to reflect higher productivity in this current than elsewhere on the Tasmanian margin. Increased productivity may have resulted from increased nutrient input swept into neritic environments by the East Australian Current as it moved south adjacent to Australia. A distinct upward increase in kaolinite (and illite) following the middle Miocene (~15 Ma) may reflect the increasing aridity of Australia and the transport of clays into the East Australian Current as it swept southward along the Australian margin.

A complete composite core record was successfully obtained for the last ~8 m.y. The successful drilling of Site 1172 capped off a highly productive and satisfying coring campaign in the Southern Ocean. Much was learned at sea, and postcruise research is expected to further contribute significantly toward understanding of Southern Ocean and antarctic environmental development and its role in Cenozoic global climate change.

BACKGROUND AND OBJECTIVES

Site 1172 is located on the western side of the East Tasman Plateau ~170 km southeast of Tasmania in a water depth of 2622 m. The site lies in cool subtropical waters just north of the Subtropical Front in an area where both the Subtropical Front and the East Australian Current have had variable influence through time, at a latitude comparable to Site 1168 west of Tasmania. Primary objectives of coring and logging at Site 1172 were to obtain (1) an Oligocene to Holocene pelagic carbonate section in the extreme southwest Pacific under long-term influence of the East Australian Current to construct moderate to high-resolution paleoceanographic and biostratigraphic histories, (2) an Eocene siliciclastic/carbonate sediment sequence for better understanding of paleoceanographic and paleoclimate development in the extreme southwestern sector of the Pacific before Antarctic Circumpolar Current development, and (3) an Eocene–Oligocene transitional sequence to determine effects of the initial opening of the Tasmanian Seaway on the paleoceanography of the Pacific Tasmanian margin region and to compare and contrast (4) changing paleoenvironmental and paleoceanographic conditions on each side of Tasmania as the Seaway opened and the Antarctic Circumpolar Current developed. This site was also expected to provide valuable information about the tectonic history of the East Tasman Plateau in relation to inferred hot spot evolution of the region.

Site 1172 is on thinned continental crust on the western side of the East Tasman Plateau. The plateau is roughly circular, 200 km across, and lies in water depths of 2200–2800 m (Exon et al., 1997). The East Tasman Plateau was located deep within Gondwana early in the Late Cretaceous, when rifting started to separate it from Tasmania and the eastern South Tasman Rise (STR) to the west and the Lord Howe Rise to the east (Exon et al., 1997). Magnetic anomalies suggest that seafloor spreading west of the STR occurred between 75 and 65 Ma (Royer and Rollet, 1997), and the East Tasman Plateau moved eastward ~150 km relative to Tasmania and the STR (Fig. **F7,** p. 72, in the "Leg 189 Summary" chapter). At about this time, seafloor spreading started to the east, thus separating the Lord Howe Rise from the East Tasman Plateau. During middle Eocene times, the East Tasman Plateau was at ~65°S, when its fast movement (55 km/Ma) north with Australia commenced.

Continental basement rocks have been dredged from the margins of the East Tasman Plateau (Exon et al., 1997). Seismic profiles and other evidence suggest that they are overlain by Cretaceous sediments, Paleogene sediments, and Neogene hemipelagic and pelagic sediments (Fig. **F2**). The late Eocene Cascade Seamount consists of volcanic breccia, hyaloclastite, and alkali olivine basalt and is part of the trace of the Balleny mantle plume (hot spot) that extends southward from the East Tasman Plateau to the Balleny Islands near the Ross Sea. The seamount is a guyot whose top lies 650 m below sea level (mbsl). Seismic profiles indicate that there has been subsidence of the central plateau and that as much as 4000 m of sediments fills the resultant depression.

Although there were almost no pre-Quaternary sediment samples from the East Tasman Plateau, circumstantial evidence suggests that above a possible volcanic horizon identified in seismic profiles, presumed to be Late Cretaceous postdrilling, the depression was filled by 500–1000 m of latest Cretaceous to Paleogene sediments and 200–500 m of Neogene carbonate oozes and chalks. Calcareous microfossils in

F2. Conceptual regional cross section through time across Site 1172, p. 54.

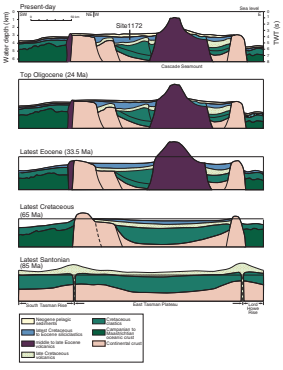

volcaniclastic sedimentary rocks from high on the seamount suggest an increase in water depth from very shallow in the latest Eocene to deep in the early Miocene (Quilty, 1997). Thus, the seamount's relief of 1500 m should approximate the minimum water depth over much of the East Tasman Plateau in the latest Eocene. However, the drilling provided an enigma by proving that the latest Eocene sediments west of the base of the seamount were deposited in upper bathyal depths (much shallower than 1500 m). At the location of Site 1172, AGSO gravity core 147/GC32 recovered 262 cm of light gray clayey foraminifer ooze of late Pleistocene or younger age (<0.46 Ma).

The only relevant Deep Sea Drilling Program (DSDP) location is Site 283 (Kennett, Houtz, et al., 1975), drilled to a depth of 592 m on the abyssal plain, 250 km east of the East Tasman Plateau in a water depth of 4756 m. Drilling at this site recovered entirely deep abyssal Paleocene and younger sediments, with a very poor biogenic record, above heavily weathered and undated pillow basalt. The sediments consist of 16 m of upper Miocene to Holocene zeolitic clay, 164 m of upper Eocene diatom ooze with nannofossils, 225 m of middle Eocene silty clay, and 283 m of Paleocene poorly fossiliferous silty clay and silty pyritic claystone. The site was located above a magnetic anomaly interpreted as Chron 32, suggesting a basement basalt age of Maastrichtian.

Site 1172 is located on multichannel seismic profiles *Tasmante* 125-4 and AGSO 202-01 and -13 (Fig. F3) in a structural low ~35 km west of the foot of the Cascade Seamount. The site is in an area of almost flat-lying sediments ~1400 m thick and overlying an older section perhaps 1500 m thick at the site. The entire sedimentary section is cut by small normal (compaction) faults. The site was designed to core down well into Paleogene sediments. For conversion from seconds below seafloor to meters below seafloor, velocities were assumed to average 1700 m/s in the Neogene sequence and 2200 m/s in the Paleogene. The upper part of the sedimentary section includes five seismic unconformities (from the top A, B, C, D, and E) whose ages were speculative; three of these unconformities were drilled (Fig. F3). Exon et al. (1997) had considered that the strong reflectors of Unconformity E probably represented middle (or late) Eocene basalt flows and volcaniclastics associated with the Cascade Seamount. Drilling proved this incorrect, and Unconformity E is probably of Late Cretaceous age.

The uppermost semitransparent but bedded sequence is above the downlapped Unconformity A at 0.37 s. Drilling proved this sequence to be carbonate ooze and chalk of Neogene age. Unconformity A proved to be upper Eocene in age. The moderately reflective and well-bedded section below the unconformity, 0.19 s thick, is siliciclastics of Eocene age. The underlying Unconformity B, at 0.5 s, truncates the underlying section. Below Unconformity B are 0.2 s of moderately reflective, thickly bedded sediments of Eocene and Paleocene age. The underlying unconformity C at 0.76 s is a strong reflector with pinch-outs beneath it. It overlies a semitransparent, irregularly bedded sequence ~0.4 s (440 m) thick of Upper Cretaceous siliciclastics.

Unconformity D at 1.19 s (1285 mbsf) is onlapped by the irregularly bedded sequence. Beneath this unconformity is a well-bedded sequence 0.2 s (220 m) thick, believed now to be siliciclastics of Late Cretaceous age. These onlap Unconformity E, the uppermost of a bundle of strong reflectors at 1.4 s (1505 mbsf), which may be within the Upper Cretaceous or the top of the Lower Cretaceous.

Sites 1172 and 1168 represent a pair of sites off the east and west margins of Tasmania, located to allow comparison between environ-

F3. A portion of multichannel seismic profile AGSO 202-13 through Site 1172, p. 55.

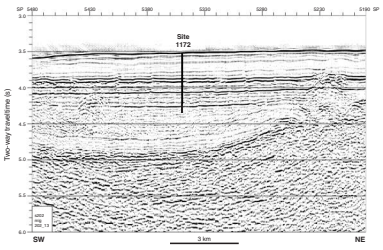

ments of sedimentation and biogeographic patterns between the southern Indian and Pacific Oceans at different stages in the development of the Southern Ocean during the Cenozoic. The comparison of the sedimentary environment and biotas in each ocean was expected to provide vital data about the nature of the ocean environment before the opening of the Tasmanian Gateway and the timing and character of developing interconnection between these oceans.

Site 1172 is well located southeast of Tasmania to monitor the paleoceanographic history of the East Australian Current, the major warm surface current of the South Pacific. This western boundary current presently flows southward along the coast of eastern Australia before turning to the east and splitting into two major branches flowing to the north and south of New Zealand. The southern branch flows eastward immediately to the south of Tasmania, where it contacts the powerful Antarctic Circumpolar Current. The strength of the East Australian Current should have varied through time in response to changing strength of the South Pacific gyral circulation. This circulation would have varied in response to changing wind forces, related to global climate change and to plate tectonics. On long time scales, critical changes in plate tectonics in the South and equatorial Pacific that should have contributed to the changing strengths of gyral circulation, and hence of the East Australian Current, include (1) constriction of the Indonesian Seaway beginning near the Eocene–Oligocene transition and continuing through the Neogene, (2) the opening of Drake Passage at the Oligocene–Miocene transition, and (3) the opening of the Tasmanian Seaway and expansion of the Southern Ocean since the Eocene–Oligocene transition.

Site 1172 represents a unique and pioneering opportunity to investigate the history of this boundary current on long time scales. No previous site in the history of ocean drilling has been suitably located to target this problem. Site 1172 appears to have been in sufficiently shallow waters through much of the Cenozoic to ensure calcareous microfossil preservation, which is so vital for isotopic, quantitative micropaleontological, and geochemical investigations of surface-water temperature changes. Changes in surface-water temperatures and in the biogeography of microfossil assemblages are expected to have resulted from changing strength of the East Australian Current.

Site 1172 is also well located to monitor changing interrelations between the East Australian Current and the Antarctic Circumpolar Current. The Antarctic Circumpolar Current was initiated during the Eocene–Oligocene transition far to the south of Tasmania with the opening of the Tasmanian Gateway, and it probably rapidly expanded northward toward Tasmania in the Oligocene because of subsidence of the South Tasman Rise. Site 1172 should have felt the effects of this expansion sometime during the Oligocene.

The East Australian Current has played a long-term role in transporting heat to high latitudes of the South Pacific. In the early Cenozoic, before the inception of the Antarctic Circumpolar Current, it flowed unimpeded to the Antarctic margin and served as a major source of heat transport to the continent (Kennett, 1977; Murphy and Kennett, 1986). With the initiation and later expansion of the circumpolar current, southward flow of the East Australian Current was interrupted and it then flowed to the east well to the north of Antarctica. This had the major effects of limiting heat transport to Antarctica, thermally isolating the continent, and contributing toward cooling and cryospheric development.

OPERATIONS

Transit to Site 1172

Site 1172, the final site of the leg, is located 275-nmi north of Site 1171 in 2622 m of water Approximately 1 mile from location, the ship slowed, the thrusters were lowered, and a beacon was deployed at 0915 hr on 23 April, initiating Site 1172.

Hole 1172A

An APC/XCB bottom-hole assembly (BHA) was made up and run to near the depth indicated by the precision depth recorder (2637.4 m below rig floor [mbrf]). Hole 1172A was spudded with the APC at 1630 hr on 23 April. The seafloor depth was calculated from the recovery of the first core as 2633.2 mbrf, or 2621.9 mbsl. Piston coring advanced to 224.8 mbsf, where Core 24H could not be retrieved from the sediment with 80,000 lb of overpull, requiring a drillover to release the core barrel. Piston cores were oriented starting with Core 3H and continued through Core 24H. Because of the ~4 m heave, heat-flow measurements were deferred until the next hole in anticipation of improving conditions. The average recovery in Hole 1172A was 102% (Table T1); however, the excessive heave resulted in many of the shallower piston cores being dominated by flow-in, in particular Cores 5H through 10H and Cores 15H and 19H.

T1. Coring summary, p. 102.

The XCB system was used to deepen the hole to 522.6 mbsf, with 85% average recovery. XCB coring was terminated because of the slow rate of penetration (ROP) (7 m/hr) and poor recovery (8%) of the last two cores. The overall average recovery for Hole 1172A was 93%.

Hole 1172B

The ship was offset 20 m north of Hole 1172A, and Hole 1172B was spudded with the APC at 1050 hr on 26 April. To obtain an appropriate stratigraphic overlap with the Hole 1172A, the bit was positioned 3 m shallower at spud-in. The estimated seafloor depth of 2633.6 mbrf (2622 mbsl) was calculated from the recovery of the first core. Piston coring advanced to 202.4 mbsf (average recovery = 102%), where 75,000 lb was required to free the core barrel (Core 22H) from the sediment. Cores were oriented starting with Core 3H and three Adara heat-flow measurements were obtained at 40.9 (Core 5H), 59.9 (Core 7H), and 88.4 mbsf (Core 10H).

Hole 1172C

The vessel was offset 20 m north of Hole 1172B, and Hole 1172C was spudded with the APC at 1130 hr on 27 April. To maintain stratigraphic overlap with the previous two holes, the bit was positioned 6 m deeper than at Hole 1172B for spud-in. The seafloor depth was estimated to be 2633.0 mbrf (2621.7 mbsl).

Piston coring advanced to 171.0 mbsf, where APC refusal was encountered. The core barrel for Core 18H required drilling over when 75,000 lb of overpull could not free the core barrel from the sediment. The average recovery was 101%, and cores were oriented beginning with Core 3H.

Hole 1172D

Following the recovery of the last core from Hole 1172C, the drill string was recovered and a rotary core barrel (RCB) BHA was assembled. Before spudding the fourth hole of the site, the vessel was offset 20 m north of Hole 1172C. Hole 1172D was spudded with the RCB at 1630 hr on 28 April and drilled ahead with a center bit in place to 343.6 mbsf with an average penetration rate of 57 m/hr. The interval from 343.6 to 372.4 mbsf was rotary cored (Cores 1R through 3R) with an average recovery of 68%; however, the first core did not recovery any material. The average recovery for the second and third core was 103%.

Following the recovery of the third core barrel, a wash barrel was dropped and was drilled ahead from 372.4 to 497.4 mbsf with an average ROP of 27 m/hr. Continuous rotary coring was initiated at 1500 hr on 29 April in Hole 1172D and extended until 2215 hr on 1 May, when operational coring time expired. The final depth of Hole 1172D was 766.5 mbsf, with an average recovery of 80%. Following a 12-hr wiper trip and hole preparation, which included the release of the bit at the bottom of the hole, the end of the pipe was placed at 160 mbsf for logging. In the first logging run, the triple-combo tool string reached a depth of 762 mbsf and the pipe was pulled to 150 mbsf while logging up to accomplish overlap with the shipboard splice. However, excessive heave caused the wireline heave compensator (WHC) to stroke out repeatedly (six times) during the logging pass. Despite the heave, the data obtained were of good quality, noting some borehole rugosity but no extensive areas of washout. Sea conditions continued to deteriorate as logging progressed (heave of ~6 m), and the WHC was abandoned during the GHMT-sonic run after stroking out six times within 10 min of activation. The GHMT-sonic also reached target depth, and good sonic and magnetic data were obtained up to the base of the pipe. The FMS was then rigged up in hopes that heave would subside to within the effective range of the WHC. The conditions did not improve within the allotted time, and the FMS run was abandoned.

After the logging equipment was rigged down, the drill string was recovered and the BHA dismantled in preparation for the voyage to Sydney, Australia. Both beacons were successfully recalled and recovered. After the drilling equipment was secured, the vessel departed for Sydney at 2100 hr on 3 May.

Transit from Site 1172 to Sydney

The 620-nmi transit from Site 1172 to Sydney was accomplished in 59.7 hr in good weather at the maximum speed possible (average = 10.4 kt). The ship docked and the first line was ashore at 1025 hr, May 6, ending Leg 189.

LITHOSTRATIGRAPHY

Introduction

At Site 1172, sediment was cored in four holes to a maximum depth of 766.50 mbsf. The sediments down to 355 mbsf contain a succession of calcareous biogenic pelagic oozes. Below this calcareous sequence, a distinct glauconitic lithologic unit was penetrated (Cores 189-1172A-

39X and 189-1172D-2R) that separates the pelagic sediments from siliciclastic sequences (Unit II).

Based on lithologic changes at Site 1172, the sediments were subdivided into the major Units I to IV with three subunits in Unit I and two subunits in Units III and IV, respectively (Table T2). This subdivision is based on the results of shipboard analyses, which include visual core observations and smear slide–based estimation of sediment components. Measurements of calcium carbonate content, sediment physical properties, lightness, and bulk mineralogy were additionally used as support in describing these units. Unit I contains white calcareous pelagic sediments. Unit II encompasses a complex series of mostly glauconitic siltstones and represents the transition from a carbonate to a siliciclastic facies. Unit III is a diatom-rich claystone with less glauconite content, and Unit IV consists of a variety of silty claystones. A general overview of the principal lithostratigraphic units of the entire cored sequence is presented in Figure F4.

Description of Lithostratigraphic Units

Unit I

Depth: 0 to 355.80 mbsf
Age: Holocene to early Oligocene
Intervals: Cores 189-1172A-1H to 39X; Cores 189-1172B-1H to 8H; and Core 189-1172C-1H to 8H
Thickness: 355.80 m

Unit I is characterized by a calcareous succession of mainly nannofossil ooze that represents the entire Neogene and some of the Oligocene at Site 1172. This sedimentary sequence is subdivided into three subunits on the basis of changes in the biogenic calcareous and noncalcareous components, as well as with the support of physical properties data.

Subunit IA

Depth: 0 to 70 mbsf
Age: Holocene to early Pliocene
Intervals: Cores 189-1172A-1H to 8H; Cores 189-1172B-1H to 8H; and Cores 189-1172C-1H to 8H
Thickness: 70 m

Subunit IA is mainly a white (N 8) foraminifer nannofossil ooze that grades occasionally to a foraminifer-bearing nannofossil ooze. In some intervals, sandy clasts contain an increased foraminiferal content. Stained fields of greenish gray to light greenish gray (5Y 7/1 to 5GY 6/1) color were sporadic throughout Subunit IA but locally abundant within layers in Core 189-1172A-3H. In Core 189-1172A-4H, alternating bands of laminated sediment show cycles at every 40 to 50 cm and every 80 to 100 cm. Bioturbation is rarely visible, although *Zoophycos* ichnofossils were observed.

Smear-slide observations indicate an average nannofossil percentage of 50% in the topmost layers, which increases downward to 90% at 70 mbsf (Fig. F5A, F6). Foraminifers are the second major component and decrease from 45% at the top of the unit to 5% at the bottom of the subunit. This variability in the calcareous content is reflected by large amplitudes in the lightness (L*) and carbonate content. Between 10 and 20 mbsf, clay is a very minor component with a maximum of 10%. Ac-

T2. Lithostratigraphic summary, p. 105.

F4. Summary of Holes 1172A to 1172D, p. 56.

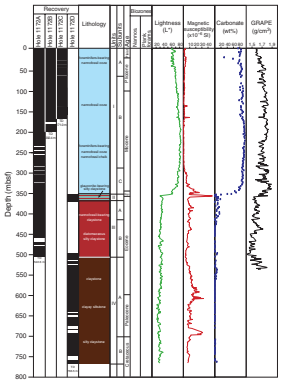

F5. Detailed summary of the 0–766.5 mbsf interval, Holes 1172A to 1172D, p. 57.

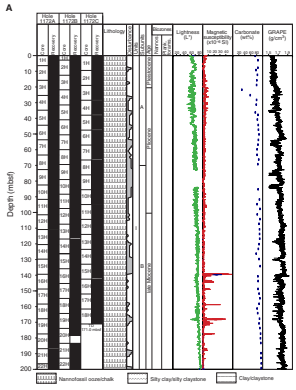

F6. Results of smear-slide analyses of Neogene and uppermost Paleogene sediments, p. 61.

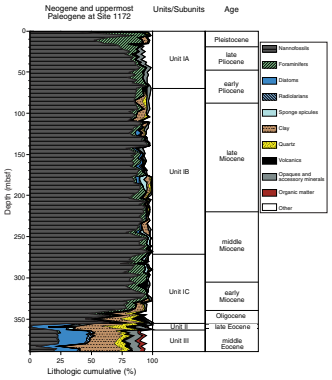

cessory and opaque minerals are rare (2%–3%) between 20 and 45 mbsf, which seems to be reflected by slightly increased values in the magnetic susceptibility record. However, magnetic susceptibility values are generally very low and appear not to be significant.

Subunit IB

Depth: 70.00 to 271.20 m
Age: early Pliocene to late Miocene
Intervals: Cores 189-1172A-8H to 30X; Cores 189-1172B-8H through 22H; and Cores 189-1172C-8H through 18H
Thickness: 201.20 m

The sediment of Subunit IB consists entirely of white and light greenish gray (N 8, 10Y 7/1, and 10Y 8/1) nannofossil ooze. Subunit IB is distinguished from Subunit IA by a considerable decrease in foraminiferal content, which is replaced almost entirely by nannofossils. This lithologic succession is not associated with a sharp boundary, but with a gradual change, which was detected in smear-slide analyses.

Subunit IB shows no signs of lithification above Core 189-1172A-29X, below which the ooze–chalk transition begins. Stained bands and thin intervals of light bluish gray color (10GY 7/1 to 5GY 8/1 or 5PB 6/1) are common and occasionally appear as faint laminations (Fig. **F7;** interval 189-1172A-26X-4, 38–55 cm). Sporadic large burrows of unknown origin are usually filled with pyrite-stained dark gray ooze. Pyrite-stained small black dots <1 mm in size are common. In Core 189-1172A-16H, several pyrite nodules 1 to 4 cm in diameter are present.

Nannofossil content in Subunit IB ranges between 79% and 94% (Fig. **F6**) and indicates a high degree of lithologic homogeneity. The remaining components show little variation. Foraminifers are consistently present with an average of 4% throughout the subunit, whereas siliceous microfossils (diatoms, radiolarians, and sponge spicules) are rare, except in a few intervals (average percentage of 1.8% in the interval between 117 and 250 mbsf). Clay was noted between 75 and 110 mbsf, between 175 and 200 mbsf, and between 231 and 245 mbsf, with an average of 3% to 6%. Trace amounts of opaque minerals, accessory minerals, and, in particular, volcanic glass are in the interval between 140 and 160 mbsf. These are reflected in slight excursions of the magnetic susceptibility record. The lightness record (L*) shows two phases of decreased values in this interval at 140 and 160 mbsf, which are also reflected in the carbonate content. At 230 mbsf, the carbonate content reaches its absolute maximum of 97 wt% for the entire sediment sequence at Site 1172.

Subunit IC

Depth: 271.20 to 355.80 m
Age: early to middle Miocene
Interval: Cores 180-1172A-30X to 39X
Thickness: 84.6 m

Subunit IC consists of foraminifer-bearing nannofossil chalk and clay-bearing nannofossil chalk of early to middle Miocene age. The boundary between Subunit IB and Subunit IC was set at the top of Core 189-1172A-30X, which follows a short interval of nonrecovery in Core 189-1172A-29X. Between these two cores, there is a considerable change within the calcareous sediment components, which requires separating those two lithologies.

F7. Stained bands in late Miocene-age nannofossil ooze, p. 62.

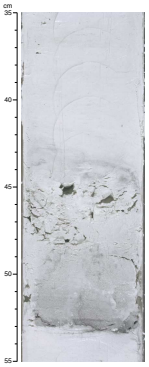

Minor lithologies in Subunit IC include nannofossil-bearing, volcanic glass-bearing clayey siltstone and a diatom- and nannofossil-bearing claystone. Colors range from white (N 8, 5Y 8/2, and 2.5Y 8/1) to pale yellow, light gray, pale olive, or light olive gray (5Y 8/1 to 5Y 6/3). Laminations of bluish gray color (5PB 6/1 to 5PB 5/1 and 5PB 8/1) are occasionally present. *Zoophycos, Chondrites,* and large burrows of unknown origin are frequent and are particularly abundant in Core 189-1172A-31X. Bioturbation is visible throughout the subunit with a distinct increase downward. Cores 189-1172A-32X and 33X are strongly bioturbated intervals and are dominated by light greenish gray colors (5BG 8/1) (Fig. **F8;** interval 189-1172A-34X-2, 100–120 cm). Lithification increases downward and pressure solution seams are common throughout the subunit (Fig. **F9;** interval 189-1172A-34X-5, 69–82 cm).

Smear-slide data indicate a compositional change in two steps through Subunit IC (Fig. **F6**). The first step is in the upper part of the subunit from Core 189-1172A-30X to 33X and is marked by decreasing nannofossils and increasing foraminifers. The second step shows a distinct increase in clay, quartz, volcanic glass, opaque minerals, and accessory minerals in the lower part of the subunit from Core 189-1172A-34X to 39X. In particular, dark grains, presumably volcanic glass, were observed throughout the subunit, occasionally in thin layers (Core 189-1172A-38X). Carbonate content and, in particular, physical properties data indicate a similar two-step change in Subunit IC (Fig. **F5A**). The occurrence of a peak in volcanic glass content with an excursion at 310 mbsf, and a distinct decline below 340 mbsf to the lower subunit boundary, is paralleled by a decrease of lightness (L*) values. This interval contains an average of 10% volcanic glass. A parallel variability is noticed in the magnetic susceptibility data, which show two distinct increases at 310 mbsf and between 340 mbsf and the end of the subunit at 355.80 mbsf.

F8. Close-up photograph of strong bioturbation in early middle Miocene-age nannofossil ooze, p. 63.

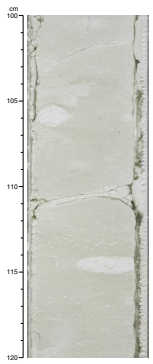

F9. Close-up photograph of the lithification of the carbonate succession, p. 64.

Unit II

Depth: 355.80 to 361.12 mbsf
Age: Oligocene to latest Eocene
Intervals: Core 189-1172A-39X and Core 189-1171D-1R to 2R
Thickness: 5.32 m

Unit II represents the transition from the pelagic sediments of Unit I to the predominantly siliciclastic sediments of Unit III. Unit II is distinguished from Subunit IC by an increase in glauconite content, a decrease in nannofossils, an abrupt decrease in carbonate content from 69 wt% at 351 mbsf to 0.3 wt% at 357 mbsf, and a sharp change in many of the physical properties data (see **"Physical Properties,"** p. 46). Although Unit II is thin, it contains a complex succession of sediments and is characterized downsection by

1. A greenish gray (5GY 6/1 and 10Y 7/1) glauconite-bearing silty diatomaceous claystone,
2. A greenish gray to dark greenish gray (10GY 5/1 and 4/1) to greenish black (5GY 2.5/1 to BG 2.5/1) glauconite-bearing silty claystone,
3. A glauconite-bearing diatomaceous clayey siltstone, and
4. A dark greenish gray (10Y 4/1) glauconitic diatomaceous clayey siltstone.

Unit II is commonly to abundantly bioturbated throughout.

The upper 2.5-m section below 355.8 mbsf contains increased glauconite as well as several distinct surfaces. Glauconite increases down to an irregular surface at 356.24 mbsf, which separates light greenish gray clay-bearing nannofossil chalk above from glauconitic greenish gray diatom- and clay-bearing nannofossil chalk below. There are small rip-up clasts a few centimeters above the contact with small burrows (<1 cm) within a few centimeters below. Glauconite varies from common to abundant (visual inspection) down to a distinct, sharp surface at 357.27 mbsf. Above the surface, pebble-sized rip-up clasts are abundant within a light greenish gray (10Y 7/1) glauconite-, diatom-, and clay-bearing nannofossil chalk, where, as below, there are angular clasts that extend ~40 cm downsection within a greenish gray (10GY 5/1) silty diatomaceous claystone. Green and dark olive glauconite grains begin below the surface (357.27 mbsf) and extend down to 357.74 mbsf. Based on biostratigraphy, a significant hiatus or condensed section of perhaps several million years is present across this distinct surface (see **"Biostratigraphy,"** p. 22). There is a 6-cm-thick volcanic ash layer at 357.93–357.99 mbsf. Glauconite abundance does not vary across a sharp color change (greenish gray [10GY 4/1] and blackish green [5GY 2.5/1]) at 358.29 to 360.6 mbsf. Glauconite begins to decrease at 360.6 mbsf and diminishes to very minor amounts at the base of the subunit at 361.12 mbsf.

Unit III

Depth: 361.12 to 503.42 mbsf
Age: late to middle Eocene
Intervals: Cores 189-1172A-39X through 54X and Cores 189-1171D-2R to 4R
Thickness: 142.30 m

Unit III is predominantly upper to middle Eocene diatom- and nannofossil-bearing claystone in the upper portion, grading to diatomaceous claystone in the lower portion. It is distinguished from Unit II by its lower glauconite content. Nannofossils decrease downsection from a minor modifier to near 0% by 438.8 mbsf. Based on this change, this unit was divided into two subunits.

Subunit IIIA

Depth: 361.12 to 433.89 mbsf
Age: late to middle Eocene
Intervals: Cores 189-1172A-39X to 47X and Cores 189-1171D-1R to 4R
Thickness: 72.77 m

Subunit IIIA is a middle to late Eocene greenish gray to dark greenish gray (10GY 5/1 and 4/1) and dark brownish gray (10YR 4/1) diatom- and nannofossil-bearing claystone to very dark brown (10YR 2/2) and very dark grayish brown (2.5Y 3/2) diatomaceous claystone. It is distinguished from Unit II by lower glauconite abundance (15%–25% above the boundary in Unit II to 2%–5% below the boundary in Unit III). A distinct cyclic color pattern is observed in this unit, alternating from greenish gray and dark greenish gray (10Y 5/1 to 4/1) to dark grayish brown (10YR 4/2) in the upper portion (361.12 to 393.40 mbsf). In the lower part of the subunit (393.40–433.89 mbsf), the pattern is generally absent, although occasionally observable from very dark grayish brown

(2.5Y 3/2) and very dark brown (10YR 4/2) to greenish gray (10Y 5/1). Bioturbation is common to abundant throughout the subunit with abundant *Zoophycos* and *Chondrites*. Glauconite is present in very minor amounts (<6%).

The pervasive color cycles that characterize most of this subunit vary in length downsection. The uppermost part contains an average cycle length of ~1.5 m, whereas at 385 mbsf the length decreases to ~0.4 m until a darker and more homogeneous interval at 412.40 mbsf, which continues down to the base of the subunit. The length of the lighter colored strata tends to decrease downsection, with the darker colored strata becoming predominant by ~400 mbsf. This coincides with a downsection increase in nannofossils from more than 20% to between 4% and 8% (Fig. **F10**). In the uppermost section, volcanic glass reaches minor modifier status before decreasing below 364 mbsf. There are very minor amounts (<8%) of volcanic glass scattered throughout the core and several thin volcanic beds at 394.45–394.47 and 395.22–395.35 mbsf.

Subunit IIIB

Depth: 433.89 to 503.40 mbsf
Age: middle Eocene
Intervals: Cores 189-1172A-47X through 54X and Core 189-1172D-4R
Thickness: 69.51 m

Subunit IIIB consists of a middle Eocene dark gray to very dark gray (5Y 3/1 to 4/1), greenish gray and dark greenish gray (5Y 4/1, 5GY 4/1, and 10Y 4/1), and dark olive-gray (5Y 3/2) diatomaceous silty claystone. It is distinguished from Subunit IIIA above by its decreasing nannofossil content and increasing quartz grains.

Colors show a cyclic pattern on a decameter scale, especially in the upper part of the unit. The color variations are faint, and there is a tendency toward a slightly lighter color below ~450 mbsf (Core 189-1172A-49X) and downsection. Clay, diatoms, and quartz are major components, but minor amounts of opaque minerals, volcanic glass, radiolarians, sponge spicules, and occasionally nannofossils are present throughout (Fig. **F10**). Planktonic foraminifers were not observed in smear slides, but rare, large benthic foraminifers are present in trace amounts from 447 to 450 mbsf. Glauconite, visible as silt- and sand-sized green/black grains, is present throughout, with occasional intervals of increasing abundance downsection on a 1- to 3-m scale. Pyrite grains appear more abundant in the lower part of the unit. Bioturbation is very common to abundant with several very large burrows, up to 37 cm in length, observed from 480 to 500 mbsf and with *Zoophycos* being very common in sections with abundant bioturbation (Fig. **F11**). Most of the distinct burrows are filled with clay of greenish gray or dark greenish gray color (5GY 4/1 and 10GY 5/1). Calcium carbonate values are very low, approaching zero, which is consistent with the very low calcareous nannofossil content.

The spectrophotometer data show little variations until ~450 mbsf and then slightly larger amplitude fluctuations toward the bottom of the subunit. Gamma-ray attenuation (GRA) bulk density data indicate an increase in density until a maximum at 1.72 g/cm³ (440 mbsf) followed by a decrease to 1.28 g/cm³ (450 mbsf) that is maintained downward.

F10. Results of smear-slide analyses with the lithologic composition of Paleogene sediments, p. 65.

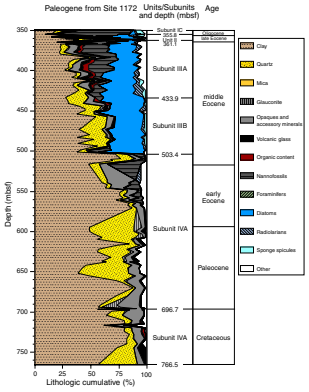

F11. Close-up photograph of abundant *Zoophycos* traces, p. 66.

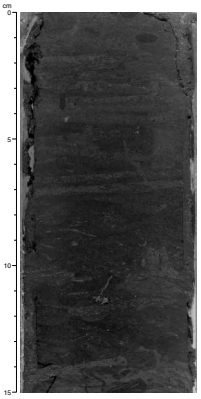

Unit IV

Depth: 503.40 to 766.50 mbsf
Age: Late Cretaceous to early Eocene
Intervals: Cores 189-1172A-54X through 56X and Cores 189-1172D-4R through 31R
Thickness: 263.10 m

Unit IV extends from 503 mbsf to the bottom of the hole at 765.97 mbsf. This unit consists mainly of claystone with low abundance of nannofossils, diatoms, glauconite, and accessory minerals in changing abundance (Fig. **F5C, F5D**). These lithologic changes were used to separate Unit IV into two subunits. Physical properties data were employed to support this separation. However, note that lower end GRA bulk density data from the rotary drilled Hole 1172D were not considered reliable because of the incompletely filled liners (see **"Physical Properties,"** p. 46). This unit also contains the K/T boundary, at which no major lithologic change was observed.

Subunit IVA

Depth: 503.40 to 695.99 mbsf
Age: middle Eocene to early Paleocene
Intervals: Cores 189-1172A-54X through 56X and Cores 189-1172D-4R to 24R-5
Thickness: 192.59 m

Subunit IVA extends from 503.40 to 695.99 mbsf and consists largely of claystone. Minor lithologies include silty claystone, nannofossil-bearing claystone, and clayey siltstone. In contrast to the overlying Subunit IIIB, Subunit IVA bears no siliceous microfossils, but it does contain an increasing abundance of opaque minerals and accessory minerals. The exact boundary was defined at changing trends in lightness and magnetic susceptibility.

The claystone of Subunit IVA is olive gray (5Y 4/2, 5Y 3/1, and 5Y 3/2) with some variations to a very dark grayish brown (2.5Y 3/2) and to a greenish gray (5GY 5/1 and 5GY 5/1). Bioturbation is abundant, with well-preserved traces of *Zoophycos* and *Chondrites*. Some individual large burrows of unknown origin are filled with pyrite. Pyrite nodules between 1 and 4 cm in diameter were found in Sections 189-1172D-4R-4, 14R-4, 18R-4, and 20R-4. Thin mollusk shell beds were observed in Sections 189-1172D-9R-2 and 10R-4. The dominant clay component varies between 50% and 85% throughout the subunit. Opaque and accessory minerals are abundant and reach a maximum between 536 and 542 mbsf with 10% and 15%, respectively (Fig. **F10**). Silt-sized grains of glauconite were observed occasionally on the core surface but were rarely found in smear slides. However, between 595 and 609 mbsf, 622 and 636 mbsf, and 691 and 696 mbsf glauconite shows relative peaks in abundance of up to 11%. These peaks correspond to the magnetic susceptibility record with slightly increased values, the older glauconite peak being recorded at the lower boundary of Subunit IVA. Nannofossils are present at 10% abundance at the top of the subunit and decrease downward to trace abundance below 565 mbsf (Fig. **F10**).

Subunit IVB

Depth: 695.99 to 766.50 mbsf
Age: Cretaceous (Maastrichtian)

Interval: Sections 189-1172D-24R-5 through 31R-CC
Thickness: 70.51 m

Subunit IVB consists of very dark olive gray (5Y 3/2), very dark gray (10YR 3/1 and 5Y 3/1), and black (5Y 2.5/1 and 5Y 2.5/2) claystone and silty claystone. Subunit IVB is darker in color and less intensely bioturbated and contains fewer glauconite grains than Subunit IVA. The sediments contain organic material (~0.85% total organic carbon [TOC], see **"Organic Geochemistry,"** p. 40) and opaque minerals (<10% by smear-slide observation; Fig. **F10**) throughout the section, which are reflected in the dark color of the sediment. Carbonate content averages 1.4 wt%, slightly higher than the averages observed in the lower half of Subunit IVA (see **"Organic Geochemistry,"** p. 40). The highest carbonate content (6.5 wt%) of Subunit IVB is observed at 762.9 mbsf (Sample 189-1172D-31R-5, 72 cm). Foraminifers and nannofossils are rare to common with good preservation. The sediment is barren of diatoms and radiolarians; however, siliceous microtubes, already observed in the Eocene sediments in Sites 1170, 1171, and 1172, are present throughout the subunit.

Sediments of this subunit are generally weakly laminated with very thin laminae frequently present throughout the subunit. Bioturbation (thin burrows of ~3 mm in diameter) is common in Cores 189-1172D-27R, 29R, and 31R and rare in other cores. Very fine sand-sized glauconite-rich layers are observed in claystones every ~50–100 cm. Although the amount of glauconite is not significant (i.e., no more than a few percent in smear slides), this periodicity may imply some paleoenvironmental signal. The dark olive-gray silty claystone below the Subunit IVA/IVB boundary, between 696.4 and 697.1 mbsf (interval 189-1172D-24R-5, 20–50 cm; Fig. **F12**), contains abundant fine to medium sand-sized grains. This sandy interval is reflected in magnetic susceptibility as a distinct positive excursion (see **"Physical Properties,"** p. 46). Carbonate particles increase downward in Section 189-1172D-26R-6, and the core catcher of Core 189-1172D-26R contains a pure limestone in which no biogenic particles are recognized. The origin of these nonbiogenic (diagenetic) limestone and carbonate components in the overlying carbonate-rich claystone remains unknown.

The boundary between Subunits IVA (Danian) and IVB (Maastrichtian) is placed at 695.99 mbsf (Sample 189-1172D-24R-5, 29.5 cm). At this horizon, a distinct change from glauconitic siltstone (of Subunit IVA) to underlying claystone (of Subunit IVB) is recognized (Fig. **F12;** interval 189-1172D-24R-5, 20–50 cm). The claystone layer immediately below the subunit boundary (interval 189-1172D-24R-5, 29.5–31.5 cm) has very little bioturbation and is dark greenish gray (5G 4/1), lighter than the underlying representative black claystones of Subunit IVB. This boundary claystone layer contains silt-sized angular quartz grains and glassy fragments. Above the subunit boundary, between 25 and 29 cm of Section 189-1172D-24R-5, small clasts (~1–3 cm) of claystone, derived from the boundary claystone layer, are observed in the glauconitic siltstone of Subunit IVA. Below the claystone layer of the subunit boundary, in the interval 189-1172D-24R-5, 32–41 cm, a very dark gray siltstone in Subunit IVA facies appears with clasts of glauconitic siltstone.

Micropaleontological evidence (see **"Biostratigraphy,"** p. 22) suggests that the K/T boundary lies between 44 and 79 cm in Section 189-1172D-24R-5. The sedimentological changes observed at the transition

F12. Close-up photograph of another distinct lithologic change that may represent the K/T boundary, p. 67.

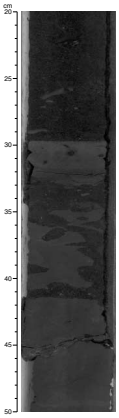

from Subunit IVB to Subunit IVA could be related to K/T boundary events and will be investigated further.

Discussion

The general trends in lithology of Site 1172 are similar to those found at other sites drilled during Leg 189 with three major phases of sedimentation:

1. The first phase is a Maastrichtian and lower Paleogene neritic and poorly ventilated siliciclastic sediment consisting of dark silty claystone and clayey siltstone. This sediment suggests stable environmental conditions during the Paleogene "Greenhouse" world.
2. This phase is followed by a period of transition with rapid changes in lithology as well as physical properties created by a highly variable environment of major reorganization in climate and oceanic conditions during the Eocene–Oligocene transition. The silty claystones are rich in authigenic glauconite, indicating extremely low sedimentation rates resulting in the entire sequence being highly condensed.
3. The youngest phase represents an open-ocean calcareous deep-water regime, which reflects a rather steady environmental system during the Neogene.

These three major periods are found in nearly all Cenozoic sequences around Antarctica.

This is the first time that Late Cretaceous sediments were drilled by the Ocean Drilling Program (ODP) in this region. The sediment recovered at Hole 1172D, on the East Tasman Plateau, is a very dark brown to black, rarely bioturbated claystone with occasional silt. It suggests a poorly ventilated, restricted shallow-water environment or restricted circulation. These sediments provide a rare window into the Late Cretaceous climate and paleoceanographic history in the extreme southwest Pacific. Postcruise studies will have major implications for Antarctic Late Cretaceous climate reconstruction, as well as the paleoceanographic history prior to the onset of the Antarctic Circumpolar Current.

As at other sites drilled during Leg 189, the Eocene–Oligocene transition at Site 1172 is remarkable sedimentologically. However, excellent recovery at Site 1172 enables a more detailed understanding of the sedimentary pattern and environment during this transition. A gradational change is present within 5 m (Fig. **F13**) from a diatom- and nannofossil-bearing silty claystone into a diatom- and clay-bearing nannofossil chalk upsection. A high glauconite content suggests a very starved environment. Glauconite increases considerably from the silty claystone upward into glauconite sand and into a glauconitic silt, and it decreases shortly after the transition into a nannofossil chalk. An ash layer at 357.9 mbsf induced a large peak in magnetic intensity and provides an excellent stratigraphic tie point. The changes in lithology and some physical properties (lightness L*, magnetic susceptibility, and GRA bulk density) as well as stratigraphic data at this boundary are documented in detail in Figure **F13.** The present stratigraphic interpretation of paleomagnetic data was made from Core 189-1172A-39X measurements, although the quality of the recorded signal in the equivalent Core 189-1172D-2R is considered to be substantially better (see **"Paleomagnetism,"** p. 36).

F13. Compilation of lithologic and stratigraphic information on Core 189-1172D-39X sediments, p. 68.

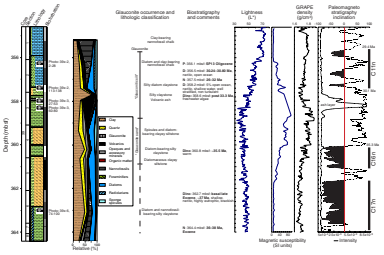

The Neogene nannofossil oozes of Unit I at Site 1172 indicate a well-oxygenated, open-marine deep-sea environment with high and relatively stable oceanic productivity, which may be affected by incursions of subantarctic surface-water masses or processes associated with frontal movements. Abundant, well-preserved diatom assemblages in the middle Miocene may indicate increased upwelling through a northward shift of the Subtropical Front. This coincides with an increase in sedimentation rates and may be related to the expansion of the East Antarctic Ice Sheet. These higher sedimentation rates may be caused by higher productivity from intensification of the Antarctic Circumpolar Current and indicate the transition from the "Doubthouse" world to the "Icehouse" world. Coarser sections with increased foraminiferal percentages may point to an increase in circulation of intermediate and bottom-water masses and associated winnowing. The variability of interaction between the east Australian current and the Antarctic Circumpolar Current system is of major importance to sedimentation at Site 1172. Results from clay X-ray diffraction (XRD) analyses of slightly darker laminated and thinly bedded intervals in the Neogene sequence indicate variable smectite content, presumably related to sedimentation of eolian dust, from Tasmania and mainland Australia. These intervals occurred particularly during the middle and late Miocene during the expansion of the Antarctic cryosphere and increasing desertification of Australia.

Clay Mineralogy

XRD analyses were completed on 41 samples from Holes 1172A and 1172D. The purpose of the clay mineral studies at Site 1172 was to (1) recognize the major variations of the paleoenvironment, as expressed by the clay mineral assemblages at a sampling interval of one for every two cores, and (2) compare the clay mineral assemblages with those recognized at Sites 1168, 1170, and 1171 drilled at comparable water depths on the western Tasmania margin, the STR, and in other areas of the Southern Ocean.

Results

The clay minerals identified include smectite, random mixed-layered clays, illite, and kaolinite. Based on the relative abundance of the clay minerals, five units were identified at Site 1172. These were designated Units C1 to C5 (Fig. F14).

Upper Pliocene to Pleistocene Unit C1, which extends from the seafloor to 50 mbsf, has a clay mineral assemblage that consists of abundant smectite (45% to 70%) and common kaolinite (15% to 25%), accompanied by random mixed-layered clays and illite (up to 15%). Unit C1 correlates to lithostratigraphic Subunit IA. Upper Miocene to upper Pliocene Unit C2, which extends from 50 to 180 mbsf, shows decreased contents of smectite (20% to 60%), increased contents of kaolinite (20% to 30%), and significant amounts of random mixed-layered clays (traces to 40%) and illite (10% to 20%). Because of the low clay content in some nannofossil oozes of lithostratigraphic Subunit IB, percentages of random mixed-layered clays >30% are probably overestimated. Unit C2 corresponds to the upper lithostratigraphic Subunit IB. Middle to upper Miocene Unit C3, which extends from 180 to 305 mbsf, shows increased contents of smectite (50% to 80%) and decreased contents of random mixed-layered clays (0% to 30%), kaolinite (10% to 20%), and

F14. Clay mineral units, p. 69.

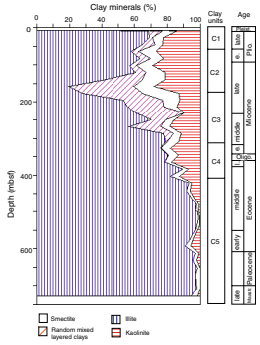

illite (0% to 10%). Unit C3 corresponds to lower lithostratigraphic Subunit IB and upper lithostratigraphic Subunit IC. Middle Eocene to middle Miocene Unit C4, which extends from 305 to 410 mbsf, contains predominant smectite (75% to 90%) increasing downhole, associated with kaolinite (10% to 20%), and illite (traces to 5%). Unit C4 corresponds to lithostratigraphic Subunit IC, Unit II, and Subunit IIIA. Upper Maastrichtian to middle Eocene Unit C5, which extends from 410 mbsf to the bottom of Hole 1172D at 766 mbsf, is characterized by almost pure smectite (95% to 100%) associated with sporadic low amounts of kaolinite and illite (up to 5%). Unit C5 correlates to lithostratigraphic Unit IV.

Paleoenvironmental Interpretation of Clay Assemblages

The clay mineral assemblage of Site 1172 is significantly different from those on the South Tasman Rise (see **"Lithostratigraphy,"** p. 9, in the "Site 1170" chapter and **"Lithostratigraphy,"** p. 10, in the "Site 1171" chapter) and western Tasmania margin (see **"Lithostratigraphy,"** p. 8, in the "Site 1168" chapter). Site 1172 is characterized by dominant smectite and an increasing trend of kaolinite, from the late middle Eocene to the early Pliocene. The kaolinite trend is absent from the other sites.

Almost exclusive smectite characterizes upper Maastrichtian to middle Eocene Unit C5. Smectite prevails in areas of low relief with alternating intervals of precipitation and aridity, and its formation is enhanced on basic volcanic substrates (Chamley, 1989; Weaver, 1989). The only visible ash layers and occurrences of volcanic glass, probably from the adjacent Cascade Seamount, were restricted to the upper Eocene and Oligocene intervals. The siliciclastic sediments consist of claystone and silty claystone, and the clay particles are most probably derived from adjacent emerged areas of the Tasmanian landbridge and Campbell Plateau (see **"Background and Objectives,"** p. 6). Therefore, the extreme predominance of smectite points to warm climates and intense weathering in the Tasmanian region adjacent to Antarctica. Uppermost Cretaceous to middle Eocene clay assemblages of almost exclusive smectite are present at other southern high-latitude sites on the Falkland Plateau (Robert and Maillot, 1983), Maud Rise (Robert and Maillot, 1990), and Kerguelen Plateau (Ehrmann, 1991), as well as in the middle Eocene of the Lord Howe Rise in the Tasman Sea (Stein and Robert, 1986). No indication of increased erosion of steep continental relief associated with tectonic activity has been found at Site 1172 on the isolated ETP. Early stages of ocean opening in the Tasman Sea were already finished, and the ETP was already separated from the South Tasman Rise and probably under the influence of a western boundary current similar to the modern East Australian Current.

Unit C4 (middle Eocene to middle Miocene) is defined by a continuous decrease of smectite upward and correlative increase of kaolinite, beginning in the late middle Eocene at ~40 Ma (close to the Zone NP16/NP17 boundary). Kaolinite is typical of warm climates with high precipitation during at least part of the year (Chamley, 1989; Weaver, 1989). Kaolinite has already been observed in middle to late Eocene high-latitude areas of the Weddell Sea and subantarctic South Atlantic (Robert and Kennett, 1992), Prydz Bay (Hambrey et al., 1991) and the western Tasmania margin (see **"Lithostratigraphy,"** p. 8, in the "Site 1168" chapter). Kaolinite formation is enhanced in warm areas of intense precipitation that increase chemical weathering of substrates, especially

where uplifted relief ensures good drainage conditions and removal of soluble chemical elements. At Site 1172, there appear to have been no such uplifted source areas during the late middle to late Eocene, as was the case on the Australo-Antarctic Gulf side of the Tasmanian region. The contrast in relief in source areas probably accounts for differences in kaolinite abundance between the western Tasmania margin and the East Tasman Plateau (see **"Lithostratigraphy,"** p. 8, in the "Site 1168" chapter, **"Lithostratigraphy,"** p. 9, in the "Site 1170" chapter, and **"Lithostratigraphy,"** p. 10, in the "Site 1171" chapter). Therefore, the increasing kaolinite may result from increased precipitation on the Australian margin of the Tasman Sea and southern transport by the East Australian Current, probably caused by intensified meridional heat transfer as ocean opening progressed between Antarctica and Tasmania. Some of the kaolinite may also have come from granitic islands forming the rim of the ETP.

The first occurrence and further development of random mixed-layered clays in Unit C3 (middle to upper Miocene) are associated with sporadically increased contents of illite. Illite and random mixed-layered clays are derived from erosion of poorly weathered substrates (Chamley, 1989; Weaver, 1989). They indicate an increase of physical weathering in the source areas during the middle Miocene, at ~13–14 Ma (Zone NN6), probably from cooler climatic conditions that followed the expansion of the East Antarctic Ice Sheet at 14–15 Ma (Kennett, 1977).

A further development of kaolinite (up to 30%) characterizes Unit C2 (upper Miocene to upper Pliocene). Because of the continued spreading in the Southern Ocean during the Oligocene and the Neogene, Australia moved into warmer latitudes and kaolinite formation increased on the emerged Australian passive margin of the Tasman Sea. Increased kaolinite may reflect intensified precipitation starting at ~8.3 Ma (lower Zone NN11). A coeval increase of kaolinite is observed at Site 823 on the northern part of the Australian margin of the Tasman Sea (Chamley et al., 1993). Increased kaolinite contents along the Australian margin of the Tasman Sea were most probably the consequence of intensified meridional heat transfer through the East Australian Current. Regional increases of kaolinite (and associated precipitation) have also been observed in the midlatitudes of the Atlantic Ocean (Robert and Chamley, 1987). Late Miocene increases of precipitation at ~8 Ma preceded the onset of ice buildup in West Antarctica in the latest Miocene (Kennett, 1977).

Unit C1, of late Pliocene and Pleistocene age, shows an increase of smectite. The clay assemblage is very similar to that of Sites 588, 590, and 591 on the Lord Howe Rise (Stein and Robert, 1986). At the same time, the clay content of the calcareous biogenic sediment of Site 1172 slightly increases (Subunit IA). The clay assemblage of Unit C1 may reflect some wind transport from central arid Australia. As observed at Site 1170 on the STR (see **"Lithostratigraphy,"** p. 9, in the "Site 1170" chapter), this pattern may have commenced during the late Pliocene, when particles from Australian arid areas reached their maximum southward extension and abundance on the Lord Howe Rise (Stein and Robert, 1986).

BIOSTRATIGRAPHY

A sedimentary succession, ranging in age from the Late Cretaceous to Quaternary, was recovered at Site 1172 (East Tasmanian Plateau). Microfossils belonging to seven major groups were investigated. Combined results suggest that there are no major breaks in the sedimentary succession from the Pleistocene to the uppermost Oligocene. In contrast, it appears that most of the Oligocene is missing, whereas the Eocene–Oligocene transitional interval is present, albeit very condensed. Underlying the upper Eocene strata, a thick middle Eocene to upper Maastrichtian section was recovered with possible breaks in the lower middle Eocene and at the Paleocene/Eocene boundary (Fig. F15).

Siliceous microfossils are rare to absent in the Holocene to Pliocene interval but are common to abundant and well preserved in the Miocene. The thin Oligocene succession yields few radiolarians, whereas diatoms remain abundant downhole. Both groups are common to locally abundant in the Eocene of Hole 1172A with good preservation. The upper Paleocene to upper Maastrichtian interval is virtually barren of siliceous microfossils.

Planktonic foraminifers and calcareous nannofossils are generally abundant, with preservation ranging from moderate to good in the Neogene and Oligocene. Although less abundant, calcareous nannofossils remain consistently present until the middle Eocene, when abundance and preservation decrease dramatically. Below the middle Eocene (Hole 1172D), the Cenozoic succession is barren of calcareous nannofossils. Planktonic foraminifers are virtually absent below the middle/upper Eocene boundary. Well-preserved and reasonably diversified calcareous microfossils reappear in the upper Maastrichtian interval.

Calcareous benthic foraminifers are consistently present throughout the Neogene–Oligocene carbonate succession. The middle Eocene sequence yields only rare agglutinating species. However, calcareous and agglutinating taxa are present in the Paleocene to upper Maastrichtian interval.

Well-preserved organic walled dinoflagellate cysts (dinocysts) and few sporomorphs are present in the Holocene–Pleistocene interval of the recovered succession at Site 1172. The remaining Neogene to lower Oligocene strata are devoid of acid-resistant organic matter. Moderate to well-preserved dinocysts are the dominant constituent of palynological associations in the upper Paleocene to lowermost Oligocene part of the succession and are persistent below this interval. Well-preserved terrestrial palynomorphs dominate the lowermost part of Hole 1172D, attributed to the late Maastrichtian to middle Paleocene.

Sedimentation rates were relatively low in the Neogene to upper Eocene interval, ranging from 0.16 to 3.2 cm/k.y. (Fig. F15). In contrast to previous Leg 189 sites, sedimentation rates were also generally low in the middle Eocene to Maastrichtian interval (between 2.6 and 1.04 cm/k.y.) (see "Age Model and Sedimentation Rates," p. 36).

F15. Age-depth plot and linear sedimentation rates, p. 70.

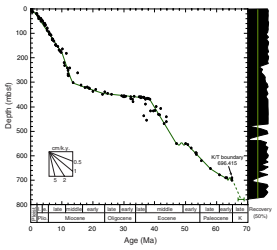

Neogene

The Pliocene/Pleistocene boundary is placed between Samples 189-1172A-1H-CC and 2H-CC on combined microfossil evidence. The upper/lower Pliocene boundary is placed between Samples 189-1172A-5H-CC and 6H-CC, whereas the Pliocene/Miocene boundary is recognized between Samples 189-1172A-9H-CC and 10H-CC. The upper/middle

Miocene boundary falls within planktonic foraminiferal Zone SN8 and nannofossil Zone CN6 but cannot be located with accuracy on the basis of the present set of samples; it must, however, be present above Sample 189-1172A-20H-CC. The middle/lower Miocene boundary is inferred to be above Sample 189-1172A-33X-CC. The Miocene/Oligocene boundary falls within the uppermost part of planktonic foraminiferal Subzone SP14b (but is normally placed for convenience at the base of Zone SN1) and at the base of nannofossil Subzone CN1a. Planktonic foraminifers indicate the passage of this boundary between Samples 189-1172A-37X-CC and 38X-CC. In terms of nannofossils, the Oligocene/Miocene boundary is associated with the last occurrence (LO) of *Reticulofenestra bisecta* (23.9 Ma), which is recognized between Samples 189-1172A-36X-CC and 37X-CC. The boundary is generally placed just above this datum.

The carbonate sequence of Site 1172 is subdivided biostratigraphically chiefly on calcareous microfossil data. The few available siliceous microfossil datums are in broad agreement with the age assignments presented above. Palynomorphs have not been analyzed in sufficient detail and/or are absent in the Neogene.

The combined paleobiotic information suggests temperate to cool temperate conditions throughout the Neogene and a deep-marine (lower bathyal to upper abyssal), well-ventilated depositional setting. To a certain extent, the Neogene encountered at Site 1172 is quite comparable with the age-equivalent interval recovered at Site 1168. A conspicuous difference is the absence of palynomorphs in this interval. It appears that in comparison with Site 1168, water masses at Site 1172 were better ventilated and more oxygen-rich, resulting in the absence of organic matter in the lower Oligocene to Neogene sediments.

Paleogene and Late Maastrichtian

The upper/lower Oligocene boundary coincides with the base of planktonic foraminiferal Subzone SP14b and is placed between Samples 189-1172A-38X-CC and 39X-CC. Part of the upper and lower Oligocene appears to be missing, as the sediments correlated to the latter zone are resting on an interval assigned to the early Oligocene planktonic foraminiferal Zone AP13.

On nannofossil evidence, it appears that much of the interval from ~27 to ~36 Ma is missing at this site. Diatoms constrain the age of the Oligocene deposits to the interval between 30.24 and 28.8 Ma (between Samples 189-1172A-39X-3, 61–63 cm, and 37X-CC).

In terms of planktonic foraminifers, the Eocene/Oligocene boundary cannot be recognized with accuracy at this site. An age of 30.24 Ma or younger can be assigned to the interval between Samples 189-1172A-39X-2, 3–5 cm, to 39X-3, 61–63 cm, on the basis of diatoms. An age of 27 to 36 Ma can be assigned to the interval between Samples 189-1172A-39X-2, 143 cm, and 39X-5, 63 cm, on the basis of nannofossils. The interval bounded by these latter samples (189-1172A-39X-2, 143 cm, and 39X-5, 63 cm) is barren of calcareous microfossils, whereas dinocysts and siliceous microfossils are consistently present. These groups suggest that the Eocene/Oligocene boundary (33.7 Ma) may be positioned between Samples 189-1172A-39X-3, 122–123 cm, and 39X-5, 22–24 cm. Combined information hence indicates that the succession, albeit condensed, is essentially complete across the Eocene–Oligocene transition.

The middle/upper Eocene boundary is recognized between Samples 189-1172A-39X-CC and 40X-CC. The bottom of Hole 1172A may be assigned to the middle middle Eocene on nannofossil and dinocyst evidence. Unfortunately, other microfossil groups cannot assist with an age assessment between the middle/upper Eocene and the K/T boundaries penetrated in Hole 1172D. Samples 189-1172D-5R-CC through 7R-CC are dated as early middle Eocene (43–49 Ma) based on nannofossil evidence, whereas Samples 189-1172D-14R-CC through 24R-CC are virtually barren of nannofossils or yield only a few specimens of nonage-diagnostic species. Dinocysts indicate the lower/middle Eocene boundary is close to Sample 189-1172D-12R-CC, whereas the Paleocene/Eocene boundary appears to be between Samples 189-1172D-19R-CC and 20R-CC. It appears that part of the lower middle Eocene is missing in Hole 1172D (Fig. **F15**).

Palynological evidence may be interpreted to indicate that the uppermost Paleocene and lowermost Eocene may be missing as well. Sample 189-1172D-23R-CC may be assigned to the Danian based on the common occurrence of the dinocyst *Alisocysta reticulata* (63–61 Ma), although unpublished reports suggest that in the Southern Hemisphere this species first appears in the uppermost Maastrichtian (P.S. Williumsen, pers. comm., 2000). The K/T boundary is presumed to be within Core 189-1172D-24R since Sample 189-1172D-24R-CC does not yield Tertiary dinocysts but does contain a typical Southern Hemisphere latest Maastrichtian assemblage. Detailed sampling within Section 189-1172D-24R-5 and subsequent palynological analysis revealed the K/T boundary to be between 189-1172D-24R-5, 77–79 and 44–46 cm, on the basis of the FO of *Trithyrodinium evittii*. The interval from Samples 189-1172D-25R-CC through 31R-CC contains Cretaceous nannofossils, including *Arkhangelskilla cymbiformis, Cribosphaerella daniae,* and *Nephrolithus frequens*. The last species is an index species for the late Maastrichtian, with an age range of 65–67 Ma in the Southern Ocean. Dinocysts from Sample 189-1172D-31R-CC indicate an age of 69 Ma or younger, whereas planktonic foraminifers confirm a Maastrichtian age for the bottom of Hole 1172D. Completeness of the K/T boundary succession will be assessed postcruise.

Paleogene Environments and the Eocene–Oligocene Transition

The Eocene–Oligocene transition is marked by a series of distinct stepwise environmental changes, reflecting increasingly cool conditions and coeval rapid deepening of the basin. A change from inner neritic depositional environments with marked freshwater influence and sluggish circulation to more offshore, deep-marine environments with increased ventilation and bottom-water current activity, marks the middle/upper Eocene boundary. Concomitant cooling is indicated by the increased numbers of endemic antarctic dinocyst species, whereas warmer episodes may be recognized as well. This trend continues throughout the upper Eocene and lowermost Oligocene (~34.0–33.3 Ma). Sediments and biota indicate increasing bottom-water ventilation and the appearance of conditions supporting highly productive surface waters, in outer-neritic to bathyal depositional settings, with increasingly cold conditions. The trend culminated in the early Oligocene (33–30 Ma) when rigorous ventilation, and generally oxygen-rich waters, precluded sedimentation of organic matter despite overall high surface-water productivity. The condensed calcareous sequence contains abun-

dant siliceous microfossils and was deposited in an oceanic bathyal environment. The Paleocene to middle Eocene dinocyst assemblages are dominated by relatively warm water, (inner) neritic, eutrophic forms. Terrestrial palynomorphs increase in relative abundance downhole and throughout, indicating warm climates in this interval. This suggests even shallower marine conditions for the older part of the succession at Site 1172, with the influence of marked runoff. Absence of foraminifers, and even nannoplankton, in most parts of the middle Eocene to Paleocene confirms the attribution to marginal marine settings. More offshore settings return in the Maastrichtian section, indicated by the return of calcareous microfossils and more offshore dinocyst assemblages. Middle to late Eocene radiolarian faunas are mainly composed of endemic taxa, whereas warm-water taxa do occur sporadically as well.

Calcareous Nannofossils

All core-catcher samples plus additional samples from critical intervals were examined for calcareous nannofossils from all four holes at Site 1172. Neogene nannofossil assemblages are similar to those recovered at Site 1168. Several index species of discoasters and ceratoliths are present, and they contribute to a higher stratigraphic resolution than that for the more southern sites (Sites 1169, 1170, and 1171; Table T3). The Oligocene–Eocene transition also yields abundant, well-preserved nannofossils. From the mid-upper Eocene through the Paleocene, nannofossils are sporadically present with variable preservation and many barren intervals. Nannofossils are generally few to common in the upper Maastrichtian (Cores 189-1172D-25R through 31R).

T3. Stratigraphic distribution of selected nannofossil species, p. 106.

The first occurrence (FO) of *Emiliania huxleyi* was not recorded in the first core-catcher sample at any of the three holes, indicating an age of older than 0.26 Ma for these samples. The LO of *Pseudoemiliania lacunosa* (0.46 Ma), marking the top of Zone NN19 (Martini, 1971) was recognized in all three holes (Table T4). The Pliocene/Pleistocene boundary is approximated by the LO of *Discoaster brouweri* (1.95 Ma).

T4. Calcareous nannofossil datum levels, p. 112.

The LO of *Discoaster pentaradiatus* (2.4 Ma) and *Discoaster surculus* (2.51 Ma) mark the base of late Pliocene Zones NN18 and NN17 (Martini, 1971), respectively. The lower/upper Pliocene boundary is marked by the LO of *Reticulofenestra psuedoumbilica* (3.65 Ma).

The Miocene/Pliocene boundary is approximated by the LO of *Discoaster quinqueramus* (5.3 Ma) recognized in the first three holes at ~80 mbsf. Nannofossil biostratigraphic resolution for the Miocene is relatively low at this latitude compared with middle to low latitudes, with only several index species present.

The LO of *Reticulofenestra bisecta* (23.9 Ma) is recognized between Samples 189-1172A-36X-CC and 37X-CC. The Oligocene/Miocene boundary is generally placed just above this datum. Another Oligocene nannofossil datum, the LO of *Chiasmolithus altus* (26.1 Ma), is present one core lower, between Sample 189-1171A-37X-CC and 38X-CC.

The LOs of *Reticulofenestra umbilica* and *Reticulofenestra reticulata* are found between Samples 189-1172A-39X-2, 143 cm, and 39X-5, 63 cm. Several samples examined between these two samples are barren of calcareous nannofossils. The truncation of the stratigraphic ranges of *R. umbilica* and *R. reticulata* and an absence of the stratigraphic interval with *Isthmolithus recurvus* and *Reticulofenestra oamaruensis* suggest that much of the interval from ~27 through ~36 Ma appears to be missing at this site.

Two more Eocene nannofossil datums were determined with moderate precision—the LO of *Chiasmolithus solitus* (40.4 Ma) between Samples 189-1172A-42X-CC and 43X-CC and the FO of *R. reticulata* (42.0 Ma) between Samples 189-1172A-43X-CC and 44X-CC. The FO of *R. umbilica* (43.7 Ma) is located between Samples 189-1172A-45X-CC and 53R-CC. This uncertainty in a long stratigraphic interval is due to the fact that many of the samples within this interval are virtually barren of nannofossils.

Samples 189-1172D-5R-CC through 7R-CC are dated as the early middle Eocene (43–49 Ma) based on the presence of *C. solitus* and the absence of *R. umbilica* and *Discoaster kuepperi*. Samples 189-1172D-14R-CC through 24R-CC are barren of nannofossils or yield only a few specimens of long-ranging species.

The interval from Samples 189-1172D-25R through 31R-CC contains Maastrichtian nannofossils, including *Arkhangelskilla cymbiformis, Cribosphaerella daniae, Eiffellithus turriseiffelii, Micula decussata,* and *Nephrolithus frequens*. The last species is an index species for the late Maastrichtian, with an age range of 65–70 Ma in the Southern Ocean.

Planktonic Foraminifers

Shipboard examination of all core-catcher samples from Hole 1172A disclosed that sediments ranging in age from Maastrichtian to Quaternary were recovered at Site 1172. The planktonic foraminiferal assemblages are typical of cool temperate regions. An apparently complete Neogene to upper Oligocene section was recognized at Site 1172. The upper Oligocene is very thin with only Subzone SP14b being recognized. The upper Oligocene rests on the lower Oligocene (Zone AP13), indicating a stratigraphic break. Beneath this is an upper to middle Eocene sequence that can be recognized on planktonic foraminifers; an underlying lower Eocene to Paleocene section is barren of planktonics. The Maastrichtian can be recognized on planktonic foraminifers. The overall sequence, with the exception of the Paleocene and Cretaceous, including the hiatuses, is almost identical to that found at Site 1168.

Planktonic foraminifers provide little biostratigraphic control throughout much of the Paleogene sequence recovered at Site 1172. Almost all of the Oligocene is missing, with only a single sample from the uppermost part being recognized. From the upper Eocene of Hole 1172A down, planktonic foraminiferal assemblages are often depauperate and barren of planktonic foraminifers below Sample 189-1172A-43X-CC. Only in the upper Maastrichtian, planktonic foraminifers return (from Sample 189-1172D-25R-CC down) with a good assemblage of high-latitude Late Cretaceous species. Cretaceous species occur sporadically in samples to Sample 189-1172D-30R-CC. Sample 189-1172-31R-CC is barren. The stratigraphic distribution of species is given in Table **T5.** The core depths of the various planktonic foraminiferal datums at Site 1172 are given in Table **T6.** A brief discussion of the salient biostratigraphic findings is provided below.

T5. Range chart of planktonic foraminifers, p. 113.

T6. Selected planktonic foraminiferal datums, p. 119.

Quaternary

The base of the Quaternary, as defined by the FO of *Globorotalia truncatulinoides,* is confined to the uppermost core in Holes 1172A (Sample 189-1172A-1H-CC). This appears to represent another example where the FO of *G. truncatulinoides* seems to be an unreliable datum in the Tasmanian region. The well-preserved assemblages are primarily temperate

in character, being dominated by such cool-water species as *Globigerina bulloides, Globorotalia crassaformis, Globorotalia inflata,* and *Neogloboquadrina pachyderma* (sinistral).

Pliocene

The late Pliocene Zone SN13, as well as Subzones SN12b and SN12a, is well represented at Site 1172 (see Table T5). The abundant and well-preserved faunas are dominated by specimens belonging to the *Globorotalia puncticulata*/*G. inflata* plexus.

Late Miocene

All of the late Miocene zones have been recognized at Site 1172, including Zone SN11. The only other record of this zone has been from Site 1168, where it is thin (just under 8 m). At Site 1170, where only this zone was missing, evidence from other microfossil groups also suggest the presence of a hiatus. At the other two sites, the absence of Zone SN11 and other zones also indicates a hiatus. At Site 1172 it is also thin, being recorded from only two samples (189-1172A-14H-CC and 15H-CC). Faunal preservation varies from good to moderate, and assemblages are common to abundant.

Middle Miocene

Zones SN5 to SN8, which are within the middle Miocene, are recognized with no conspicuous breaks. Over the interval of the upper part of Zone SN7 into Zone SN8, the faunas have typically moderate to good preservation with fairly low abundances reflecting some dissolution. In the lower part of Zone SP7, dissolution effects become less and both preservation and abundances improve. As with all other sites, specimens of *Globigerinoides quadrilobatus* are absent, but *Globigerinoides trilobus* was recorded from only one sample (189-1172A-31X-CC). Warm-water species with subtropical affinities are absent, which is surprising because the East Australian Current should have bathed this area at that time. *Orbulina universa* and *Praeorbulina* are both rare.

Early Miocene

Zones SN2 and SN4 are not recognized at Site 1172. Zone SN4 is based on the presence of *G. trilobus* without *Praeorbulina curva,* and as noted above, *G. trilobus* has been identified only from the middle Miocene at this site, so its absence does not indicate a hiatus. Zone SP2 also has not been recognized here, but as the whole of the lower Miocene at this site is thin (38 m), it may be present within a core and so not sampled. As at most of the other sites *Globoquadrina dehiscens* is rare, but Zone SN1 is recognizable.

Late Oligocene/Early Miocene Hiatus

The entire upper Oligocene, which encompasses some 6.8 m.y., is missing at Site 1172. The early Miocene Zone SN1 (Sample 189-1172A-26X-CC) unconformably overlies sediments containing *Subbotina angiporoides,* indicating an early Oligocene age (Zone AP13) for Sample 189-1172A-27X-CC. This hiatus is correlative to that at Site 1170, but there Subzone SP14b overlies Zone AP13. By contrast, the Oligocene–Mio-

cene transition appears to be continuous at Site 1168, where the upper Oligocene (Zone SP14) is ~300 m thick.

Early Oligocene

The lower Oligocene succession at Site 1172 is the thinnest of all the sites, being recognized in a single sample (189-1172A-39X-2, 5–7 cm) from 356.15 mbsf. Here *S. angiporoides* is present without *Subbotina linaperta* or *Globigerinatheka index*. Sample 189-1172A-39X-CC contains both *S. angiporoides* and *S. linaperta,* indicating the late Eocene Zone AP11. Thus, the lower Oligocene must be confined to Core 189-1172A-39X.

Eocene/Oligocene Boundary

The Eocene/Oligocene boundary has not been recognized at Site 1172, but as noted above, it must be within Core 189-1172A-39X. Further details await the results of shore-based studies.

Late to Middle Eocene

Late and middle Eocene faunas are present at Site 1172. Although these are very well preserved, their abundance declines from the highest sample where they are rare to Sample 189-1172D-7R-CC, where only a trace is present. The presence of *G. index* in Sample 189-1172D-2R-CC indicates Zone AP12. Samples 189-1172A-39X-CC and 3R-CC have been referred to Zone AP12 on the appearance of *S. linaperta*. *Acarinina primitiva* is the only planktonic foraminifer species found in Sample 189-1172D-7R-CC, indicating a level within the interval of Zones AP7 to AP10. Below this, the samples are barren of planktonic foraminifers.

Late Cretaceous

Late Cretaceous assemblages are encountered in Sample 189-1172D-25R-CC. They are low-diversity and low abundance assemblages that are well preserved. The faunas are typical of the Austral Realm assemblages from the subantarctic region (Huber, 1991). The absence of key zonal taxa (such as *Abathomphalus mayaroensis*) precludes assignment to the global Late Cretaceous zonal scheme. However, the presence of *Rugoglobigerina rugosa* indicates a Campanian to Maastrichtian age. Sample 189-1172D-26R-CC contains the same assemblage but is less well preserved. Samples below this are generally composed of single species in low numbers. None were found in Sample 189-1172D-31R-CC.

Benthic Foraminifers, Ostracodes, and Bolboforma

Similar to Sites 1170 and 1171, benthic foraminiferal assemblages at Site 1172 change from neritic to upper bathyal faunas in the Paleocene and Eocene to lower bathyal to abyssal faunas in the Oligocene and Neogene. The transition, however, is not abrupt. Reconstruction of water depths in the Cretaceous to middle middle Eocene is limited by very restricted faunas, but these suggest a change from upper bathyal to neritic depths. This trend is reversed in the upper middle Eocene, when a barren interval is followed by upper bathyal faunas. The uppermost Oligocene is most likely still marked by middle to lower bathyal depths,

whereas the Neogene interval is dominated by lower bathyal to upper abyssal faunas.

The finely agglutinated foraminifer *Spiroplectammina* is the most persistent genus in the Cretaceous to middle Eocene interval. Van Morkhoven et al. (1986) describe *S. spectabilis* as having an upper depth range of middle to upper bathyal in the Paleocene and upper bathyal to outer neritic in the Eocene. The presence of planktonic foraminifers and calcareous benthic foraminifers belonging to the genera *Bulimina* and *Anomalinoides* in the uppermost Cretaceous (Samples 189-1172D-26R-CC to 25R-CC) suggest that, at least for this interval, more open marine conditions must have prevailed and that water depths of 200–400 m were likely. The Paleocene to upper middle Eocene samples are almost without exception virtually barren (189-1172D-23R-CC through 5R-CC) or entirely barren (189-1172A-4R-CC and 52X-CC through 44X-CC). Limited occurrences of *Spiroplectammina* spp. and other agglutinated taxa (e.g., *Glomospira* spp. and *Reophax* spp.) suggest a restricted environment. It has to be noted that sample spacing is wide and that more diverse and diagnostic faunas might be found within the cores. In this interval, two samples (189-1172A-56X-CC and 53X-CC) were found to contain *Elphidium,* a genus only found at neritic depths. In summary, this implies a shallowing of water depths from upper bathyal at the end of the Cretaceous to neritic in the middle middle Eocene.

The barren interval near the end of the middle Eocene is followed by a mostly calcareous benthic fauna with *Cibicidoides* spp., *Globocassidulina* spp., and costate *Uvigerina* spp. (Samples 189-1172D-3R-CC through 2R-CC and Samples 189-1172A-43X-CC through 39X-CC). The presence of rare planktonic foraminifers supports the conclusion that this interval was deposited in upper bathyal water depths. Most of the upper Eocene and Oligocene section is highly condensed, and more detailed sampling will provide information on the history of subsidence during this crucial interval. However, the presence of *Hanzawaia mantaensis* in Sample 189-1172A-37X-CC suggests that the latest Oligocene was still marked by bathyal water depths. Van Morkhoven et al. (1986) describe this species from upper to middle, and occasionally neritic, depths, but the co-occurrence with *Cibicidoides mundulus* and *Fontbotia wuellerstorfi* implies lower bathyal depths.

A notable difference between the Neogene benthic foraminiferal assemblages at this site and at previous sites is the early occurrence of *F. wuellerstorfi.* Both *C. mundulus* and *F. wuellerstorfi* are present from the uppermost Oligocene to lowermost upper Pliocene (Samples 189-1172A-37X-CC through 5H-CC), with the exception that *C. mundulus* is likely absent across the Miocene/Pliocene boundary (Samples 189-1172A-14H-CC through 8H-CC). Similar to Site 1171, *Melonis barleeanus* is present in the lower Neogene, but it plays a much lesser role than at Sites 1168 to 1170. *Sigmoilopsis schlumbergeri* is consistently present within the Pliocene and Pleistocene (Samples 189-1172A-11H-CC through 1H-CC). This is unlike Site 1170, where the few specimens were very badly preserved. Site 1172 shows high abundances of *Uvigerina hispida* and *Uvigerina peregrina* from the uppermost Pliocene to the topmost samples (189-1172A-7H-CC to 1H-CC). Similar abundance patterns were not recorded at the other sites, but in the same interval *Chilostomella oolina* is an abundant species. This species is also recorded in one sample near the top at Site 1168, in the topmost samples of Site 1169, and in the top sample at both Sites 1170 and 1171.

Most samples in the biogenic carbonate sequence (189-1172A-38X-CC to 1X-CC) contain a few ostracode valves. In the Cretaceous–Paleocene sequence, only one valve is recorded. *Bolboforma* spp. are absent.

Radiolarians

Radiolarians are common in the Miocene and Eocene but are absent or rare in the Holocene through Pliocene and Oligocene intervals. No radiolarians were recovered from the Paleocene to Cretaceous. Standard radiolarian zones cannot be applied for the radiolarian sequence of Site 1172 because of the near absence of age-diagnostic species (Table T7). Characteristics of the radiolarian assemblages are summarized below.

T7. Selected radiolarian datums, p. 120.

Quaternary–Neogene

The Holocene through Pliocene radiolarian faunas (Samples 189-1172A-1H-CC through 12H-CC, 189-1172B-1H-CC through 12H-CC, and 189-1172C-1H-CC through 12H-CC) are mainly composed of only two or three spumellarian species, including *Stylacontarium acquilonium,* and are identical to the same age interval of Site 1168. The Miocene radiolarians of Site 1172 are marked by an absence of antarctic species. The faunas are very similar to those of age-equivalent intervals of Sites 1170 and 1171. Differences are expressed in terms of the continuous occurrence of temperate artiscinid forms and the sporadic occurrence of tropical artiscinid species at Site 1172. Samples 189-1172A-13H-CC through 26X-CC, 189-1172B-13H-CC through 22H-CC, and 189-1172C-13H-CC through 22H-CC are assigned to the late Miocene. The Miocene/Pliocene boundary is placed approximately at the last consistent occurrence (LCO) of *Stichocorys delmontensis* at 5.18–6.90 Ma, and the boundary between the upper and middle Miocene by the last abundant occurrence (LAO) of *Cyrtocapsella japonica* at 11.6 Ma. The *C. japonica* LAO is a global event and is also recognized at Sites 1168, 1170, and 1171. At Site 1172 this bioevent is not recorded between the LO of *C. japonica* (at 9.9–10.6 Ma) in Sample 189-1172A-21H-CC and the LAO of *Cyrtocapsella tetrapera* (at 12.5 Ma) in Sample 189-1172A-27X-CC. A hiatus or condensed zone from 11.6 through 12.5 Ma may, therefore, be placed between Samples 189-1172A-26X-CC and 27X-CC.

Paleogene

Samples 189-1172A-32X-CC through 37X-CC are barren of radiolarians or yield only a few specimens. Oligocene faunas have been recorded from one sample only (189-1172A-38X-CC). The late and middle Eocene radiolarians consist mainly of antarctic species associated with a few tropical species. Age-diagnostic species for the antarctic, however, are sporadic. Eocene subantarctic or temperate faunas have never been reported, so those recovered from Site 1172 are unique in linking tropical and antarctic faunas and provide new insights into their evolution.

The LO of *Lychnocanoma amphitrite* (at 32.8 Ma), which is a presumed synchronous bioevent in the tropical regions, is recognized between Samples 189-1172A-39X-CC and 40X-CC, although the Eocene/Oligocene boundary (at 33.7 Ma) is placed within Core 189-1172A-39X based on other evidence. This discrepancy is probably caused by the diachronicity of the LO of *L. amphitrite* between the subantarctic and the tropics. Another bioevent, the FO of *Eucyrtidium antiquum,* is known to occur at 32.96 Ma in the antarctic. This bioevent is recorded in Sample

189-1172A-40X-CC. Hence, both bioevents are apparently older at Site 1172 than in antarctic and tropical regions. Samples 189-1172D-2R-CC and 3R-CC are late Eocene in age, based on the absence of *E. antiquum* and the co-occurrences of *Eucyrtidium cheni* and *Eucyrtidium spinosum*.

The middle/upper Eocene boundary is placed between Samples 189-1172A-46X-CC and 48X-CC, as the FO of *L. amphitrite* (at 36.4–37.3 Ma) is recognized below Sample 189-1172A-46X-CC and the LO of *Spongatractus pachystylus* (at 37.3–38.8 Ma) is above Sample 189-1172A-49X-CC. Samples 189-1172A-49X-CC through 56X-CC and 189-1172D-4R-CC through 14R-CC are correlated to the middle Eocene. The FO of *Dictyomitra amygdala* (approximately lower–middle Eocene in the North Pacific; Shilov, 1995) is recognized between Samples 189-1172D-14R-CC and 15R-CC. The middle Eocene Samples 189-1172A-51X-CC and 52X-CC commonly contain two lower Eocene reworked species: *Amphisphaera goruna* and *Spongatractus balbis*. In other middle Eocene samples of Site 1172A, no significant amounts of reworked radiolarians are found.

Samples 189-1172D-15R-CC through 22R-CC contain rare, poorly preserved unidentifiable radiolarians. Samples 189-1172D-23R-CC and 24R-CC are barren of radiolarians.

Diatoms, Silicoflagellates, and Sponge Spicules

Core-catcher material from Holes 1172A and 1172D was analyzed for diatoms, sponge spicules, and silicoflagellates. Samples were treated with 40% HCl to remove the carbonate component. Intervals rich in organic matter were treated with up to 40% H_2O_2 prior to acid treatment.

Diatoms are confined to discrete intervals at Site 1172. Abundance data for diatoms, sponge spicules, and silicoflagellates are presented in Table **T8.** Samples 189-1172A-1H-CC through 12H-CC are barren or contain "few" diatoms with moderate to good preservation. There is an abrupt downhole increase in biogenic silica between Samples 189-1172A-12H-CC (110.05 mbsf) and 13H-CC (120.76 mbsf). Samples 189-1172A-13H-CC through 18H-CC contain an abundant, well-preserved, and diverse open-ocean flora. Throughout this interval, there are fluctuations in the dominance of subantarctic and temperate/warm taxa, suggesting meridional shifts in the position of the Subtropical Convergence at this site during the late Miocene. Samples 189-1172A-19X-CC through 28X-CC contain less abundant, lower diversity floras, whereas Samples 189-1172A-29X-CC through 37X-CC are barren or contain only rare diatom occurrences.

T8. Relative abundance of selected diatom taxa, sponge spicules, and silicoflagellates, Holes 1172A and 1172D, p. 121.

There is a second abrupt downhole increase in biogenic silica between Samples 189-1171A-37X-CC (345.10 mbsf) and 38X-CC (353.76 mbsf). Samples 189-1172A-38X-CC and 39X-2, 3–5 cm, and 189-1171D-2R-CC (early Oligocene) contain a well-preserved open-ocean flora plus a noteworthy proportion (~30%) of well-preserved neritic diatoms. The Eocene section (Samples 189-1172A-39X-CC and below) contains an abundant and generally well-preserved neritic flora in association with open-ocean taxa in varying proportions (~2%–10% of the total assemblage, see below). Similar neritic assemblages to those observed at Sites 1170 and 1171 are present at Site 1172. Although *Pyxilla* is generally broken throughout the sequence, diatom preservation is mostly very good. In particular, whole frustules and chains (e.g., *Paralia sulcata* vars.) remain intact, suggesting a quiescent environment and/or sluggish circulation. Eocene and early Oligocene neritic diatoms are considered to be in situ because of such preservation and their high

abundance. Samples 189-1172A-39X-CC through 41X-CC (upper middle to upper Eocene) contain ~2% open-ocean diatoms, whereas Samples 189-1172A-42X-CC through 49X-CC (middle Eocene) contain a slightly greater proportion of open-ocean taxa, decreasing downhole from ~10% to 5% of the total assemblage. This information suggests that during the late Eocene, the depositional setting may have shallowed or become slightly more restricted again before opening to deeper waters. Samples 189-1172-50X-CC through 53X-CC comprise an entirely neritic diatom flora with no open-ocean influences. This is also supported by dinocyst evidence (see **"Palynology,"** p. 32). High abundances of high productivity indicators (e.g., *Chaetoceros* resting spores) found in Samples 189-1172A-42X-CC through 53X-CC suggest eutrophic conditions for the middle Eocene (see also **"Palynology,"** p. 32). Samples 189-1172A-54X-CC and below contain only rare occurrences or are barren of diatoms. However, pyritized diatoms are present in low abundance at the K/T boundary. Initial analyses suggest a shallow (neritic) marine setting by the common occurrence of *Stephanopyxis* spp.

The sporadic occurrence of planktonic diatoms in the Oligocene to Quaternary interval curtails any detailed diatom biostratigraphy for this interval. Three bioevents only are recognized in Hole 1172A (see Table **T9**). These are the LO of *Denticulopsis dimorpha* (10.7 Ma), placed between core-catcher samples of Cores 189-1172A-23H and 24H, and the FO of *Rocella vigilans* (30.24 Ma) and *Cavitatus (Synedra) jouseanus* (30.64 Ma), both placed between Samples 189-1172A-39X-2, 3–5 cm, (356.14 mbsf) and 39X-3, 61–63 cm (358.22 mbsf). Diatom biostratigraphic markers are not present in the Eocene to Cretaceous sediments (Holes 1172A and 1172D).

T9. Diatom bioevents, Holes 1172A and 1172D, p. 125.

Palynology

Onboard palynological analysis included a few selected core-catcher and core samples from Site 1172, comprising critical intervals from Hole 1172A to assist in dating and/or to assess the potential for future, more detailed studies. Similarly, a selection of core-catcher and core samples was analyzed from Hole 1172D (cf. Table **T10**).

T10. Distribution of organic walled dinocysts and sporomorph percentages, Holes 1171A and 1172D, p. 126.

Hole 1172A

Samples 189-1172A-1H-CC and 4H-CC yielded abundant (189-1172A-1H-CC) to a few (189-1172A-4H-CC) Pleistocene–Pliocene dinoflagellate cysts, dominated by *Protoperidinium* cysts like *Brigantedinium* spp. and *Multispinula quanta* (Sample 189-1172A-1H-CC) or oligotrophic warm-water representative of *Impagidinium* (Sample 189-1172A-4H-CC). This indicates good potential for future detailed studies of the younger Neogene.

Further analysis of samples from Hole 1172A was limited to the presumed Eocene–Oligocene transition (Cores 189-1172A-37X to 40X) and the lowermost Cores 189-1172A-50X to 56X to provide (additional) age control. Palynomorphs are consistently present in great abundance from Sample 189-1172D-39R-2, 18–20 cm, down. Above this horizon, samples are devoid of acid-resistant organic matter. The Eocene–Oligocene succession of Hole 1172A is similar to those recorded at Sites 1170 and 1171. Also in this case, the lower Oligocene is palynologically barren and thus provides further evidence of the inception of the influence of well-oxygenated (bottom) water masses.

Dinocysts are generally the most abundant category of palynomorphs in productive samples from Hole 1172A. In addition, pollen, spores, foraminifer organic linings, and acritarchs are present, albeit generally in low relative abundances. The few identified sporomorph taxa may be compared with established records from New Zealand and Australia and indicate cooling and increasing humidity from the middle middle Eocene to the late Eocene. Moreover, as stated for previous sites, again they are comparable to those reported by Mohr (1990) from approximately age-equivalent sediments from across Antarctica.

Palynomorphs are generally well preserved, and dinocyst concentrations are high, but assemblages are often of relatively low diversity for Eocene standards and may be totally dominated by a single taxon. In terms of quantitative distribution patterns, the middle to upper Eocene interval is quite comparable to the correlative successions of Holes 1170D and 1171D.

Dinocyst Stratigraphy

Middle to late Eocene (and earliest Oligocene) Hole 1172D assemblages are approximately identical to those reported from age-equivalent records from nearby sites and even to presumed coeval successions recovered from the other side of Antarctica, as well as those from Northern Hemisphere high-latitude sites (see **"Palynology,"** p. 30, in the "Site 1170" chapter and **"Palynology,"** p. 36, in the "Site 1171" chapter). Applied dinocyst events are listed in Table **T11.** For the middle to late Eocene, the dinocyst datums are reasonably consistent with results from the calcareous nannofossils from Hole 1172D.

T11. Selected dinocyst datums, Holes 1172A and 1172D, p. 128.

Eocene–Oligocene Transition

The palynological succession of the Eocene–Oligocene transition (viz., the interval from Sample 189-1172A-38X-CC to 40R-CC) is quite comparable with that of Hole 1170D. The youngest available productive sample of the Eocene–Oligocene interval in Hole 1172A (189-1172A-39X-6, 18–20 cm) contains a few operculae of *Enneadocysta partridgei,* as well as several specimens of *Stoveracysta kakanuiensis*. Representatives of an undescribed Protoperidinioid genus, provisionally assigned to *Brigantedinium*?, dominate the assemblage. The latter phenomenon indicates a highly productive setting, as motile stages of this group feed predominantly on diatoms. The typical composition of the sample, together with the very few (parts of) specimens of *E. partridgei,* would suggest an age close to 33.3 Ma or slightly younger (i.e., near the extinction of *E. partridgei;* see also **"Palynology,"** p. 30, in the "Site 1170" chapter and **"Palynology,"** p. 36, in the "Site 1171" chapter). Overlying samples are barren, and thus, no interpretations can be provided on possible missing section.

The underlying Sample 189-1172A-39X-5, 22–24 cm, yields an assemblage typical for the early late Eocene (~35.5 Ma) with warm-water influence exemplified by the presence of *Schematophora speciosa, Aireiana verrucosa,* and *Hemiplacophora semilunifera*. Representatives of the cosmopolitan *Deflandrea phosphoritica* group dominate this sample. The dinocyst assemblage of this sample suggests eutrophic neritic marine conditions (see **"Palynology,"** p. 30, in the "Site 1170" chapter and **"Palynology,"** p. 36, in the "Site 1171" chapter). The palynological results from samples from the so-called "glauconitic unit" suggest its relative stratigraphic completeness across the Eocene–Oligocene transition

interval. In a sample taken from just below the inception of the dominantly glauconitic aspect (189-1172D-39X-6, 64–66 cm), endemic antarctic species and/or bipolar high-latitude taxa are dominant (notably *Spinidinium macmurdoense*), suggesting relatively cool conditions. The assemblage, with consistent *Alterbidinium distinctum,* indicates an age of ~36.5 Ma for this sample. The underlying Sample 189-1172A-39X-CC is again dominated by cosmopolitan taxa.

The palynological succession of the Eocene–Oligocene transition is, thus, strongly suggestive of a stepwise series of changes from the late middle Eocene to the earliest Oligocene. Relatively warm conditions in inner neritic environments, with eutrophic conditions caused by river input, rather rapidly evolve into an apparently bathyal setting with high surface-water productivity and cool temperate to cold conditions in a stepwise pattern (see also **"Diatoms, Silicoflagellates, and Sponge Spicules,"** p. 31).

Middle Eocene

The top of the middle Eocene is recognized by the FAO of *A. distinctum* (between Samples 189-1172A-50X-CC and 40X-CC; ~37 Ma). The age of the base of Hole 1172A (Sample 189-1172A-56X-CC) is difficult to assess. The base appears to lie just below the onset of the *Enneadocysta*-acme sensu Raine et al. (1997) at ~43 Ma, whereas it is positioned below the FO of *Cerebrocysta bartonensis*. This sample is also marked by the presence of a conspicuous morphotype of the *Deflandrea phosphoritica* group, "*Deflandrea convexa*." Apparently, the environmental conditions associated with the development of this morphotype occurred during the middle middle Eocene of New Zealand (Wilson, 1988). The available information would indicate that the base of Hole 1172A has an age of ~44 Ma. Combined with results from Hole 1172D, a possible hiatus straddling the lower middle Eocene is indicated by the conjunction of the LO of *Wilsonidinium ornatum* and *Hystrichokolpoma spinosa* between Samples 189-1172D-12R-CC and 189-1172A-56X-CC.

Hole 1172D

Palynomorphs are consistently present in selected samples from Hole 1172D, albeit in low abundances in some cases. Dinocysts are common, and locally abundant, in productive samples from Hole 1172D and are assigned to the late Maastrichtian to early Eocene. In addition, pollen, spores, foraminifer organic linings, and acritarchs are also common in the upper samples and are persistent downhole. In the lowermost portion of Hole 1170D, in the upper Paleocene to Maastrichtian, sporomorphs are quantitatively significant and locally dominant (Table **T10**). These late Maastrichtian–Paleocene assemblages throughout are indicative of warm climates. Palynomorphs are generally well preserved and dinocyst assemblages are often of relatively low diversity for Eocene standards and may be totally dominated by a single taxon. In terms of quantitative distribution patterns, the lower Eocene to Paleocene interval is quite different from the correlative successions of Hole 1171D. Notably, representatives of *Glaphyrocysta* are particularly abundant in the Paleocene section of Hole 1172D, whereas they were only in the background in presumed coeval assemblages from Hole 1171D.

Dinocyst Stratigraphy

Relatively little is known from the Maastrichtian to the middle Eocene in terms of southern high-latitude dinocysts. Most meaningful information is derived from New Zealand and Antarctica (Seymour Island) sites (e.g., Wilson, 1988; Wrenn and Hart, 1988). However, these dinocyst successions still await chronostratigraphic calibration. Applied dinocyst events are listed in Table **T11.** For the Paleocene to lower Eocene interval, dinocysts are the sole source of biostratigraphic information (also see Fig. **F15**).

Assemblages indicative of a late early Eocene age characterize the topmost analyzed sample from Hole 1172D, Sample 189-1172D-12R-CC, with the presence of *Wilsonidinium ornatum* (the LO at ~50 Ma). Assemblages from the Samples 189-1172D-13R-CC and 19R-CC are not particularly age diagnostic. A late Paleocene age (~58 Ma) is indicated for Sample 189-1172D-20R-CC based on the occurrence of *Cerodinium boloniensis* and associated *Cerodinium* morphotypes. A possible hiatus is indicated by a rather abrupt compositional change of the palynological association between Samples 189-1172D-20R-CC and 21R-CC, where dominating sporomorphs give way to dominating dinocysts. In addition, the classic (and globally identified) oldest *Apectodinium* acme (or any *Apectodinium* acme) was not recorded in the available material, indicating that Paleocene–Eocene transitional strata may be missing.

Sample 189-1172D-23R-CC may be assigned to the Danian on the basis of the co-occurrence of the dinocysts *Alisocysta reticulata* and *Trithyrodinium evittii*. The K/T boundary is presumed to be within Core 189-1172D-24R since Sample 189-1172D-24R-CC does not yield Tertiary dinocysts but does contain a typical Southern Hemisphere latest Maastrichtian assemblage, dominated by *Manumiella druggii*. Subsequent palynological analyses of available samples from Section 189-1172D-24R-5 revealed the K/T boundary to be between interval 189-1172D-24R-5, 79–77 and 46–44 cm, on the basis of the FO of *T. evittii*. The lowermost sample analyzed, Sample 189-1172D-31R-CC, still contains abundant *M. druggii*. It also yields representatives of undescribed species of *Spiniferites* and *Impagidinium* and the age-diagnostic taxon *Acanthaulax wilsonii*. Combined with nannofossil information, microfossil assemblages indicate an age of younger than 67 Ma for this sample.

Paleoenvironment

The quantitative dinocyst distribution in the Eocene generally indicates somewhat restricted, eutrophic, neritic conditions throughout the succession. For further discussion, see **"Palynology,"** p. 30, in the "Site 1170" chapter because the assemblages in this site are comparable to those in Site 1172. The late Maastrichtian to middle Eocene dinocyst assemblages are dominated by relatively warm water, (inner) neritic, eutrophic forms. Terrestrial palynomorphs increase in relative abundance downhole, and throughout they indicate warm climates in this interval. This suggests shallow marine conditions for the older part of the succession at Site 1172, with marked influence of runoff. Only the lowermost Sample 189-1172D-31R-CC yields significant numbers of the typically offshore taxon *Impagidinium*. The upper Maastrichtian succession may hence represent a regressive sequence.

Age Model and Sedimentation Rates

The combined microfossil biostratigraphy at Site 1172 yielded 74 bioevents with age significance. Principal trends through this section are shown in Figure F15. Datums are from the combined microfossil bioevents from Holes 1172A, 1172B, 1172C, and 1172D and 59 magnetic polarity datums (see "Paleomagnetism," p. 36). The bioevents (Table T12) are comprised of 22 FO events, 48 LO events, three acme event, and one LAO event. All events are plotted according to their mean depth at Site 1172 and by their ages as defined in "Biostratigraphy," p. 9, in the "Explanatory Notes" chapter). The FO events may have been estimated to be too shallow and the LO events may have been estimated as being deep, based on the limited sampling interval. Stratigraphic positions of these datums will be refined with further study. See individual microfossil group discussion for more detailed bioevent data.

T12. Age-diagnostic biostratigraphic events, p. 129.

Sedimentation rates are moderate from the middle middle Miocene to the Pleistocene (2.0–3.2 cm/k.y.) with no obvious hiatuses. This section of the age-depth plot is well constrained by 25 bioevents and 35 paleomagnetism datums.

Sedimentation rates dropped abruptly to 0.43 cm/k.y. for the remainder of the Miocene to the upper lower Oligocene. No hiatuses are suggested by the 19 datums that define this interval. The lower Oligocene to upper Eocene interval shows an even slower sedimentation rate (0.16 cm/k.y.). A condensed section or intermingling of short periods of sedimentation and times of nondeposition are clearly indicated through the carbonate-glauconitic siltstone transition (see "Lithostratigraphy," p. 10). Nine bioevents spanning 6.5 Ma are within 8.98 m. Though no major fossil group provides age control through this boundary, all major groups contribute to interpreting this key interval.

Sedimentation rates increase to 1.8 cm/k.y. across the middle/upper Eocene boundary. Biostratigraphic control is poor through the remainder of Site 1172 because of the lack of consistent microfossil appearances, except for the dinocysts, which provide the only age control through the Paleogene. An ~3-m.y. hiatus is inferred across the lower/middle Eocene boundary at 550 mbsf. A correlative hiatus was also recognized at Site 1171 (see "Age Model and Sedimentation Rates," p. 39, in the "Site 1171" chapter). Sedimentation rates are 1.04 cm/k.y. until the lowermost Paleocene, where another hiatus is indicated by dinocyst datums. A change in lithology is also seen in this interval (see "Lithostratigraphy," p. 10). The length of this hiatus is unclear and requires shore-based analysis for clarification.

Sedimentation rates double in the upper Maastrichtian (2.6 cm/k.y.), which spans the bottom 80 m of core. Calcareous nannofossils, moderately preserved in this section, and dinocysts provide the only age control for this section. Detailed shore-based work will provide additional data.

PALEOMAGNETISM

Introduction

After alternating-field (AF) demagnetization to 20 mT, the natural remanent magnetization (NRM) of whole-round sections from Site 1172 was measured at 5-cm intervals using the pass-through cryogenic mag-

netometer. An exception was made for cores whose liners or end caps were deformed, because these could damage the magnetometer. These deformed cores were measured as archive-half cores. The nonmagnetic core barrel assembly was used for even-numbered cores in Holes 1172A and 1172C and for odd-numbered cores, starting with Core 3H in Hole 1172B. The comparison between results from cores collected with the nonmagnetic corer and with those from the standard corer is discussed in the "Appendix" chapter as are results of experiments investigating the effect of core splitting on magnetization and other coring-related magnetic experiments. The Tensor tool is usually employed to orient the APC cores beginning with the third core from each hole, but the poor determination of the declination of the cores at this site precluded such orientation.

Oriented discrete samples were routinely collected from Holes 1172A and 1172D. These were used to aid in the interpretation of the long-core record of magnetization by providing additional measurements of polarity and basic magnetic characterization. Most of them were demagnetized at 5, 10, 15, 20, 30, 40, and 50 mT to permit principal component analysis. For rock-magnetic characterization, measurements were made of the demagnetization behavior of anhysteretic remanent magnetization (ARM) given in 0.2 direct-current (DC) and 200-mT alternating-current (AC) fields and isothermal remanent magnetization (IRM) in a DC field of 1 T. Some discrete samples were progressively saturated up to 1.0 T to study the hardness of the IRM.

Results

Long-Core Measurements

The long-core measurements for the APC cores are presented in Figures F16 and F17, which show inclination and intensity for Holes 1172A, 1172B, and 1172C. The magnetostratigraphic interpretation was based primarily upon Hole 1172B. The intensity of magnetization was between 10^{-5} and 10^{-4} mA/m, so that measurements again approached the noise level of the instrument and the background noise from core liners. However, in Holes 1172B and 1172C a useful magnetic record emerged, which allowed us to establish a continuous magnetostratigraphy from the late Pleistocene down to the middle Miocene. Using sequences of reversals, we also determined that, for the most part, the depth shift between Holes 1172B and 1172C was <1 m.

In the first 110 m, we identified successively at 12.5 mbsf the onset of the Brunhes Chron; at 19.5 mbsf, the onset of the Olduvai Subchron; at 46.25 mbsf, the onset of the Gauss Chron; at 78.9 mbsf, the onset of Subchron C3n.4n; and at 107.4 mbsf, the onset of Subchron C3An.2n. In both records, the Jaramillo Subchron was missing, which indicates the presence of an early Pleistocene hiatus. The duration of the hiatus must be <1 m.y. because Subchron C3n.3n was identifiable in Hole 1172C.

Figure F17 shows the long-core measurements and interpreted magnetostratigraphy for the depth interval of 100–200 mbsf. Unfortunately, weather conditions were poor during the drilling of Hole 1172A, resulting in substantial disturbed sequences, but conditions in the two other holes permitted the magnetostratigraphy to be completed, although it may require some refinement from postcruise analysis. From 200 to 300 mbsf, the magnetostratigraphy is poorly defined with only the onset of Chron C5n and the termination of Subchron C5An.1n possibly discernible (Fig. F18).

F16. Long-core measurements from 0 to 100 mbsf, p. 71.

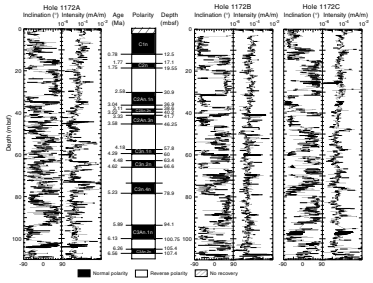

F17. Long-core measurements from 100 to 200 mbsf, p. 72.

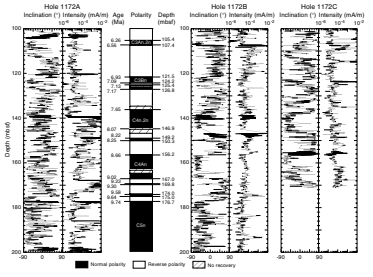

F18. Long-core measurements from 200 to 300 mbsf, Hole 1172A, p. 73.

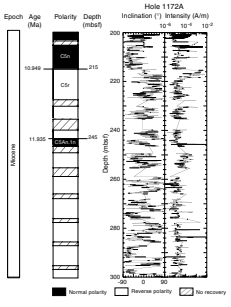

The interval from 300 to 400 mbsf is of particular interest because it contains the remarkable Eocene/Oligocene boundary section, which was recovered in Core 189-1172A-39X and subsequently in Core 189-1172D-2R. Curiously, the RCB core has a much better paleomagnetic record (Fig. F19). Chron 11n is identified between 356.2 and 358.5 mbsf, which is consistent with the diatom datum of 30.2–30.8 Ma for this interval and within the weaker constraints of 26–32 Ma from calcareous nannofossils and post–33.3 Ma from dinocysts. We were not able to trace the magnetostratigraphy through the boundary, but it seems likely that the predominantly reversed chrons between ~30 and 35 Ma are represented by the reversed interval between 350 and 360 mbsf. Immediately below this we interpret Subchron 16n.2n, which is consistent with a dinocyst datum of 35.5 Ma at a depth of 359 ± 1 mbsf. This then places Subchron 17n.1n below 367.7 mbsf, which is consistent with the dinocyst datum of 36.5 Ma at 361.8 ± 0.96 mbsf. Below this depth, the interval is dominated by the higher Eocene sedimentation rate.

In the Eocene section and below, we encountered severe difficulty in interpreting the magnetostratigraphy from the inclination data because there was a strong normal overprint. However, it was clear from the intensity record that intensity fluctuations correlated with the minor indications of magnetozones in the inclination. Therefore, we used the intensity of the z-component to interpret the magnetostratigraphy. Initially, we simply removed the bias that represented the normal overprint and recovered a more easily interpreted record of the magnetozones. Eventually, it should be possible to improve this method by first detrending the data and then applying a sum and difference calculation to separate the constant overprint from the opposed normal and reversed z-component magnetization. An example of the initial application of the technique is shown in Figure F20.

Discrete Samples

Samples were analyzed in a similar manner to that used at previous sites, and the results are presented in Figures F21 and F22. For the most part, the intensity of saturation IRM and ARM, and hence their ratio, were all consistent over much of the cored depth in the sampled holes. A notable exception is in an interval centered ~340 mbsf. There is a gradual increase in intensity associated with an increase in volcanic glass and the ratio of ARM:IRM increases, probably reflecting the fine grain size of the particles in the glass and devitrified products.

Age-Depth Relationship

The combination of data from the APC part of Hole 1172A and the APC Holes 1172B and 1172C provides an excellent magnetostratigraphy and, hence, age-depth determination for this interval to 200 mbsf. The results are given in Table T13 and Figures F16 and F17. The record was sufficiently good enough to demonstrate that Subchron 1r.1n (the Jaramillo) was missing, indicating a lower Pleistocene hiatus. Although the quality of the record deteriorates considerably in the older intervals, a relatively complete magnetostratigraphy was achieved and, for the most part, found to be consistent with the biostratigraphic data (Fig. F21). The magnetostratigraphy across the Eocene/Oligocene boundary constrained the timing of events, but unfortunately across the sus-

F19. Long-core measurements from 300 to 400 mbsf, Holes 1172A and 1172D, p. 74.

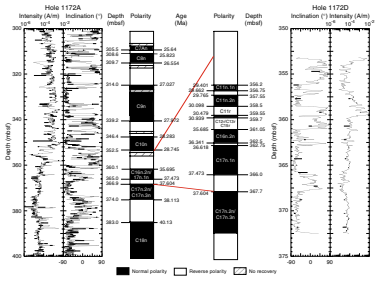

F20. Recovery of magnetostratigraphy from z-intensity, Hole 1172D, p. 75.

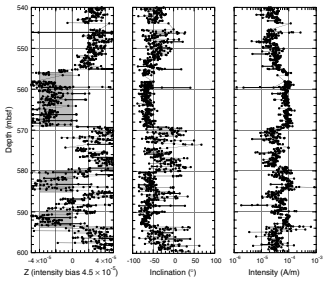

F21. Variation of magnetic properties, Holes 1172A and 1172D, p. 76.

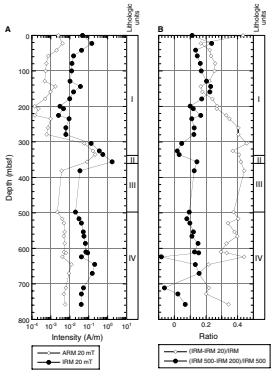

F22. Age-depth relationship from paleomagnetic data for the Cenozoic, Hole 1172B, p. 77.

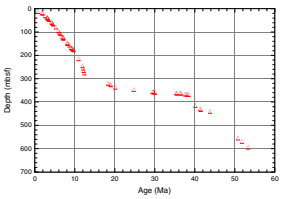

T13. Magnetostratigraphic results, p. 131.

pected K/T boundary, there was no strong indication of Chron 29R in the inclination record.

COMPOSITE DEPTHS

Multisensor track (MST) and spectral reflectance (L*) data collected from Holes 1172A, 1172B, 1172C, and 1172D were used to determine depth offsets in the composite section. Magnetic susceptibility, GRA bulk density, and spectral reflectance measurements were the primary parameters used for core-to-core correlation at Site 1172. GRA bulk density and magnetic susceptibility data were collected at 2-cm intervals on all APC cores recovered from Holes 1172A, 1172B, and 1172C, except for Cores 189-1172A-23H and 24H, on which measurements were made at 3-cm intervals. Magnetic susceptibility and GRA bulk density were collected at 3-cm intervals on the XCB cores from Hole 1172A and the RCB cores from Hole 1172D. Spectral reflectance data were collected at 2-cm intervals on cores from Holes 1172A, 1172B, 1172C, and 1172D (see **"Physical Properties,"** p. 46, and **"Lithostratigraphy,"** p. 10, for details about MST and spectral reflectance data).

The data used to construct the composite section and determine core overlaps in the APC interval are presented on a composite depth scale in Figure **F23.** The depth offsets that comprise the composite section for Holes 1172A, 1172B, 1172C, and 1172D are given in Table **T14.** The composite data show that the APC cores from Site 1172 provide a continuous overlap to 146 mcd (base of Core 189-1172C-14H). Spectral reflectance and magnetic susceptibility data were the primary basis for interhole correlation. The interhole correlations (Fig. **F23**) show that ~50 cm to 1 m of material is missing between cores in each hole.

Cores 189-1172A-5H through 10H are severely disturbed by flow-in. These cores were not used in the composite construction and are only adjusted by the cumulative composite correction resulting from alignment of cores upsection. Below Core 14H in Holes 1172A, 1172B, and 1172C, low signal variability in the spectral reflectance, magnetic susceptibility, and GRA bulk density data precluded definitive core-to-core correlation. On the mcd scale, these cores only have a cumulative composite correction added; no further alignment was attempted.

Rotary drilling operations at Hole 1172D were designed so that an overlap of several cores occurred with the XCB-cored interval of Hole 1172A at the Eocene/Oligocene boundary. Composite alignment of the color reflectance, magnetic susceptibility, and GRA bulk density data (Figure **F24**) show that Cores 189-1172A-38X through 40X contain the same sedimentary horizons as Cores 189-1172D-2R and 3R. Core 189-1172D-2R spans the gap between Cores 189-1172A-38X and 39X, and Core 189-1172D-3R spans the gap between Cores 189-1172A-39X and 40X.

Stretching and compression of sedimentary features in aligned cores indicate distortion of the cored sequence. Because significant distortion occurred within individual cores on depth scales of <9 m, it was not possible to align every feature in the MST and color reflectance records accurately by simply adding a constant to the mbsf core depth. Core-scale changes will require postcruise processing to align smaller sedimentary features. Only after allowing variable adjustments of peaks within each core can an accurate estimate of core gaps be made.

Following construction of the composite depth section for Site 1172, a continuous spliced record was assembled for the aligned cores over

F23. Smoothed spectral reflectance and magnetic susceptibility data for the upper 140 mcd, p. 78.

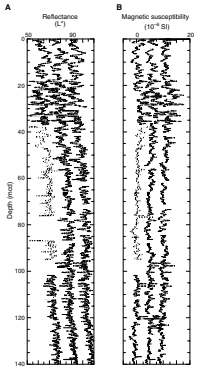

T14. Composite depth section, p. 132.

F24. Smoothed GRA bulk density, spectral reflectance, and magnetic susceptibility data for the Eocene/Oligocene boundary interval, p. 79.

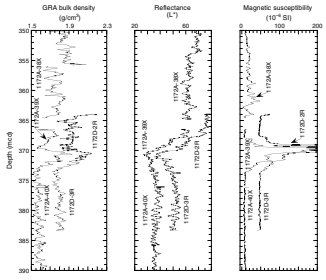

the upper 140 mcd (base of Core 189-1172C-14H). The Site 1172 splice (Table T15) can be used as a sampling guide to recover a single sedimentary sequence between 0 and 140 mcd. The splice primarily utilizes cores from Holes 1172A as the backbone, with cores from Holes 1172B and 1172C patched in across core gaps. Intervals having significant disturbance or distortion were avoided. For example, Cores 189-1172A-5H through 10H are severely affected by flow-in. Cores from Hole 1172B and 1172C had sufficient overlap over this 50-m interval and were used to maintain a continuous splice.

T15. Splice tie points, p. 133.

ORGANIC GEOCHEMISTRY

The shipboard organic geochemistry program at Site 1172 included studies of volatile hydrocarbons, total organic and inorganic carbon, total nitrogen, total sulfur, and hydrogen and oxygen indexes. Rock-Eval pyrolysis and gas chromatography were performed (see "Organic Geochemistry," p. 20, in the "Explanatory Notes" chapter) on headspace residues sampled at one per core. The CNS analysis and carbon coulometry (see "Organic Geochemistry," p. 20, in the "Explanatory Notes" chapter) were performed on samples taken from Sections 1, 3, and 5 in each core.

Sedimentary Geochemistry

Results

Carbonate ($CaCO_3$) content for the strata sampled at Site 1172 ranges from 0 to >95 wt% (Fig. F25; Table T16). In general, the carbonate distribution exhibits a two-tiered profile as observed at Sites 1170 and 1171. Here at Site 1172, sediments from ~355 to 766 mbsf commonly contain <5 wt% $CaCO_3$ (with broader zones of elevated values up to 20% from ~360 to 410 mbsf and >5 wt% from ~500 to 545 mbsf), whereas carbonate content increases to mostly >85% above 355 mbsf. Within the upper high–carbonate content strata, carbonate content values are consistently >90 wt% from ~175 to 335 mbsf. From the seafloor to ~175 mbsf, carbonate content displays an overall declining trend with values mostly >80 wt%. A decrease to ~30 wt% is observable at ~22 mbsf.

The TOC content for most intervals at Site 1172 is <1 wt% (Fig. F25; Tables T16, T17). Total nitrogen content ranges from 0 to 0.07 wt% (Fig. F25; Table T16); nitrogen content covaries with the TOC content (Fig. F25). From ~370 to 766 mbsf, total sulfur content ranges from 0.2 to ~1.4 wt% (Fig. F26; Table T16). Zones of elevated total sulfur content >1 wt% exist at ~455 mbsf and below ~635 mbsf. No appreciable sulfur content was noted above ~370 mbsf. We calculated the C/S ratios for strata below ~370 mbsf at the site assuming that all of the sulfur exists as pyrite. The C/S method of estimating paleosalinities is discussed in "Organic Geochemistry," p. 37, in the "Site 1168" chapter, "Organic Geochemistry," p. 40, in the "Site 1170" chapter, and "Organic Geochemistry," p. 44, in the "Site 1171" chapter; the implications of these ratios at Site 1172 are discussed below.

Organic matter type was assessed using Rock-Eval pyrolysis and CNS analyses; Rock-Eval pyrolysis data were obtained only for samples from ~400 mbsf to total depth. A discussion of this methodology is included in "Organic Geochemistry," p. 37, in the "Site 1168" chapter, and

F25. Plots of carbonate, total organic carbon, total nitrogen, C/N ratios, and hydrogen index values, p. 80.

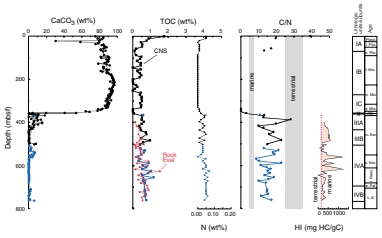

T16. Values for inorganic carbon, calcium carbonate, total carbon, total organic carbon, total nitrogen, total sulfur, hydrogen, and C/N and C/S ratios, p. 134.

T17. Results of Rock-Eval analyses, p. 138.

F26. Total sulfur content compared to C/S ratios, p. 81.

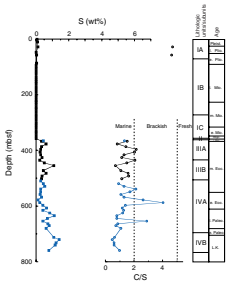

"Organic Geochemistry," p. 40, in the "Site 1170" chapter. The hydrogen index (HI) values from Rock-Eval pyrolysis range from 68 to 775 mg of hydrocarbon per gram of TOC at Site 1172 (Fig. F25; Table T17). The highest HI values are between ~560 and 620 mbsf. The oxygen index values vary between 31 to 778 mg of CO_2 per gram of TOC. The T_{max} values obtained from Rock-Eval pyrolysis range from 402° to 598°C, although the most reliable T_{max} values cluster between 400° and 420°C (Table T17). The T_{max} values provide an estimate of organic matter thermal maturity with the "oil window" generally considered to range between T_{max} values of 435° and 465°C (see "Organic Geochemistry," p. 37, in the "Site 1168" chapter, "Organic Geochemistry," p. 40, in the "Site 1170" chapter, and "Organic Geochemistry," p. 44, in the "Site 1171" chapter).

Discussion

The high carbonate content of Oligocene through Holocene sediments at Site 1172 primarily reflects dominance of calcareous nannofossils; foraminifers are secondary in importance (see "Biostratigraphy," p. 22). This observation is similar to those made for Sites 1168, 1169, 1170, and 1171. The overall upward increase in carbonate content through the sequence is again a direct consequence of a change from shallow marine to pelagic open-ocean conditions. Here, the transition from carbonate-poor to carbonate-rich sediments appears to be relatively abrupt, although sampling at higher resolution demonstrates that the change in carbonate content is gradational from ~343 to 356 mbsf. This observation suggests that more sampling across this boundary at Sites 1168, 1170, and 1171 may provide important information with regard to the nature of this carbonate-rich/carbonate-poor boundary. Specifically, the presence of a condensed section can be inferred if the carbonate content increases gradationally across the boundary at all sites, whereas the presence of an unconformity can be considered where an abrupt change in carbonate content is observed. In either case, a relatively rapid change in depositional environments is recorded at all Leg 189 sites penetrating the Eocene/Oligocene boundary interval.

In the upper ~360 mbsf at Site 1172, the CNS results indicate TOC content values commonly up to 0.5 wt%. However, Rock-Eval pyrolysis verification of the organic carbon content was not performed on these samples. At previous sites, Rock-Eval pyrolysis results indicate very little organic carbon content in the Oligocene and younger carbonate-rich sediment. For this reason, and because CNS results are determined by difference, the organic carbon content determined by CNS analysis is considered questionable. Therefore, two modes of carbonate and total organic carbon preservation are inferred to exist at Site 1172, as at the other Leg 189 sites.

The TOC content values determined by Rock-Eval pyrolysis and CNS analysis mostly provide similar TOC content profiles below ~360 mbsf at Site 1172, although the absolute values differ for each method. Replicate Rock-Eval pyrolysis analyses were not performed, so some of the highest and lowest TOC content and HI values may be erroneous. In general, average organic carbon content displays a downward increase from the uppermost middle Eocene to the Upper Cretaceous (~370 mbsf to total depth). Organic matter type (as determined by Rock-Eval pyrolysis) is best characterized as dominantly marine through this trend, but shows an overall downward decrease in marine character.

However, the CNS analyses suggest a mixed marine-oxidized marine or marine-terrestrial signature. The total sulfur content also increases downward, and C/S ratios become increasingly marine downward in the core. Various issues regarding the organic carbon content and type will be resolved through postcruise analyses.

The overall increase in the marine character of organic matter at Site 1172 is similar to observations from Site 1171. Interestingly, organic matter type is bundled into four intervals at Site 1172—Upper Cretaceous to upper Paleocene, upper Paleocene to lower Eocene, lower Eocene to middle Eocene, and middle Eocene to the Eocene/Oligocene boundary. The upper three intervals appear to correspond to intervals in organic matter type identified at Site 1171. This similarity between geochemical parameters is significant because it suggests regional-scale changes in Paleogene Pacific Ocean seafloor and water-column conditions along the STR.

Relatively elevated TOC contents exist in the middle Eocene and the upper Paleocene/lower Eocene; both of these intervals contain very labile marine organic matter. The upper Paleocene/lower Eocene interval contains C/S values indicative of fluctuations between marine and brackish depositional settings, whereas at Site 1171, Paleocene through lowermost Eocene sediments show alternations between horizons containing marine and terrestrial organic matter. These alternations in organic matter type at Site 1171, and in C/S ratios at Site 1172, suggest rapidly changing environmental conditions across the Paleocene/Eocene boundary on the STR.

The middle Eocene interval of slightly elevated organic carbon content is more marine in character than surrounding sediment and exists at the base of a decreasing trend in the Th/U values (see **"Downhole Measurements,"** p. 48). Here, the Th/U ratios attain values indicative of dysoxic to anoxic seafloor conditions. Elevated TOC content was also observed in the middle Eocene sediment at Sites 1170 and 1171. At Site 1170, the middle Eocene organic matter is best characterized as terrestrial, whereas at Site 1171 the organic matter is considered marine. These observations suggest that a middle Eocene episode of elevated organic carbon burial was widespread in shallow and deep marine environments around the STR.

The T_{max} values obtained from Rock-Eval pyrolysis of sub-Oligocene samples at Site 1172 display three distinct populations. First, a group of T_{max} values fall between ~400° and 425°C, which is interpreted to represent mostly immature organic matter relative to thermal maturation and hydrocarbon generation. A second population exists at nearly 600°C, which we attribute to the presence of bitumen in the sediments. The third population lies between the first two and likely represents a "smearing" of the output signal during Rock-Eval pyrolysis of samples containing a mix of immature organic matter and bitumen.

Volatile Hydrocarbons

Results

Concentrations of volatile hydrocarbon gases were measured from every core using the standard ODP headspace-sampling technique and gas chromatographic analysis. Profiles of methane content and various methane and heavier volatile hydrocarbon ratios are presented in Figure **F27** (also see Table **T18**). Methane only occurred in minor concentrations (~2–185 ppmv) at the base of the hole. Here, the ratio of meth-

F27. Headspace gas analysis, p. 82.

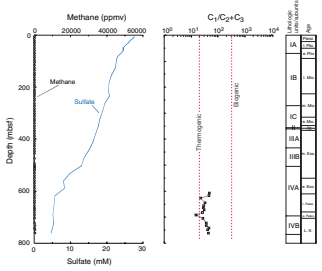

T18. Headspace gas composition, p. 139.

ane vs. ethane (C_1/C_2) shows maximum values at ~610 mbsf and from ~740 to 760 mbsf.

Discussion

The low headspace-gas content of sediment at Site 1172 is unique compared to the other sites drilled on Leg 189. At Sites 1168, 1169, 1170, and 1171, low gas content was mostly confined to the upper carbonate-rich lithologies and was considered to be a function of very little organic matter as a source of gas and pore-water profiles with sulfate reduction limiting methanogenesis. At Site 1172 the gas is likely best characterized as biogenic in origin. Here, low gas content continues downhole into the organic carbon–bearing siliciclastic sediments, where pore-water profiles show the presence of appreciable dissolved sulfate; hence, sulfate reduction processes are likely inhibiting methanogenesis (see "Inorganic Geochemistry," p. 43). This observation is unusual because the total organic carbon content (0.5%–1%) of these low-gas sediments appears to be sufficient to have already driven sulfate concentrations to zero.

INORGANIC GEOCHEMISTRY

Forty-five whole-round samples were collected from Hole 1172A (36) and Hole 1172D (9) for interstitial water (IW) analysis at the following frequency: three per core in the upper 60 m, one per core from 60 to 100 mbsf, and one every third core to total depth. Thirty-five of the IW samples were used for shipboard analyses; the balance of samples from the upper 60 mbsf of the hole were archived for shore-based analyses, with one exception. The whole-round sample collected from Core 189-1172D-19R showed visual signs of disturbance and evidence of contamination with drilling fluid (surface seawater) and was thus excluded from the data set. Results of IW analyses are reported in Table T19 and Figure F28.

T19. Interstitial water data, p. 140.

Chloride, Sodium, and Salinity

Chloride (Cl^-) and sodium (Na^+) concentrations increase immediately below the seafloor and remain above mean seawater concentrations in the upper 500 mbsf (Fig. F28A). The increase in Cl^- at the top of the hole centered at ~30 mbsf is a 1.6% increase from 557 mM in the uppermost sample to 566 mM. Maximum Cl^- values in the upper 500 mbsf reach 574 mM (2.8% increase) at 530 mbsf. Not surprisingly, with such minor variations in Na^+ and Cl^-, salinity changes very little in the upper 530 mbsf. Below ~500 mbsf, Cl^-, Na^+, and salinity are highly variable. Chloride values reach a minimum of 476 mM (14.8% decrease from the standard seawater value), yet concentrations higher than seawater are also observed in this interval (567 mM at 691 mbsf). The low-Cl^- fluids at Site 1172 are in what appears to be an overall background increase in the Cl^- profile with depth (Fig. F28A). Thus, the actual freshening may be greater by ~2%, or a total of 17%, because of the elevated pore-fluid Cl^- (574 mM) immediately above the horizon of freshening.

The presence of low-Cl^- waters on the East Tasman Plateau and at sites on the STR and western Tasmania margin demonstrates that the observed pore-water freshening is clearly a regional phenomenon. Although a determination of the origin of the low-Cl^- waters requires

F28. Concentration-depth profiles for interstitial water chemistry, p. 83.

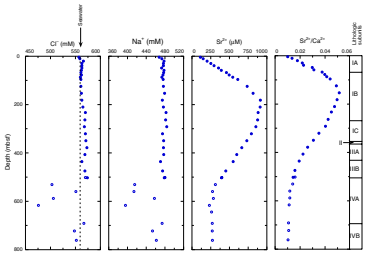

shore-based analyses, Site 1172 profiles provide new insight into the possible mechanisms. At Sites 1168, 1170, and 1171, pore-water freshening coincided with the onset of methanogenesis, suggesting a possible link either to methane hydrate dissociation or as an organic matter degradation by-product. However, at Site 1172, pore-water freshening is present without appreciable methane (see "Volatile Hydrocarbons," p. 42, in "Organic Geochemistry"). Together with the previous observations that the low-Cl^- fluids are found below the calculated base of the gas hydrate stability zone, the lack of methane suggests that neither gas hydrate dissociation nor a methanogenic by-product universally explains the regional extent of low-Cl^- pore fluids. The other possible hypotheses to describe low-Cl^- pore fluids include (1) dehydration reactions of hydrous minerals, such as clays and biogenic opal; (2) clay-membrane ion filtration; and perhaps (3) connate fluids. Postcruise isotopic analysis of the IW will be required to determine the origin of these regionally extensive low-Cl^- pore waters.

Strontium

Strontium (Sr^{2+}) increases with depth in the upper ~200 mbsf, reaching a maximum of 914 µM, at 181 mbsf (Fig. F28A). Below ~200 mbsf, Sr^{2+} decreases downhole reaching a fairly constant value of ~270 µM at ~500 mbsf. As observed at the previous sites, the increase in Sr^{2+} concentration and Sr^{2+}/Ca^{2+} ratios (Fig. F28A) coincides with Neogene–Oligocene pelagic carbonates, indicating that these sediments are actively undergoing recrystallization (e.g., Baker et al., 1982).

Sulfate, Ammonium, Alkalinity, and pH

Unlike the setting at the other deep penetration sites, complete sulfate reduction is not achieved by the base of the cored interval (Fig. F28B). Sulfate decreases gradually from seawater values to 4 mM, with a steeper gradient across the boundary between lithostratigraphic Units III and IV (~500 mbsf) (see "Lithostratigraphy," p. 10). Alkalinity increases downsection in the upper 300 mbsf, decreases across Unit II, then increases again reaching a maximum of 11 mM at ~500 mbsf. Below 500 mbsf, alkalinity declines to a minimum of 1.2 mM at 691 mbsf. The pH varies inversely with alkalinity (r = 0.86) reaching a minimum of 7.0 and a maximum of 8.6 at the alkalinity maximum and minimum, respectively. Ammonium steadily increases downcore to 500 mbsf (984 µM), below which the profile is highly variable, ranging from 542 to 1277 µM. The variability in NH_4^+ may correspond to fluctuations in pH and alkalinity (i.e., when alkalinity is high, NH_4^+ is high, and vice versa).

The major changes in SO_4^{2-}, NH_4^+, and alkalinity are largely a function of microbially mediated organic matter degradation. Despite appreciable TOC concentrations (0.5–1 wt%) and the presence of very labile marine organic matter (see "Sedimentary Geochemistry," p. 40, in "Organic Geochemistry"), sulfate reduction is not complete and methane does not increase significantly within the cored sequence.

Silica

Dissolved silica concentrations range from 45 to 1149 µM in the upper 500 mbsf, with several distinct negative shifts (~58 and 320 mbsf) in

a generally increasing profile (Fig. F28B). Below 500 mbsf, $H_4SiO_4^0$ drops precipitously, reaching a minimum of 45 µM.

The distinct shifts in pore-fluid $H_4SiO_4^0$ correspond to shifts in biogenic silica abundance in the sediments (see "Biostratigraphy," p. 22, and "Lithostratigraphy," p. 10). In particular, the negative $H_4SiO_4^0$ excursions are in intervals that are barren or contain only trace amounts of diatoms and radiolarians. The rapid decrease below 500 mbsf is likely a response to the general absence of biogenic silica. The transformation of opal-A to opal-CT may also play a role in the $H_4SiO_4^0$ decrease (e.g., Baker, 1986).

Magnesium, Potassium, Calcium, and Lithium

Similar to previous sites, Mg^{2+} and K^+ concentrations decrease from the topmost sample to minimum values of 19.5 and 3.3 mM, respectively, at the base of the cored interval (Fig. F28C). The magnitude of the decrease is similar for both elements—65% for Mg^{2+} and 68% for K^+. Lithium concentrations steadily increase to 584 µM at ~500 mbsf. Below ~500 mbsf, Li^+ concentrations decrease and are slightly variable, ranging from 415 to 263 µM. In the upper 500 mbsf, the Ca^{2+} and Li^+ profiles are very similar, with Ca^{2+} increasing to a maximum of ~28 mM (~2.7 times normal seawater). Below 500 mbsf, Ca^{2+} decreases and is more variable than Li^+ over the same interval, ranging from 20.8 to 25.2 mM.

Gradients in Ca^{2+}, Mg^{2+}, K^+, and Li^+ profiles are largely the result of silicate mineral alteration. As at the previous sites, the Mg^{2+} and K^+ decreases are correlated (r = 0.92). However, in contrast to the previous sites, Mg^{2+} and Ca^{2+} are strongly inversely correlated (r = 0.987) in the upper 500 mbsf (Fig. F29). This relationship has been noted at numerous DSDP and ODP sites and has been interpreted to be the result of alterations involving sedimentary volcanic material or basaltic material at depth (i.e., Layer II) (e.g., Lawrence et al., 1975; Lawrence and Gieskes, 1981). The strong positive correspondence between Ca^{2+} and Li^+ (r = 0.915) (Fig. F29) also suggests that the production of Li^+ is controlled by volcanic material alteration. Volcanic material from the nearby Cascade Seamount was observed in smear-slide sediment analysis, in particular in lithostratigraphic Units II and III (see "Lithostratigraphy," p. 10). Below Unit III, there is little indication of ash. The coincident maximums of Li^+ and Ca^{2+} at the base of Unit III (~500 mbsf), the decrease of each below, and the lack of correspondence between Mg^{2+} and Ca^{2+} below Unit III indicate that the reactions are being driven by sedimentary volcanic material rather than from basaltic rocks at depth.

F29. Crossplots of Mg^{2+} vs. Ca^{2+} for Hole 1172A and Ca^{2+} vs. Li^+, Holes 1172A and 1172D, p. 86.

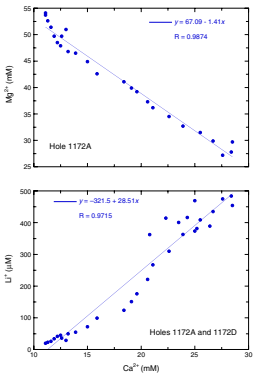

Summary

Many of the same reactions noted at Sites 1168–1171 control the IW chemical profiles at Site 1172. In contrast, however, Site 1172 shows clear evidence of volcanic material alteration, which results in large increases in Ca^{2+} and Li^+ and contributes to the consumption of Mg^{2+} and K^+. The presence of fresher pore waters on the East Tasman Plateau has demonstrated that the low-Cl^- fluids are a regional feature in the older sediments. In addition, the pore-water freshening observed at Site 1172 is not coincident with methanogenesis, which likely eliminates gas hydrates as a possible source of the low-Cl^- fluids at this site.

PHYSICAL PROPERTIES

The physical properties program at Site 1172 included MST and thermal conductivity measurements of whole-round cores and compressional wave (*P*-wave) velocity, moisture and density (MAD), and vane shear-strength measurements of split cores. Three in situ temperature measurements were made in Hole 1171B using the Adara tool.

Multisensor Track

Measurements of magnetic susceptibility, *P*-wave velocity, and GRA density were taken at 2- to 3-cm intervals in all core sections from Holes 1172A, 1172B, 1172C, and 1172D. *P*-wave velocities were recorded at 2-cm intervals for Hole 1172A to a depth of ~225 mbsf, but were not taken in the XCB-cored sections.

Downcore variability in magnetic susceptibility (Fig. **F30A**) correlates well with the lithostratigraphic units (see **"Lithostratigraphy,"** p. 10). The glauconite-bearing sediments of the condensed section in Unit II are marked by a prominent increase in magnetic susceptibility. Magnetic susceptibility (Fig. **F30A**) is negatively correlated with GRA and discrete bulk density (Fig. **F30B**) in both carbonate-rich and clay-rich intervals of the hole, except in lithostratigraphic Unit IV. The K/T boundary is also characterized by a rapid increase in magnetic susceptibility (see **"Lithostratigraphy,"** p. 10).

Density generally increases between the seafloor and ~750 mbsf, following a normal compaction and dewatering trend (Fig. **F30B**). This overall trend is interrupted by an interval of high-porosity diatomaceous silty claystones in lithostratigraphic Unit III. All major features of the GRA density records are also seen in the discrete density data and both data sets correlate well with other physical parameters and lithostratigraphic units. GRA density and discrete density, however, show some offset downcore. GRA values are higher than discrete density values in carbonate-rich sections (between approximately the seafloor and 220 mbsf), because the MST is optimized for mixed sediments. GRA densities are lower than densities from discrete measurements in Hole 1172D (355 mbsf to total depth). This difference in measured density is expected because the RCB cores in Hole 1172D did not fill the core liner.

Acoustic Velocity

Compressional ultrasonic velocities were obtained on the split-core sections at a sampling interval of one per section in cores from Holes 1172A and 1172D (PWS3; x-direction) (Figs. **F31, F32**). When possible, discrete velocity was measured in longitudinal directions (PWS1; z-direction down to ~80 mbsf for Hole 1172A), transverse directions were recorded in some cores only (PWS2; y-direction between the seafloor and 70 mbsf for Hole 1172A).

As expected for the sediment types encountered at this site, average velocities vary between 1550 m/s in the soft-surface sediments and up to 2100 m/s in the more consolidated sediments at 750 mbsf (PWS3; Table **T20;** Fig. **F32**). In general, the core velocity corresponds well to the downhole logging data, except within lithostratigraphic Subunit IC, where the combined influence of the XCB coring and the relatively

F30. Magnetic susceptibility, GRA density, and wet bulk density vs. depth, Holes 1172A and 1172D, p. 87.

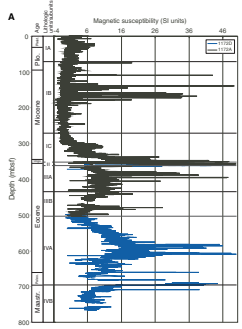

F31. *P*-wave velocities measured for discrete samples and in whole cores vs. depth, Hole 1172A, p. 89.

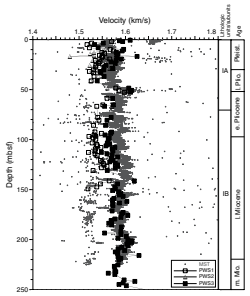

F32. *P*-wave velocities measured for discrete samples vs. depth, Hole 1172A, p. 90.

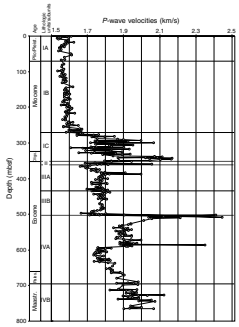

T20. *P*-wave velocities measured at discrete intervals, p. 141.

high lithologic variability degrade the core velocity measurements (see "Downhole Measurements," p. 48).

A comparison of the continuous velocity profile obtained with the MST and the discrete values for the interval between 0 and 230 mbsf is shown in Figure F32. Within lithostratigraphic Unit I, acoustic velocity increases with depth below the seafloor from values slightly higher than seawater velocity to average values of 1.6 km/s (PWS1) (Figs. F31, F32). Velocity is variable within Subunit IC with high values associated with relatively dark clay-bearing layers and low values associated with lighter carbonate-rich layers. At the ooze–chalk transition, which corresponds to the Subunit IB/IC boundary at ~273 mbsf, the acoustic velocity increases by 150 m/s. The limestone at the base of lithostratigraphic Subunit IC near the Eocene–Oligocene transition (see "Lithostratigraphy," p. 10) is characterized by an acoustic velocity of 2.2 km/s. The relatively porous diatom-silty claystone of lithostratigraphic Unit III (see "Lithostratigraphy," p. 10) has lower *P*-wave velocities.

Thermal Conductivity

Thermal conductivity was measured on Section 3 of each core from Hole 1172A to a depth at which induration prevented insertion of the needles (~220 mbsf; Fig. F33). Values generally increase with depth, corresponding to a general downhole decrease in porosity (Figs. F33, F34; Table T21).

In Situ Temperature Measurements

The Adara tool was deployed three times at Site 1172, and this deployment yielded three acceptable temperature records. The temperature at the seafloor (2.46°C) was determined using the mudline stops. Examination of the penetration temperature records indicates a normal deployment (see "Physical Properties," p. 45, in the "Site 1168" chapter).

Heat Flow

The geothermal gradient was determined using the four points of the temperature profile (Fig. F35). The solution of the least-squares regression gives a geothermal gradient of 46°C/km, which is lower than the 58°C/km at Site 1168 (see "Physical Properties," p. 45, in the "Site 1168" chapter) and the 52°C/km at Site 1170 (see "Physical Properties," p. 49, in the "Site 1170" chapter). Data for all Leg 189 sites show higher values than the Cape Sorell No. 1 exploration well (27°C/km) on the continental shelf 100 km to the northeast of Site 1168 on the western Tasmania margin (Willcox et al., 1989). The average of the thermal conductivities measured from 0 through 89 mbsf in Hole 1172B is 1.182 W/(m·K). Using the average conductivity and the geothermal gradient, a heat flow of 55 mW/m² is calculated. This heat-flow value is considerably higher than values reported from sedimentary basins and slopes near western Tasmania north of Site 1168 and Mesozoic continental margins in the mid-Atlantic (~40 mW/m²; see "Physical Properties," p. 45, in the "Site 1168" chapter).

F33. Thermal conductivity vs. depth measured on whole cores, p. 91.

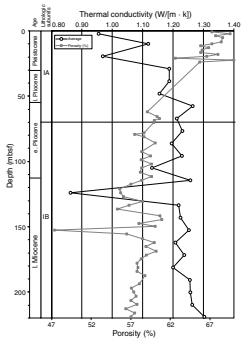

F34. Wet bulk density, water content, and porosity measured at discrete intervals vs. depth, p. 92.

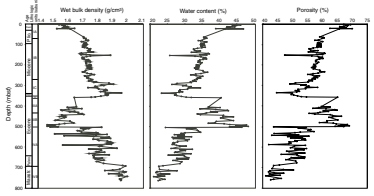

T21. Thermal conductivity measured on whole-core sections, Hole 1172A, p. 145.

F35. Temperature vs. depth, p. 93.

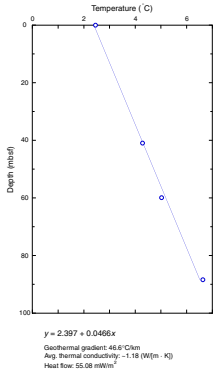

Undrained Shear Strength

One measurement of vane shear strength was taken per section for Hole 1172A to the depth at which induration prevented insertion of the vane (~270 mbsf; the ooze–chalk transition). The results are displayed in Figure F36 and Table T22. Undrained shear strength increases with depth in the upper 110 mbsf from ~10 to 50 kPa. The data show an overall increase with depth down to 170 mbsf, but with relatively high variability. Variations in shear strength between the seafloor and 130 mbsf correlate well overall with the GRA density (Fig. F36). As already observed in shear strength data from Sites 1168 and 1170, the uppermost Pliocene and upper and lower Miocene are characterized by higher mean values and greater variability and shear strength.

F36. Undrained shear strength from miniature vane-shear measurements and GRA density vs. depth, Hole 1172A, p. 94.

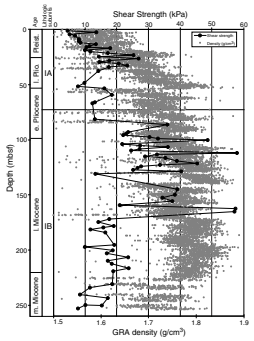

T22. Undrained shear strength from miniature vane-shear measurements, Hole 1172A, p. 146.

T23. Index properties measured at discrete intervals, Hole 1172A, p. 147.

Moisture and Density

Bulk density generally increases with depth below seafloor, except in Unit III, where a high-porosity diatomaceous claystone is found (Table T23). Water content and porosity mirror the magnetic susceptibility record with the exception of Subunits IVA and IVB. First-order variations in the MAD downcore profiles correspond to the lithostratigraphic units (see "Lithostratigraphy," p. 10) and with changes in sedimentation rates (see "Biostratigraphy," p. 22). The discrete wet bulk density data (Fig. F34) correlate very well with the GRA data and can be used to calibrate and correct GRA density (see "Multisensor Track," p. 46; Fig. F30B).

DOWNHOLE MEASUREMENTS

Logging Operations

Downhole logging was conducted in Hole 1172D after it had been drilled to a depth of 766.5 mbsf with a 9.785-in drill bit. The hole had been cored between 343.6–372.4 mbsf and 497.4–766.5 mbsf. The remaining sections of the hole had been drilled ahead with a center bit (see "Operations," p. 9). After a wiper trip (see "Downhole Measurements," p. 47, in the "Site 1168" chapter) and displacing the hole with sepiolite mud, the RCB bit was released and the pipe was set at 160 mbsf in preparation for logging. The pipe was raised by 10 m during the first tool-string run only (Fig. F37). Three tool-string runs were planned; the triple combo, the GHMT-sonic, and the FMS. However, operational difficulties resulted in measurements only being taken with the first two tool strings. Details of the logging operations are shown in Figure F37.

F37. Details of the logging operations, Hole 1172D, p. 95.

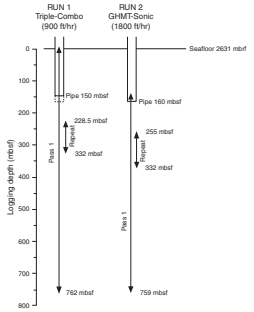

The heave was heavy throughout logging operations, routinely exceeding 6 m and reaching a maximum of 10 m. The wireline heave compensator (WHC) stroked out on six occasions during the main run of the triple combo, resulting in ~40% of the data being collected without heave compensation. After returning the triple combo to the rig floor, it was discovered that the caliper on the hostile-environment lithodensity sonde had sustained minor damage to the caliper wear plate.

While logging with the GHMT-sonic, the WHC stroked out continually, resulting in all of the data being collected without heave compensation. A decision was made to rig up and run in with the FMS and assess heave conditions again before opening the pads on this tool. The

WHC was turned on when the tool was going down through the open formation, but it stroked out almost immediately. When attempting to restart the WHC, a serious oil leak from the cylinder end assembly was discovered and, bearing in mind the time constraints and the weather conditions, a decision was made to cancel any further logging.

Results/Data Quality

The principal results are shown in Figures **F38, F39, F40.** The hole conditions were variable, with a particularly rugose borehole between ~165 and 200 mbsf, ~415 and 500 mbsf, and ~685 and 695 mbsf. The main cause of error in the data, however, will be the lack of heave compensation, which will make it very difficult to determine accurate depths for each set of measurements. This will be a particular problem for core/log integration and cyclostratigraphic analysis.

There is generally good agreement between log density and core density values, with both data sets showing stepwise variations downhole (Fig. **F41**). Core porosities are similar to the log values down to ~400 mbsf (Fig. **F42**), but below this there is a relatively large disparity in the two data sets until the very bottom of the hole (>700 mbsf). Core *P*-wave velocity measurements are considerably lower and more variable than the log values between 150 and 300 mbsf (Fig. **F43**), but below this depth there is relatively good agreement between the data.

Core/Log Correlation

Preliminary comparisons between the log data and the core lithology (see **"Lithostratigraphy,"** p. 10) show that major fluctuations in the logs are often correlative with distinct changes in the sediments. Some examples are given below:

1. All the log data show a marked change at ~350 mbsf (Figs. **F38, F40**), which is close to the downcore transition from carbonates to glauconitic claystone and siltstone. The increased glauconite concentrations at this level are particularly evident as a pronounced spike in K concentrations (Fig. **F40**).
2. At ~505 mbsf, density and porosity show distinct increases and decreases respectively, in association with an increase in velocities that suggests an increase in formation lithification at this depth. This horizon correlates with the bottom of the siliceous ooze bearing unit in the core.
3. Increased log U values between ~620 and 640 mbsf are present at approximately the same depth as the occurrence of a very dark gray organic-bearing (~10%) silty claystone.
4. A spike in magnetic susceptibility values at ~695–700 mbsf (see **"Physical Properties,"** p. 46), ~0.5 m below the K/T boundary (~696.5 mbsf; see **"Lithostratigraphy,"** p. 10, and **"Biostratigraphy,"** p. 22), is evident in both the core and log results.

F38. Caliper, gamma-ray, resistivity, and magnetic susceptibility values, Hole 1172D, p. 96.

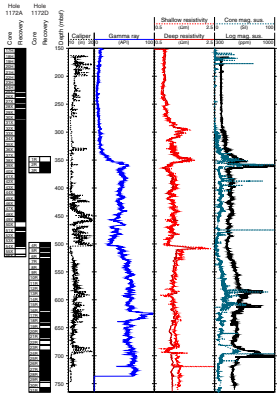

F39. Velocity, density, porosity, and photoelectric effect values, Hole 1172D, p. 97.

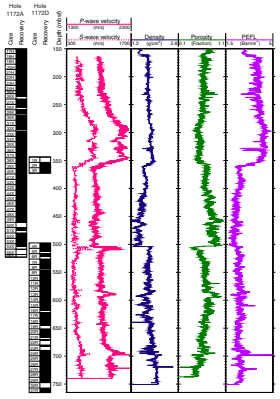

F40. Total gamma-ray and spectral gamma-ray values, Hole 1172D, p. 98.

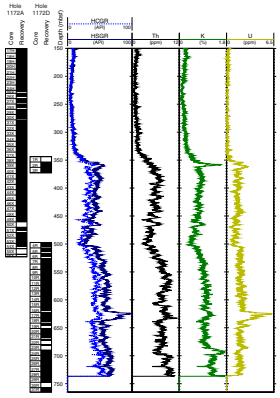

F41. Downhole log bulk density plotted with core bulk density, p. 99.

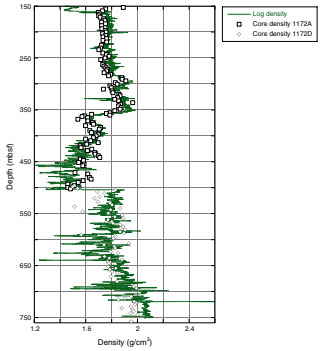

F42. Downhole neutron porosity plotted with core porosity, p. 100.

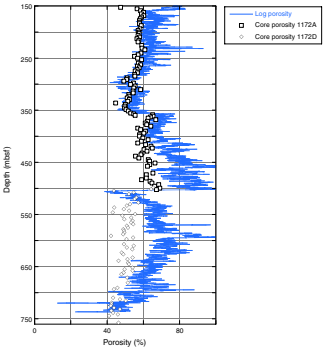

F43. Downhole *P*-wave velocities from the logs, p. 101.

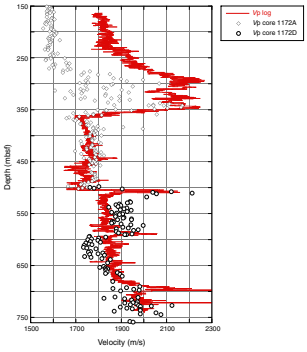

REFERENCES

Baker, P.A., 1986. Pore-water chemistry of carbonate-rich sediments, Lord Howe Rise, Southwest Pacific Ocean. *In* Kennett, J.P., von der Borch, C.C., et al., *Init. Repts. DSDP,* 90 (Pt. 2): Washington (U.S. Govt. Printing Office), 1249–1256.

Baker, P.A., Gieskes, J.M., and Elderfield, H., 1982. Diagenesis of carbonates in deep-sea sediments: evidence from Sr^{2+}/Ca^{2+} ratios and interstitial dissolved Sr^{2+} data. *J. Sediment. Petrol.,* 52:71–82.

Chamley, H., 1989. *Clay Sedimentology:* Berlin (Springer-Verlag).

Chamley, H., Robert, C., and Müller, D.W., 1993. The clay-mineralogical record of the last 10 million years off northeastern Australia. *In* McKenzie, J.A., Davies, P.J., Palmer-Julson, A., et al., *Proc. ODP, Sci. Results,* 133: College Station, TX (Ocean Drilling Program), 461–470.

Ehrmann, W.U., 1991. Implications of sediment composition on the southern Kerguelen Plateau for paleoclimate and depositional environment. *In* Barron, J., Larsen, B., et al., *Proc. ODP, Sci. Results,* 119: College Station, TX (Ocean Drilling Program), 185–210.

Exon, N.F., Berry, R.F., Crawford, A.J., and Hill, P.J., 1997. Geological evolution of the East Tasman Plateau, a continental fragment southeast of Tasmania. *Aust. J. Earth Sci.,* 44:597–608.

Hambrey, M.J., Ehrmann, W.U., and Larsen, B., 1991. Cenozoic glacial record of the Prydz Bay continental shelf, East Antarctica. *In* Barron, J., Larsen, B., et al., *Proc. ODP, Sci. Results,* 119: College Station, TX (Ocean Drilling Program), 77–132.

Huber, B.T., 1991. Paleogene and early Neogene planktonic foraminifer biostratigraphy of Sites 738 and 744, Kerguelen Plateau (southern Indian Ocean). *In* Barron, J., Larsen, B., et al., *Proc. ODP, Sci. Results,* 119: College Station, TX (Ocean Drilling Program), 427–449.

Kennett, J.P., 1977. Cenozoic evolution of Antarctic glaciation, the circum-Antarctic Ocean, and their impact on global paleoceanography. *J. Geophys. Res.,* 82:3843–3860.

Kennett, J.P., Houtz, R.E., et al., 1975. *Init. Repts. DSDP,* 29: Washington (U.S. Govt. Printing Office).

Lawrence, J.R., and Gieskes, J.M., 1981. Constraints on water transport and alteration in the oceanic crust from the isotopic composition of pore water. *J. Geophys. Res.,* 86:7924–7934.

Lawrence, J.R., Gieskes, J.M., and Broecker, W.S., 1975. Oxygen isotope and cation composition of DSDP pore waters and the alteration of Layer II basalts. *Earth Planet. Sci. Lett.,* 27:1–10.

Martini, E., 1971. Standard Tertiary and Quaternary calcareous nannoplankton zonation. *In* Farinacci, A. (Ed.), *Proc. 2nd Int. Conf. Planktonic Microfossils Roma:* Rome (Ed. Tecnosci.), 2:739–785.

Mohr, B.A.R., 1990. Eocene and Oligocene sporomorphs and dinoflagellate cysts from Leg 113 drill sites, Weddell Sea, Antarctica. *In* Barker, P.F., Kennett, J.P., et al., *Proc. ODP, Sci. Results,* 113: College Station, TX (Ocean Drilling Program), 595–612.

Murphy, M.G., and Kennett, J.P., 1986. Development of latitudinal thermal gradients during the Oligocene: oxygen-isotope evidence from the southwest Pacific. *In* Kennett, J.P., von der Borch, C.C., et al., *Init. Repts. DSDP,* 90: Washington (U.S. Govt. Printing Office), 1347–1360.

Quilty, P.G., 1997. Eocene and younger biostratigraphy and lithofacies of the Cascade Seamount, East Tasman Plateau, southwest Pacific Ocean. *Aust. J. Earth Sci.,* 44:655–665.

Raine, J.I., Askin, R.A., Crouch, E.M., Hannah, M.J., Levy, R.H., and Wrenn, J.H., 1997. Palynomorphs. *In* Hannah, M.J., and Raine, J.I. (Eds), *Southern Ocean Late Cretaceous/Early Cenozoic Biostratigraphic Datums.* Inst. Geol. Nucl. Sci., Sci. Rep., 97:25–33.

Robert, C., and Chamley, H., 1987. Cenozoic evolution of continental humidity and paleoenvironment, deduced from the kaolinite content of oceanic sediments. *Palaeogeogr., Palaeoecol., Palaeoclimatol.,* 60:171–187.

Robert, C., and Kennett, J.P., 1992. Paleocene and Eocene kaolinite distribution in the South Atlantic and Southern Ocean: Antarctic climatic and paleoceanographic implications. *Mar. Geol.,*103:99–110.

Robert, C., and Maillot, H., 1983. Paleoenvironmental significance of clay mineralogical and geochemical data, Southwest Atlantic, DSDP Legs 36 and 71. *In* Ludwig, W.J., Krasheninnikov, V.A., et al., *Init. Repts. DSDP,* 71: Washington (U.S. Govt. Printing Office), 317–343.

————, 1990. Paleoenvironments in the Weddell Sea area and Antarctic climates, as deduced from clay mineral associations and geochemical data, ODP Leg 113. *In* Barker, P.F., Kennett, J.P., et al., *Proc. ODP, Sci. Results,* 113: College Station, TX (Ocean Drilling Program), 51–70.

Royer, J.-Y., and Rollet, N., 1997. Plate-tectonic setting of the Tasmanian region. *In* Exon, N.F., and Crawford, A.J. (Eds.), *West Tasmanian Margin and Offshore Plateaus: Geology, Tectonic and Climatic History, and Resource Potential*. Aust. J. Earth Sci., 44:543–560.

Shilov, V.V., 1995. Eocene–Oligocene radiolarians from Leg 145, North Pacific. *In* Rea, D.K., Basov, I.A., Scholl, D.W., and Allan, J.F. (Eds.), *Proc. ODP, Sci. Results,* 145: College Station, TX (Ocean Drilling Program), 117–132.

Stein, R., and Robert, C., 1986. Siliciclastic sediments at Sites 588, 590 and 591: Neogene and Paleogene evolution in the Southwest Pacific and Australian climate. *In* Kennett, J.P., von der Borch, C.C., et al., *Init. Repts. DSDP,* 90 (Pt. 2): Washington (U.S. Govt. Printing Office), 1437–1455.

van Morkhoven, F.P.C.M., Berggren, W.A., and Edwards, A.S., 1986. Cenozoic cosmopolitan deep-water benthic foraminifera. *Bull. Cent. Rech. Explor.—Prod. Elf-Aquitaine,* 11.

Weaver, C.E., 1989. *Clays, Muds, and Shales:* New York (Elsevier).

Willcox, J.B., Baillie, P., Exon, N.F., Lee, C.-S., and Thomas, B., 1989. The geology of western Tasmania and its continental margin—with particular reference to petroleum potential. *Bureau Mineral Resources (Australia),* Record 1989/13:27.

Williams, G.L., Brinkhuis, H., et al., 1998. Cenozoic dinocyst events. *In* De Gracianski, et al. (Eds.), *Sequence Stratigraphy of European Basins*. Spec. Publ.—Soc. Econ. Paleontol. Mineral., 60.

Wilson, G.J., 1988. Paleocene and Eocene dinoflagellate cysts from Waipawa, Hawkes Bay, New Zealand. *N.Z. Geol. Surv. Paleontol. Bull.,* 57.

Wrenn, J.H., and Hart, G.F., 1988. Paleogene dinoflagellate cyst biostratigraphy of Seymour Island, Antarctica. *Mem.—Geol. Soc. Am.,* 169:321–447.

Figure F1. Postdrilling interpretation for local seismic profile AGSO 125-4, across Site 1172, showing broad ages and lithostratigraphic units. Drilling directly dated the three upper unconformities (A–C) and helped control the possible ages of the lower unconformities (D and E). Note the thick middle Eocene and Miocene to Holocene, and the virtually absent Oligocene and late Eocene sections at this site. TD = total depth.

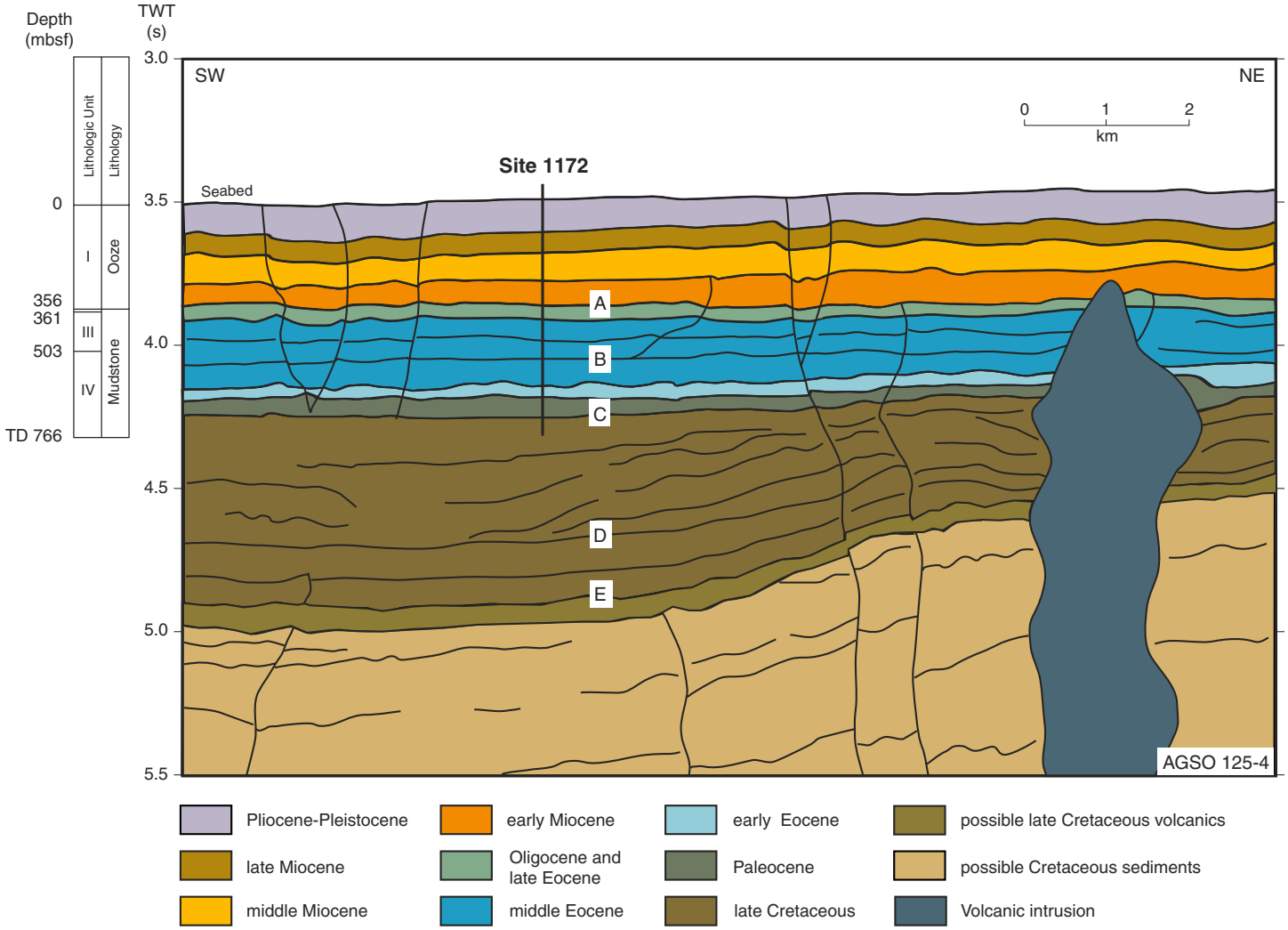

Figure F2. Conceptual regional cross section through time across Site 1172, west and southwest from the Tasman Sea oceanic crust, across the East Tasman Plateau, and onto the abyssal plain between it and the South Tasman Rise, based loosely on seismic profiles AGSO 125-03 and -04 and 202-01 and -13 and limited other geological information (Exon et al., 1997) and information from Site 1172 drilling. Note the formation of oceanic crust east and west of the plateau in the latest Cretaceous as the plateau separated from the South Tasman Rise and the Lord Howe Rise, moving east-northeast relative to Australia/Tasmania/STR. Note also the phase of volcanism in the middle to late Eocene that formed the Cascade Seamount and other volcanic features. TWT = two-way traveltime.

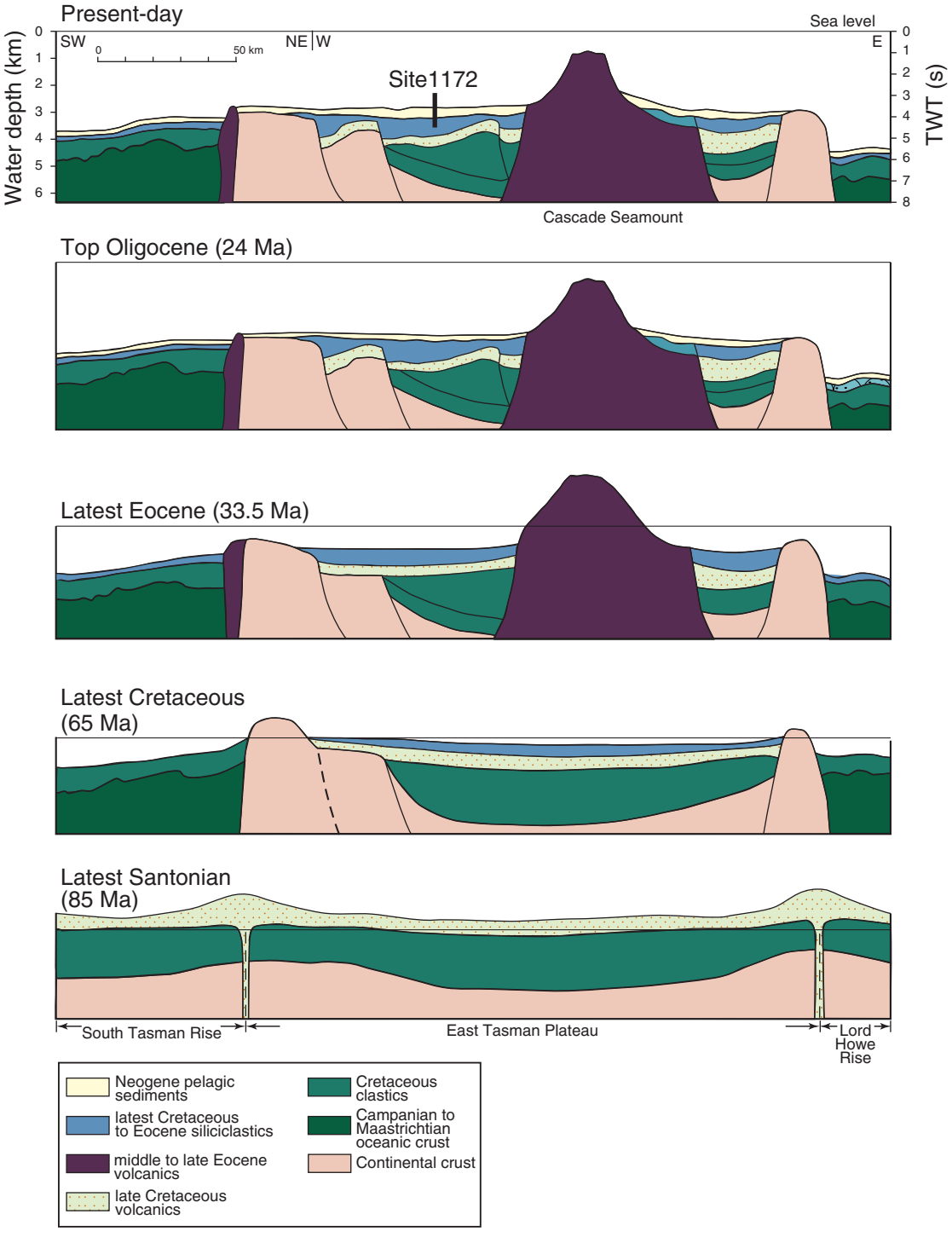

Figure F3. A portion of multichannel seismic profile AGSO 202-13 through Site 1172 showing the interval penetrated during coring. SP = shotpoint.

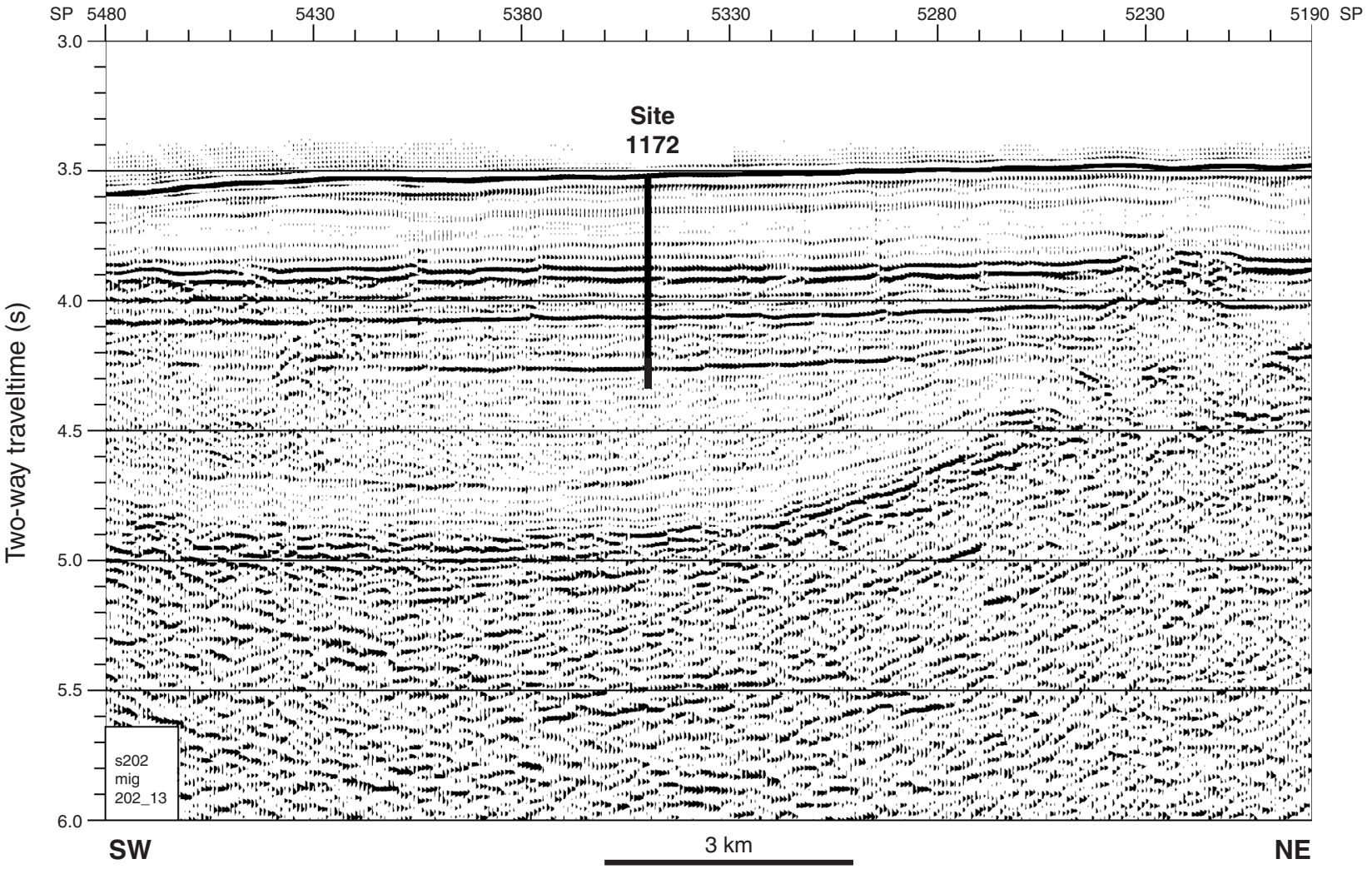

Figure F4. Summary of Holes 1172A to 1172D with core recovery, lithostratigraphic units, biozonation, physical properties data, and carbonate content (see "Physical Properties," p. 46, and "Organic Geochemistry," p. 40). Nannos. = nannofossils. Plank. forams. = planktonic foraminifers. TD = total depth.

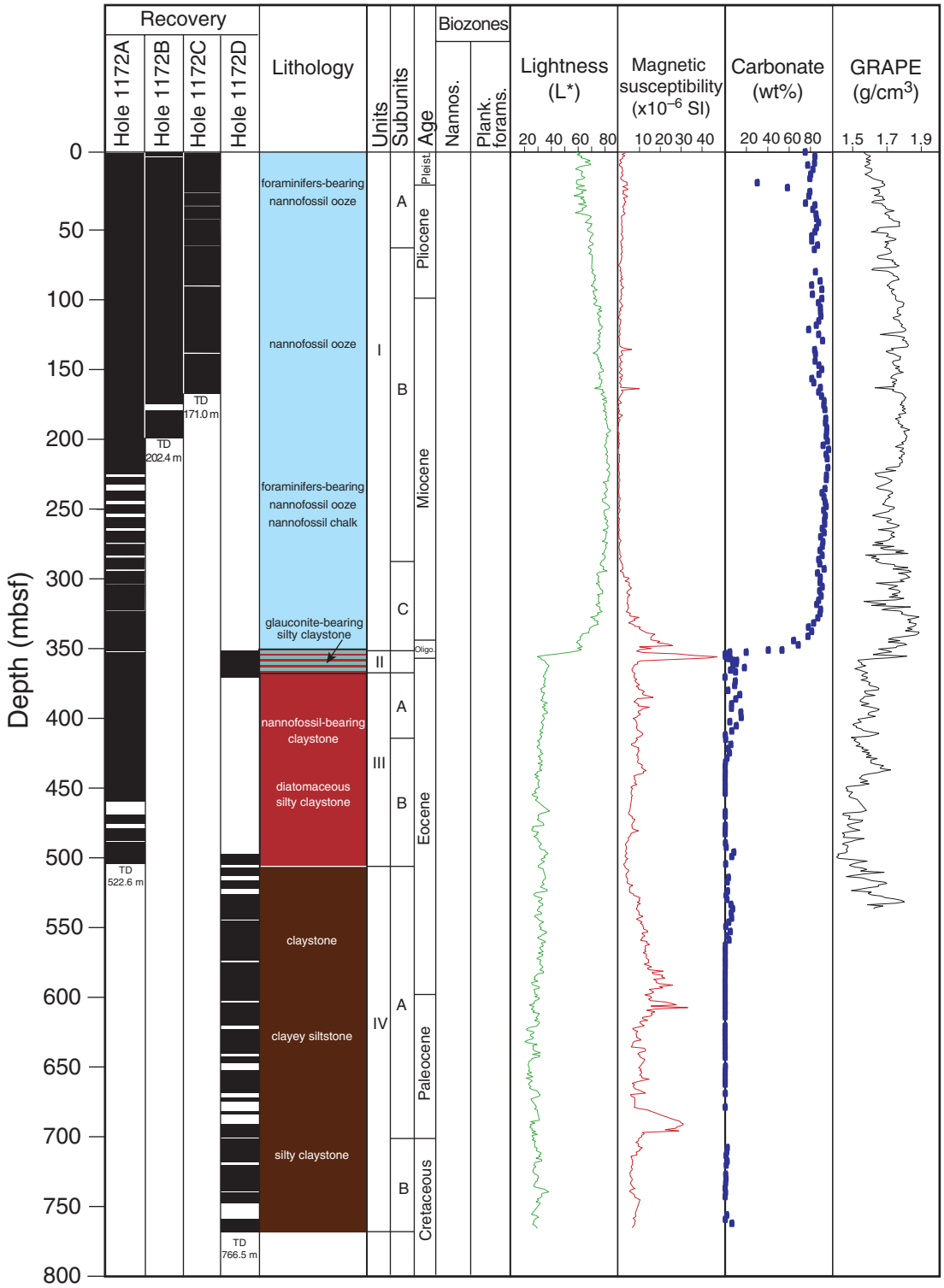

Figure F5. Detailed summary of the 0–766.5 mbsf interval of Holes 1172A to 1172D with core recovery, principal lithology, and relative core disturbance (range 0 to 4 from nil to major disturbance), lithologic units, biozonation, physical properties data and carbonate content. **A.** Summary for the 0–200 mbsf interval. Nannos. = nannofossils. Plank. forams. = planktonic foraminifers. TD = total depth. (Continued on next three pages.)

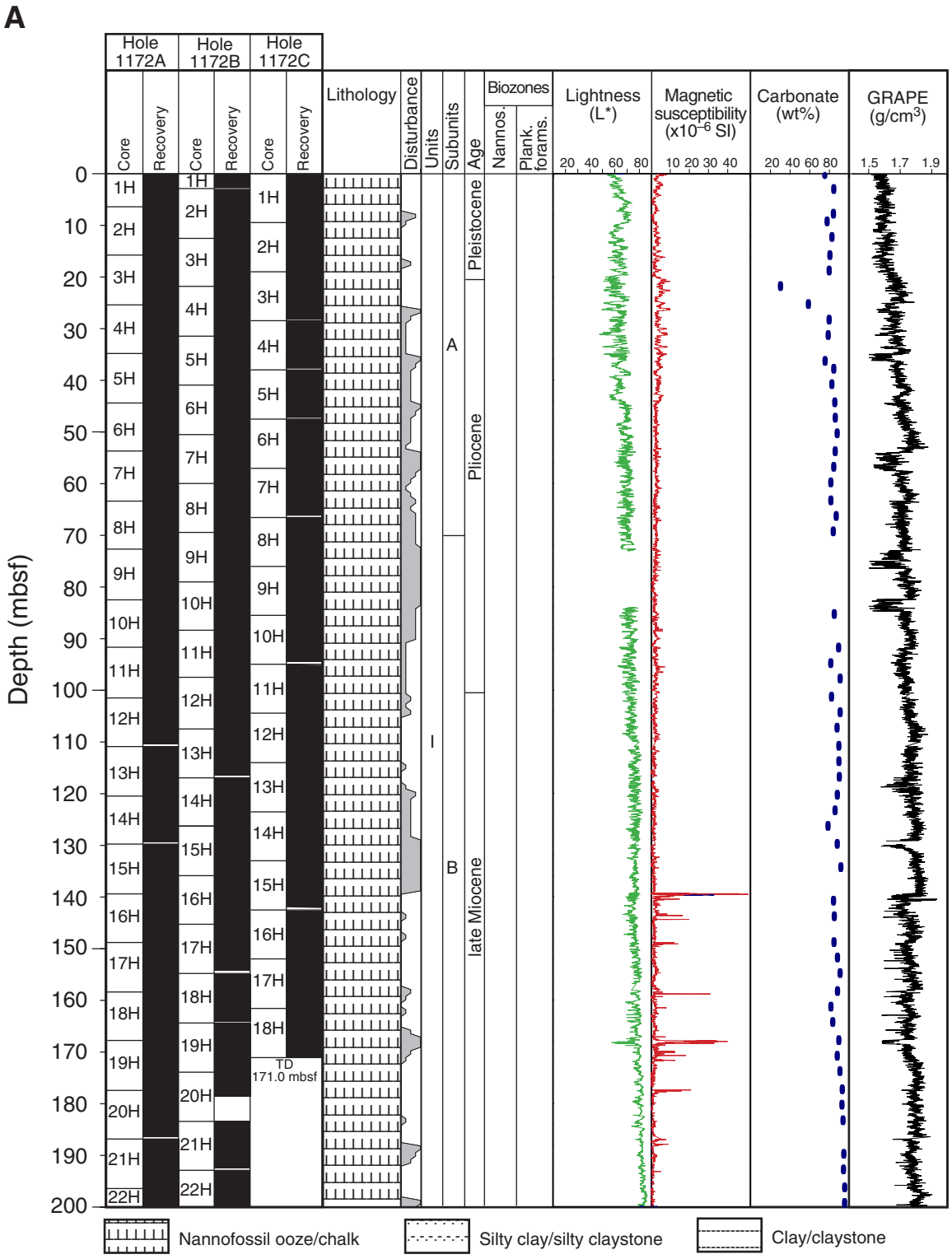

Figure F5 (continued). B. Summary for the 200–400 mbsf interval.

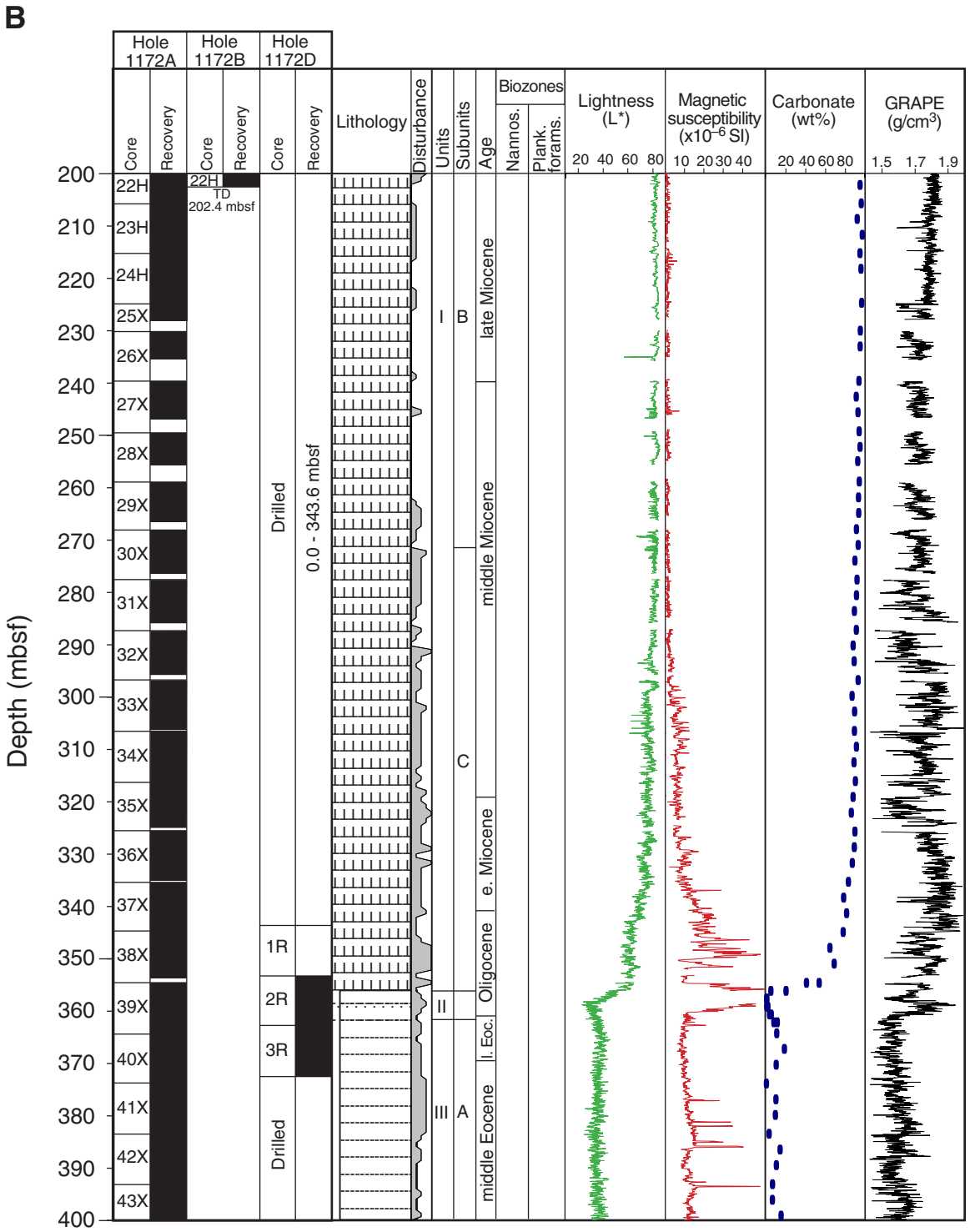

Figure F5 (continued). C. Summary for the 400–600 mbsf interval.

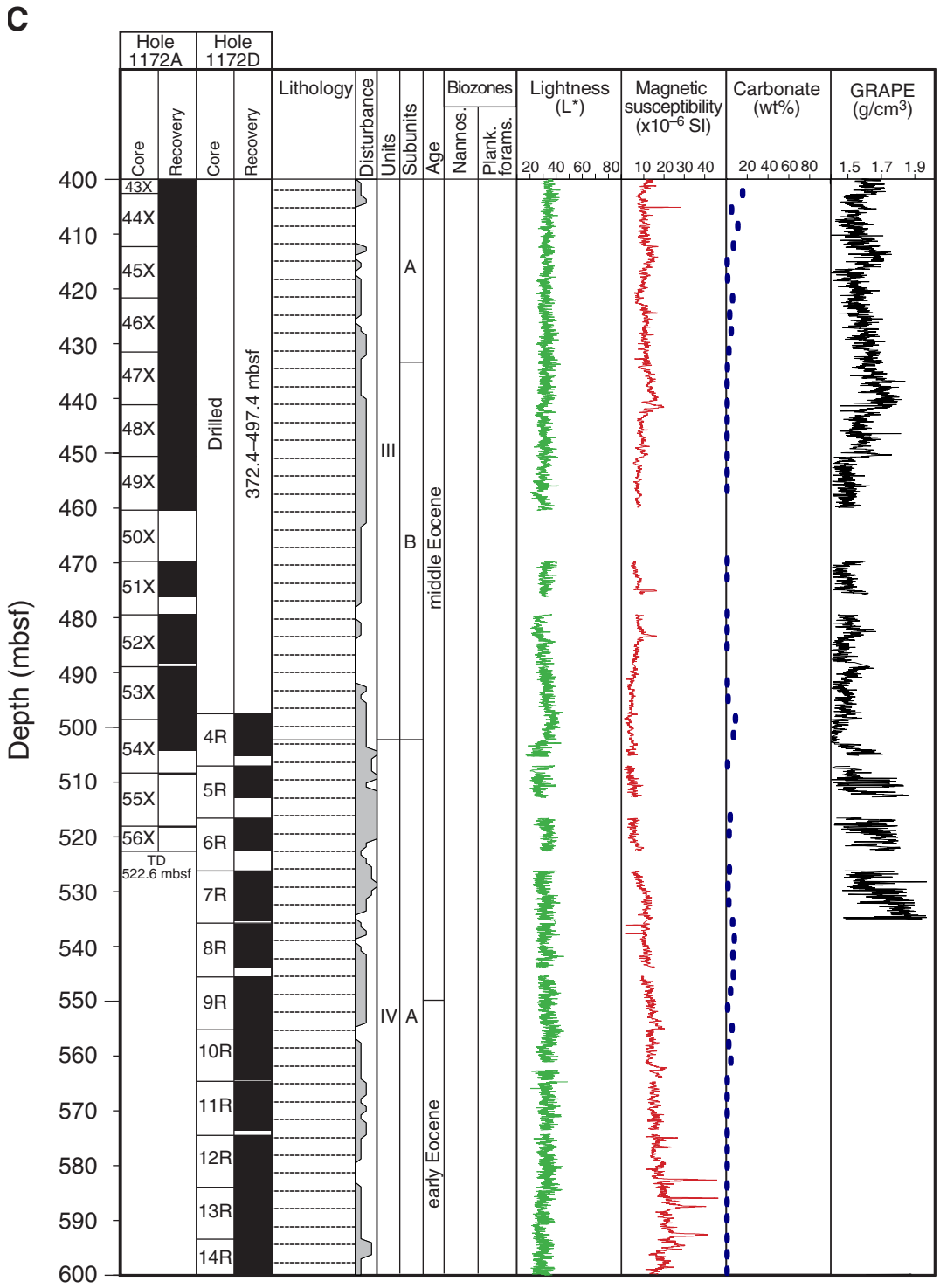

Figure F5 (continued). D. Summary for the 600–766.5 mbsf interval.

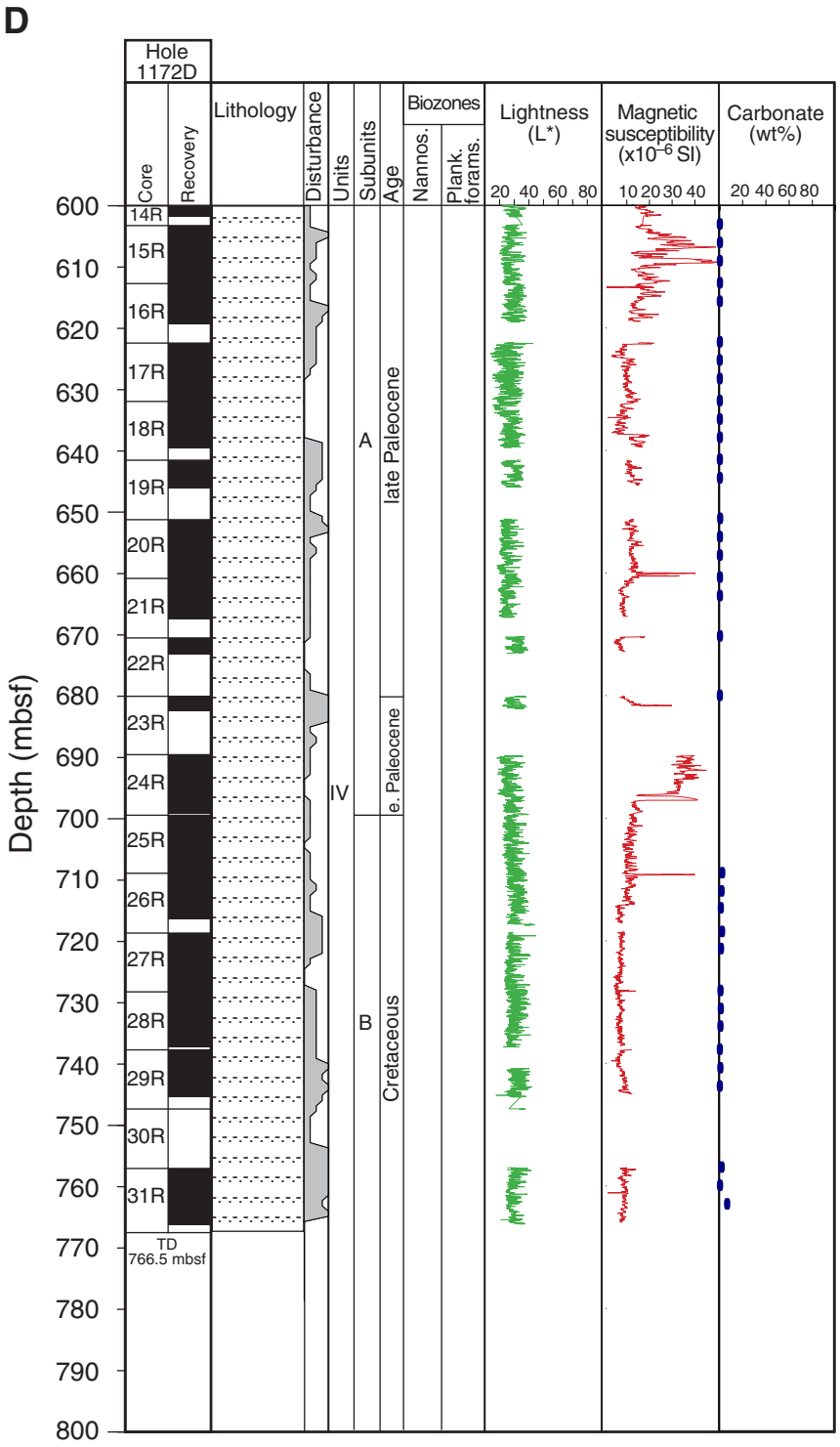

Figure F6. Results of smear-slide analyses of Neogene and uppermost Paleogene sediments of Site 1172.

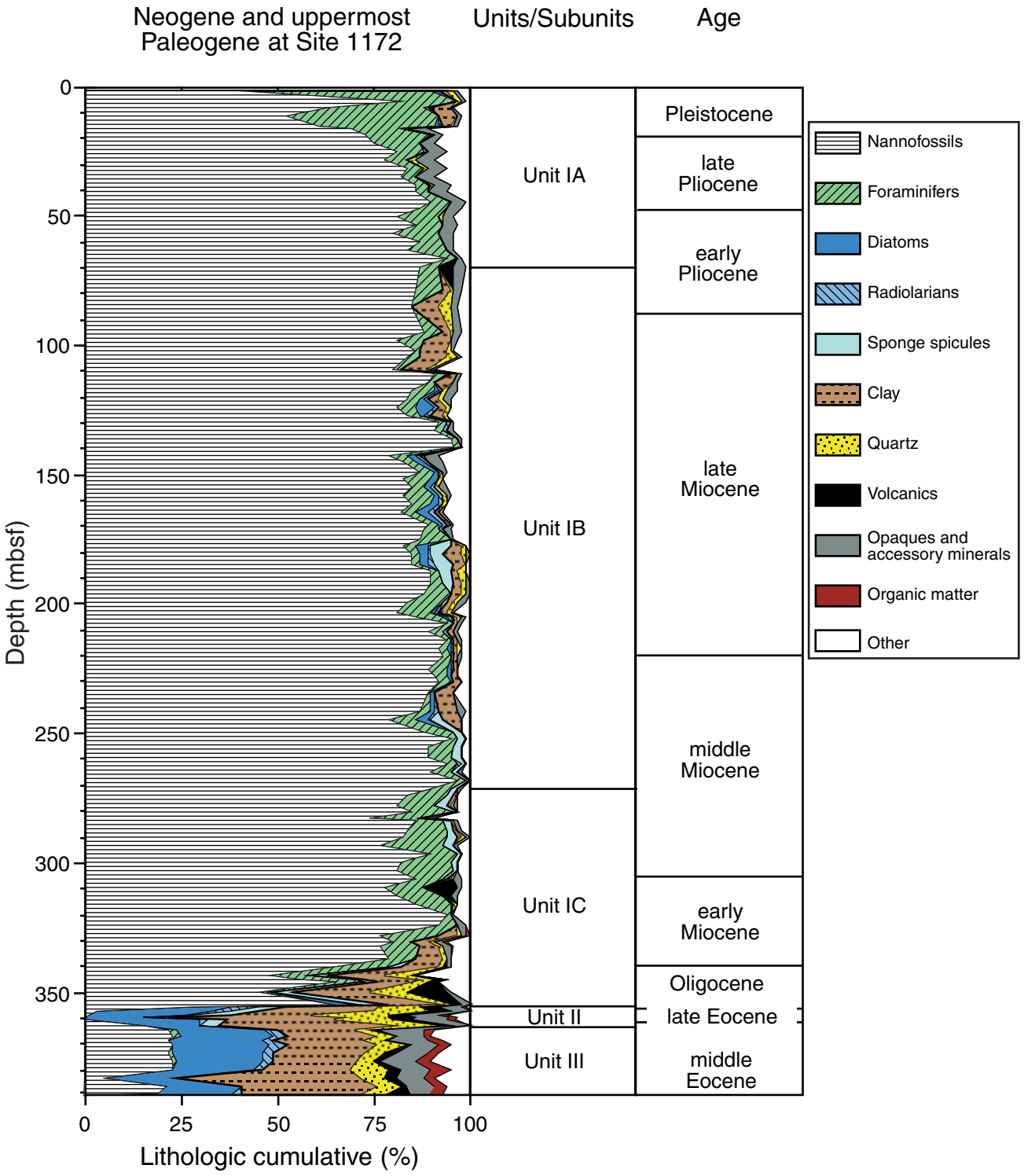

Figure F7. Close-up photograph of stained bands in late Miocene-age nannofossil ooze from Site 1172. These stains are present as faint laminations or as surfaces (interval 189-1172-26X-4, 35–55 cm).

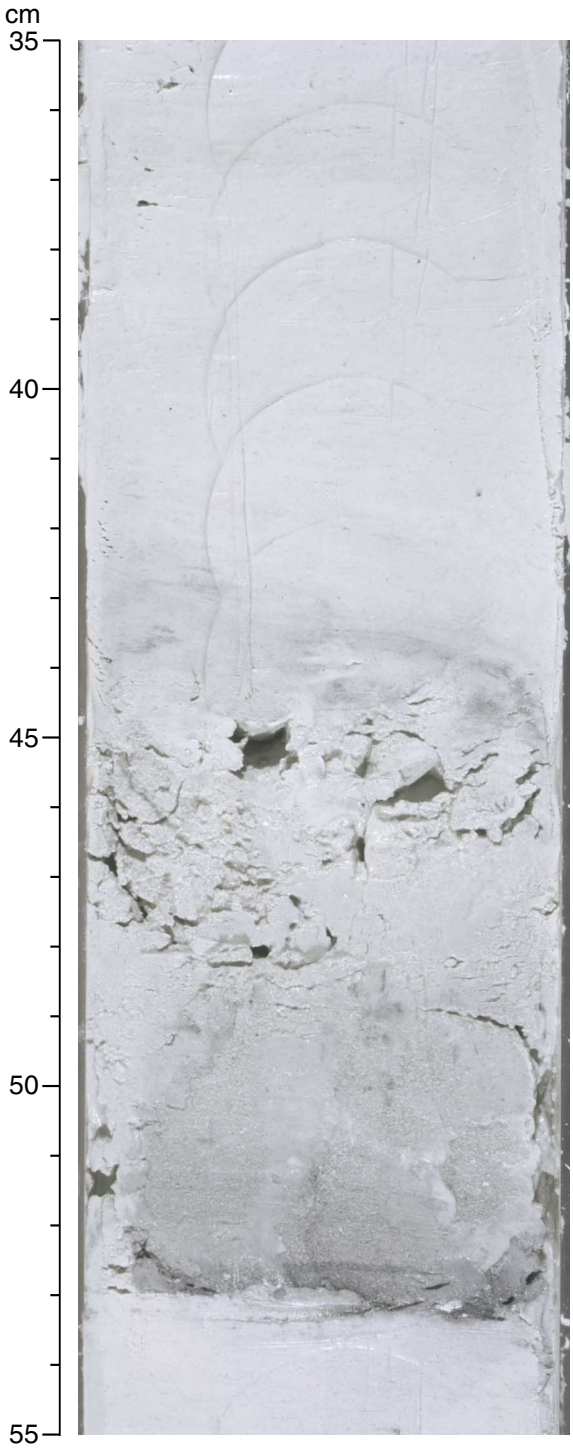

Figure F8. Close-up photograph of strong bioturbation in early middle Miocene-age nannofossil ooze at Site 1172. In contrast to the late Miocene sequences, the early and middle Miocene sediments are increasingly bioturbated downward (interval 189-1172-34X-2, 100–120 cm).

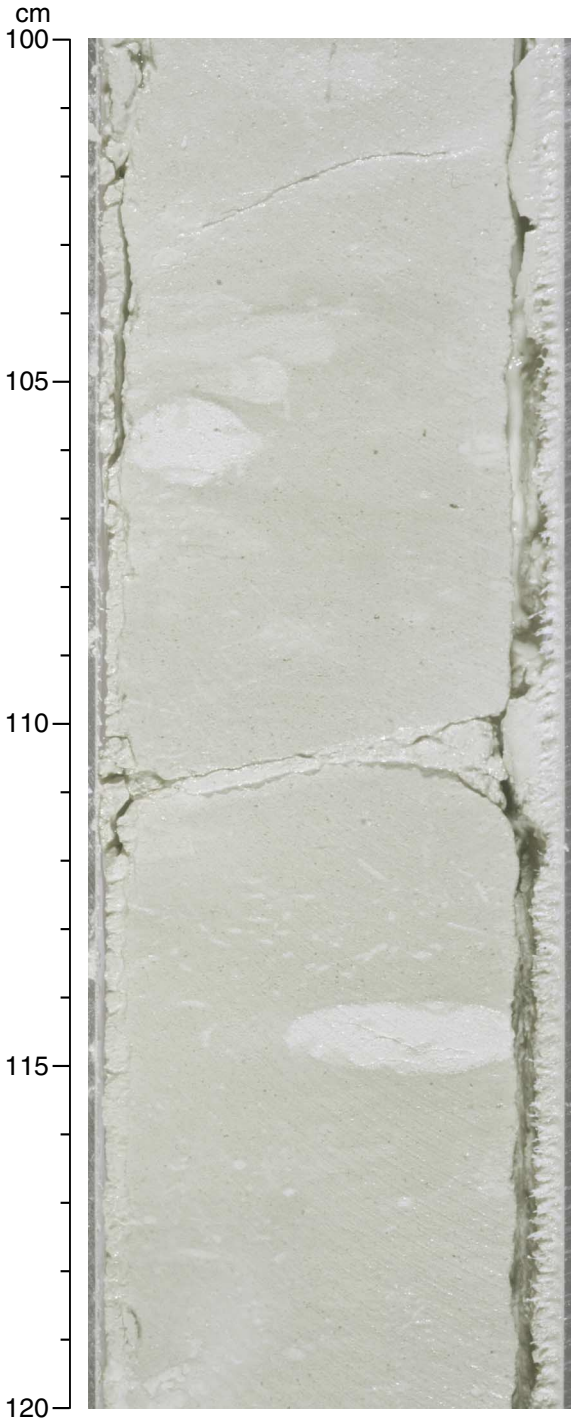

Figure F9. Close-up photograph of the lithified middle Miocene carbonate succession showing pressure solution seams that commonly accompany such lithification (interval 189-1172A-34X-5, 69–82 cm).

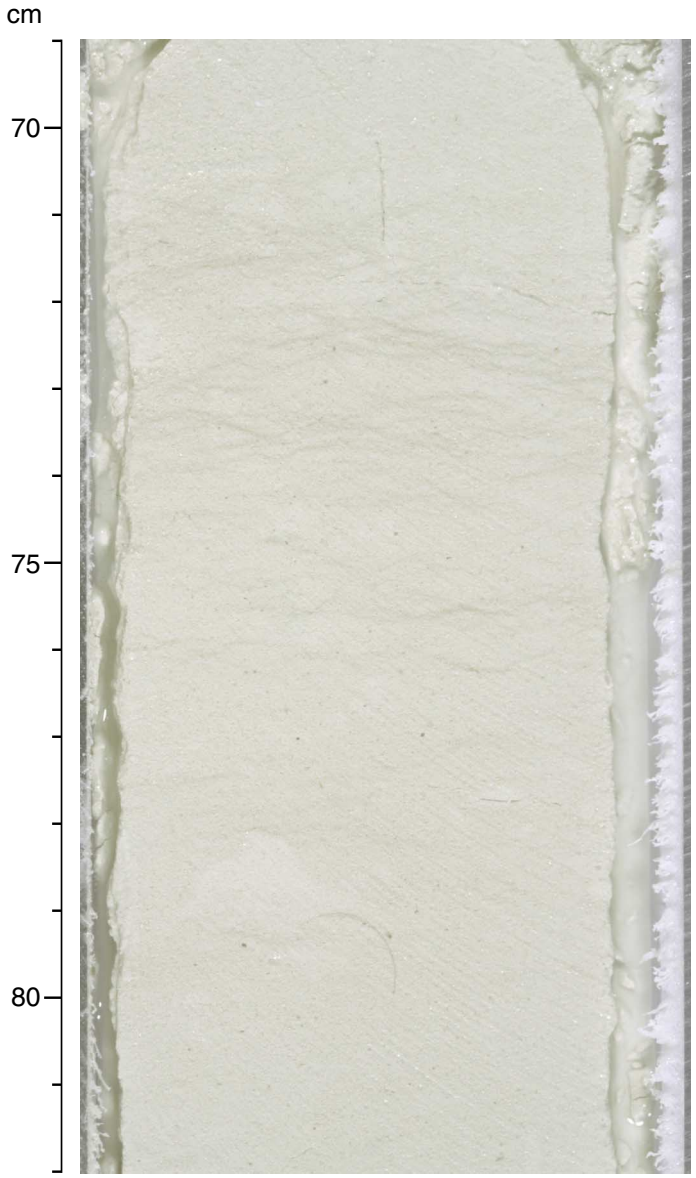

Figure F10. Results of smear-slide analyses of Paleogene sediments of Site 1172.

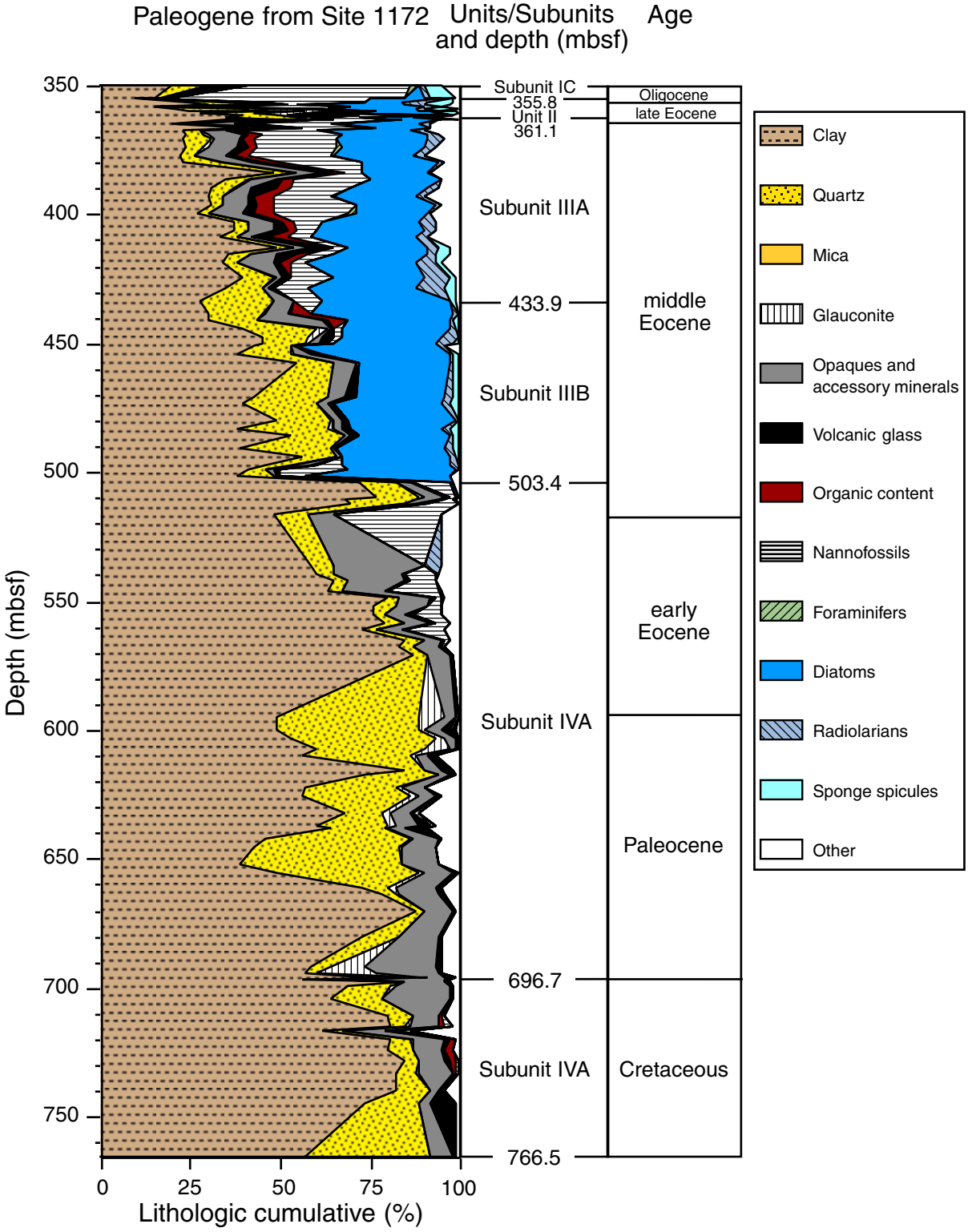

Figure F11. Close-up photograph of abundant *Zoophycos* traces in middle Eocene claystone interval 189-1172A-52X-3, 0–15 cm.

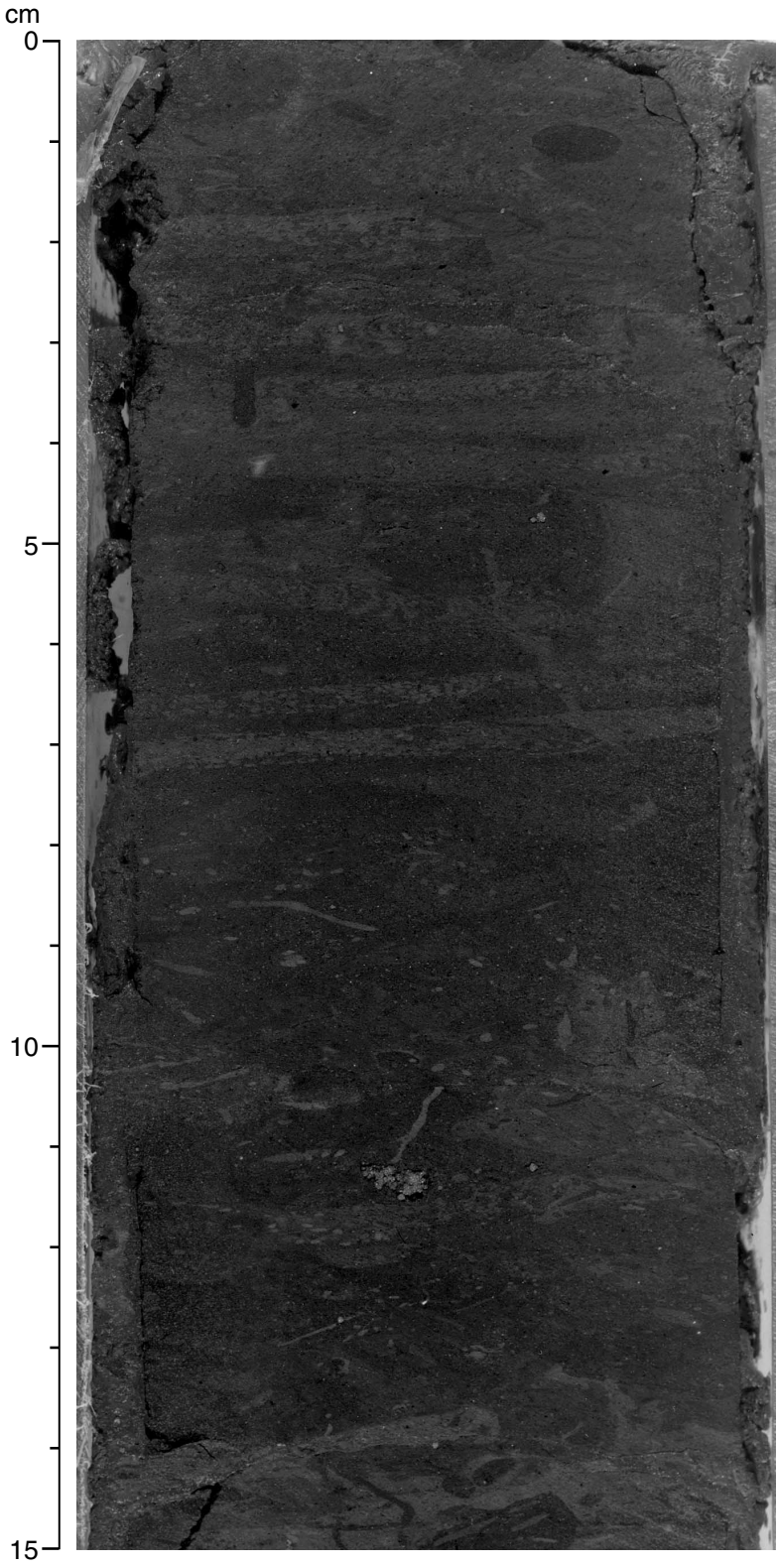

Figure F12. Close-up photograph of distinct lithologic change from glauconitic siltstone to an underlying claystone. Dinocysts suggest that the Cretaceous/Tertiary boundary at Site 1172 is below 44 cm (interval 189-1172D-24R-5, 20–50 cm).

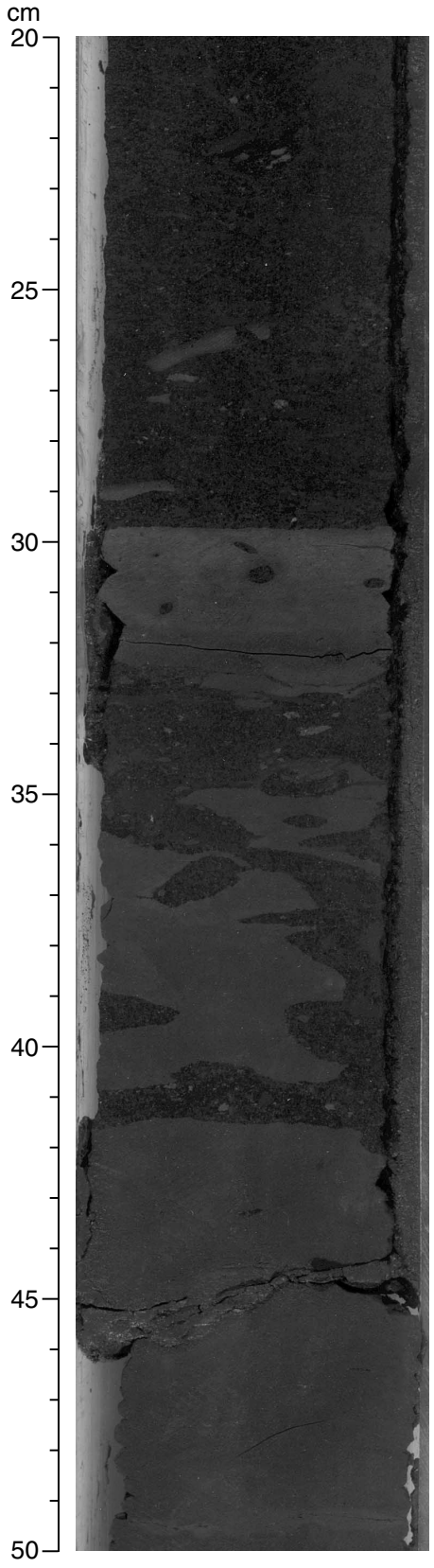

Figure F13. Compilation of lithologic and stratigraphic information of Core 189-1172D-39X sediments (Unit IV, Eocene–Oligocene Transition). The paleomagnetostratigraphic data series seems not to match the exact depth interval. The ash layer identified in the lithologic column is suspected to be responsible for the intensity peak at 358 mbsf. See Figure **F3,** p. 40, in the "Explanatory Notes" chapter for the key to lithologic and bioturbation symbols. P = planktonic foraminifers, D = diatoms, N = nannofossils, Dino = dinocysts.

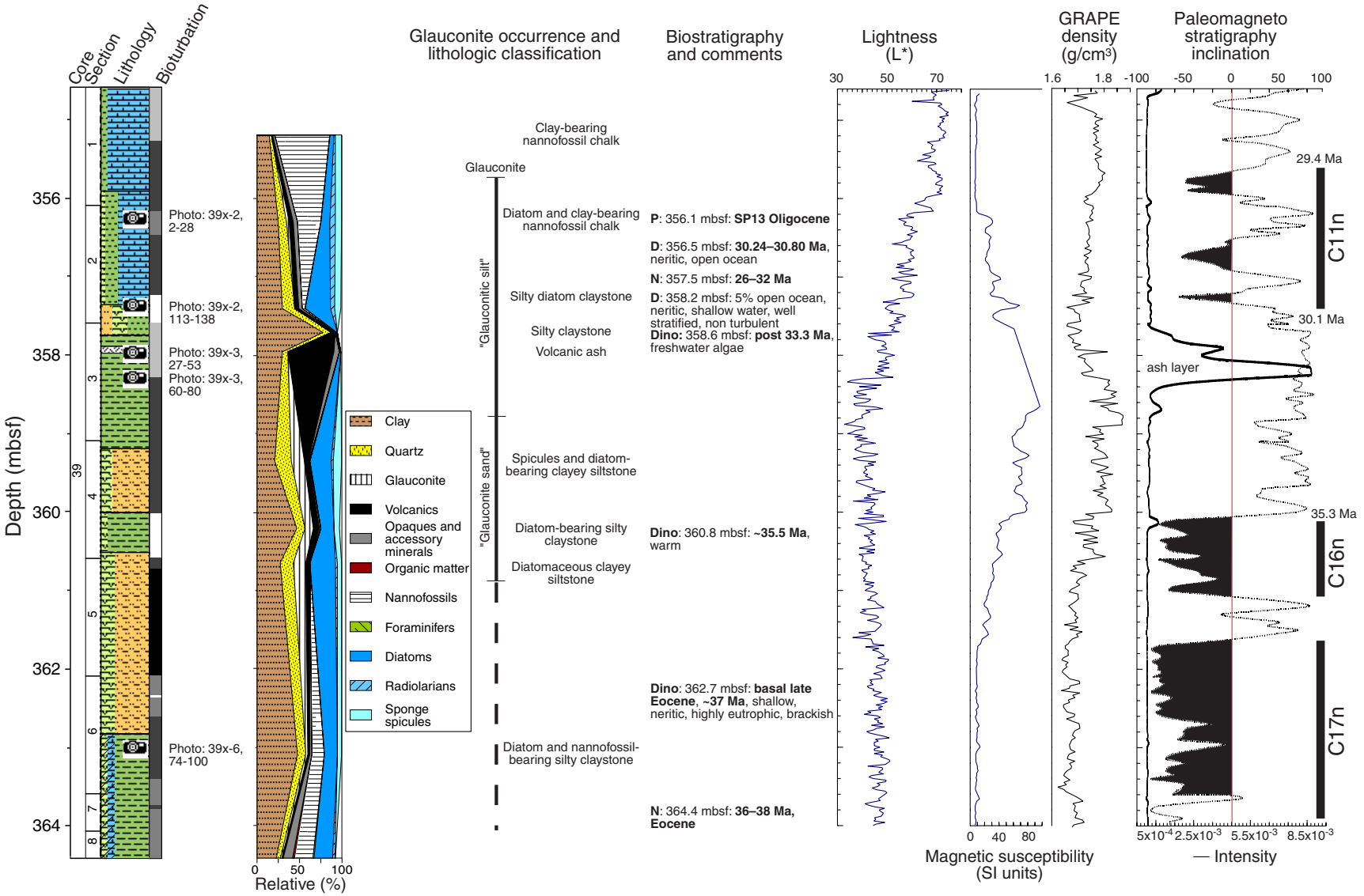

Figure F14. Clay mineral units of Site 1172, East Tasman Plateau.

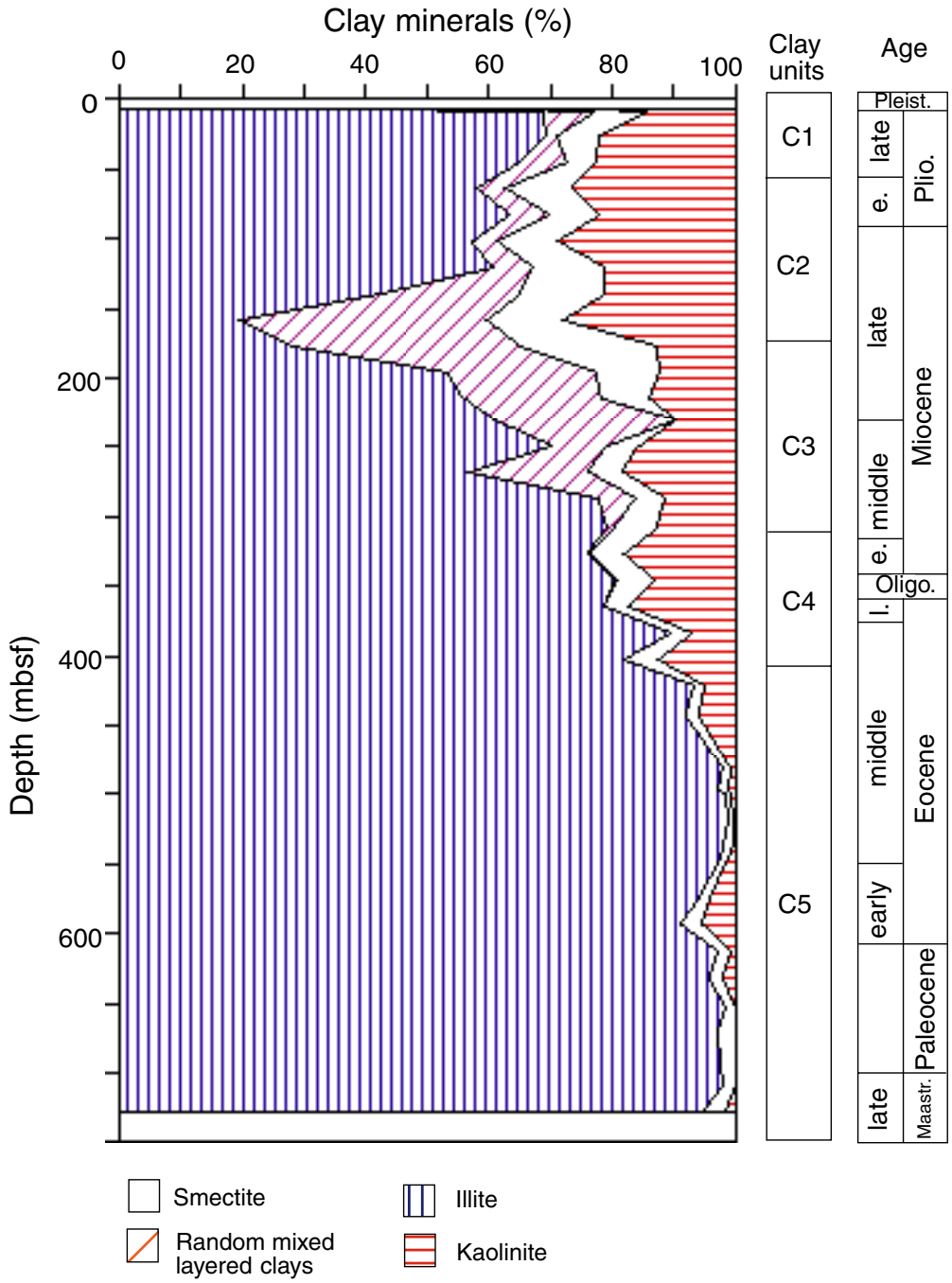

Figure F15. Site 1172 age-depth plot and linear sedimentation rates. The age-depth plot uses multiple microfossil and paleomagnetic datums for Site 1172. The events used are listed in Table **T12,** p. 129, and in **"Paleomagnetism,"** p. 36. Below 281 mcd, there is a constant offset of 9.78 m from mbsf. For mbsf values of all datums, see Table **T12,** p. 129.

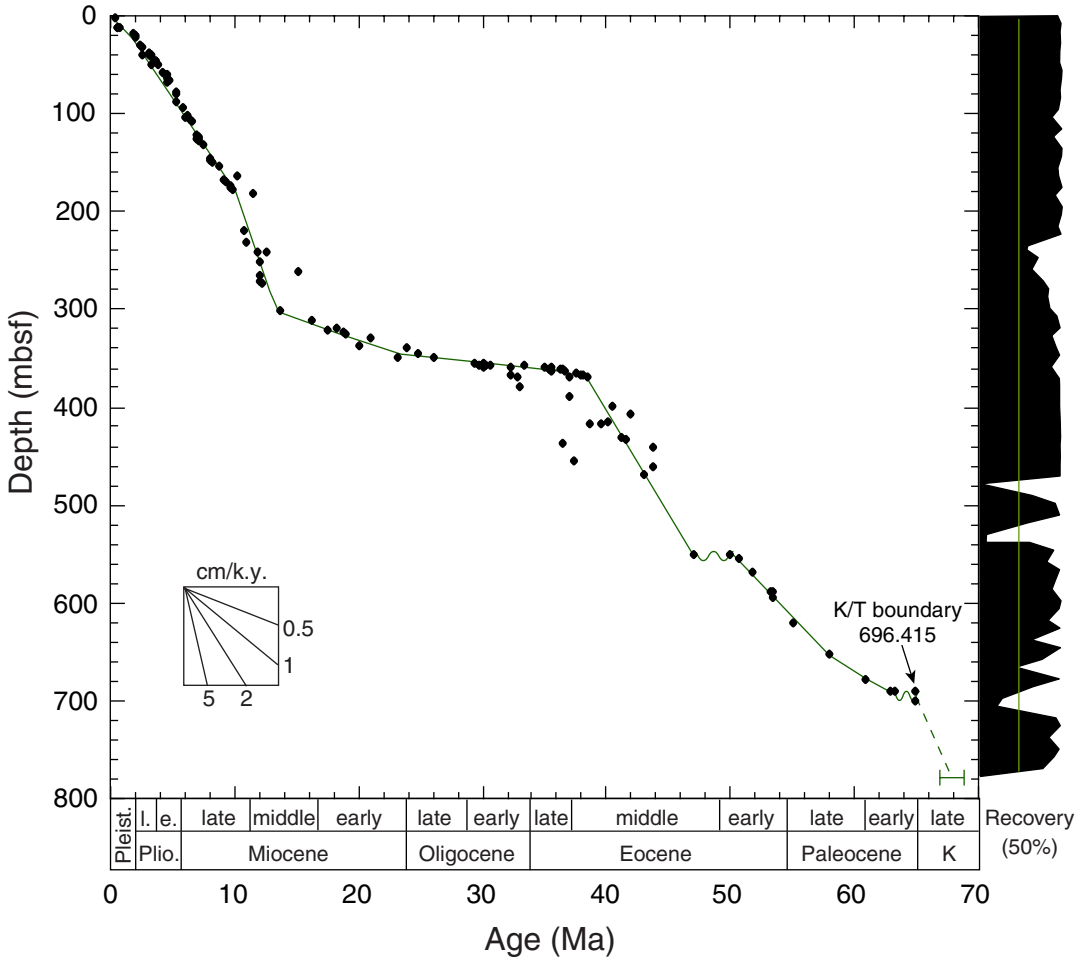

Figure F16. Long-core measurements from 0 to 100 mbsf for Holes 1172A, 1172B, and 1172C showing inclination, intensity, and interpreted magnetostratigraphy.

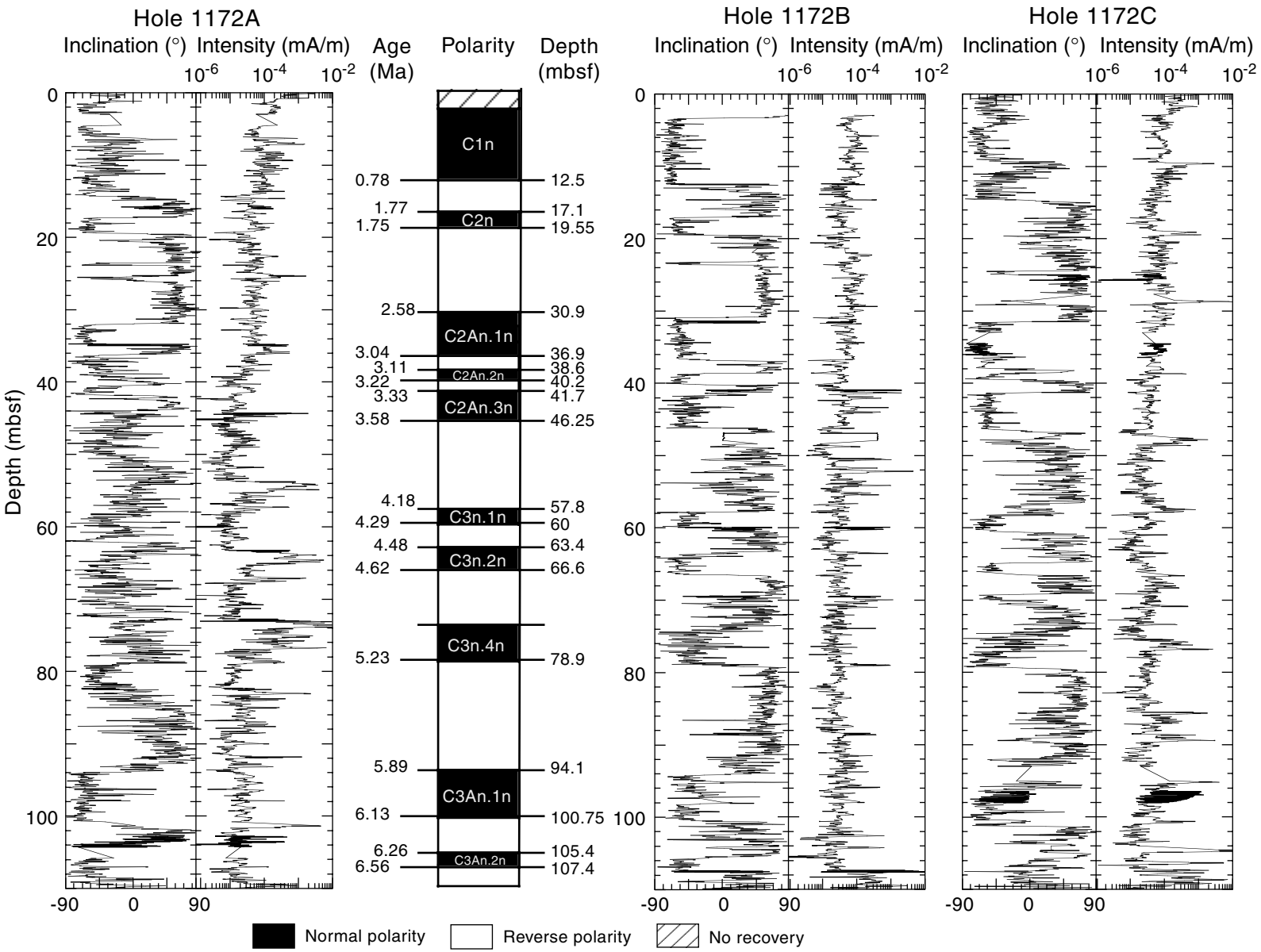

Figure F17. Long-core measurements from 100 to 200 mbsf for Holes 1172A, 1172B, and 1172C showing inclination, intensity, and interpreted magnetostratigraphy.

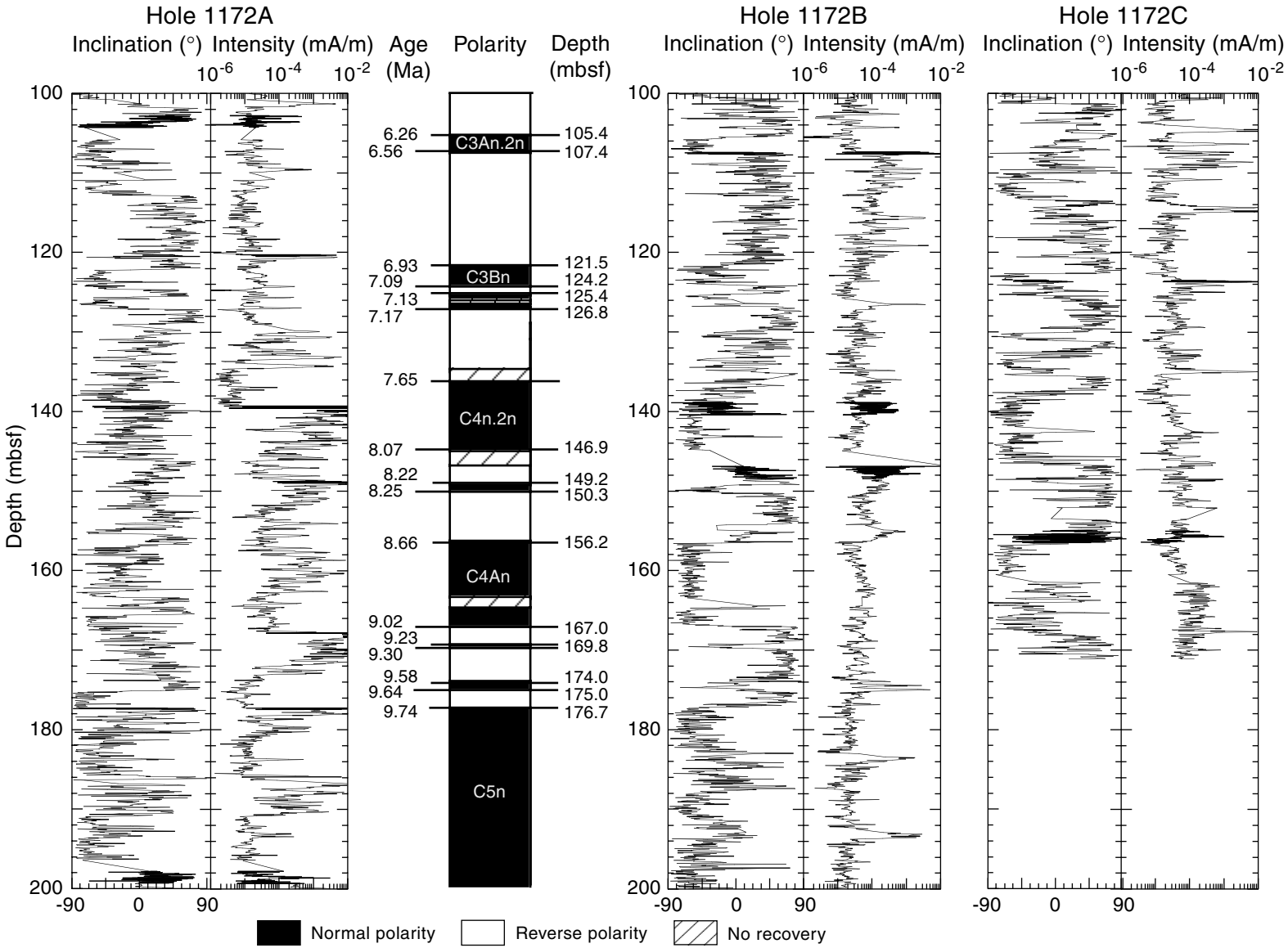

Figure F18. Long-core measurements from 200 to 300 mbsf for Hole 1172A showing inclination, intensity, and interpreted magnetostratigraphy.

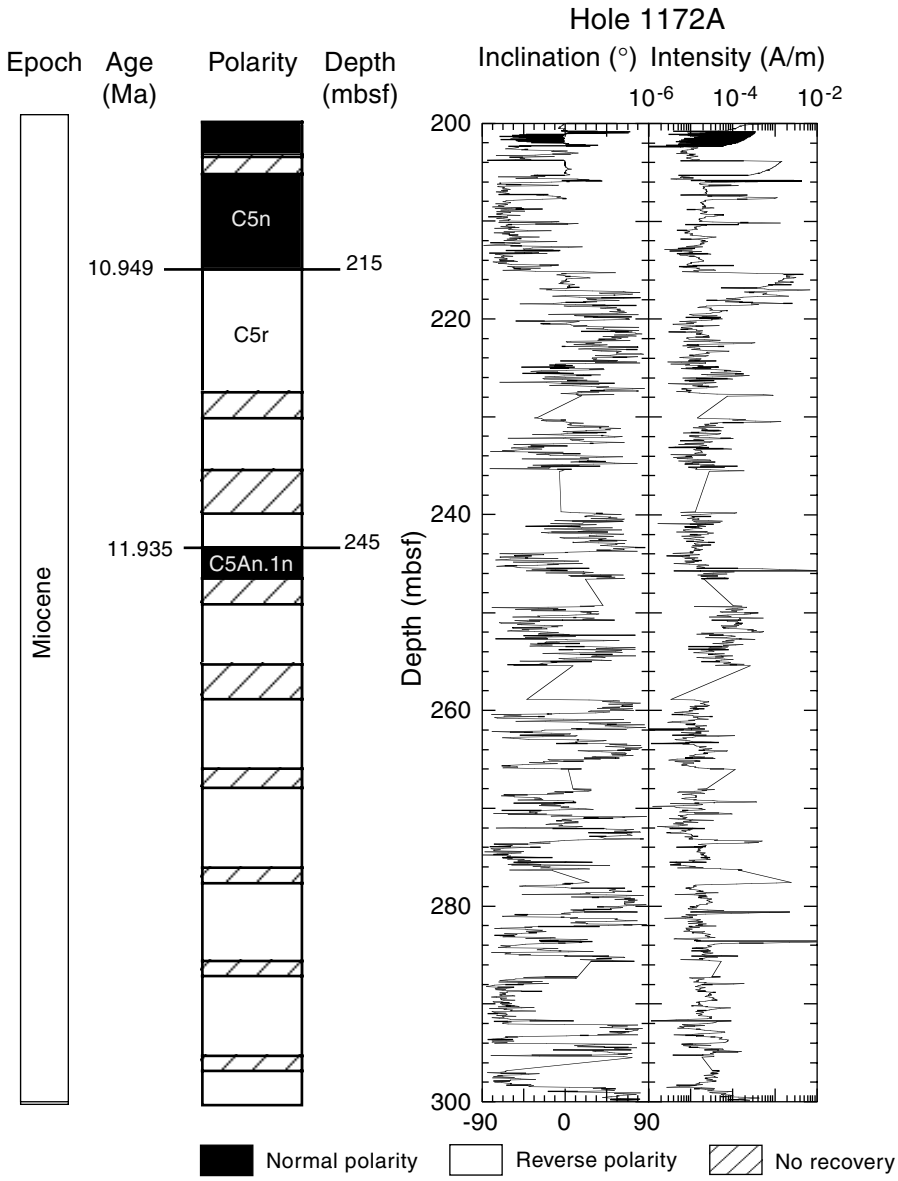

Figure F19. Long-core measurements from 300 to 400 mbsf for Hole 1172A and from 350 to 375 mbsf for Hole 1172D showing inclination, intensity, and interpreted magnetostratigraphy.

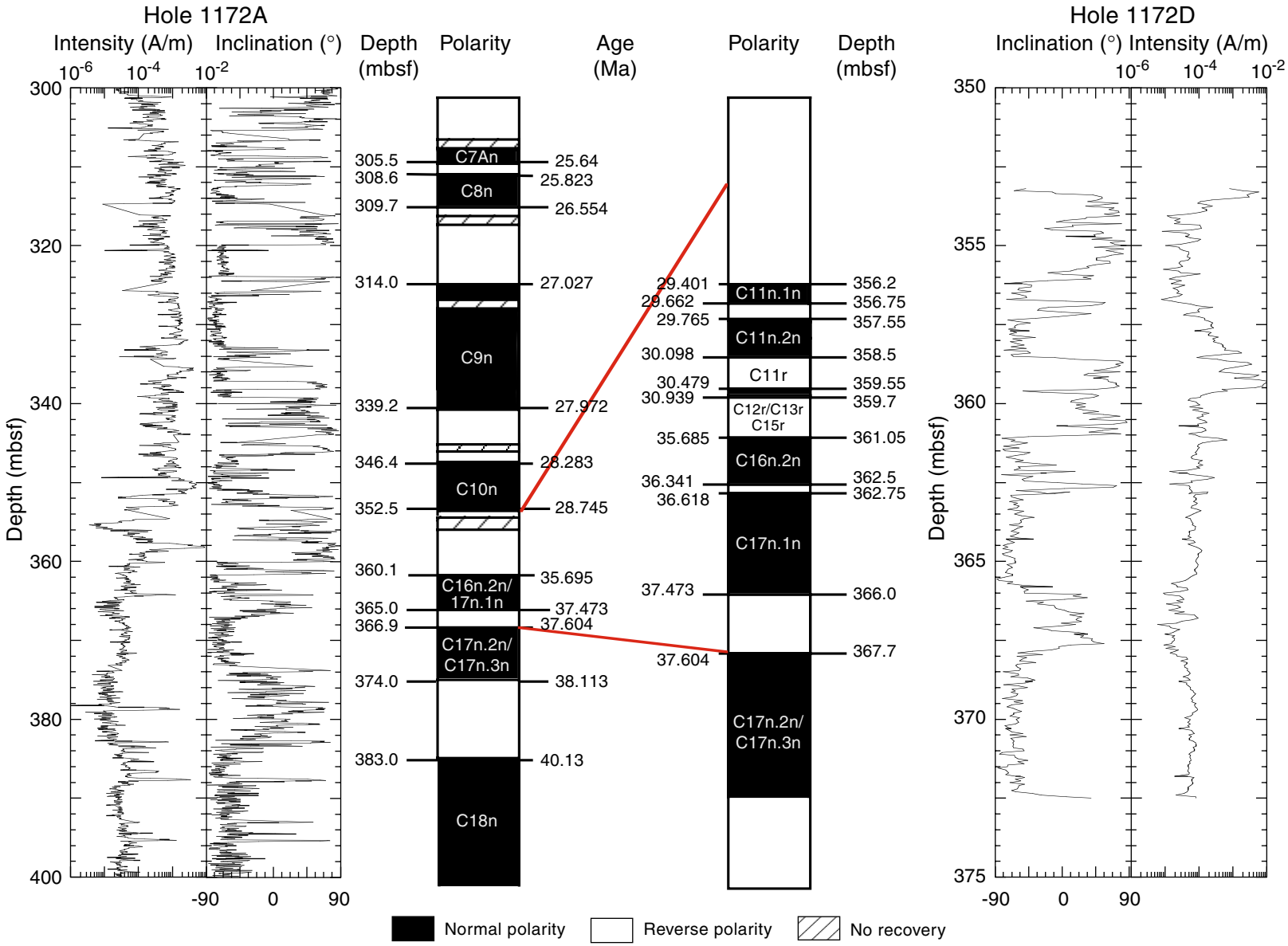

Figure F20. Recovery of magnetostratigraphy from the z-intensity of Hole 1172D.

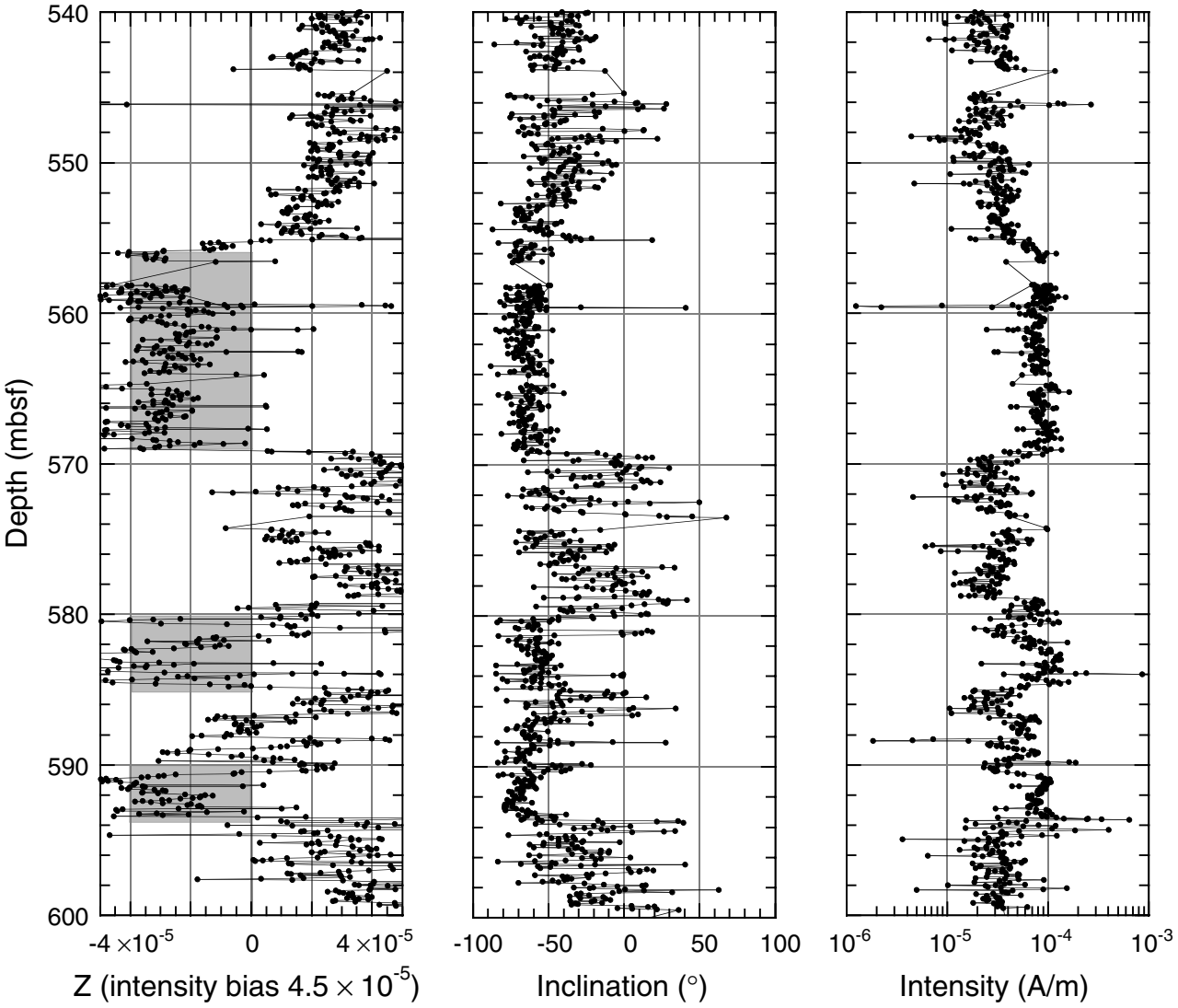

Figure F21. Variation of magnetic properties in Holes 1172A and 1172D. **A.** Variation of intensity of ARM and IRM. **B.** Variation of normalized IRM demagnetized between 0 and 20 mT and normalized IRM acquired between 200 and 500 mT.

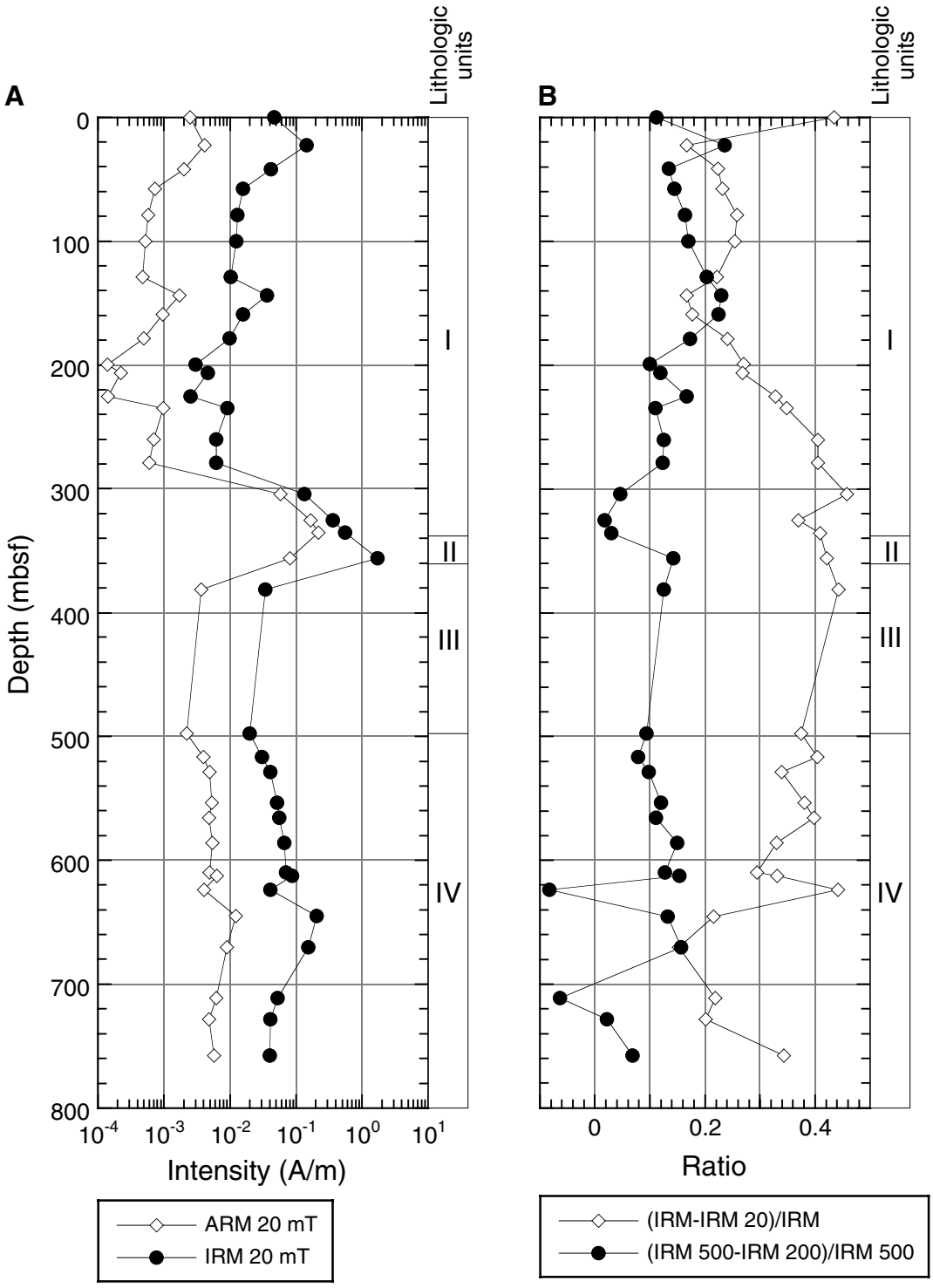

Figure F22. Age-depth relationship from paleomagnetic data for the Cenozoic for Hole 1172B.

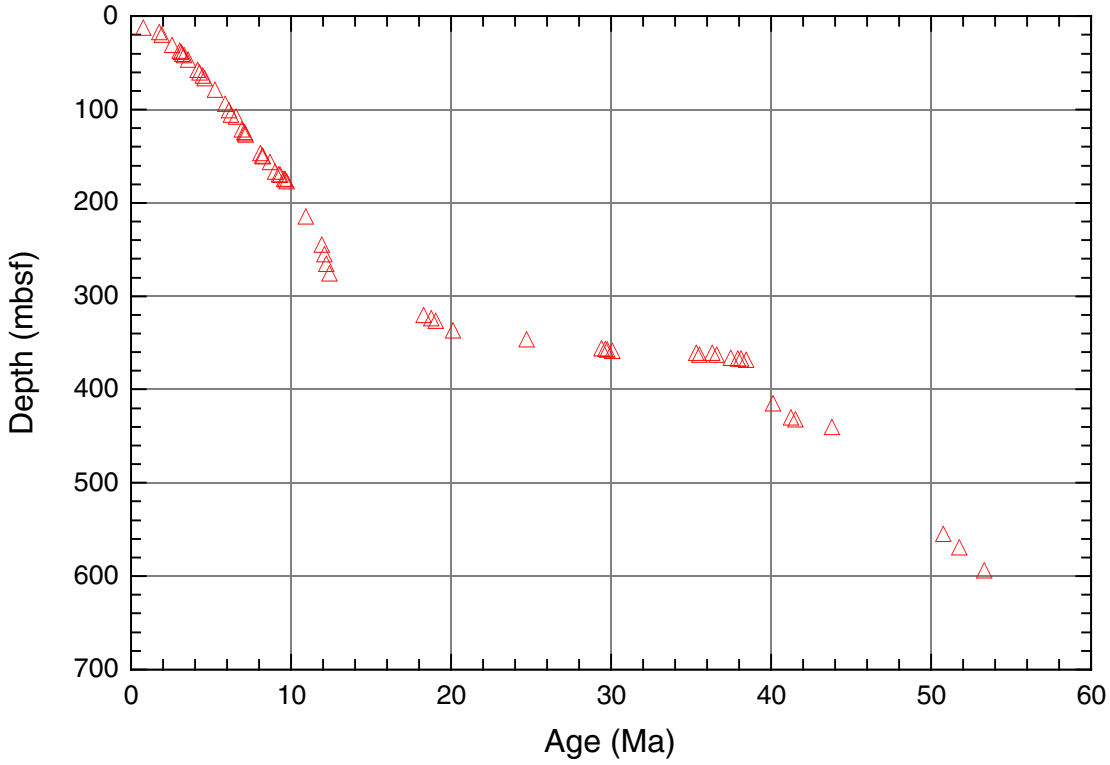

Figure F23. A. Smoothed (21-cm Gaussian) spectral reflectance data (L*) for the upper 140 mcd from Holes 1172A (left), 1172B (middle), and 1172C (right). Holes 1172B and 1172C are offset from Hole 1172A by constants (10 and 20 L* units, respectively). **B.** Smoothed (21-cm Gaussian) magnetic susceptibility data for the upper 140 mcd from Holes 1172A (left), 1172B (middle), and 1172C (right). Holes 1172B and 1172C are offset from Hole 1172A by constants (5×10^{-6} and 10×10^{-6}, respectively). Note that cores in Hole 1172A designated by dashed lines (Cores 189-1172A-5H through 10H) are severely disturbed by flow-in and were not utilized in constructing the composite section or sampling splice. These five Hole 1172A cores have only a cumulative composite correction added; no further alignment was attempted.

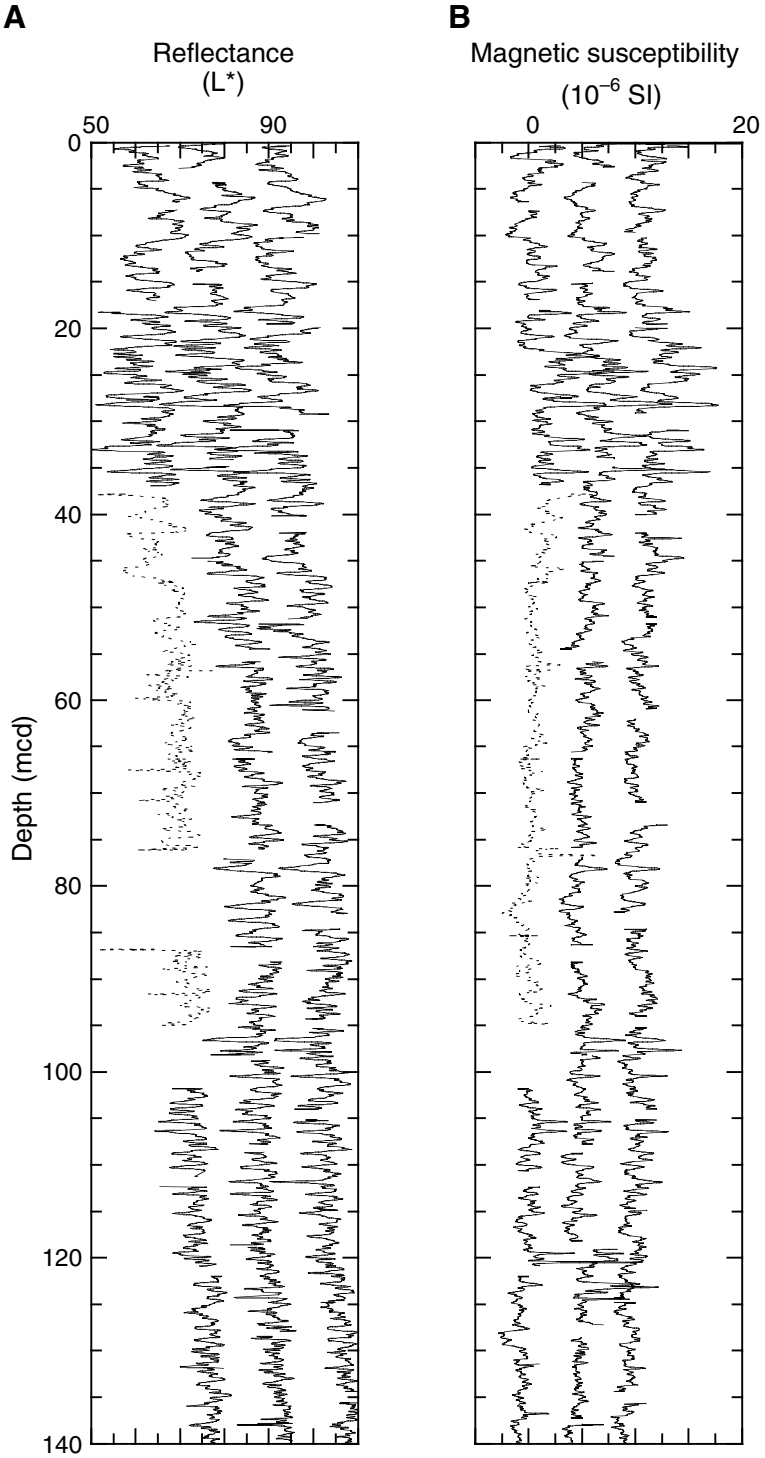

Figure F24. A. Smoothed (21-cm Gaussian) GRA bulk density data for the Eocene/Oligocene boundary interval in Holes 1172A (left) and 1172D (right). Hole 1172D is offset from Hole 1172A by a constant (0.2 g/cm^3). **B.** Smoothed (21-cm Gaussian) spectral reflectance data (L*) for the Eocene/Oligocene boundary interval in Holes 1172A (left) and 1172D (right). Hole 1172D is offset from Hole 1172A by a constant (10 L* units). **C.** Smoothed (21-cm Gaussian) magnetic susceptibility data for the Eocene/Oligocene boundary interval in Holes 1172A (left) and 1172D (right). Hole 1172D is offset from Hole 1172A by a constant (30 × 10^{-6} SI).

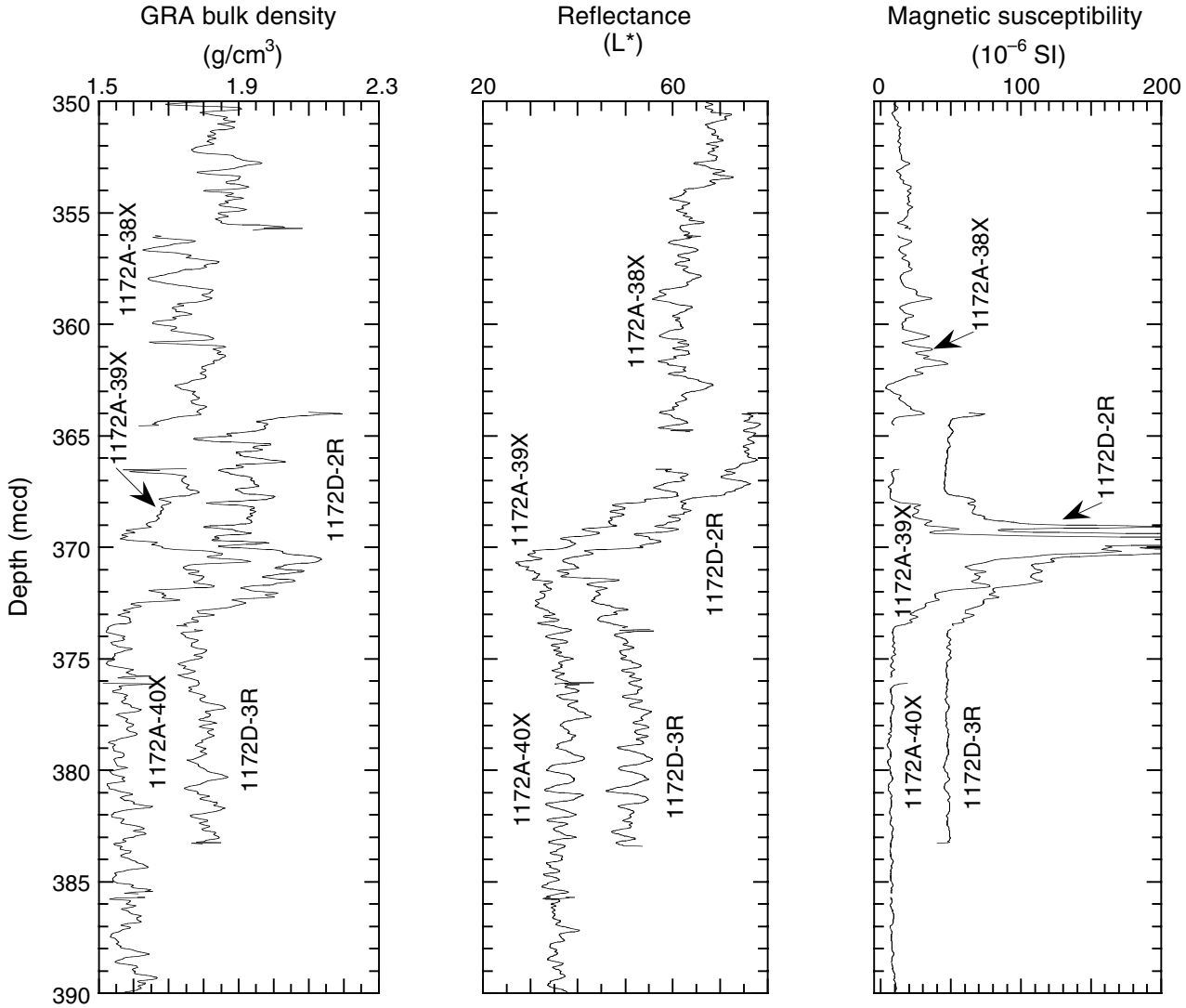

Figure F25. Plots of carbonate, total organic carbon (TOC) (squares = CNS analyzer data; dots = Rock-Eval pyrolysis values), total nitrogen, C/N ratios, and hydrogen index values for Site 1172. Data from Hole 1172A are presented in black, and data from Hole 1172D are shown in blue. Shaded areas on the C/N ratio plot delineate typical marine and terrestrial organic matter fields. Lithostratigraphic and preliminary biostratigraphic units are on the right side of the figure.

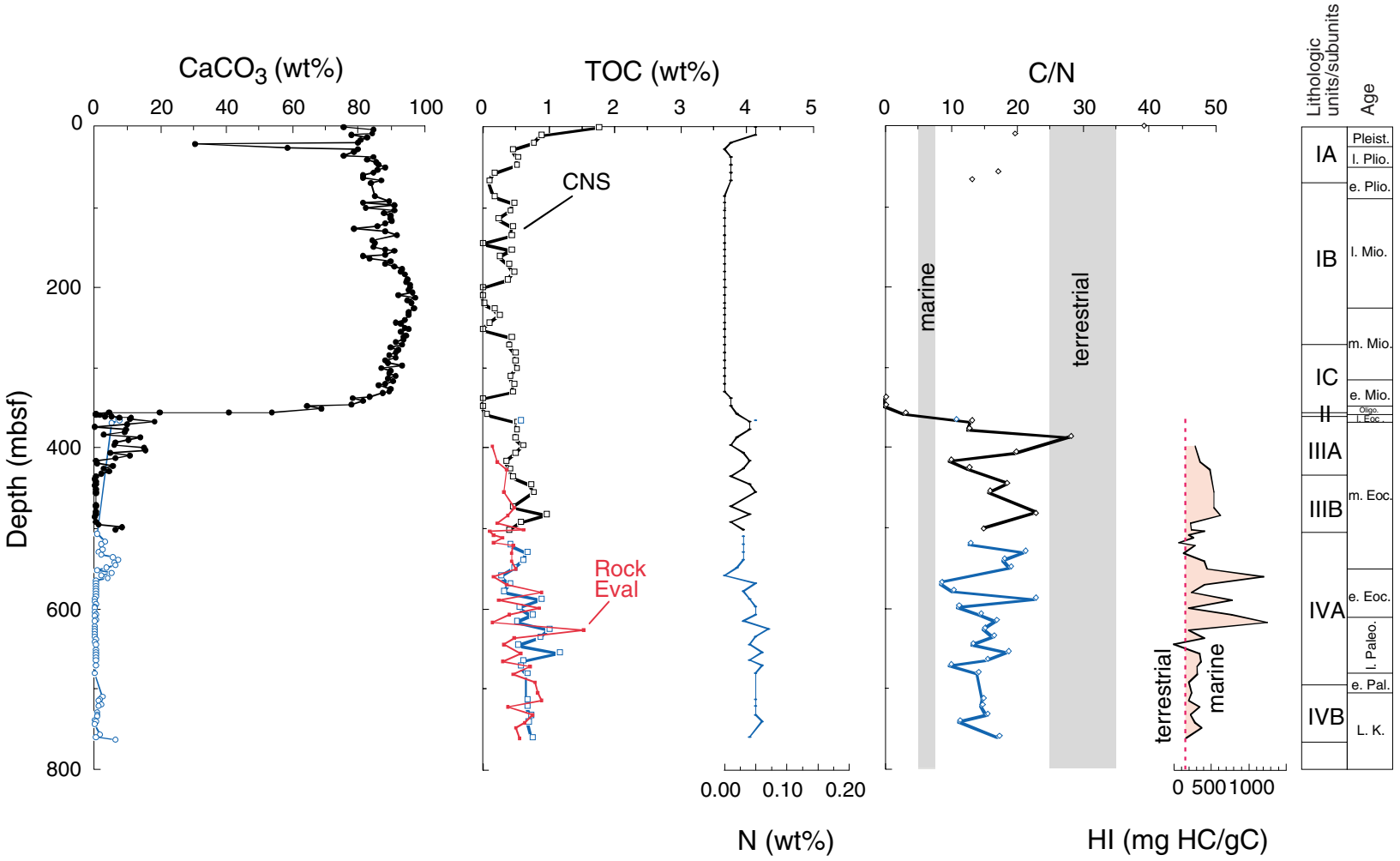

Figure F26. Total sulfur content (squares) compared to C/S ratios (circles) for Site 1172. Dashed lines = transitions between marine, brackish, and freshwater environments. Lithostratigraphic and preliminary biostratigraphic units are on the right side of the diagram.

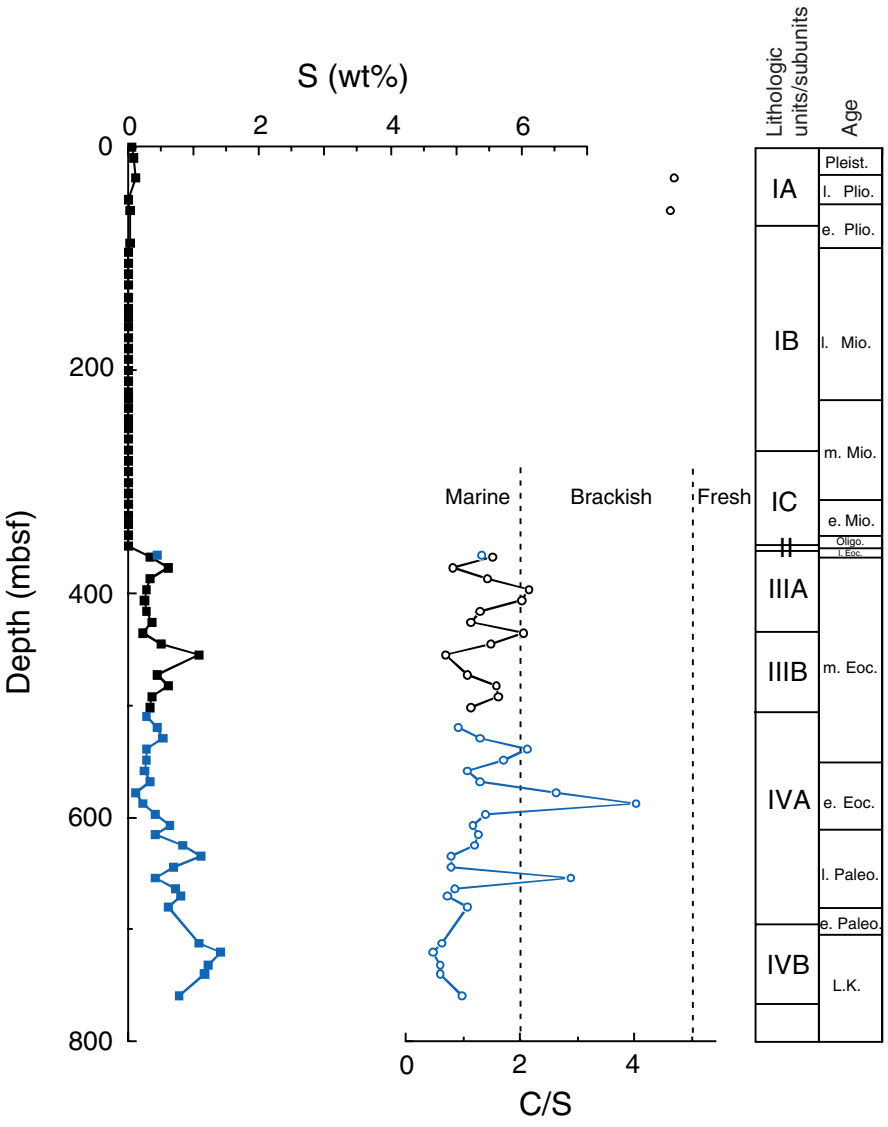

Figure F27. Methane (C_1) and dissolved sulfate (SO_4^{2-}) concentrations and methane vs. ethane plus propane ratio (C_1/C_2+C_3) from headspace gas analysis at Site 1172. Dashed lines = biogenic and thermogenic fields on the C_1/C_2+C_3 plot. Lithostratigraphic and preliminary biostratigraphic units are on the right side of the diagram.

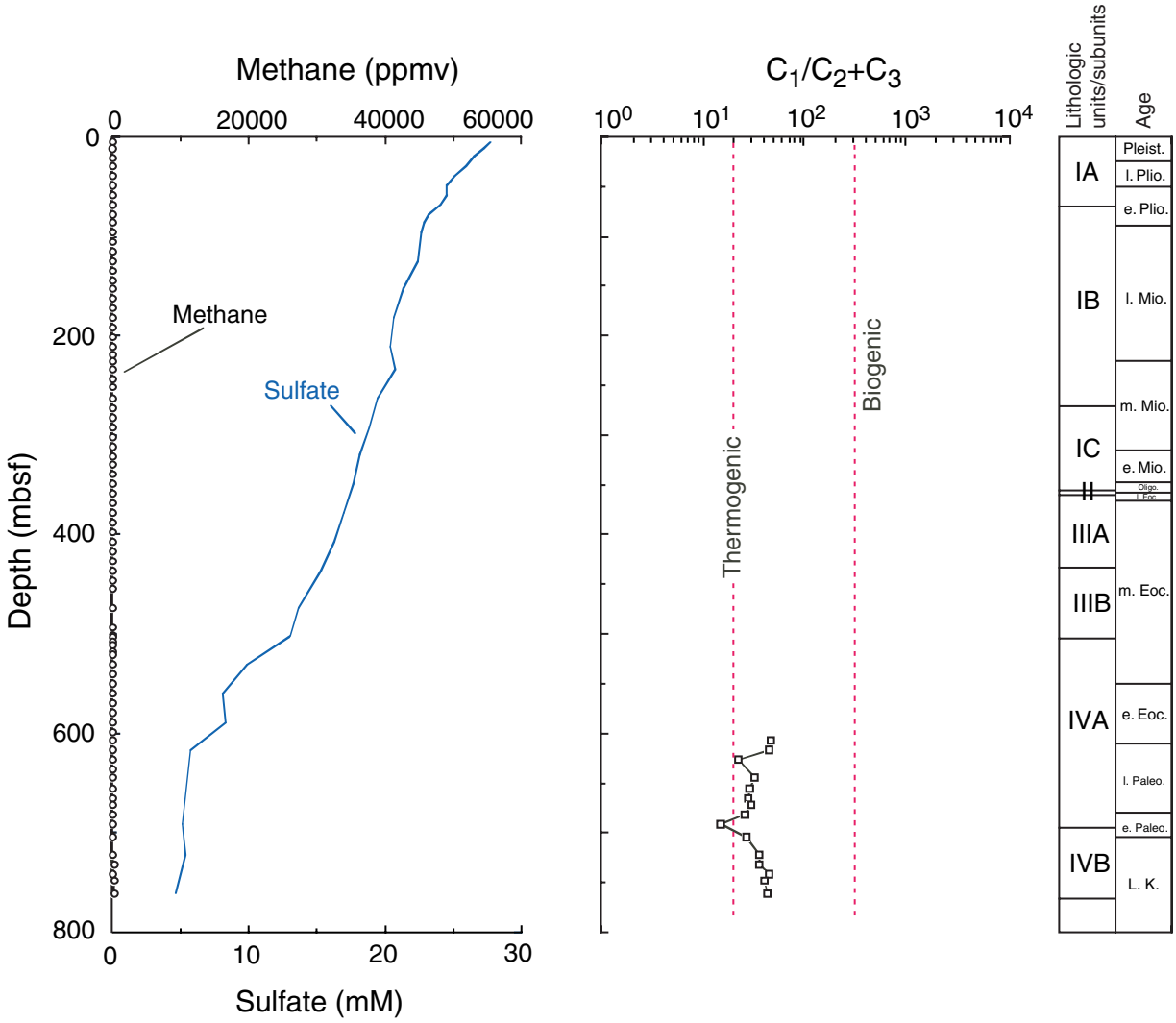

Figure F28. Concentration-depth profiles for interstitial water chemistry at Site 1172. Solid circles = samples collected from Hole 1172A. Open circles = samples from Hole 1172D. Approximate locations of lithostratigraphic boundaries are also shown (see "Lithostratigraphy," p. 10). (Continued on next two pages.)

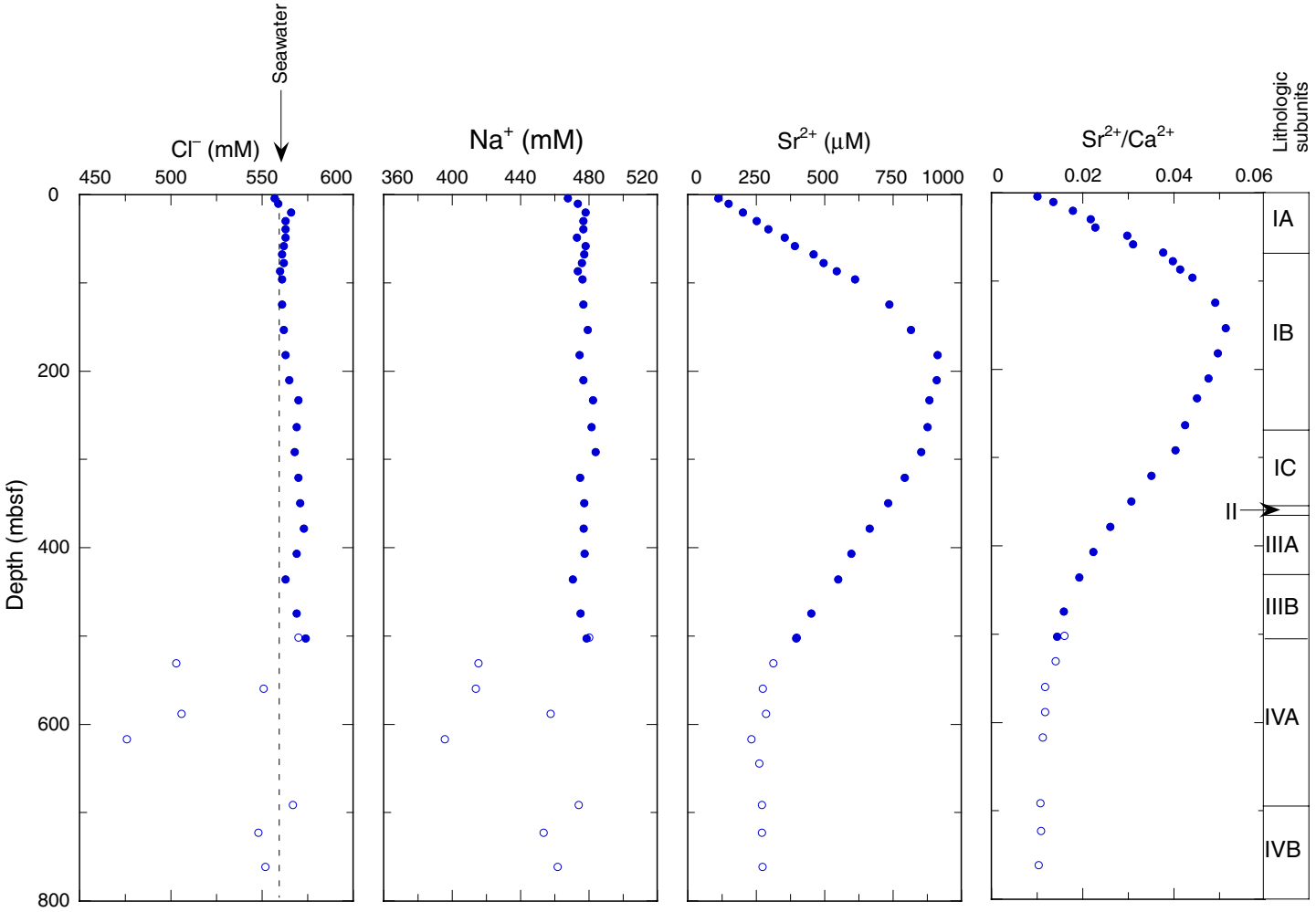

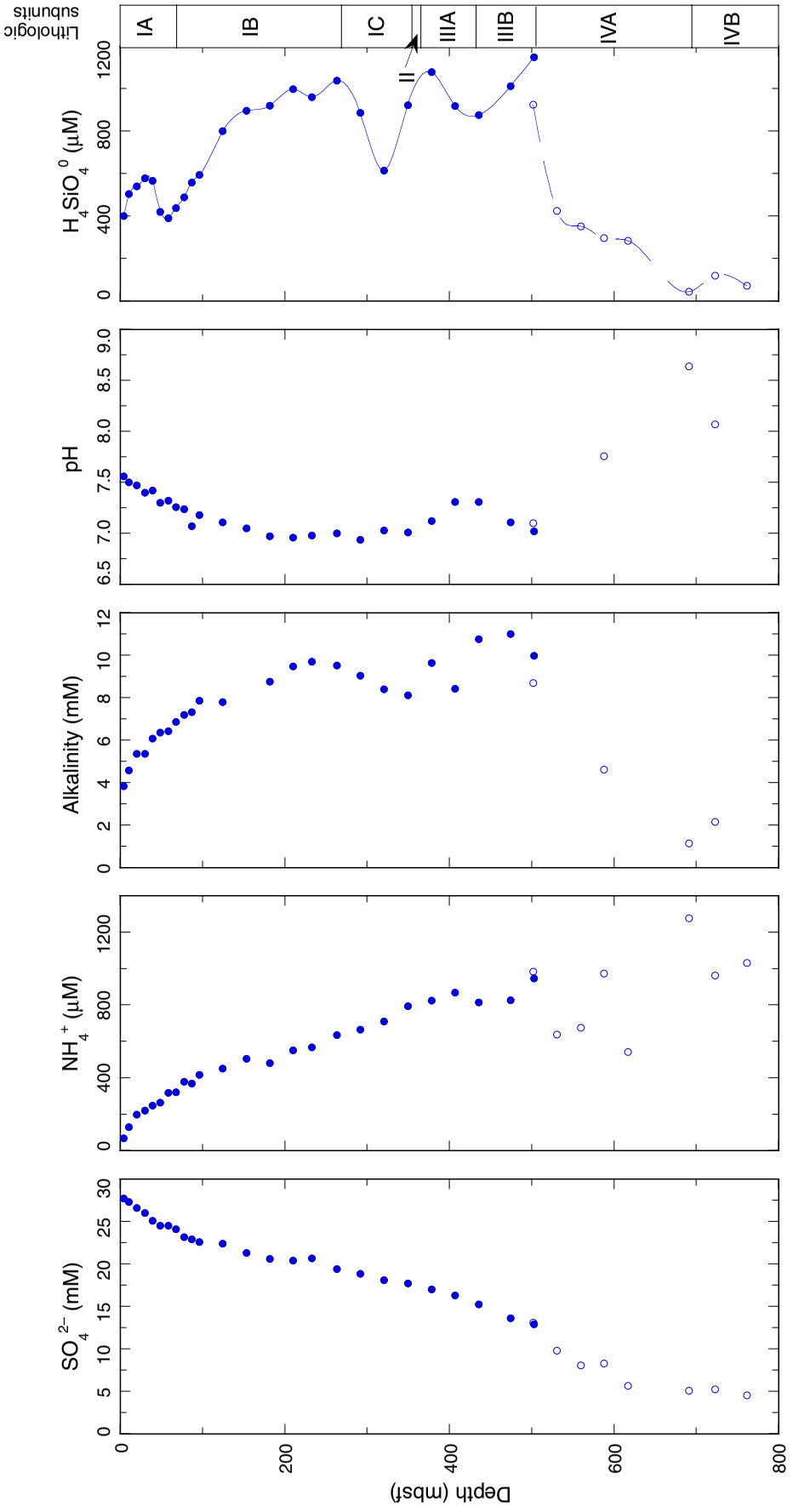

Figure F28 (continued).

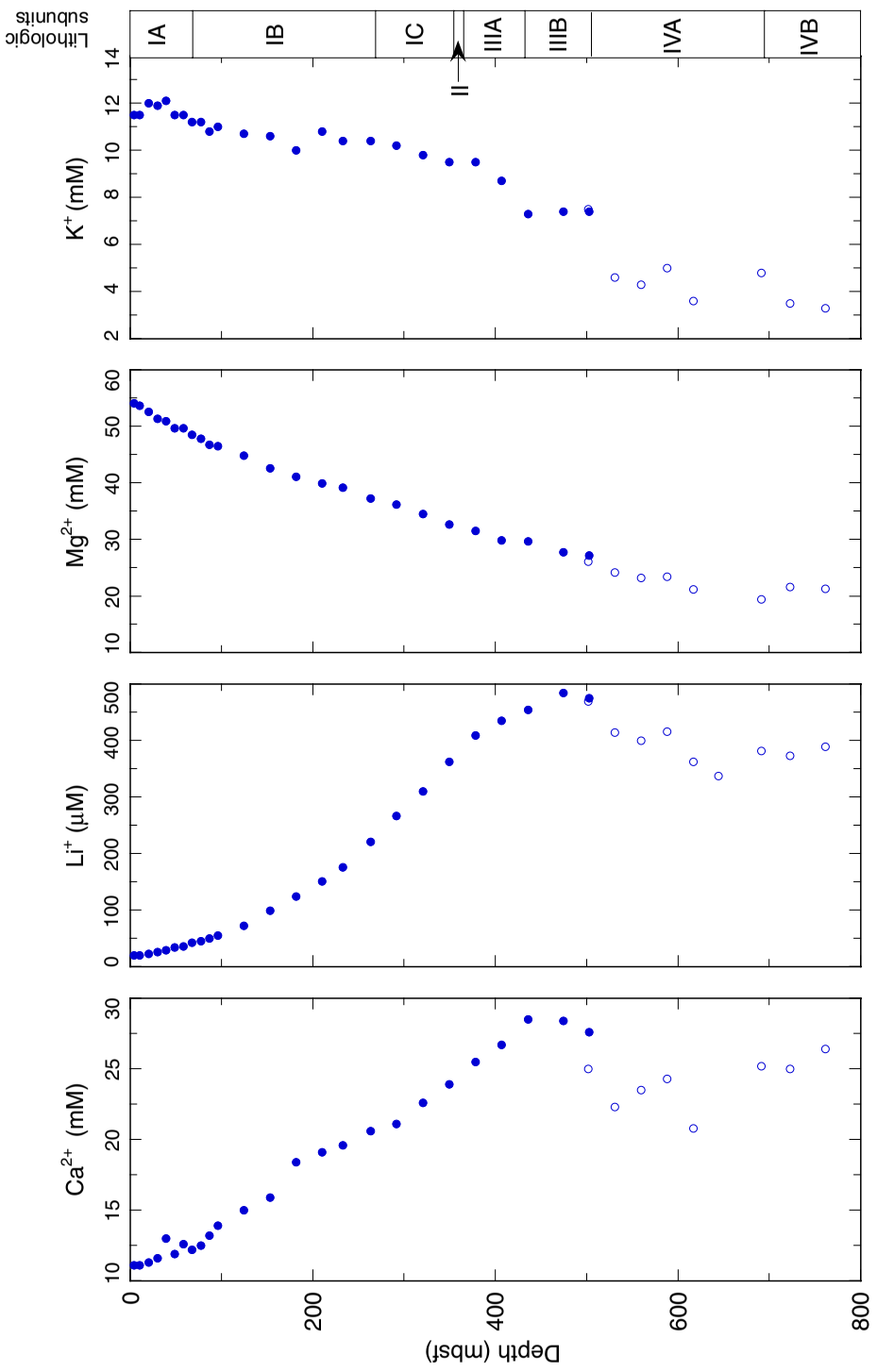

Figure F28 (continued).

Figure F29. Crossplots of Mg^{2+} vs. Ca^{2+} for Hole 1172A and Ca^{2+} vs. Li^{+} for Holes 1172A and 1172D. Approximate locations of lithostratigraphic boundaries also shown (see **"Lithostratigraphy,"** p. 10).

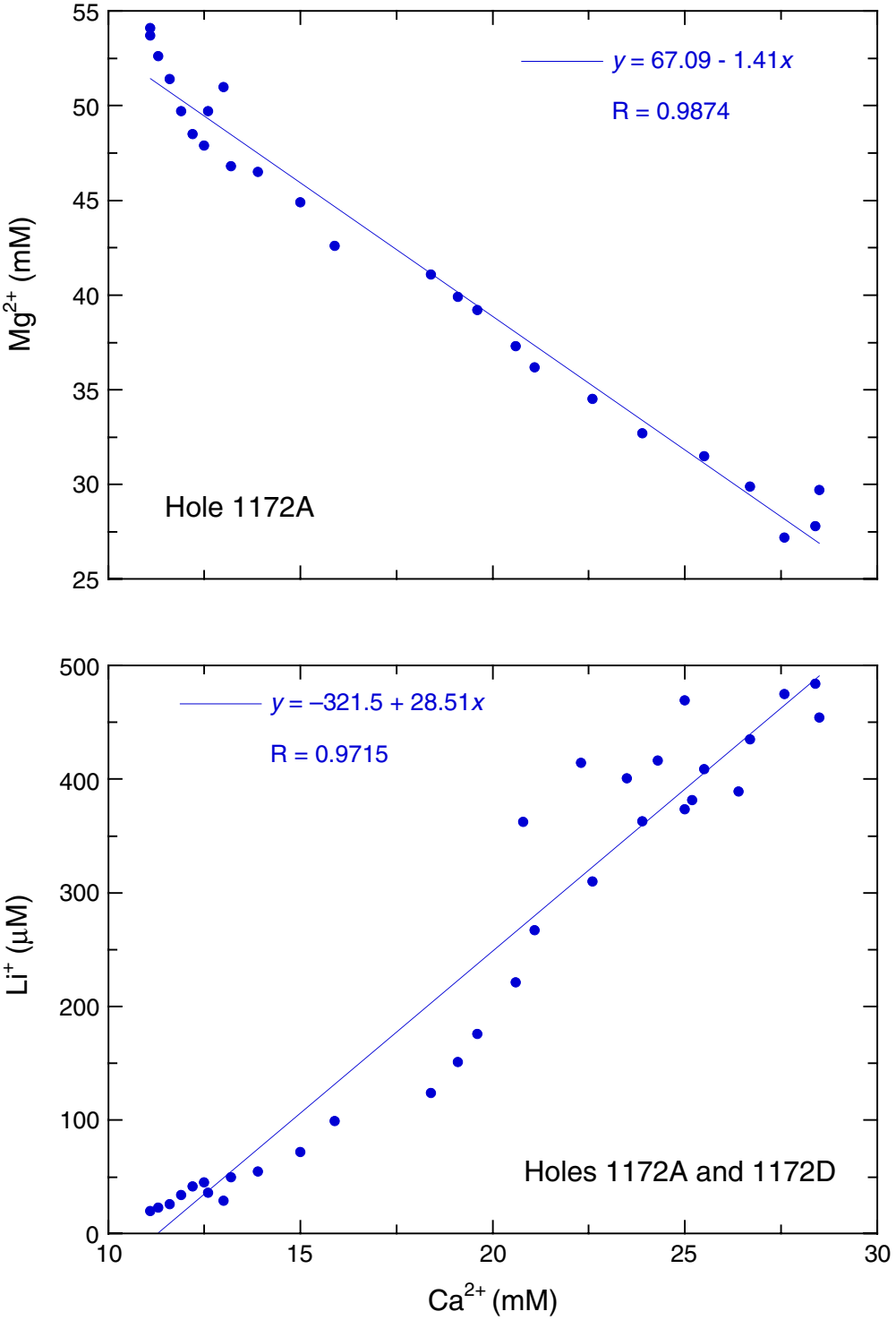

Figure F30. A. Magnetic susceptibility measured on whole cores by the MST vs. depth for Holes 1172A and 1172D. (Continued on next page.)

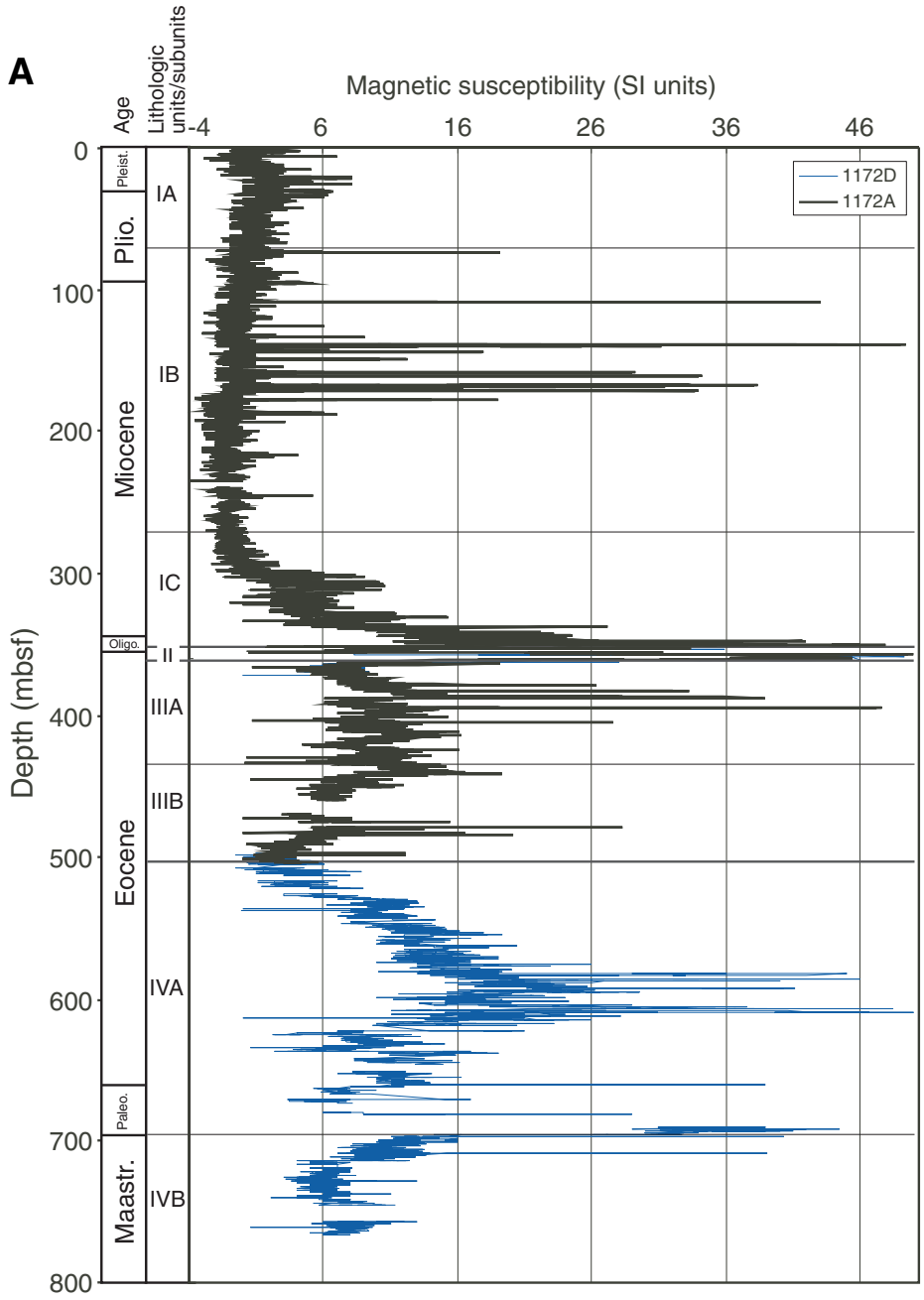

Figure F30 (continued). B. GRA density (dots) and wet bulk density determined for discrete samples (open circles) vs. depth for Holes 1172A and 1172D.

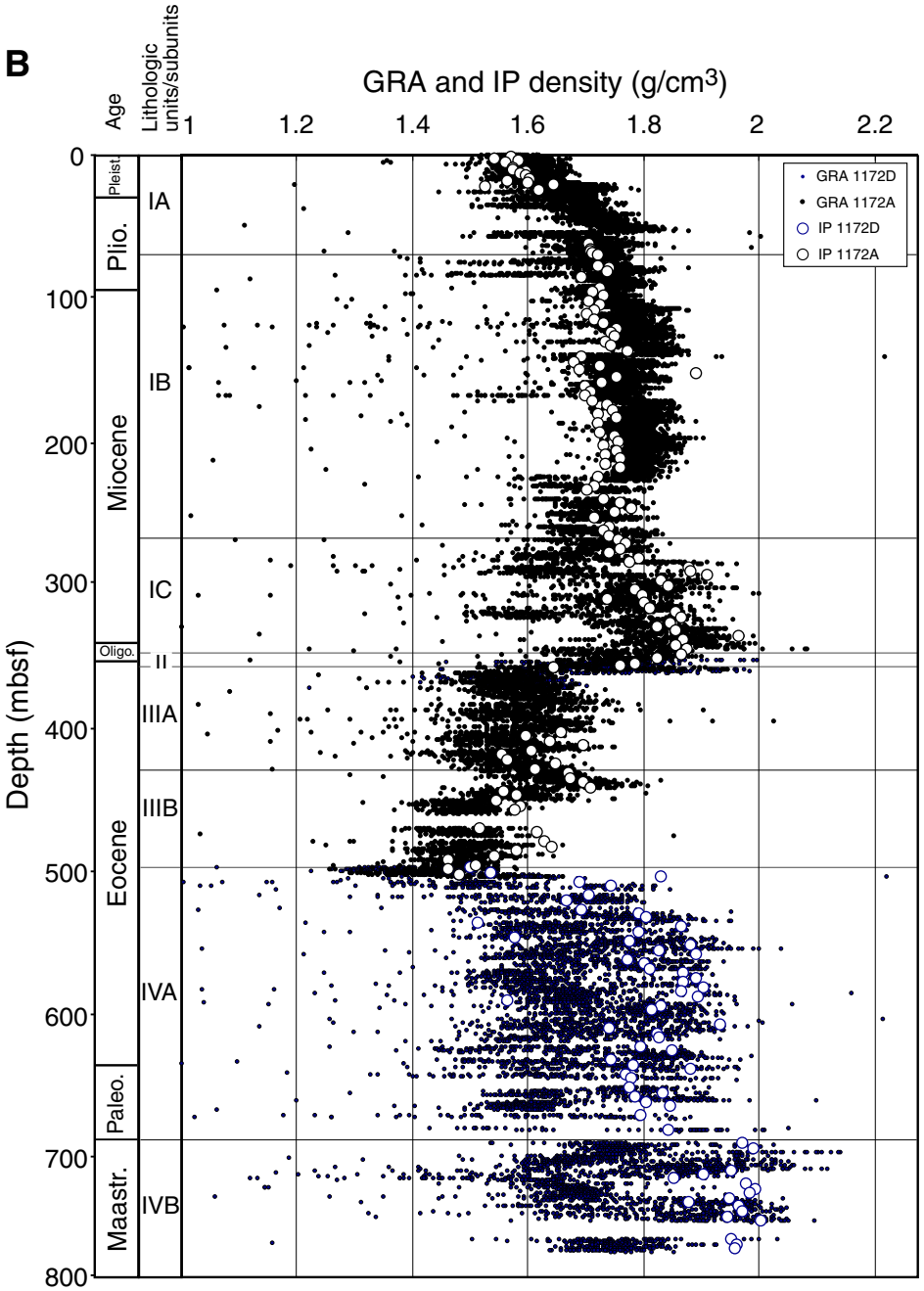

Figure F31. *P*-wave velocities (PWS1, PWS2, and PWS3) measured for discrete samples and *P*-wave velocities measured in whole cores (MST) vs. depth for the upper part of Hole 1172A. See Figure **F38B,** p. 102, in the "Site 1168" chapter, for an illustration of the three directions of measurement.

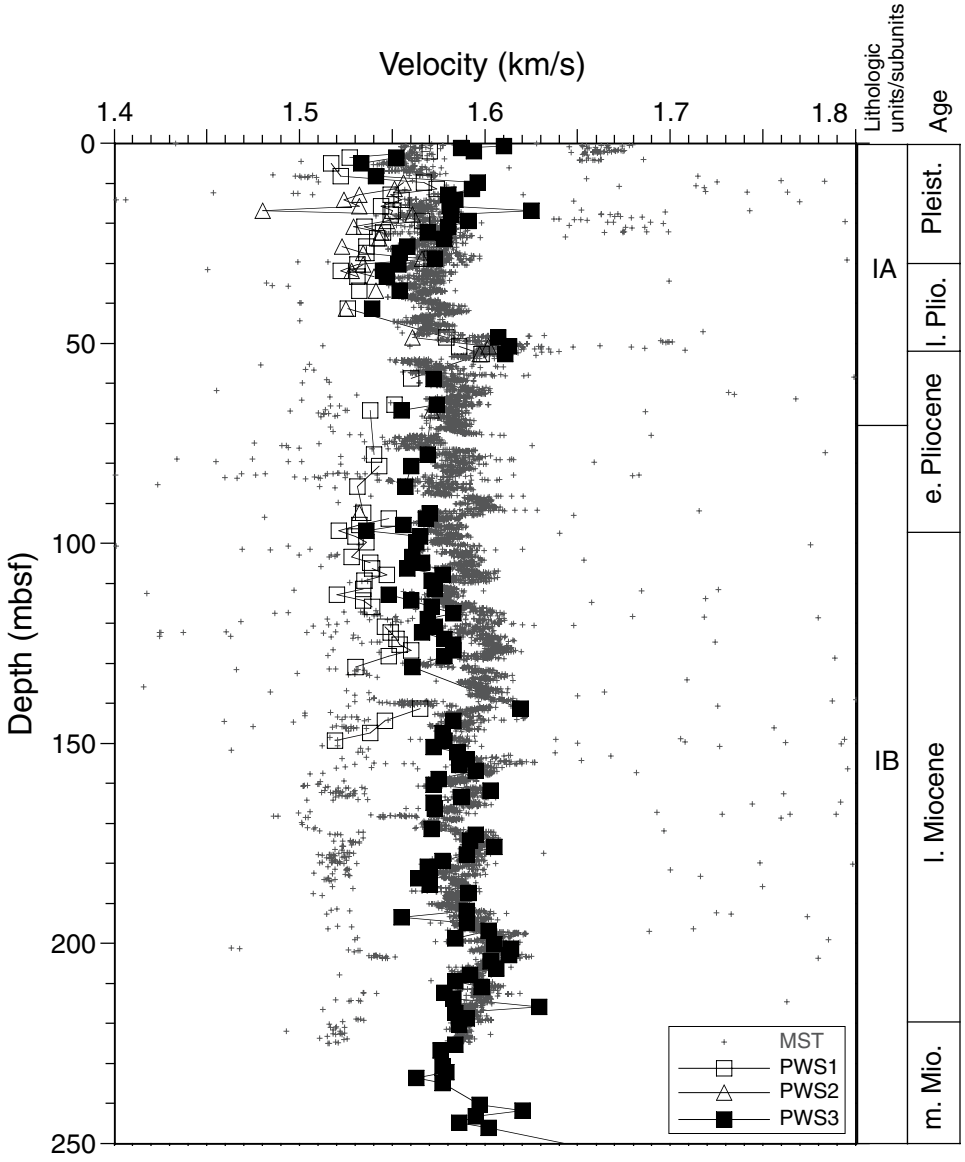

Figure F32. *P*-wave velocities (PWS3) measured for discrete samples vs. depth for Hole 1172A.

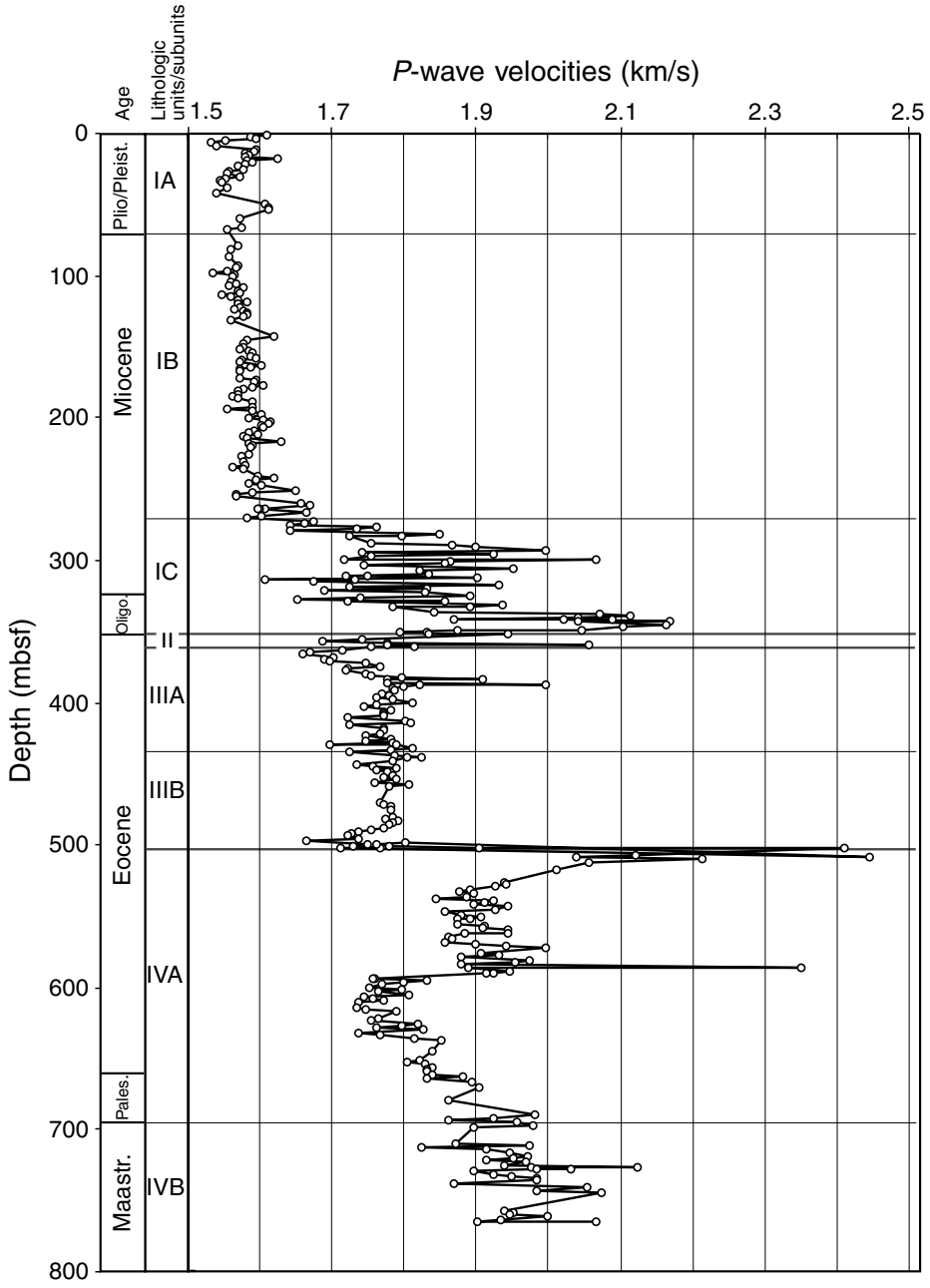

Figure F33. Thermal conductivity and porosity measured on whole cores vs. depth for Hole 1172A.

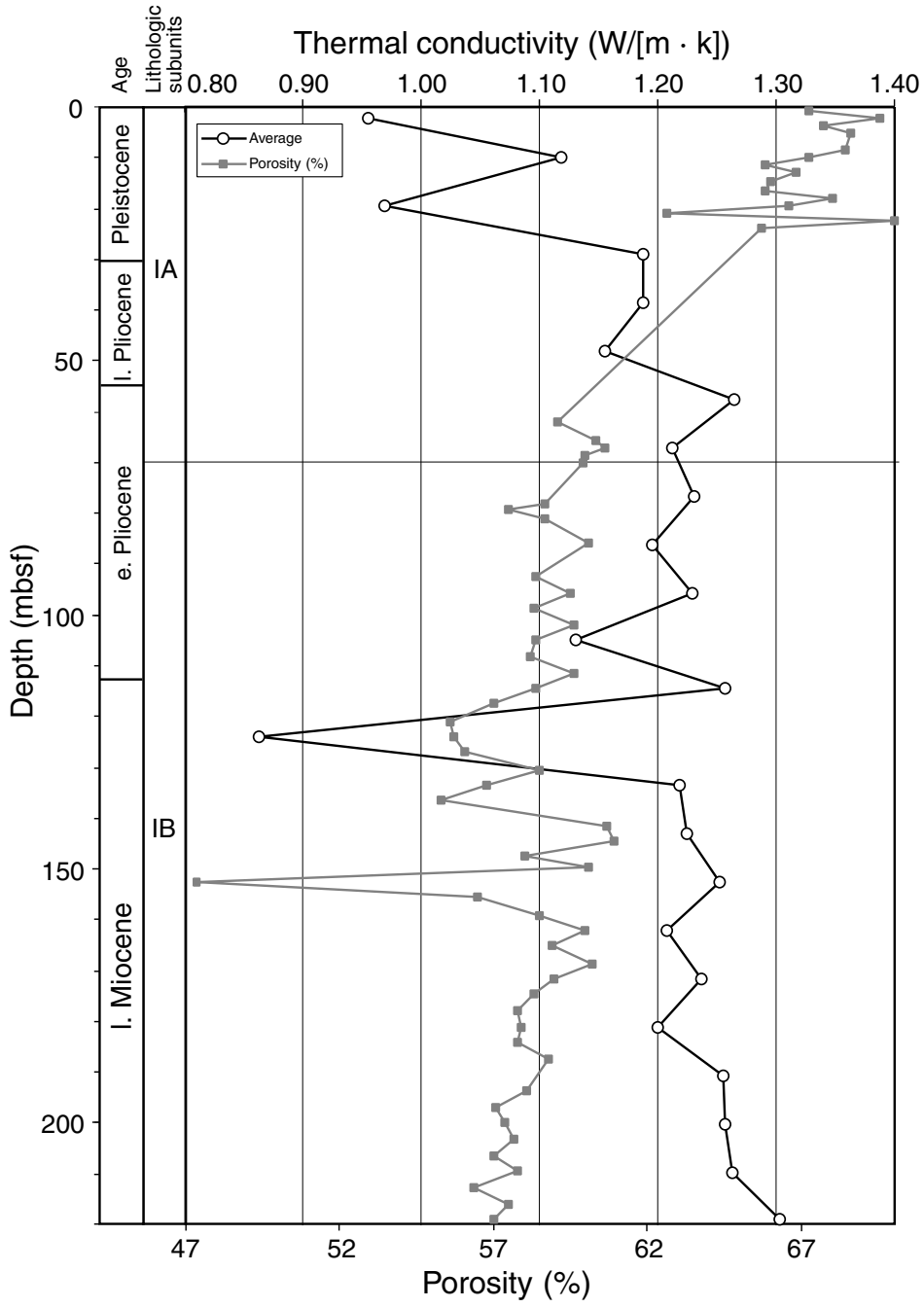

Figure F34. Wet bulk density, water content, and porosity measured at discrete intervals vs. depth for Site 1172.

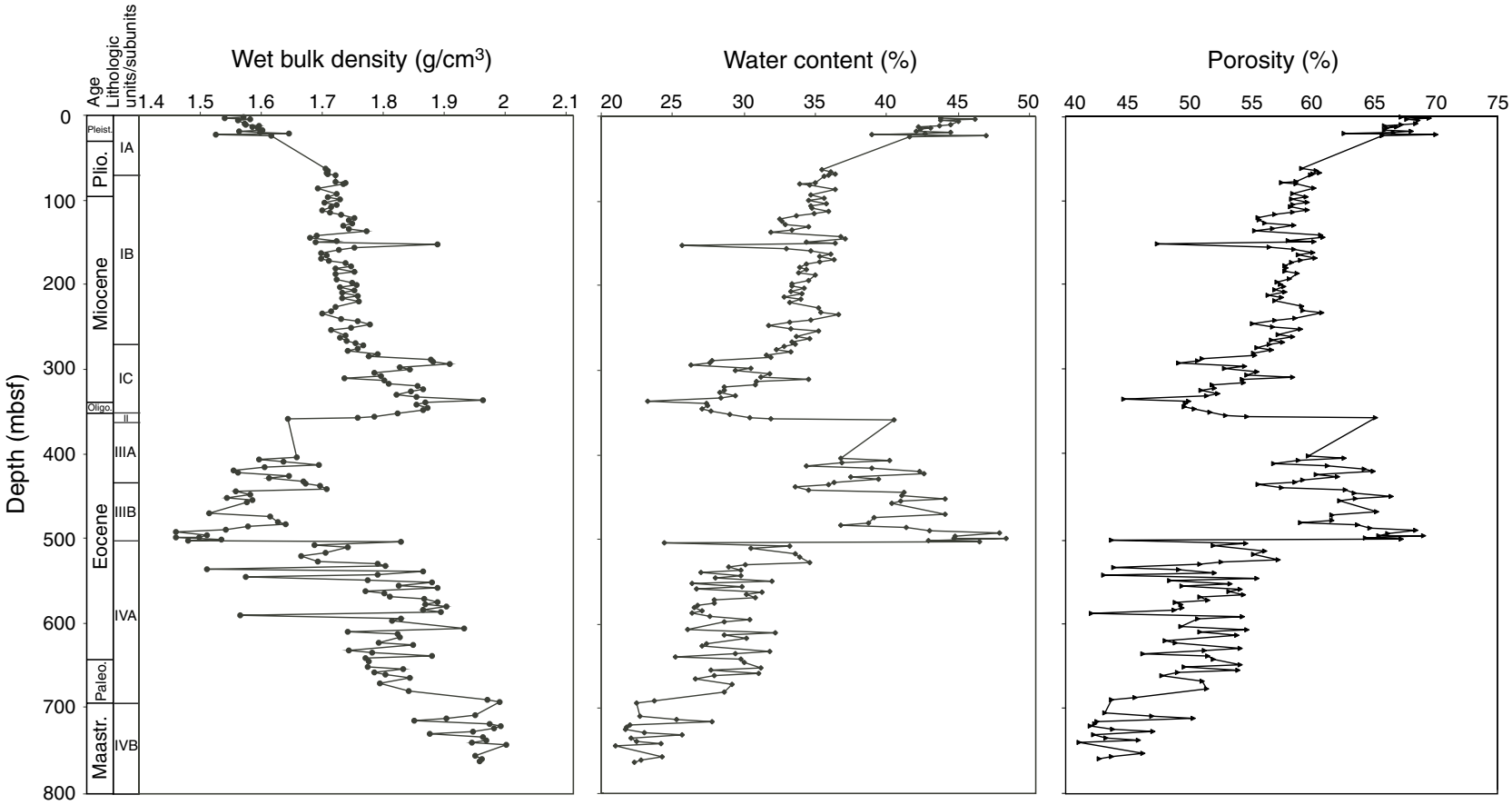

Figure F35. Temperature vs. depth for Site 1172.

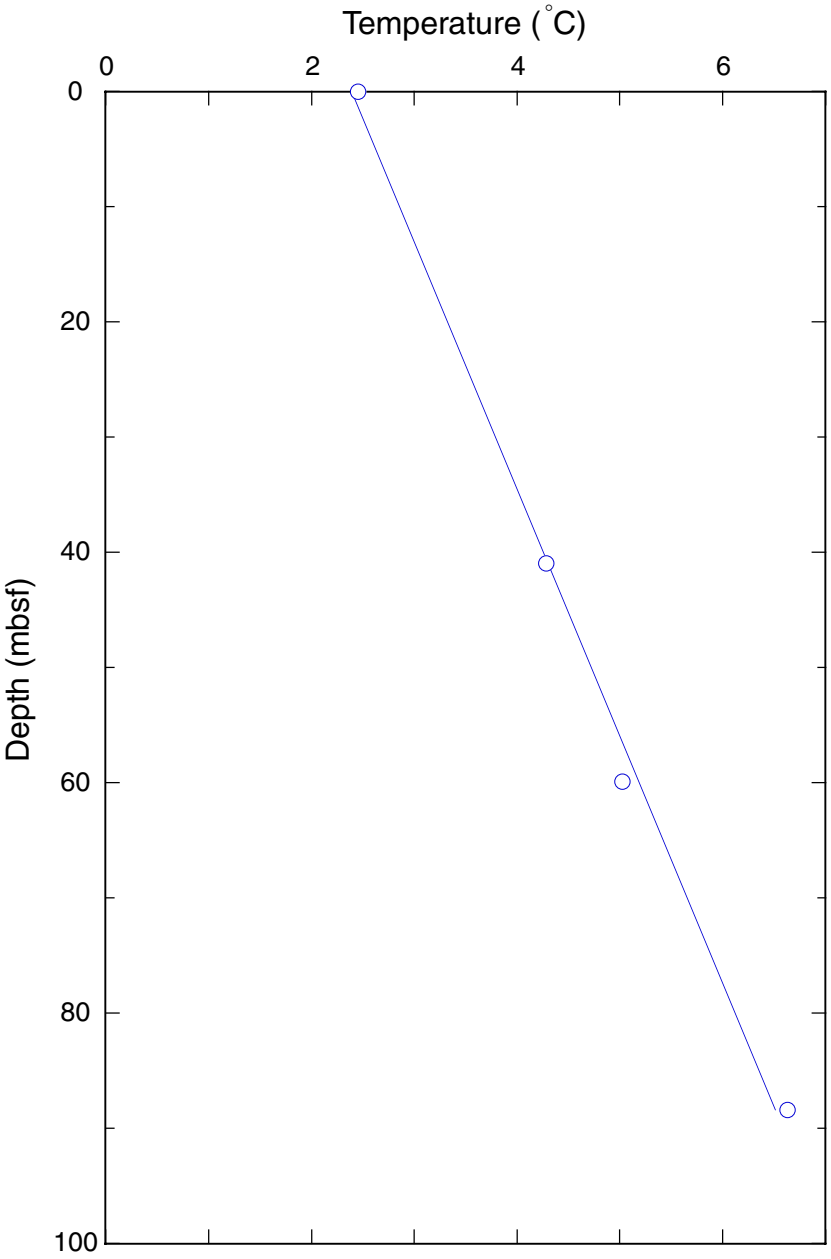

$y = 2.397 + 0.0466x$

Geothermal gradient: 46.6°C/km
Avg. thermal conductivity: ~1.18 (W/[m · K])
Heat flow: 55.08 mW/m^2

Figure F36. Undrained shear strength from miniature vane-shear measurements (line) and GRA density (dots) vs. depth for Hole 1172A.

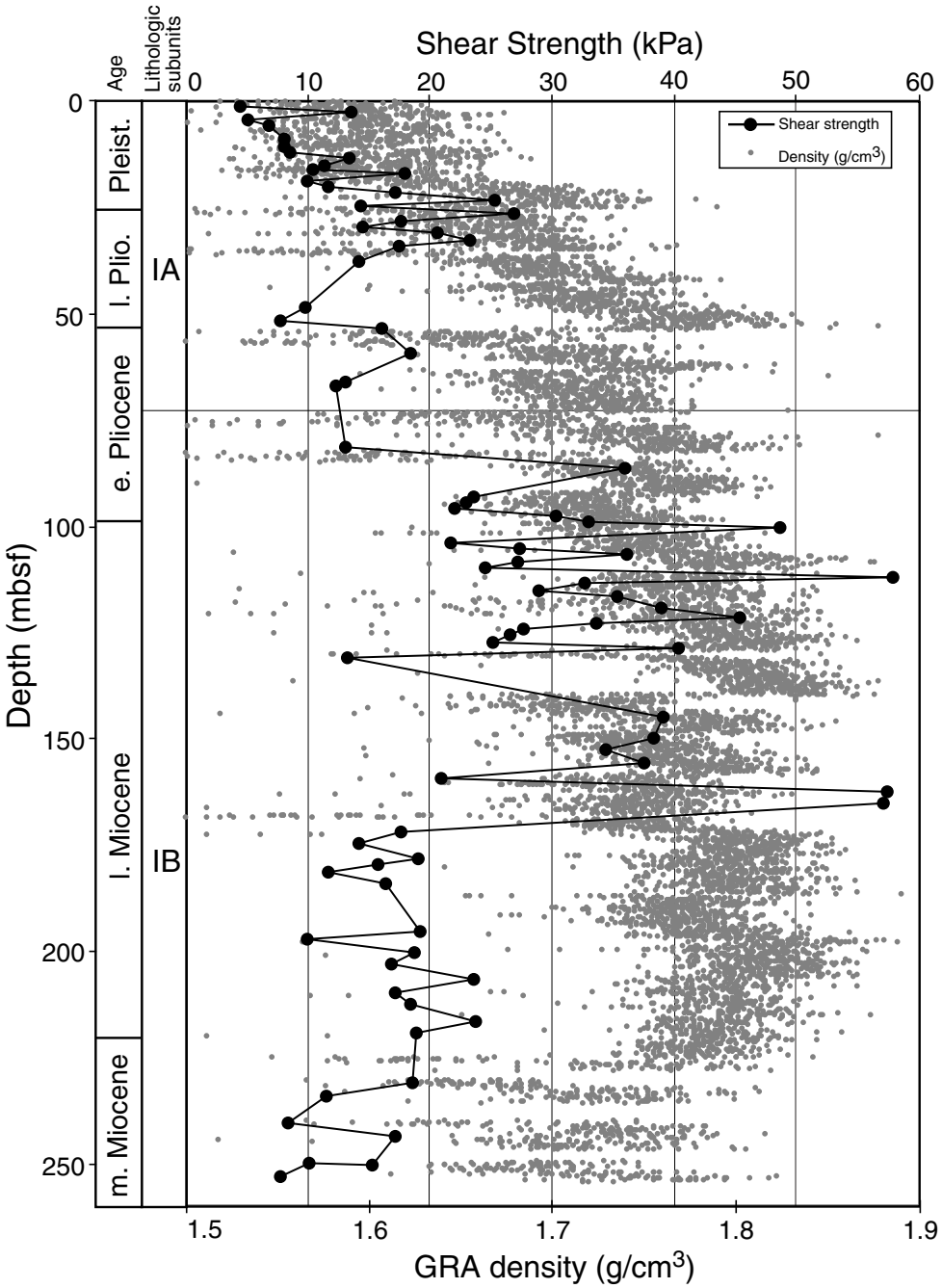

Figure F37. Details of the logging operations in Hole 1172D. Depths are shown in either meters below rig floor (mbrf) or meters below seafloor (mbsf).

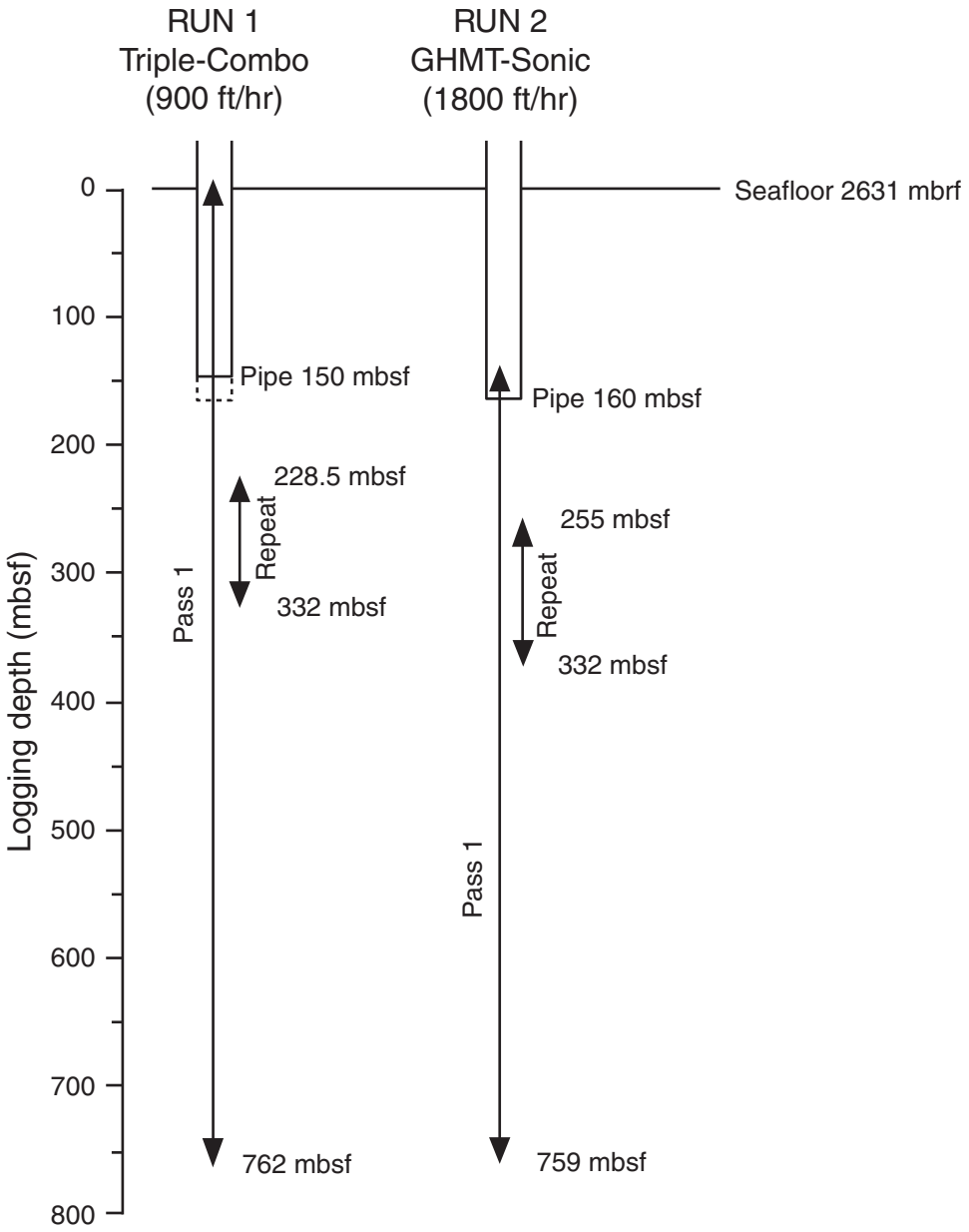

Figure F38. Caliper, gamma-ray, resistivity, and magnetic susceptibility (log and core) values from Hole 1172D.

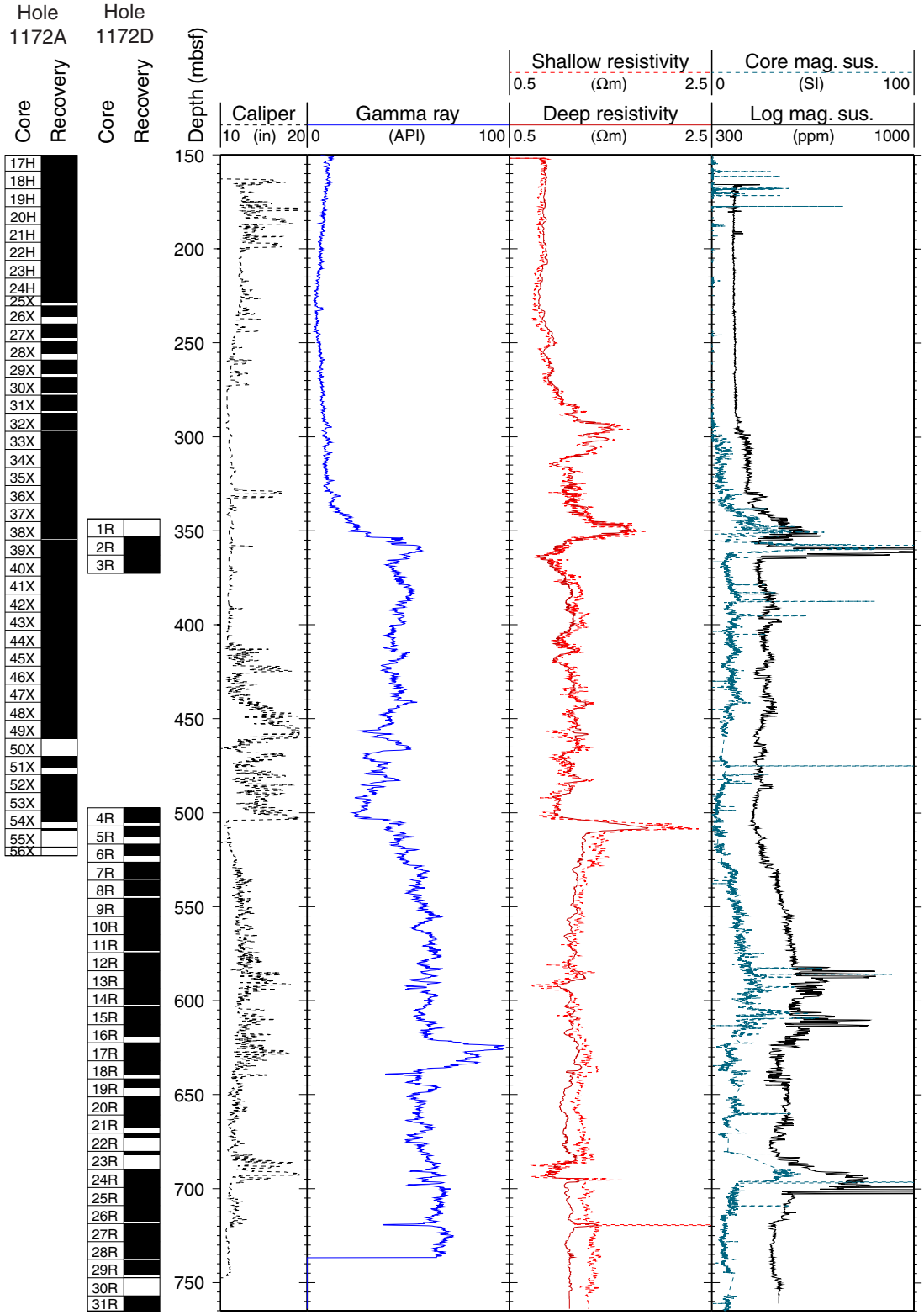

Figure F39. Velocity, density, porosity, and photoelectric effect (PEFL) values from Hole 1172D.

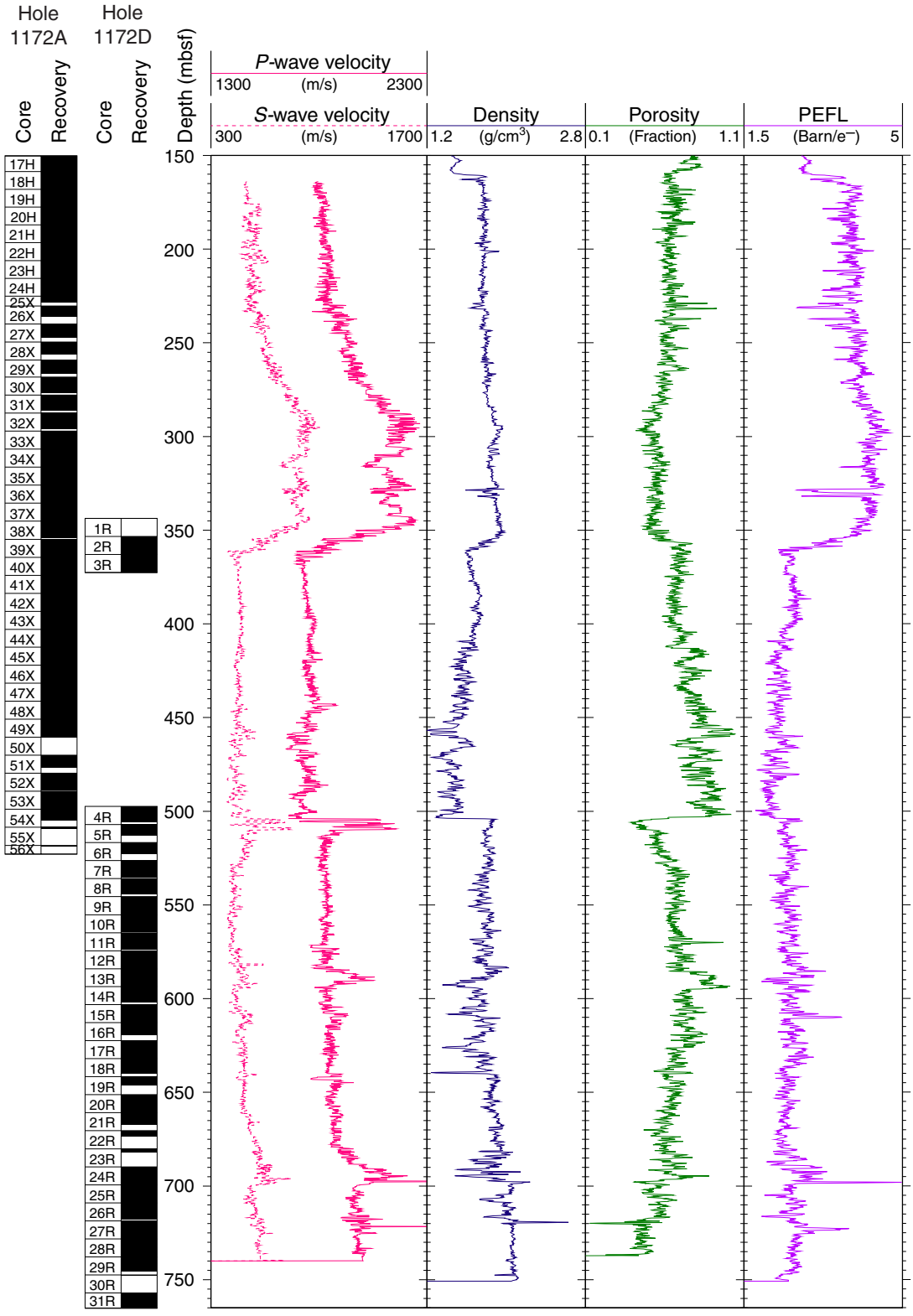

Figure F40. Total gamma-ray and spectral gamma-ray values from Hole 1172D. HSGR = total gamma radiation (from Th, K, and U). HCGR = gamma radiation from Th and K only.

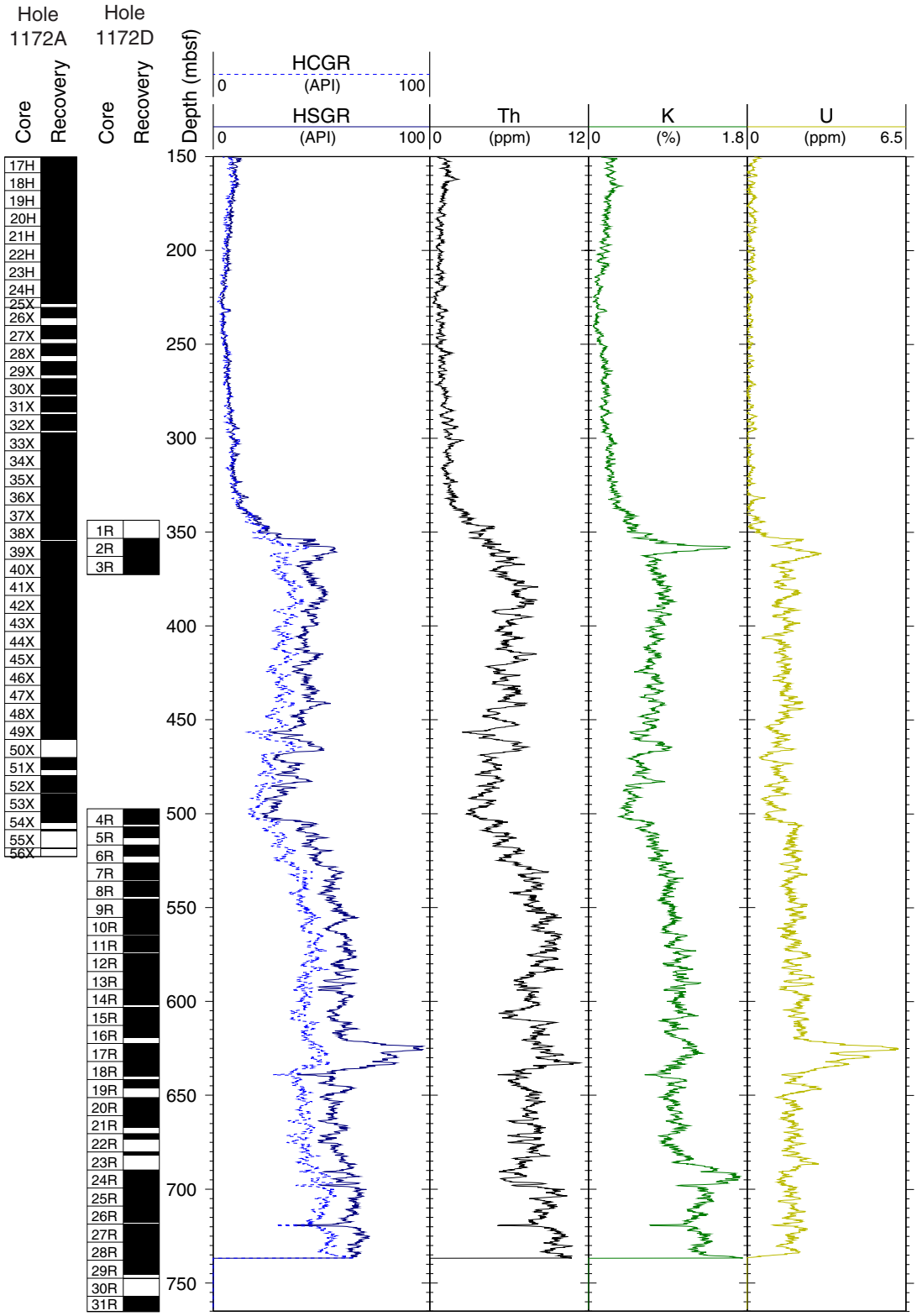

Figure F41. Downhole log bulk density plotted with core bulk density.

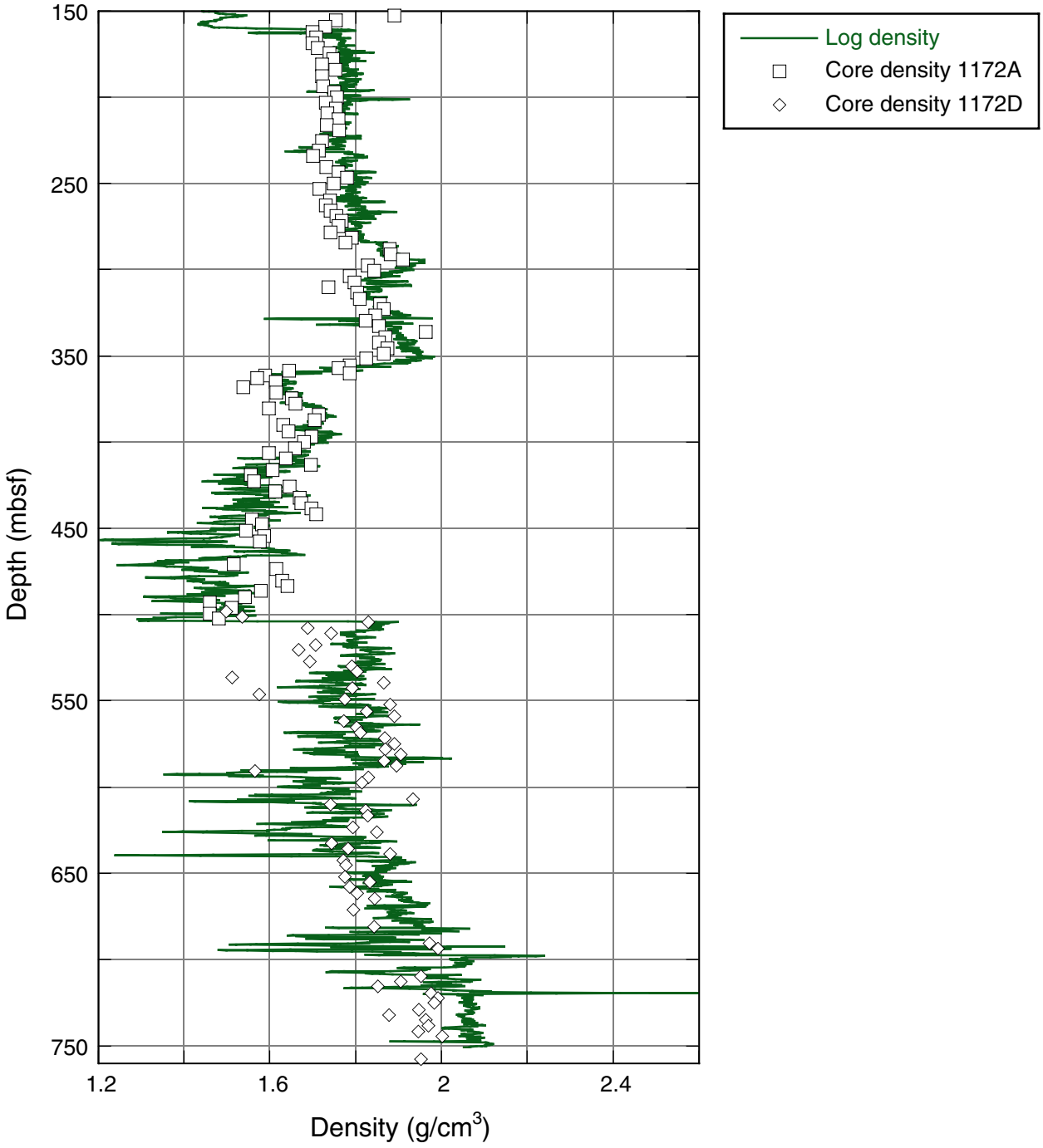

Figure F42. Downhole neutron porosity plotted with core porosity.

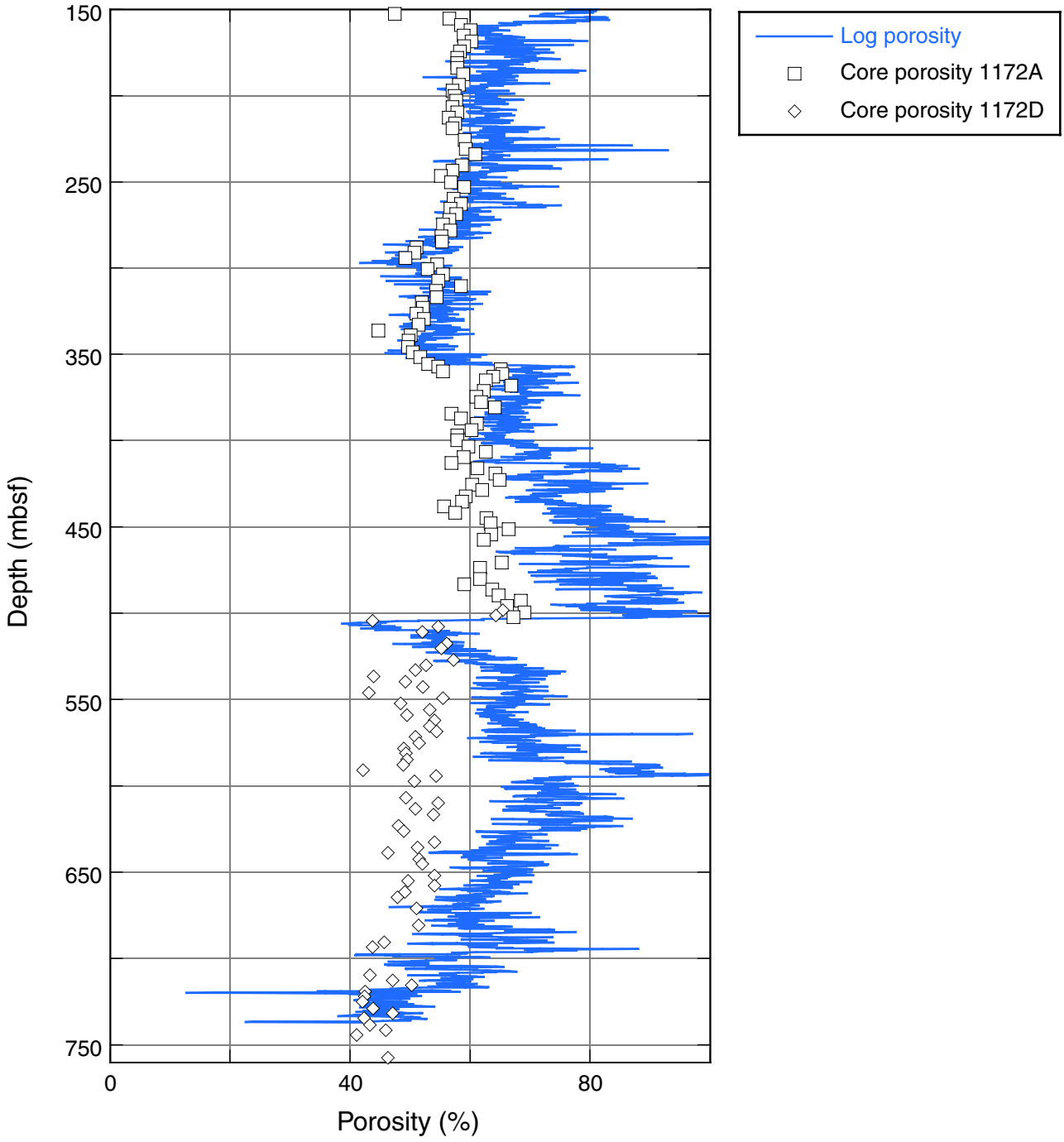

Figure F43. Downhole *P*-wave velocities (V_p) from the logs plotted with the V_p measured vertically on half cores.

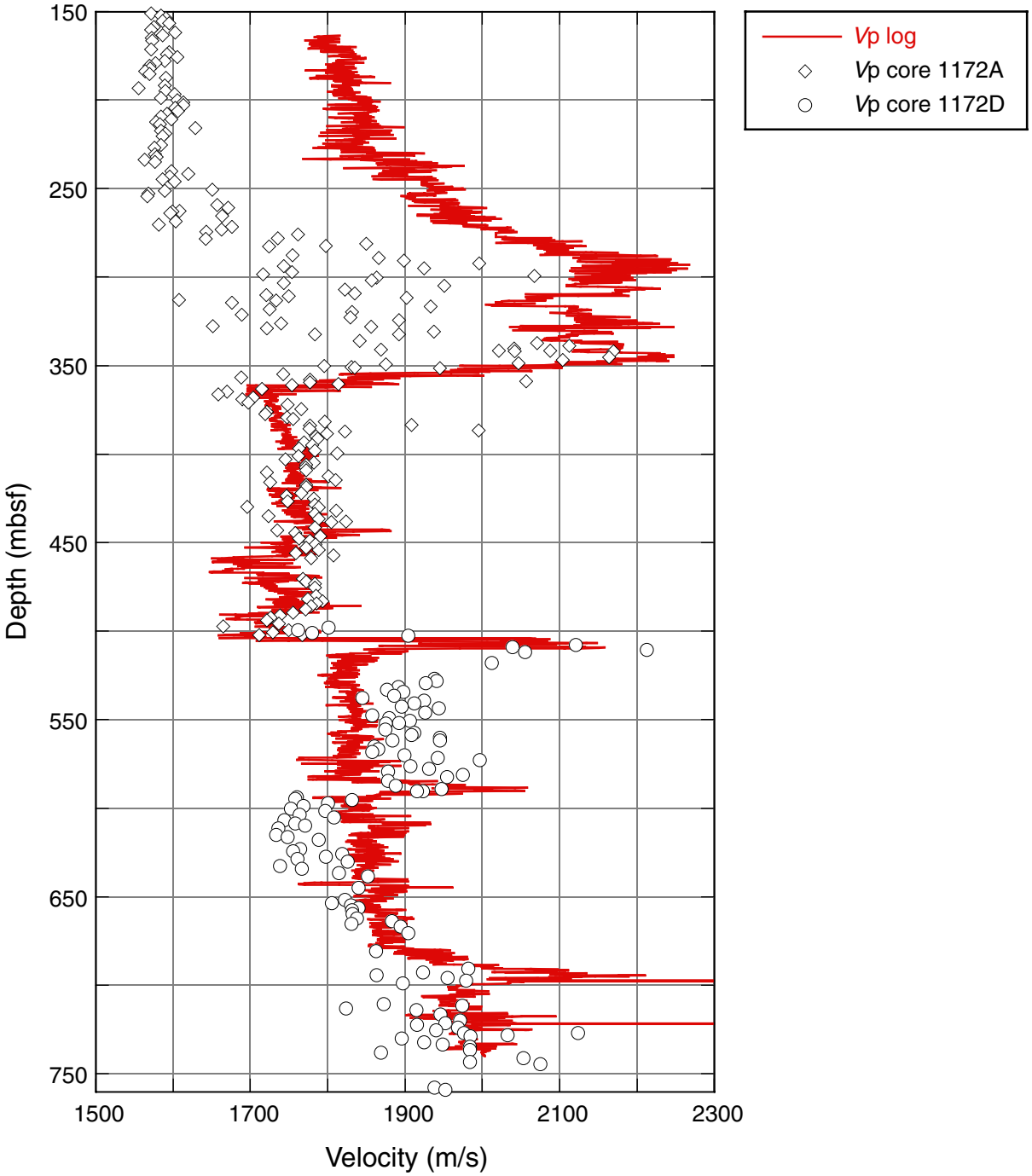

Table T1. Coring summary, Site 1172. (Continued on next two pages.)

Hole 1172A
Latitude: 43°57.5854′S
Longitude:149°55.6961′E
Time on site: 246.08 hr (0915 hr, 23 April–1520 hr, 3 May 2000)
Time on hole: 72.25 hr; 3 days, 15 min (0915 hr, 23 April–0930 hr, 26 April 2000)
Seafloor (drill pipe measurement from rig floor, mbrf): 2633.2
Distance between rig floor and sea level (m): 11.3
Water depth (drill pipe measurement from sea level, m): 2621.9
Total depth (from rig floor, mbrf): 3155.8
Total penetration (mbsf): 522.6
Total length of cored section (m): 522.6
Total core recovered (m): 483.72
Core recovery (%): 92.6
Total number of cores: 56

Hole 1172B
Latitude: 43°57.5750′S
Longitude: 149°55.7010′E
Time on hole: 24.75 hr; 1 day, 45 min (0930 hr, 26 April–1015 hr, 27 April 2000)
Seafloor (drill pipe measurement from rig floor, mbrf): 2633.6
Distance between rig floor and sea level (m): 11.3
Water depth (drill pipe measurement from sea level, m): 2622.0
Total depth (from rig floor, mbrf): 2836.0
Total penetration (mbsf): 202.4
Total length of cored section (m): 202.4
Total core recovered (m): 206.7
Core recovery (%): 102.1
Total number of cores: 22

Hole 1172C
Latitude: 43°57.5684′S
Longitude: 149°55.7077′E
Time on hole: 25.25 hr; 1 day, 1 hr, 15 min (1015 hr, 26 April–1130 hr, 28 April 2000)
Seafloor (drill pipe measurement from rig floor, mbrf): 2633.0
Distance between rig floor and sea level (m): 11.3
Water depth (drill pipe measurement from sea level, m): 2621.7
Total depth (from rig floor, mbrf): 2804.0
Total penetration (mbsf): 171.0
Total length of cored section (m): 171.0
Total core recovered (m): 172.64
Core recovery (%): 101.0
Total number of cores: 18

Hole 1172D
Latitude: 43°57.5545′S
Longitude: 149°55.7169′E
Time on hole: 123.83 hr; 5 days,3 hr, 50 min (1130 hr, 28 April–1520 hr, 3 May 2000)
Seafloor (drill pipe measurement from rig floor, mbrf): 2633.0
Distance between rig floor and sea level (m): 11.3
Water depth (drill pipe measurement from sea level, m): 2621.7
Total depth (from rig floor, mbrf): 3399.5
Total penetration (mbsf): 766.5
Total length of cored section (m): 297.9
Total length of drilled intervals (m): 468.6
Total core recovered (m): 237.09
Core recovery (%): 79.6
Total number of cores: 31
Total number of drilled intervals (DI): 2

Core	Date (2000)	Time (local)	Depth (mbsf) Top	Depth (mbsf) Bottom	Length (m) Cored	Length (m) Recovered	Recovery (%)
189-1172A-							
1H	23 April	1650	0.0	6.3	6.3	6.29	99.8
2H	23 April	1745	6.3	15.8	9.5	9.90	104.2
3H	23 April	1900	15.8	25.3	9.5	9.79	103.1
4H	23 April	1940	25.3	34.8	9.5	9.86	103.8
5H	23 April	2125	34.8	44.3	9.5	9.75	102.6
6H	23 April	2215	44.3	53.8	9.5	9.72	102.3
7H	23 April	2315	53.8	63.3	9.5	10.04	105.7
8H	24 April	0015	63.3	72.8	9.5	9.97	105.0
9H	24 April	0235	72.8	82.3	9.5	9.79	103.1
10H	24 April	0335	82.3	91.8	9.5	9.85	103.7

Table T1 (continued).

Core	Date (2000)	Time (local)	Depth (mbsf) Top	Depth (mbsf) Bottom	Length (m) Cored	Length (m) Recovered	Recovery (%)
11H	24 April	0430	91.8	101.3	9.5	9.59	101.0
12H	24 April	0530	101.3	110.8	9.5	8.80	92.6
13H	24 April	0630	110.8	120.3	9.5	10.01	105.4
14H	24 April	0725	120.3	129.8	9.5	9.00	94.7
15H	24 April	0820	129.8	139.3	9.5	10.04	105.7
16H	24 April	1030	139.3	148.8	9.5	9.97	105.0
17H	24 April	1155	148.8	158.3	9.5	9.52	100.2
18H	24 April	1255	158.3	167.8	9.5	9.61	101.2
19H	24 April	1355	167.8	177.3	9.5	10.02	105.5
20H	24 April	1455	177.3	186.8	9.5	9.20	96.8
21H	24 April	1555	186.8	196.3	9.5	10.06	105.9
22H	24 April	1655	196.3	205.8	9.5	9.93	104.5
23H	24 April	1755	205.8	215.3	9.5	9.52	100.2
24H	24 April	1930	215.3	224.8	9.5	9.90	104.2
25X	24 April	2105	224.8	230.1	5.3	3.26	61.5
26X	24 April	2200	230.1	239.7	9.6	5.79	60.3
27X	24 April	2250	239.7	249.3	9.6	7.21	75.1
28X	24 April	2345	249.3	258.9	9.6	6.40	66.7
29X	25 April	0035	258.9	268.0	9.1	7.42	81.5
30X	25 April	0125	268.0	277.6	9.6	8.50	88.5
31X	25 April	0220	277.6	287.2	9.6	8.35	87.0
32X	25 April	0315	287.2	296.8	9.6	8.64	90.0
33X	25 April	0405	296.8	306.5	9.7	9.62	99.2
34X	25 April	0455	306.5	316.1	9.6	9.89	103.0
35X	25 April	0545	316.1	325.7	9.6	8.87	92.4
36X	25 April	0640	325.7	335.3	9.6	9.43	98.2
37X	25 April	0730	335.3	344.9	9.6	9.85	102.6
38X	25 April	0825	344.9	354.6	9.7	8.91	91.9
39X	25 April	0915	354.6	364.2	9.6	9.80	102.1
40X	25 April	1015	364.2	373.8	9.6	9.85	102.6
41X	25 April	1135	373.8	383.4	9.6	9.70	101.0
42X	25 April	1235	383.4	393.0	9.6	9.70	101.0
43X	25 April	1340	393.0	402.6	9.6	9.88	102.9
44X	25 April	1445	402.6	412.2	9.6	9.92	103.3
45X	25 April	1555	412.2	421.8	9.6	9.96	103.8
46X	25 April	1655	421.8	431.4	9.6	9.91	103.2
47X	25 April	1750	431.4	441.0	9.6	9.94	103.5
48X	25 April	1855	441.0	450.6	9.6	9.90	103.1
49X	25 April	2020	450.6	460.2	9.6	9.90	103.1
50X	25 April	2150	460.2	469.8	9.6	0.08	0.8
51X	25 April	2305	469.8	479.4	9.6	6.49	67.6
52X	26 April	0040	479.4	489.0	9.6	9.30	96.9
53X	26 April	0205	489.0	498.6	9.6	9.85	102.6
54X	26 April	0350	498.6	508.3	9.7	5.97	61.6
55X	26 April	0555	508.3	518.0	9.7	0.82	8.5
56X	26 April	0755	518.0	522.6	4.6	0.35	7.6
				Totals:	522.6	483.72	92.6
189-1172B-							
1H	26 April	1120	0.0	2.9	2.9	2.84	97.9
2H	26 April	1205	2.9	12.4	9.5	9.88	104.0
3H	26 April	1255	12.4	21.9	9.5	9.75	102.6
4H	26 April	1345	21.9	31.4	9.5	9.92	104.4
5H	26 April	1500	31.4	40.9	9.5	9.96	104.8
6H	26 April	1550	40.9	50.4	9.5	9.69	102.0
7H	26 April	1700	50.4	59.9	9.5	9.98	105.1
8H	26 April	1800	59.9	69.4	9.5	9.93	104.5
9H	26 April	1900	69.4	78.9	9.5	9.85	103.7
10H	26 April	2005	78.9	88.4	9.5	10.20	107.4
11H	26 April	2100	88.4	97.9	9.5	9.71	102.2
12H	26 April	2155	97.9	107.4	9.5	10.10	106.3
13H	26 April	2255	107.4	116.9	9.5	9.17	96.5
14H	26 April	2355	116.9	126.4	9.5	9.61	101.2
15H	27 April	0100	126.4	135.9	9.5	9.76	102.7
16H	27 April	0210	135.9	145.4	9.5	9.97	105.0
17H	27 April	0310	145.4	154.9	9.5	8.97	94.4
18H	27 April	0415	154.9	164.4	9.5	9.27	97.6
19H	27 April	0520	164.4	173.9	9.5	9.68	101.9
20H	27 April	0620	173.9	183.4	9.5	9.28	97.7

Table T1 (continued).

Core	Date (2000)	Time (local)	Depth (mbsf) Top	Depth (mbsf) Bottom	Length (m) Cored	Length (m) Recovered	Recovery (%)
21H	27 April	0725	183.4	192.9	9.5	9.29	97.8
22H	27 April	0850	192.9	202.4	9.5	9.89	104.1
				Totals:	202.4	206.70	102.1
189-1172C-							
1H	27 April	1200	0.0	9.5	9.5	9.55	100.5
2H	27 April	1245	9.5	19.0	9.5	9.61	101.2
3H	27 April	1340	19.0	28.5	9.5	9.45	99.5
4H	27 April	1430	28.5	38.0	9.5	9.54	99.4
5H	27 April	1510	38.0	47.5	9.5	9.41	99.1
6H	27 April	1600	47.5	57.0	9.5	9.49	99.9
7H	27 April	1655	57.0	66.5	9.5	9.20	96.8
8H	27 April	1745	66.5	76.0	9.5	9.77	102.8
9H	27 April	1835	76.0	85.5	9.5	9.86	103.8
10H	27 April	1935	85.5	95.0	9.5	9.01	94.8
11H	27 April	2025	95.0	104.5	9.5	9.95	104.7
12H	27 April	2120	104.5	114.0	9.5	10.04	105.7
13H	27 April	2215	114.0	123.5	9.5	9.87	103.9
14H	27 April	2310	123.5	133.0	9.5	9.67	101.8
15H	28 April	0005	133.0	142.5	9.5	9.01	94.8
16H	28 April	0105	142.5	152.0	9.5	9.85	103.7
17H	28 April	0220	152.0	161.5	9.5	9.44	99.4
18H	28 April	0400	161.5	171.0	9.5	9.92	104.4
				Totals:	171	172.64	101.0
189-1172D-							
Drilled			0.0	343.6			
1R	29 April	0430	343.6	353.2	9.6	0.00	0.0
2R	29 April	0555	353.2	362.8	9.6	9.82	102.3
3R	29 April	0710	362.8	372.4	9.6	9.89	103.0
Drilled			372.4	497.4			
4R	29 April	1500	497.4	507.0	9.6	8.03	83.7
5R	29 April	1730	507.0	516.6	9.6	6.02	62.7
6R	29 April	2000	516.6	526.2	9.6	6.11	63.7
7R	29 April	2225	526.2	535.8	9.6	9.10	94.8
8R	30 April	0020	535.8	545.4	9.6	8.24	85.8
9R	30 April	0210	545.4	555.1	9.7	9.93	102.4
10R	30 April	0350	555.1	564.7	9.6	9.27	96.6
11R	30 April	0540	564.7	574.3	9.6	8.91	92.8
12R	30 April	0730	574.3	583.9	9.6	10.02	104.4
13R	30 April	0920	583.9	593.5	9.6	9.78	101.9
14R	30 April	1100	593.5	603.1	9.6	8.42	87.7
15R	30 April	1305	603.1	612.7	9.6	9.90	103.1
16R	30 April	1505	612.7	622.3	9.6	6.38	66.5
17R	30 April	1700	622.3	631.9	9.6	9.96	103.8
18R	30 April	1905	631.9	641.5	9.6	7.68	80.0
19R	30 April	2120	641.5	651.1	9.6	4.46	46.5
20R	30 April	2330	651.1	660.7	9.6	9.80	102.1
21R	1 May	0125	660.7	670.3	9.6	6.56	68.3
22R	1 May	0350	670.3	680.0	9.7	2.79	28.8
23R	1 May	0545	680.0	689.7	9.7	2.11	21.8
24R	1 May	0730	689.7	699.3	9.6	9.38	97.7
25R	1 May	0910	699.3	708.9	9.6	9.93	103.4
26R	1 May	1145	708.9	718.5	9.6	8.52	88.8
27R	1 May	1345	718.5	728.1	9.6	9.77	101.8
28R	1 May	1535	728.1	737.7	9.6	9.15	95.3
29R	1 May	1800	737.7	747.3	9.6	7.76	80.8
30R	1 May	1945	747.3	756.9	9.6	0.11	1.2
31R	1 May	2215	756.9	766.5	9.6	9.29	96.8
				Coring totals:	297.9	237.09	79.6
				Drilled totals:	468.6		
				Totals:	766.5		

Table T2. Lithostratigraphic summary, Site 1172.

Lithostratigraphic units and subunits	Series	Core intervals	Lithology	Depth (mbsf)	Comments
IA	Holocene to early Pliocene	1172A-1H to 8H; 1172B-1H to 8H; 1172C-1H to 8H	Nannofossil foraminifer ooze, foraminifer-bearing nannofossil ooze, and nannofossil ooze	0-70.0	Foraminifers decrease downsection.
IB	early Pliocene to late Miocene	1172A-8H to 30X; 1172B-8H to 22H; 1172C-8H to 18H	Nannofossil ooze	70.0-271.2	
IC	early Miocene to middle Miocene	1172A-30X to 39X; 1171D-1R	Foraminifer-bearing nannofossil chalk, nannofossil chalk, clay- and foraminifer- bearing nannofossil chalk, foraminiferal-and clay-bearing nannofossil chalk	271.2-355.8	Increase in clay and foraminifers downsection.
II	Oligocene to latest Eocene	1172A-39X; 1171D-2R	Diatom- and clay-bearing nannofossil chalk, silty diatomaceous claystone, spicules- and diatom-bearing clayey siltstone, diatom-bearing silty claystone, and diatomaceous clayey siltstone	355.8-361.1	Transitional unit. Major lithologic changes, very slow sedimentation rates (condensed section).
IIIA	late to middle Eocene	1172A-39X to 47X; 1171D-2R to 3R	Diatom- and nannofossil-bearing claystone, diatom-bearing claystone, diatom claystone, and nannofossil-bearing diatom silty claystone	361.1-433.9	Increasing dissolution of calcareous microfossils.
IIIB	middle Eocene	1172A-47X to 54X; 1172D-4R	Diatomaceous silty claystone and diatom-bearing silty claystone	433.9-503.4	Nearly total absence of calcareous microfossils.
IVA	middle Eocene to early Paleocene	1172A-54X to 56X; 1172D-4R to 24R-5	Claystone, nannofossil-bearing claystone, silty claystone, and organic-bearing silty claystone	503.4-696.0	Significant increase in glauconite just above the K/T boundary.
IVB	Cretaceous (Maastrichtian)	1172D-24R-5 to 31R	Claystone and silty claystone	696.0-766.5	Excellent preservation of calcareous microfossils in upper portion.

Table T3. Stratigraphic distribution of selected nannofossil species, Site 1172. (**See table notes.** Continued on next five pages.)

Core, section, interval (cm)	Depth (mbsf)	Preservation	Group abundance	*Ahmuellerella octoradiata*	*Amaurolithus amplificus*	*Amaurolithus delicatus*	*Amaurolithus ninae*	*Amaurolithus primus*	*Amaurolithus tricorniculatus*	*Arkhangelskiella cymbiformis*	*Calcidiscus leptoporus*	*Calcidiscus macintyrei*	*Calcidiscus premacintyrei*	*Chiasmolithus altus*	*Chiasmolithus expansus*	*Chiasmolithus oamaruensis*	*Chiasmolithus solitus*	*Chiasmolithus* spp.	*Coccolithus miopelagicus*	*Coccolithus pelagicus*	*Cribrosphaerella daniae*	*Cyclicargolithus abisectus*	*Cyclicargolithus floridanus*	*Dictyococcites bisectus*	*Dictyococcites callidus*	*Discoaster bellus*	*Discoaster brouweri*	*Discoaster calcaris*	*Discoaster challengeri*	*Discoaster intercalaris*	*Discoaster lodoensis*	*Discoaster loeblichii*	*Discoaster pentaradiatus*
189-1172A-																																	
1H-CC, 10-15	6.24	G	A																														
2H-CC, 9-14	16.15	G	A																														
3H-CC, 15-20	25.54	G	A									A															R						
4H-CC, 12-17	35.11	G	A									C															R						R
5H-CC, 0-5	44.50	G	A									C																					R
6H-CC, 11-16	53.97	G	A																														
7H-CC, 27-32	63.79	G	A																														
8H-CC, 15-20	73.22	M	A					R			F	F								A							F	R					R
9H-CC, 0-7	82.52	M	A								F	F								C							R			R			
10H-CC, 15-20	92.10	M	A								A	A								A											R		
11H-CC, 7-12	101.34	M	A			F	R	R			A									C							R			F			
12H-CC, 10-15	110.05	M	A								F	F								A										R			
13H-CC, 26-31	120.76	M	A								F																			C	R		
14H-CC, 10-16	129.24	M	A								C	C								A							R		R		F		
15H-CC, 22-27	139.79	M	A								F	F																	C		C		
16H-CC, 22-27	149.22	M	A								F	C								A									F				
17H-CC, 19-24	158.27	M	A									C																					
18H-CC, 0-6	167.85	M	A									C															R						R
19H-CC, 28-34	177.76	M	A									C															R						R
20H-CC, 5-11	186.44	M	A									C																					
21H-CC, 33-38	196.81	M	A									C																					
22H-CC, 21-26	206.18	M	A									C																					
23H-CC, 12-17	215.27	M	A									C																					
24H-CC, 15-20	225.15	M	A									C																					
25X-CC, 14-19	228.01	M	A									C																					
26X-CC, 29-34	235.84	M	A									C							C														
27X-CC, 25-30	246.86	M	A									C											C										
28X-CC, 16-21	255.65	M	A									C											C										
29X-CC, 22-27	266.27	M	A								C	F	F							C			F			R							
30X-CC, 10-15	276.45	M	A										C						F	A			C										
31X-CC, 21-26	285.90	M	A								C		C							C			A										
32X-CC, 31-36	295.79	M	A								C	F	F						F	C			C										
33X-CC, 19-24	306.37	M	A								F		C						F	C			C										
34X-CC, 23-28	316.34	M	A								F	F	F							C			A										
35X-CC, 24-29	324.92	M	A																	A		F	C										
36X-CC, 21-26	335.08	M	A																F	C		C	C										
37X-CC, 38-43	345.10	M	A																	C		C	C	C									
38X-CC, 24-29	353.76	M	A											A						C		F	A	C									
39X-CC, 27-33	364.34	M	A													A																	
40X-CC, 26-31	374.00	M	A												C									R									
41X-CC, 31-36	383.60	M	A												C	R																	
42X-CC, 51-56	393.18	M	A																														
43X-CC, 33-38	402.83	M	A														C																
44X-CC, 32-37	412.47	P	C														R																
45X-CC, 41-46	422.11	P	C																														
46X-CC, 36-41	431.66	P	R																														
47X-CC, 36-41	441.29		B																														
48X-CC, 36-41	450.85	P	R																														
49X-CC, 43-48	460.45		B																														
50X-CC, 0-8	460.20		B																														
51X-CC, 43-48	476.19		B																														
52X-CC, 39-44	488.65		B																														
53X-CC, 34-39	498.80	P	C												F		F																
54X-CC, 12-17	504.44	M	A														C																
55X-CC, 26-31	509.07	P	F															F															
56X-CC, 23-33	518.23	P	C																														
189-1172B-																																	
1H-CC, 8-13	2.79	G	A																														

Table T3 (continued).

Core, section, interval (cm)	Depth (mbsf)	Preservation	Group abundance	*Discoaster quinqueramus*	*Discoaster* spp.	*Discoaster surculus*	*Discoaster triradiatus*	*Discoaster variabilis*	*Eiffellithus turriseiffelii*	*Ericsonia formosa*	*Gephyrocapsa* >4.5 µm	*Gephyrocapsa* spp. (small)	*Helicosphaera kamptneri*	*Helicosphaera* spp.	*Micula decussata*	*Neococcolithes dubius*	*Nephrolithus coraystus*	*Nephrolithus frequens*	*Pontosphaera* spp.	*Prediscosphaera cretacea*	*Pseudoemiliania lacunosa*	*Reticulofenestra dictyoda*	*Reticulofenestra gelida*	*Reticulofenestra perplexa*	*Reticulofenestra psuedoumbilica*	*Reticulofenestra reticulata*	*Reticulofenestra samodurovii*	*Reticulofenestra* spp.	*Reticulofenestra umbilicata*	*Sphenolithus heteromorphus*	*Sphenolithus moriformis*	*Triquetrorhabdulus rugosus*	*Zygrhablithus bijugatus*
189-1172A-																																	
1H-CC, 10-15	6.24	G	A								A																						
2H-CC, 9-14	16.15	G	A								A										C												
3H-CC, 15-20	25.54	G	A																		C												
4H-CC, 12-17	35.11	G	A																														
5H-CC, 0-5	44.50	G	A			R																											
6H-CC, 11-16	53.97	G	A			R																	C		F								
7H-CC, 27-32	63.79	G	A																				C		C								
8H-CC, 15-20	73.22	M	A			F	R						F										C		C								
9H-CC, 0-7	82.52	M	A	R		F		F															C										
10H-CC, 15-20	92.10	M	A										F										D										
11H-CC, 7-12	101.34	M	A			R																	D		C								
12H-CC, 10-15	110.05	M	A			F		R															A		F								
13H-CC, 26-31	120.76	M	A	R		R		R															C		F							R	
14H-CC, 10-16	129.24	M	A					C																	F								
15H-CC, 22-27	139.79	M	A					C															A		C								
16H-CC, 22-27	149.22	M	A					C															C	R									
17H-CC, 19-24	158.27	M	A					C															C										
18H-CC, 0-6	167.85	M	A																				C										
19H-CC, 28-34	177.76	M	A																				C										
20H-CC, 5-11	186.44	M	A																				C										
21H-CC, 33-38	196.81	M	A																				C										
22H-CC, 21-26	206.18	M	A																				C										
23H-CC, 12-17	215.27	M	A																				C										
24H-CC, 15-20	225.15	M	A																				C										
25X-CC, 14-19	228.01	M	A																				C										
26X-CC, 29-34	235.84	M	A																				C										
27X-CC, 25-30	246.86	M	A																				C										
28X-CC, 16-21	255.65	M	A																				C										
29X-CC, 22-27	266.27	M	A																				A	C	R								
30X-CC, 10-15	276.45	M	A					R							F								F										
31X-CC, 21-26	285.90	M	A		A																				F						F		
32X-CC, 31-36	295.79	M	A		C																										F		
33X-CC, 19-24	306.37	M	A		A																				A					C	C		
34X-CC, 23-28	316.34	M	A		C																				C								
35X-CC, 24-29	324.92	M	A		C																				A						C		
36X-CC, 21-26	335.08	M	A		A																										C		
37X-CC, 38-43	345.10	M	A		A																										C		
38X-CC, 24-29	353.76	M	A																												C		
39X-CC, 27-33	364.34	M	A																							C			A				
40X-CC, 26-31	374.00	M	A																							F	C		A				R
41X-CC, 31-36	383.60	M	A																							C			C				
42X-CC, 51-56	393.18	M	A																							C			C				
43X-CC, 33-38	402.83	M	A																							C			C				
44X-CC, 32-37	412.47	P	C																										R				
45X-CC, 41-46	422.11	P	C																										C				
46X-CC, 36-41	431.66	P	R																														
47X-CC, 36-41	441.29		B																														
48X-CC, 36-41	450.85	P	R																														
49X-CC, 43-48	460.45		B																														
50X-CC, 0-8	460.20		B																														
51X-CC, 43-48	476.19		B																														
52X-CC, 39-44	488.65		B																														
53X-CC, 34-39	498.80	P	C																			C											
54X-CC, 12-17	504.44	M	A																									A					R
55X-CC, 26-31	509.07	P	F							R																	R	F					
56X-CC, 23-33	518.23	P	C																														
189-1172B-																																	
1H-CC, 8-13	2.79	G	A								A	A																					

Table T3 (continued).

Core, section, interval (cm)	Depth (mbsf)	Preservation	Group abundance	*Ahmuellerella octoradiata*	*Amaurolithus amplificus*	*Amaurolithus delicatus*	*Amaurolithus ninae*	*Amaurolithus primus*	*Amaurolithus tricorniculatus*	*Arkhangelskiella cymbiformis*	*Calcidiscus leptoporus*	*Calcidiscus macintyrei*	*Calcidiscus premacintyrei*	*Chiasmolithus altus*	*Chiasmolithus expansus*	*Chiasmolithus oamaruensis*	*Chiasmolithus solitus*	*Chiasmolithus* spp.	*Coccolithus miopelagicus*	*Coccolithus pelagicus*	*Cribrosphaerella daniae*	*Cyclicargolithus abisectus*	*Cyclicargolithus floridanus*	*Dictyococcites bisectus*	*Dictyococcites calidus*	*Discoaster bellus*	*Discoaster brouweri*	*Discoaster calcaris*	*Discoaster challengeri*	*Discoaster intercalaris*	*Discoaster lodoensis*	*Discoaster loeblichii*	*Discoaster pentaradiatus*
2H-CC, 14-19	12.73	G	A																														
3H-CC, 12-17	22.10	G	A																														
4H-CC, 11-16	31.77	G	A																								R						R
5H-CC, 15-20	41.31	G	A																														
6H-CC, 3-10	50.52	G	A																														
7H-CC, 13-18	60.33	G	A			R																											
8H-CC, 21-26	69.78	M	A																														
9H-CC, 23-28	79.20	M	A																														
10H-CC, 45-50	89.05	M	A																														
11H-CC, 0-5	98.06	M	A		R				R																								
12H-CC, 33-38	107.95	M	A																														
13H-CC, 69-74	116.52	M	A																														
14H-CC, 9-14	126.46	M	A																											R			
15H-CC, 16-21	136.11	M	A																													R	
16H-CC, 30-35	145.82	M	A																								F			R		R	
17H-CC, 0-7	154.30	M	A									C																				F	
18H-CC, 14-19	164.12	M	A								A	A																					
19H-CC, 16-21	174.03	M	A								C	C							F														
20H-CC, 8-16	183.10	M	A								A	A																					
21H-CC, 14-19	192.64	M	A								C	C							C														
22H-CC, 30-35	202.74	M	A								C	F								C													
189-1172C-																																	
1H-CC, 7-15	9.47	G	A																														
2H-CC, 9-14	19.06	G	A																														
3H-CC, 12-17	28.40	G	A									C															R						
4H-CC, 22-27	37.89	G	A																								R						R
5H-CC, 10-15	47.36	G	A																														
6H-CC, 18-23	56.94	G	A																														
7H-CC, 8-14	66.14	G	A			R																											
8H-CC, 15-20	76.22	G	A			R																											
9H-CC, 27-32	85.81	M	A																														
10H-CC, 0-6	94.45	M	A																														
11H-CC, 21-26	104.90	M	A		R																												
12H-CC, 29-34	114.49	M	A																														
13H-CC, 11-16	123.82	M	A																														
14H-CC, 12-17	133.12	M	A																														
15H-CC, 0-8	141.93	M	A									F															R		R			C	R
16H-CC, 14-20	152.29	M	A									C																				F	
17H-CC, 0-10	161.34	M	A								C	C															R					R	
18H-CC, 23-31	171.34	M	A								A	A								A													
189-1172D-																																	
2R-CC, 8-13	362.97	M	A													C								F									
3R-CC, 12-17	372.64	M	A													C								F									
4R-CC, 13-18	505.38	P	R														R						R										
5R-CC, 12-17	512.97	P	F														F																
6R-CC, 8-13	522.66	P	F														F																
7R-CC, 15-20	535.25	P	F														F																
8R-CC, 7-12	543.99	M	F												F		F			F					C								
9R-CC, 15-22	555.26	M	C														F														R		
10R-CC, 0-7	564.30		B																														
11R-CC, 0-7	573.54		B																														
12R-CC, 23-28	584.27		B																														
13R-CC, 0-5	593.63		B																														
14R-CC, 0-6	601.86		B																														
15R-CC, 22-27	612.95		B																														
16R-CC, 0-6	619.02		B																														
17R-CC, 17-22	632.21		B																														
18R-CC, 0-5	639.53		B																														
19R-CC, 23-28	645.91		B																														

Table T3 (continued).

Core, section, interval (cm)	Depth (mbsf)	Preservation	Group abundance	*Discoaster quinqueramus*	*Discoaster* spp.	*Discoaster surculus*	*Discoaster triradiatus*	*Discoaster variabilis*	*Eiffellithus turriseiffelii*	*Ericsonia formosa*	*Gephyrocapsa* >4.5 µm	*Gephyrocapsa* spp. (small)	*Helicosphaera kamptneri*	*Helicosphaera* spp.	*Micula decussata*	*Neococcolithes dubius*	*Nephrolithus corystus*	*Nephrolithus frequens*	*Pontosphaera* spp.	*Prediscosphaera cretacea*	*Pseudoemiliania lacunosa*	*Reticulofenestra dictyoda*	*Reticulofenestra gelida*	*Reticulofenestra perplexa*	*Reticulofenestra psuedoumbilica*	*Reticulofenestra reticulata*	*Reticulofenestra samodurovii*	*Reticulofenestra* spp.	*Reticulofenestra umbilica*	*Sphenolithus heteromorphus*	*Sphenolithus moriformis*	*Triquetrorhabdulus rugosus*	*Zygrhablithus bijugatus*
2H-CC, 14-19	12.73	G	A								A										C											
3H-CC, 12-17	22.10	G	A																		C											
4H-CC, 11-16	31.77	G	A			R															C											
5H-CC, 15-20	41.31	G	A																		C		F									
6H-CC, 3-10	50.52	G	A																				F									
7H-CC, 13-18	60.33	G	A			R																	C									
8H-CC, 21-26	69.78	M	A			R																	C									
9H-CC, 23-28	79.20	M	A			R																	C									
10H-CC, 45-50	89.05	M	A	R																			C									
11H-CC, 0-5	98.06	M	A	R																												
12H-CC, 33-38	107.95	M	A																													
13H-CC, 69-74	116.52	M	A			R																										
14H-CC, 9-14	126.46	M	A					R																								R
15H-CC, 16-21	136.11	M	A					F															A									
16H-CC, 30-35	145.82	M	A	R		R		F						C																		
17H-CC, 0-7	154.30	M	A					C						F																		
18H-CC, 14-19	164.12	M	A					F															A		A							
19H-CC, 16-21	174.03	M	A																													
20H-CC, 8-16	183.10	M	A																									A			F	
21H-CC, 14-19	192.64	M	A																									A				
22H-CC, 30-35	202.74	M	A																									A				
189-1172C-																																
1H-CC, 7-15	9.47	G	A								C										F											
2H-CC, 9-14	19.06	G	A																		F											
3H-CC, 12-17	28.40	G	A																		F											
4H-CC, 22-27	37.89	G	A			R															F											
5H-CC, 10-15	47.36	G	A																				C									
6H-CC, 18-23	56.94	G	A																				C									
7H-CC, 8-14	66.14	G	A																				C									
8H-CC, 15-20	76.22	G	A																				C									
9H-CC, 27-32	85.81	M	A	R																			C									
10H-CC, 0-6	94.45	M	A	R																												
11H-CC, 21-26	104.90	M	A	R																												
12H-CC, 29-34	114.49	M	A	R																												
13H-CC, 11-16	123.82	M	A	R																												R
14H-CC, 12-17	133.12	M	A	R																												R
15H-CC, 0-8	141.93	M	A											F																		
16H-CC, 14-20	152.29	M	A																				A									
17H-CC, 0-10	161.34	M	A					C																	R							
18H-CC, 23-31	171.34	M	A																				A									
189-1172D-																																
2R-CC, 8-13	362.97	M	A							R																C			A			
3R-CC, 12-17	372.64	M	A							R																C			A			
4R-CC, 13-18	505.38	P	R																									R				
5R-CC, 12-17	512.97	P	F																									F				
6R-CC, 8-13	522.66	P	F																								R	F				
7R-CC, 15-20	535.25	P	F																								R	F				
8R-CC, 7-12	543.99	M	F													R			R			R						F				
9R-CC, 15-22	555.26	M	C		F					R																		C				
10R-CC, 0-7	564.30		B																													
11R-CC, 0-7	573.54		B																													
12R-CC, 23-28	584.27		B																													
13R-CC, 0-5	593.63		B																													
14R-CC, 0-6	601.86		B																													
15R-CC, 22-27	612.95		B																													
16R-CC, 0-6	619.02		B																													
17R-CC, 17-22	632.21		B																													
18R-CC, 0-5	639.53		B																													
19R-CC, 23-28	645.91		B																													

Table T3 (continued).

Core, section, interval (cm)	Depth (mbsf)	Preservation	Group abundance	*Ahmuellerella octoradiata*	*Amaurolithus amplificus*	*Amaurolithus delicatus*	*Amaurolithus ninae*	*Amaurolithus primus*	*Amaurolithus tricorniculatus*	*Arkhangelskiella cymbiformis*	*Calcidiscus leptoporus*	*Calcidiscus macintyrei*	*Calcidiscus premacintyrei*	*Chiasmolithus altus*	*Chiasmolithus expansus*	*Chiasmolithus oamaruensis*	*Chiasmolithus solitus*	*Chiasmolithus* spp.	*Coccolithus miopelagicus*	*Coccolithus pelagicus*	*Cribrosphaerella daniae*	*Cyclicargolithus abisectus*	*Cyclicargolithus floridanus*	*Dictyococcites bisectus*	*Dictyococcites calidus*	*Discoaster bellus*	*Discoaster brouweri*	*Discoaster calcaris*	*Discoaster challengeri*	*Discoaster intercalaris*	*Discoaster lodoensis*	*Discoaster loeblichii*	*Discoaster pentaradiatus*
20R-CC, 7-12	660.85		B																														
21R-CC, 5-11	667.20		B																														
22R-CC, 17-23	673.03		B																														
23R-CC, 28-33	682.06		B																														
24R-CC, 0-6	699.02	G	R																														
25R-CC, 14-20	709.17	G	F							F											R												
26R-6, 100-105	717.13	M	C							F																							
27R-CC, 0-5	728.22	M	F							F											R												
28R-CC, 0-7	737.18	M	F							F											R												
29R-CC, 32-37	745.41		B																														
30R-CC, 6-11	747.36		B																														
31R-CC, 17-22	766.14	M	F	R						F											R												

Notes: Preservation: G = good, M = moderate, P = poor. Abundance: A = abundant, C = common, F = few, R = rare B = barren.

Table T3 (continued).

Core, section, interval (cm)	Depth (mbsf)	Preservation	Group abundance	*Discoaster quinqueramus*	*Discoaster* spp.	*Discoaster surculus*	*Discoaster tridradiatus*	*Discoaster variabilis*	*Eiffellithus turriseiffelii*	*Ericsonia formosa*	*Gephyrocapsa* >4.5 µm	*Gephyrocapsa* spp. (small)	*Helicosphaera kamptneri*	*Helicosphaera* spp.	*Micula decussata*	*Neococcolithes dubius*	*Nephrolithus corystus*	*Nephrolithus frequens*	*Pontosphaera* spp.	*Prediscosphaera cretacea*	*Pseudoemiliania lacunosa*	*Reticulofenestra dictyoda*	*Reticulofenestra gelida*	*Reticulofenestra perplexa*	*Reticulofenestra psuedoumbilica*	*Reticulofenestra reticulata*	*Reticulofenestra samodurovii*	*Reticulofenestra* spp.	*Reticulofenestra umbilica*	*Sphenolithus heteromorphus*	*Sphenolithus moriformis*	*Triquetrorhabdulus rugosus*	*Zygrhablithus bijugatus*
20R-CC, 7-12	660.85		B																													
21R-CC, 5-11	667.20		B																													
22R-CC, 17-23	673.03		B																													
23R-CC, 28-33	682.06		B																													
24R-CC, 0-6	699.02	G	R																													
25R-CC, 14-20	709.17	G	F						R						R																	
26R-6, 100-105	717.13	M	C						R									F		F												
27R-CC, 0-5	728.22	M	F												R			R														
28R-CC, 0-7	737.18	M	F															R														
29R-CC, 32-37	745.41		B																													
30R-CC, 6-11	747.36		B																													
31R-CC, 17-22	766.14	M	F						R						R		R	R		R												

Table T4. Calcareous nannofossil datum levels, Site 1172.

Hole	Bioevent	Age (Ma)	Interval (cm)		Depth (mbsf)		Mean (mbsf)	Error bar (m)
			Top	Bottom	Top	Bottom		
1172A								
	LO *Pseudoemiliania lacunosa*	0.46	1H-CC	2H-CC	6.24	16.15	11.195	4.955
	LO *Discoaster brouweri*	1.95	2H-CC	3H-CC	16.15	25.45	20.800	4.650
	LO *Discoaster pentaradiatus*	2.40	3H-CC	4H-CC	25.45	35.11	30.280	4.830
	LO *Discoaster surculus*	2.50	4H-CC	5H-CC	35.11	44.50	39.805	4.695
	LO *Reticulofenestra pseudoumbilica*	3.75	5H-CC	6H-CC	44.50	53.97	49.235	4.735
	LO *Amaurolithus primus*	4.60	6H-CC	7H-CC	53.97	63.79	58.880	4.910
	LO *Discoaster quinqueramus*	5.30	8H-CC	9H-CC	73.22	82.52	77.870	4.650
	LO *Coccolithus miopelagicus*	11.00	25X-CC	26X-CC	228.01	235.84	231.925	3.915
	LO *Cyclicargolithus floridanus*	11.90	26X-CC	27X-CC	235.84	246.86	241.350	5.510
	LO *Sphenolithus heteromorphus*	13.60	32X-CC	33X-CC	295.79	306.37	301.080	5.290
	LO *Calcidiscus premacintyrei*	17.40	34X-CC	35X-CC	316.14	324.92	320.530	4.390
	LO *Reticulofenestra bisecta*	23.90	36X-CC	37X-CC	335.08	345.10	340.090	5.010
	LO *Chiasmolithus altus*	26.10	37X-CC	38X-CC	345.10	353.76	349.430	4.330
	LO *Reticulofenestra umbilica*	32.30	39X-2, 143	39X-5, 63	356.69	360.39	358.540	1.850
	LO *Reticulofenestra reticulata*	35.00	39X-2, 143	39X-5, 63	356.69	360.39	358.540	1.850
	LO *Chiasmolithus solitus*	40.40	42X-CC	43X-CC	393.18	402.83	398.005	4.825
	LO *Reticulofenestra reticulata*	42.00	43X-CC	44X-CC	402.83	412.47	407.650	4.820
	FO *Reticulofenestra umbilica*	43.70	45X-CC	53X-CC	422.11	498.80	460.455	38.345
1172B								
	FO *Emiliania huxleyi*	0.26	Top of core	1H-CC	0.00	2.79	1.400	1.400
	LO *Pseudoemiliania lacunosa*	0.46	1H-CC	2H-CC	2.79	12.73	7.760	4.970
	LO *Discoaster surculus*	2.50	3H-CC	4H-CC	22.10	31.77	26.940	4.840
	LO *Reticulofenestra pseudoumbilica*	3.75	4H-CC	5H-CC	31.77	41.31	36.540	4.770
	LO *Amaurolithus primus*	4.60	6H-CC	7H-CC	50.52	60.33	55.430	4.910
	LO *Discoaster quinqueramus*	5.30	9H-CC	10H-CC	79.20	89.05	84.130	4.930
	LO *Amaurolithus amplificus*	6.00	11H-CC	12H-CC	98.06	107.95	103.010	4.950
	LO *Discoaster loeblichii*	7.40	14H-CC	15H-CC	126.46	136.11	131.290	4.830
1172C								
	LO *Pseudoemiliania lacunosa*	0.46	Top of core	1H-CC	0.00	9.47	4.735	4.735
	LO *Discoaster brouweri*	1.95	2H-CC	3H-CC	19.06	28.40	23.730	4.670
	LO *Discoaster surculus*	2.50	3H-CC	4H-CC	28.40	37.89	33.145	4.745
	LO *Reticulofenestra pseudoumbilica*	3.75	4H-CC	5H-CC	37.89	47.36	42.625	4.735
	LO *Amaurolithus primus*	4.60	6H-CC	7H-CC	56.94	66.14	61.540	4.600
	LO *Discoaster quinqueramus*	5.30	8H-CC	9H-CC	76.22	85.81	81.015	4.795
	LO *Amaurolithus amplificus*	6.00	10H-CC	11H-CC	94.45	104.90	99.675	5.225
	LO *Discoaster loeblichii*	7.40	14H-CC	15H-CC	133.12	141.93	137.525	4.405
1172D								
	LO *Reticulofenestra umbilica*	32.30	2R-CC	3R-CC	362.97	372.64	367.805	4.835
	LO *Chiasmolithus solitus*	40.40	4R-CC	5R-CC	505.38	512.97	509.175	3.795
	LO *Arkhangelskiella cymbiformis*	65.00	24R-5,41	25R-5, 40	696.11	705.70	700.905	4.795
	LO *Eiffellithus turriseiffelii*	65.00	24R-5,41	25R-5, 40	696.11	705.70	700.905	4.795

Notes: The mean depth of each datum is assigned at the midpoint between two samples. LO = last occurrence, FO = first occurrence.

Table T5. Range chart of planktonic foraminifers, Site 1172. (**See table note.** Continued on next five pages.)

Hole, core, section, interval (cm)	Depth (mbsf)	*Acarinina primitiva*	*Catapsydrax dissimilis*	*Catapsydrax unicavus*	*Chiloguembelina cubensis*	*Dentoglobigerina praedehiscens*	*Dentoglobigerina venezuelana*	*Globigerellinoides multispinus*	*Globigerina bulloides*	*Globigerina eamsi*	*Globigerina falconensis*	*Globigerina officinalis*	*Globigerina praebulloides*	*Globigerina quinqueloba*	*Globigerinatheka index*	*Globigerinella aequilateralis*	*Globigerinella obesa*	*Globigerinella praecalida*	*Globigerinita glutinata*	*Globigerinita uvula*	*Globigerinoides immaturus*	*Globigerinoides obliquus*	*Globigerinoides parawoodi*	*Globigerinoides quadrilobatus*	*Globigerinoides ruber*	*Globigerinoides trilobus*	*Globoquadrina dehiscens*	*Globorotalia cibaoensis*	*Globorotalia conica*	*Globorotalia conomiozea*	*Globorotalia crassacarina*	*Globorotalia crassaconica*	*Globorotalia crassaformis* (sin)	*Globorotalia crassula*	*Globorotalia explicationis*	*Globorotalia inflata* (sin)	Zone/ Subzone	Age	
189-																																							
1172A-1H-CC	6.24								X		X			X		X	X			X													X	X		X	SN14	Pleistocene	
1172A-2H-CC	16.15								X		X			X		X	X			X											X	X	X	X		X	SN13	late	Pliocene
1172A-3H-CC	25.54								X		X			X		X				X													X	X		X				
1172A-4H-CC	35.11								X		X									X												X	X			X			
1172A-5H-CC	44.50								X		X			X		X				X													X	X		X				
1172A-6H-CC	53.97								X		X			X		X				X											X	X	X			X	SN12b		
1172A-7H-CC	63.79								X		X			X			X			X	X		X								X		X	X				early	
1172A-8H-CC	73.22								X		X			X			X			X											X		X		X		SN12a		
1172A-9H-CC	82.52								X		X			X			X			X	X										X		X							
1172A-10H-CC	92.10								X		X			X																X			X			SN11	late	Miocene
1172A-11H-CC	101.34								X					X						X										X									
1172A-12H-CC	110.05								X					X						X	X									X									
1172A-13H-CC	120.76								X					X						X	X									X									
1172A-14H-CC	129.24								X					X						X	X									?						SN10		
1172A-15H-CC	139.79								X					X						X	X																late	
1172A-16H-CC	149.22								X					X						X	X									?				X		SN9		
1172A-17H-CC	158.27								X					X						X						X								X					
1172A-18H-CC	167.85								X											X							X							X		SN8		
1172A-19H-CC	177.76								X				X	X						X	X													X			middle	
1172A-20H-CC	186.44								X											X	X					X	X												
1172A-21H-CC	196.81								X				X	X						X	X				X		X							X		SN7		
1172A-22H-CC	206.18								X				X	X				X		X	X						X		X										
1172A-23H-CC	215.27								X				X	X						X				X			X												
1172A-24H-CC	225.15								X				X	X						X																			
1172A-25X-CC	228.01								X				X	X						X																			
1172A-26X-CC	235.84								X				X	X						X							X												
1172A-27X-CC	246.86								X				X	X						X																			
1172A-28X-CC	255.65												X	X						X																SN6		
1172A-29X-CC	266.27								X				X	X						X							X												
1172A-30X-CC	276.45								X				X																							SN5		
1172A-31X-CC	285.90												X	X						X						X												
1172A-32X-CC	295.79								X				X	X						X																			
1172A-33X-CC	306.37												X	X						X							X												
1172A-34X-CC	316.34		X										X	X						X							X									SN3	early	
1172A-35X-CC	324.92		X										X	X						X							X												
1172A-36X-CC	335.08		X	X									X														X									SN1		
1172A-37X-CC	345.10		X			X							X							X							X												

Table T5 (continued).

Hole, core, section, interval (cm)	Depth (mbsf)	*Globorotalia juanai*	*Globorotalia limbata*	*Globorotalia miotumida*	*Globorotalia miozea*	*Globorotalia panda*	*Globorotalia peripheroronda*	*Globorotalia pliozea*	*Globorotalia praemenardii*	*Globorotalia praescitula*	*Globorotalia pseudokugleri*	*Globorotalia puncticulata*	*Globorotalia puncticuloides*	*Globorotalia scitula*	*Globorotalia sphericomiozea*	*Globorotalia triangula*	*Globorotalia truncatulinoides*	*Globorotalia zealandica*	*Globoturborotalita suteri*	*Globoturborotalita apertura*	*Globoturborotalita brazieri*	*Globoturborotalita connecta*	*Globoturborotalita decoraperta*	*Globoturborotalita nepenthes*	*Globoturborotalita woodi*	*Hedbergella silteri*	*Heterohelix globulosa*	*Neogloboquadrina dutertrei*	*Neogloboquadrina humerosa*	*Neogloboquadrina pachyderma* (dex)	*Neogloboquadrina pachyderma* (sin)	*Orbulina suturalis*	*Orbulina universa*	*Paragloborotalia bella*	*Paragloborotalia continuosa*	*Paragloborotalia mayeri*	Zone/ Subzone	Age		
189-																																								
1172A-1H-CC	6.24													X		X	X														X		X			SN14	Pleistocene		
1172A-2H-CC	16.15													X																X	X		X							
1172A-3H-CC	25.54											X	X	X		X														X	X		X			SN13	late	Pliocene	
1172A-4H-CC	35.11											X	X	X																			X							
1172A-5H-CC	44.50											X	X	X		X																	X							
1172A-6H-CC	53.97											X	X	X															X				X			SN12b			
1172A-7H-CC	63.79											X	X																X				X				early		
1172A-8H-CC	73.22							X				X	X	X	X					X									X	X	X		X			SN12a			
1172A-9H-CC	82.52							X				X	X		X					X													X							
1172A-10H-CC	92.10							X					?		X					X									X	X	X		X			SN11	late	Miocene	
1172A-11H-CC	101.34			X											X																		X							
1172A-12H-CC	110.05			X											X																		X							
1172A-13H-CC	120.76			X											?																		X							
1172A-14H-CC	129.24			X																			X		X								X			SN10			
1172A-15H-CC	139.79			X																					X															
1172A-16H-CC	149.22			X				?						X	?										X				X			X		X		SN9			
1172A-17H-CC	158.27			X																					X				X			X	X	X					
1172A-18H-CC	167.85			X		X								X									X		X								X			SN8			
1172A-19H-CC	177.76			X		X								X									X		X								X							
1172A-20H-CC	186.44			X		X																	X		X								X	X						
1172A-21H-CC	196.81			X		X								X									X		X								X	X						
1172A-22H-CC	206.18			X	X	X																			X								X							
1172A-23H-CC	215.27			X	X	X																X			X								X	X						
1172A-24H-CC	225.15			X	X	X												?				X			X								X	X						
1172A-25X-CC	228.01			X	?																	X			X								X	X						
1172A-26X-CC	235.84			X	X	X																X		X	X								X							
1172A-27X-CC	246.86			X	X	X	X														X	X			X								X	X						
1172A-28X-CC	255.65				X	X	X			X	X							X								X							X			SN6			
1172A-29X-CC	266.27				X	X	X				X			X				X								X		X													
1172A-30X-CC	276.45				X	X	X							X				X								X														
1172A-31X-CC	285.90				X	X					X							X			X	X	X			X										SN5			
1172A-32X-CC	295.79			X	X	X												X				X				X														
1172A-33X-CC	306.37				X	X				X	X							X				X				X								X						
1172A-34X-CC	316.34					X					X							X				X				X								X	X		SN3	early		
1172A-35X-CC	324.92																					X				X								X	X						
1172A-36X-CC	335.08																		X																	SN1			
1172A-37X-CC	345.10																																							

Table T5 (continued).

Hole, core, section, interval (cm)	Depth (mbsf)	*Paragloborotalia nana*	*Paragloborotalia nympha*	*Praeorbulina curva*	*Pulleniatina obliquiloculata*	*Pulleniatina primalis*	*Rugoglobigerina rugosa*	*Sphaeroidinellopsis seminulina*	*Subbotina angiporoides*	*Subbotina eocaena*	*Subbotina linaperta*	*Subbotina patagonica*	*Tenuitella gemma*	*Tenuitella minutissima*	*Tenuitellinata angustiumbilicata*	*Turborotalia euapertura*	*Turborotalia pomeroli*	Zone/ Subzone	Age		
189-																		SN14	Pleistocene		
1172A-1H-CC	6.24																				
1172A-2H-CC	16.15																	SN13	late	Pliocene	
1172A-3H-CC	25.54																				
1172A-4H-CC	35.11																				
1172A-5H-CC	44.50																				
1172A-6H-CC	53.97																	SN12b			
1172A-7H-CC	63.79																		early		
1172A-8H-CC	73.22																	SN12a			
1172A-9H-CC	82.52																				
1172A-10H-CC	92.10																	SN11	late	Miocene	
1172A-11H-CC	101.34																				
1172A-12H-CC	110.05																				
1172A-13H-CC	120.76																				
1172A-14H-CC	129.24																	SN10			
1172A-15H-CC	139.79																				
1172A-16H-CC	149.22																	SN9			
1172A-17H-CC	158.27				X																
1172A-18H-CC	167.85		X			?												SN8			
1172A-19H-CC	177.76																		middle		
1172A-20H-CC	186.44		X															SN7			
1172A-21H-CC	196.81																				
1172A-22H-CC	206.18																				
1172A-23H-CC	215.27		X																		
1172A-24H-CC	225.15													X							
1172A-25X-CC	228.01		X																		
1172A-26X-CC	235.84													X							
1172A-27X-CC	246.86		X											X							
1172A-28X-CC	255.65		X											X				SN6			
1172A-29X-CC	266.27													X							
1172A-30X-CC	276.45		X	X										X				SN5			
1172A-31X-CC	285.90		X	X										X							
1172A-32X-CC	295.79		X	X										X							
1172A-33X-CC	306.37			X										X							
1172A-34X-CC	316.34																	SN3	early		
1172A-35X-CC	324.92													X							
1172A-36X-CC	335.08											X			X	X		SN1			
1172A-37X-CC	345.10											X				X					

Table T5 (continued).

Hole, core, section, interval (cm)	Depth (mbsf)	*Acarinina primitiva*	*Catapsydrax dissimilis*	*Catapsydrax unicavus*	*Chiloguembelina cubensis*	*Dentoglobigerina praedehiscens*	*Dentoglobigerina venezuelana*	*Globigerellinoides multispinus*	*Globigerina bulloides*	*Globigerina eamsi*	*Globigerina falconensis*	*Globigerina officinalis*	*Globigerina praebulloides*	*Globigerina quinqueloba*	*Globigerinatheka index*	*Globigerinella aequilateralis*	*Globigerinella obesa*	*Globigerinella praecalida*	*Globigerinita glutinata*	*Globigerinita uvula*	*Globigerinoides immaturus*	*Globigerinoides obliquus*	*Globigerinoides parawoodi*	*Globigerinoides quadrilobatus*	*Globigerinoides ruber*	*Globigerinoides trilobus*	*Globoquadrina dehiscens*	*Globorotalia cibaoensis*	*Globorotalia conica*	*Globorotalia conomiozea*	*Globorotalia crassacarina*	*Globorotalia crassaconica*	*Globorotalia crassaformis* (sin)	*Globorotalia crassula*	*Globorotalia explicationis*	*Globorotalia inflata* (sin)	Zone/ Subzone	Age	
1172A-38X-CC	353.76												X																							SP14b	e. l.	Oligocene
1172A-39X-2, 5-7	356.15			X								X																								AP13	e. l.	Oligocene
1172D-2R-CC	362.97														X																					AP12	late to middle	Eocene
1172A-39X-CC	364.34		X																																	AP10 to AP11	late to middle	Eocene
1172D-3R-CC	372.64				X																																late to middle	Eocene
1172A-40X-CC	374.00		X																																	AP10 to AP12	late to middle	Eocene
1172A-41X-CC	383.60		X																																		late to middle	Eocene
1172A-42X-CC	393.18														X																					AP9 to AP12	late to middle	Eocene
1172A-43X-CC	402.83						X																													Barren	late to middle	Eocene
1172D-7R-CC	535.25	X																																		AP7 to AP10	late to middle	Eocene
																																				Barren interval		
1172D-25R-CC	709.17							X																												Campanian to Maastrichtian	late Cretaceous	
1172D-26R-CC	717.13							X																													late Cretaceous	
1172D-27R-CC	728.22							X																												ND	late Cretaceous	
1172D-28R-CC	737.18																																				late Cretaceous	
1172D-29R-CC	745.41																																				late Cretaceous	
1172D-30R-CC	747.36																																			Campanian to Maastrichtian	late Cretaceous	
1172D-31R-CC	766.14																																			ND	late Cretaceous	

Note: X = present, ? = questionably identified/present, ND = not determined.

Table T5 (continued).

Hole, core, section, interval (cm)	Depth (mbsf)	*Globorotalia juanai*	*Globorotalia limbata*	*Globorotalia miotumida*	*Globorotalia miozea*	*Globorotalia panda*	*Globorotalia peripheroronda*	*Globorotalia pliozea*	*Globorotalia praemenardii*	*Globorotalia praescitula*	*Globorotalia pseudokugleri*	*Globorotalia puncticulata*	*Globorotalia puncticuloides*	*Globorotalia scitula*	*Globorotalia sphericomiozea*	*Globorotalia triangula*	*Globorotalia truncatulinoides*	*Globorotalia zealandica*	*Globoturborotalita apertura*	*Globoturborotalita brazieri*	*Globoturborotalita connecta*	*Globoturborotalita decoraperta*	*Globoturborotalita nepenthes*	*Globoturborotalita woodi*	*Hedbergella silteri*	*Heterohelix globulosa*	*Neogloboquadrina dutertrei*	*Neogloboquadrina humerosa*	*Neogloboquadrina pachyderma* (dex)	*Neogloboquadrina pachyderma* (sin)	*Orbulina suturalis*	*Orbulina universa*	*Paragloborotalia bella*	*Paragloborotalia continuosa*	*Paragloborotalia mayeri*	Zone/ Subzone	Age	
1172A-38X-CC	353.76										?																								SP14b	l.	Oligocene
1172A-39X-2, 5-7	356.15																	X																X	AP13	e.	
1172D-2R-CC	362.97																	X																	AP12	late to middle	Eocene
1172A-39X-CC	364.34																	X																	AP10 to AP11		
1172D-3R-CC	372.64																	X																			
1172A-40X-CC	374.00																	X																	AP10 to AP12		
1172A-41X-CC	383.60																																				
1172A-42X-CC	393.18																																		AP9 to AP12		
1172A-43X-CC	402.83																																		Barren		
1172D-7R-CC	535.25																																		AP7 to AP10		
																																		Barren interval		
1172D-25R-CC	709.17																								X	X									Campanian to Maastrichtian		late Cretaceous
1172D-26R-CC	717.13																								X	X											
1172D-27R-CC	728.22																																				
1172D-28R-CC	737.18																																		ND		
1172D-29R-CC	745.41																																				
1172D-30R-CC	747.36																									X									Campanian to Maastrichtian		
1172D-31R-CC	766.14																																		ND		

Table T5 (continued).

Hole, core, section, interval (cm)	Depth (mbsf)	*Paragloborotalia nana*	*Paragloborotalia nympha*	*Praeorbulina curva*	*Pulleniatina obliquiloculata*	*Pulleniatina primalis*	*Rugoglobigerina rugosa*	*Sphaeroidinellopsis seminulina*	*Subbotina angiporoides*	*Subbotina eocaena*	*Subbotina linaperta*	*Subbotina patagonica*	*Tenuitella gemma*	*Tenuitella minutissima*	*Tenuitellinata angustiumbilicata*	*Turborotalia euapertura*	*Turborotalia pomeroli*	Zone/ Subzone	Age	
1172A-38X-CC	353.76																	SP14b	l.	Oligocene
1172A-39X-2, 5-7	356.15								X									AP13	e.	
1172D-2R-CC	362.97								X	X								AP12	late to middle	Eocene
1172A-39X-CC	364.34								X		X							AP10 to AP11		
1172D-3R-CC	372.64								X		X									
1172A-40X-CC	374.00								X		X							AP10 to AP12		
1172A-41X-CC	383.60								X		X									
1172A-42X-CC	393.18										X	X						AP9 to AP12		
1172A-43X-CC	402.83										X							Barren		
1172D-7R-CC	535.25																	AP7 to AP10		
																		Barren interval		
1172D-25R-CC	709.17						X											Campanian to Maastrichtian		late Cretaceous
1172D-26R-CC	717.13						X													
1172D-27R-CC	728.22																			
1172D-28R-CC	737.18																	ND		
1172D-29R-CC	745.41																			
1172D-30R-CC	747.36																	Campanian to Maastrichtian		
1172D-31R-CC	766.14																	ND		

Table T6. Selected planktonic foraminiferal datums, Hole 1172A.

Bioevent	Age (Ma)	Interval (cm)		Depth (mbsf)		Mean (mbsf)	Error bar (m)
		Top	Bottom	Top	Bottom		
FO *Globorotalia truncatulinoides*	1.96	1H-CC	2H-CC	6.24	16.15	11.20	4.96
FO *Globorotalia inflata*	3.20	5H-CC	6H-CC	44.50	53.97	49.24	4.74
LO *Globorotalia pliozea*	4.60	7H-CC	8H-CC	63.79	73.22	68.51	4.72
FO *Globorotalia puncticulata*	5.30	9H-CC	10H-CC	82.52	92.10	87.31	4.79
FO *Globorotalia conomiozea*	6.90	13H-CC	14H-CC	120.76	129.24	125.00	4.24
LO *Paragloborotalia continuosa*	8.00	15H-CC	16H-CC	139.79	149.22	144.51	4.72
LO *Paragloborotalia nympha*	10.10	17H-CC	18H-CC	158.27	167.85	163.06	4.79
LO *Paragloborotalia mayeri*	11.40	19H-CC	20H-CC	177.76	186.44	182.10	4.34
FO *Paragloborotalia mayeri*	12.10	27X-CC	28X-CC	246.86	255.65	251.26	4.40
FO *Orbulina suturalis*	15.10	28X-CC	29X-CC	255.65	266.27	260.96	5.31
FO *Praeorbulina curva*	16.30	33X-CC	34X-CC	306.37	316.34	311.36	4.98
FO *Globoturborotalita connecta*	20.90	35X-CC	36X-CC	324.92	335.08	330.00	5.08
FO *Globoquadrina dehiscens*	23.20	37X-CC	38X-CC	345.10	353.76	349.43	4.33
LO *Subbotina angiporoides*	30.00	38X-CC	39X, 2-5	353.76	356.15	354.96	1.19

Note: FO = first occurrence, LO = last occurrence.

Table T7. Selected radiolarian datums, Site 1172.

Bioevent	Age (Ma)	Sample Top	Sample Bottom	Depth (mbsf) Top	Depth (mbsf) Bottom	Mean (mbsf)	Error (m)
Hole 1172A							
LO *Stylatractus universus*	0.45	1H-CC	2H-CC	6.24	16.15	11.195	9.91
LAO *Cyrtocapsella tetrapera*	12.50	26X-CC	27X-CC	235.84	246.86	241.350	11.02
LO *Lychnocanoma amphitrite*	32.80	39X-CC	40X-CC	364.34	374.00	369.170	9.66
FO *Eucyrtidium antiquum*	32.96	40X-CC	41X-CC	374.00	383.60	378.800	9.60
FO *Eucyrtidium spinosum*	37.00	41X-CC	42X-CC	383.60	393.18	388.390	9.58
LO *Spongatractus pachystylus*	37.30-38.80	48X-CC	49X-CC	450.85	460.45	455.650	9.60
Hole 1172B							
LO *Stylatractus universus*	0.45	1H-CC	2H-CC	2.79	12.73	7.760	9.94

Notes: No datum at Hole 1172C. LO = last occurrence, LAO = last abundant occurrence, FO = first occurrence.

Table T8. Relative abundance of selected diatom taxa, sponge spicules, and silicoflagellates, Holes 1172A and 1172D. (See table notes. Continued on next three pages.)

Core, section, interval (cm)	Depth (mbsf)	Preservation	Group abundance	*Actinocyclus curvatulus*	*Actinocyclus ingens*	*Actinocyclus ingens* var. *nodus*	*Actinocyclus ingens* var. *ovalis*	*Actinocyclus karstenii*	*Actinocyclus octonarius* var. *tenellus*	*Actinocyclus* spp.	*Actinoptychus bipunctatus*	*Actinoptychus senarius*	*Actinoptychus* spp.	*Arachnodiscus marylandica*	*Arachnodiscus* sp.	*Asteromphalus kennettii*	*Asteromphalus* spp.	*Azpeitia nodulifer*	*Azpeitia* sp.	*Azpeitia tabularis* group	*Biddulphia* spp.	*Cestodiscus* sp.	*Chaetoceros* resting spores	*Cocconeis* spp.	*Corethron criophilum*	*Coscinodiscus marginatus*	*Coscinodiscus oculus-iridis*	*Coscinodiscus radiatus*	*Coscinodiscus rhombicus*	*Coscinodiscus* spp.	*Dactyliosolen antarcticus*	*Denticulopsis dimorpha*	*Denticulopsis hustedtii*	*Ethmodiscus rex*	*Fragilariopsis reinholdii*	cf. *Grammatophora* sp.	*Hemiaulus* spp.	*Hemidiscus cuneiformis*	*Hemidiscus karstenii*	*Hemidiscus* sp.	*Navicula* spp.	*Nitzschia marina*	*Paralia sulcata*
189-1172A-																																										
1H-CC, 10-15	6.24		B																																							
2H-CC, 9-14	16.15	G	F						R		R												R													R						F
3H-CC, 15-20	25.54	M	R								R													R													R						R
4H-CC, 12-17	35.11	G	T																																							
5H-CC, 0-5	44.50		B																																							
6H-CC, 11-16	53.97		B																																							
7H-CC, 27-32	63.79		B																																							
8H-CC, 15-20	73.22		B																																							
9H-CC, 0-7	82.52		B																																							
10H-CC, 15-20	92.10		B																																							
11H-CC, 7-12	101.34	MP	R										R					R																									
12H-CC, 10-15	110.05	MP	R		R																																					
13H-CC, 26-31	120.76	G	A									F						A		F						C									A		A		R		
14H-CC, 10-16	129.24	G	A									F					C	A		A		R			R	F					R			A		A				
15H-CC, 22-27	139.79	G	A		D			R				F						F						F		A							F		T						
16H-CC, 22-27	149.22	G	A		R		D					R		R										R		R									A	R		R		F	
17H-CC, 19-24	158.27	G	A				C																	F			R								C					
18H-CC, 0-6	167.85	G	A				R								R	D								C										C					
19H-CC, 28-34	177.76	G	F				F											F						F										R					
20H-CC, 5-11	186.44	G	F									F												F											R					R
21H-CC, 33-38	196.81	G	F	R	F											R		F						R											F					
22H-CC, 21-26	206.18	M	F		F																			R																
23H-CC, 12-17	215.27	M	R		R																		T			T														
24H-CC, 15-20	225.15	M	F	R	F																					F						F								
25X-CC, 14-19	228.01	M	F	F	R															F															F					
26X-CC, 29-34	235.84	P	F															F														F								R
27X-CC, 25-30	246.86	G	C		C	R																		R		R		R												
28X-CC, 16-21	255.65	G	F		F													R																						
29X-CC, 22-27	266.27	P	T												T															R										
30X-CC, 10-15	276.45	P	T																											R										R
31X-CC, 21-26	285.90	P	T																											T										
32X-CC, 31-36	295.79	P	T																																					T
33X-CC, 19-24	306.37		B																																					
34X-CC, 23-28	316.34		B																																					
35X-CC, 24-29	324.92		B																																					
36X-CC, 21-26	335.08		B																																					

Table T8 (continued).

Core, section, interval (cm)	Depth (mbsf)	*Paralia sulcata* var.	*Paralia sulcata* var. *crenulata*	*Podosira* spp.	*Proboscia barboi*	*Proboscia praebarboi*	*Pterotheca* spp.	*Pyxilla fragments*	*Pyxilla fragments*	*Rhizosolenia bergonii*	*Rhizosolenia* spp.	*Rocella vigilans*	*Rodella praentitida*	*Rossiella* spp.	*Sceptroneis* spp.	*Stephanopyxis grunowii*	*Stephanopyxis turris*	*Synedra jouseana*	*Synedra linearis*	*Thalassionema nitzschioides* var. *parva*	*Thalassiosira eccentrica*	*Thalassiosira leptopus*	*Thalassiosira oestrupii*	*Thalassiosira* spp.	*Thalassiothrix antarctica*	*Triceratium* spp.	*Trigonium alterans*	*Trinacria* spp.	*Xanthiopyxis* spp.	Silicoflagellate tests	Sponge spicules
189-1172A-																															
1H-CC, 10-15	6.24																														C
2H-CC, 9-14	16.15																F													F	A
3H-CC, 15-20	25.54																														A
4H-CC, 12-17	35.11																							R							
5H-CC, 0-5	44.50																														C
6H-CC, 11-16	53.97																														T
7H-CC, 27-32	63.79																														T
8H-CC, 15-20	73.22																														F
9H-CC, 0-7	82.52																R														A
10H-CC, 15-20	92.10																														C
11H-CC, 7-12	101.34																R														A
12H-CC, 10-15	110.05																R														A
13H-CC, 26-31	120.76																				F	F			C					C	
14H-CC, 10-16	129.24				R															F	C	C			R		R			A	A
15H-CC, 22-27	139.79																														
16H-CC, 22-27	149.22																					C			F					C	A
17H-CC, 19-24	158.27																					C							R	F	A
18H-CC, 0-6	167.85			R	R																	C			C					C	A
19H-CC, 28-34	177.76																					R			R						A
20H-CC, 5-11	186.44																														A
21H-CC, 33-38	196.81																								F						A
22H-CC, 21-26	206.18																														A
23H-CC, 12-17	215.27																														A
24H-CC, 15-20	225.15																														C
25X-CC, 14-19	228.01																														A
26X-CC, 29-34	235.84																								F			R			
27X-CC, 25-30	246.86																								C			R		C	A
28X-CC, 16-21	255.65								R																F						A
29X-CC, 22-27	266.27																														C
30X-CC, 10-15	276.45																T						T								C
31X-CC, 21-26	285.90																														C
32X-CC, 31-36	295.79	T																													
33X-CC, 19-24	306.37																														A
34X-CC, 23-28	316.34																														
35X-CC, 24-29	324.92																														
36X-CC, 21-26	335.08																														

Table T8 (continued).

Core, section, interval (cm)	Depth (mbsf)	Preservation	Group abundance	*Actinocyclus curvatulus*	*Actinocyclus ingens*	*Actinocyclus ingens* var. *nodus*	*Actinocyclus ingens* var. *ovalis*	*Actinocyclus karstenii*	*Actinocyclus octonarius* var. *tenellus*	*Actinocyclus* spp.	*Actinoptychus bipunctatus*	*Actinoptychus senarius*	*Actinoptychus* spp.	*Arachnodiscus marylandica*	*Arachnodiscus* sp.	*Asteromphalus kennettii*	*Asteromphalus* spp.	*Azpeitia nodulifer*	*Azpeitia* sp.	*Azpeitia tabularis* group	*Biddulphia* spp.	*Cestodiscus* sp.	*Chaetoceros* resting spores	*Cocconeis* spp.	*Corethron criophilum*	*Coscinodiscus marginatus*	*Coscinodiscus oculus-iridis*	*Coscinodiscus radiatus*	*Coscinodiscus rhombicus*	*Coscinodiscus* spp.	*Dactyliosolen antarcticus*	*Denticulopsis dimorpha*	*Denticulopsis hustedtii*	*Ethmodiscus rex*	*Fragilariopsis reinholdii*	cf. *Grammatophora* sp.	*Hemiaulus* spp.	*Hemidiscus cuneiformis*	*Hemidiscus karstenii*	*Hemidiscus* sp.	*Navicula* spp.	*Nitzschia marina*	*Paralia sulcata*
37X-CC, 38-43	345.10		B																																						
38X-CC, 24-29	353.76	MG	A																	C						R			R												
39X-2, 3-5	356.13	G	A																																						
39X-3, 61-63	358.21	MG	C										R						F	C																					
39X-CC, 27-33	364.34	MP	C																R							R			R						C						
40X-CC, 26-31	374.00	P	C									R											F						R						C						
41X-CC, 31-36	383.60	MP	C									R										R	R			R			C						F						
42X-CC, 51-56	393.18	P	C																			F	F						C						R						C
43X-CC, 33-38	402.83	P	C																F			F	F						F						F						
44X-CC, 32-37	412.47	MP	A																			F													C						
45X-CC, 41-46	422.11	MG	A							R					R							F	A			R			A												
46X-CC, 36-41	431.66	MP	A																			F						C	F						R						
47X-CC, 36-41	441.29	MP	A									F											A						F						R						
48X-CC, 36-41	450.85	P	C												R								C						F												
49X-CC, 43-48	460.45	MG	A																				A						F												
50X-CC, 0-8	460.20	MG	A																				A						R						F						
51X-CC, 43-48	476.19	MG	A																				A			R									F						
52X-CC, 39-44	488.65	MG	A																				A																		
53X-CC, 34-39	498.80	MG	A																				A						F						F						
54X-CC, 12-17	504.44	P	R																										T												
55X-CC, 26-31	509.07	P	T																																						
56X-CC, 23-33	518.23		B																																						
189-1172D-																																									
2R-CC, 8-13	362.97	M	C							C													C						C						R						
3R-CC, 12-17	372.64	MP	C							F		R											C						R						C						
4R-CC, 13-18	505.38	P	T																										R												

Notes: Samples below 505.38 mbsf are barren of silicified diatoms. Preservation: G = good, M = moderate, MG = moderate-good, MP = moderate-poor, P = poor. Abundance: D = dominant, A = abundant, C = common, F = few, R = rare, T = trace, B = barren.

Table T8 (continued).

Core, section, interval (cm)	Depth (mbsf)	*Paralia sulcata* var.	*Paralia sulcata* var. *crenulata*	*Podosira* spp.	*Proboscia barboi*	*Proboscia praebarboi*	*Pterotheca* spp.	*Pyxilla fragments*	*Pyxilla fragments*	*Rhizosolenia bergonii*	*Rhizosolenia* spp.	*Rocella vigilans*	*Rodella praentitida*	*Rossiella* spp.	*Sceptroneis* spp.	*Stephanopyxis grunowii*	*Stephanopyxis turris*	*Synedra jouseana*	*Synedra linearis*	*Thalassionema nitzschioides* var. *parva*	*Thalassiosira eccentrica*	*Thalassiosira leptopus*	*Thalassiosira oestrupii*	*Thalassiosira* spp.	*Thalassiothrix antarctica*	*Triceratium* spp.	*Trigonium alterans*	*Trinacria* spp.	*Xanthiopyxis* spp.	Silicoflagellate tests	Sponge spicules
37X-CC, 38-43	345.10																														C
38X-CC, 24-29	353.76					C						C	R		R	R	C	A												F	A
39X-2, 3-5	356.13					C						C	R					A	C											F	C
39X-3, 61-63	358.21		F						C							C	C												F		C
39X-CC, 27-33	364.34		C						C																				C	R	
40X-CC, 26-31	374.00		A						C							C	F												C		C
41X-CC, 31-36	383.60		C			F			A		F					R	C												F	F	C
42X-CC, 51-56	393.18				F				A							F	C												R		F
43X-CC, 33-38	402.83		C						A								C							R					F		C
44X-CC, 32-37	412.47		D					R	A							C													C		C
45X-CC, 41-46	422.11		A						A							C	A							F		R			C		C
46X-CC, 36-41	431.66		C						A		R					A	A									C			C		F
47X-CC, 36-41	441.29		F					R	A							A	A													F	F
48X-CC, 36-41	450.85								A		C			R			C											R	R		C
49X-CC, 43-48	460.45								A							F	A											F	A	R	C
50X-CC, 0-8	460.20						C		A		F				R	A	A												C		C
51X-CC, 43-48	476.19		C	R			F		A		R				R	C	C												C		F
52X-CC, 39-44	488.65		R				F		A							C	A								R				C	F	C
53X-CC, 34-39	498.80		C				R		C	C	R					C	C									F			C	F	
54X-CC, 12-17	504.44								R							R															F
55X-CC, 26-31	509.07																														
56X-CC, 23-33	518.23																														
189-1172D-																															
2R-CC, 8-13	362.97		C	R					C							C	C												C	F	F
3R-CC, 12-17	372.64		C	C					C						R		C												C		
4R-CC, 13-18	505.38		R						R																						

Table T9. Diatom bioevents, Holes 1172A and 1172D.

Bioevent	Age (Ma)	Interval (cm)		Depth (mbsf)		Mean (mbsf)	Error bar (m)
		Top	Bottom	Top	Bottom		
LO *Denticulopsis dimorpha*	10.70	23H-CC	24H-CC	215.27	225.15	220.21	9.88
FO *Rocella vigilans* (small)	30.24	39X-2, 3–5	39X-3, 61–63	356.14	358.22	357.18	2.08
FO *Cavitatus (Synedra) jouseanus*	30.62	39X-2, 3–5	39X-3, 61–63	356.14	358.22	357.18	2.08

Note: LO = last occurrence, FO = first occurrence.

Table T10. Distribution of organic walled dinoflagellate cysts (dinocysts; number of specimens counted) and percentages of the major other palynomorph groups in selected samples, Holes 1172A and 1172D. (Continued on next page.)

Core, section, interval (cm)	Depth (mbsf)	Preservation	Group abundance	*N* (palynomorphs)	*N* (dinocysts)	*N* (sporomorphs)	*N* (foraminifer linings)	*N* (acritarchs)	Sporomorphs (%)	Foraminifer linings (%)	Acritarchs (%)	*Acanthaulax wilsonii*	*Xenicodinium*? sp.	*Achomosphaera alcicornu*	*Aireiana verrucosa*	*Alisocysta circumtabulata*	*Alisocysta reticulata*	*Alterbidinium distinctum*	*Alterbidinium* spp.	*Areoligera senonensis*	*Areosphaeridium diktyoplokum*	*Batiacasphaera compta*	*Brigantedinium* spp.	*Brigantedinium*? sp.	*Cassidium fragile*	*Cerebrocysta bartonensis*	*Cerodinium boloniensis*	*Cerodinium* spp.	*Cordosphaeridium fibrospinosum*	*Corrudinium* sp. (G&F '83)	*Corrudinium* sp. A	*Cribroperidinium* spp.	*Deflandrea phosphoritica* group	*Dinopterygium cladoides*	*Elytrocysta* spp.	*Enneadocysta partridgei*	*Enneadocysta pectiniformis*	*Eocladopyxis* sp.	*Exochosphaeridium bifidum*	*Florentinia mantellii*	*Gelatia inflata*
189-1172A-																																									
1H-CC, 10-15	6.24	G	F	x	x																		5																			
4H-CC, 12-17	35.11	G	T	x	x																																				
8H-CC, 15-20	73.22		B	x	x																																			
12H-CC, 10-15	110.05		B	x	x																																			
37X-CC, 38-43	345.10		B	x	x																																			
38X-CC, 24-29	353.76		B	x	x																																			
39X-2, 18-20	356.28		B	x	x																																			
39X-2, 135-137	357.45		B	x	x																																			
39X-3, 122-124	358.82	M	C	160	157	6	3	0	3.8	1.9	0.0													125								11		2	1					
39X-5, 22-24	360.82	G	A	250	244	5	1	0	2.0	0.4	0.0			1	1			2	4											1	1	200			1					1
39X-6, 64-66	362.74	G	A	233	228	7	5	2	3.0	2.1	0.9							1	7		1											60		1	2	1				
39X-CC, 27-33	364.34	G	A	221	207	8	6	1	3.6	2.7	0.5							1	2											1		130		3	6	3				
40X-CC, 26-31	374.00	G	A	231	217	7	11	3	3.0	4.8	1.3								10													150		3	10					
50X-CC, 0-8	460.20	G	A	250	248	1	3	1	0.4	1.2	0.4								1			1				6						30			205					
51X-CC, 43-48	476.19	G	A	146	251	2	6	10	1.4	4.1	6.8															1						180			31					
53X-CC, 34-39	498.80	G	A	100	229	5	3	6	5.0	3.0	6.0															3						175			20					
56X-CC, 23-33	518.23	G	C	106	232	6	6	4	5.7	5.7	3.8															2						185			23					
189-1172D-																																									
12R-CC, 23-28	584.27	G	A	181	116	27	12	12	14.9	6.6	6.6								4										1		2	40	1				13			
13R-CC, 0-5	593.63	M	F	x	x																								1			1								
19R-CC, 23-28	645.91	M	R	x	x																							1				1		1						
20R-CC, 7-12	660.85	G	A	129	101	20	5	4	15.5	3.9	3.1								6								1	9	2					1						
21R-CC, 5-11	667.20	M	C	45	27	20	3	2	44.4	6.7	4.4					1			1								1	1						1						
22R-CC, 17-23	673.03	G	A	208	206	1	1	0	0.5	0.5	0.0								1								1	1												
23R-CC, 28-33	682.06	M	F	108	86	40	8	4	37.0	7.4	3.7						4		30								2	10						1						
24R-5, 12-14	698.93	M	A	159	130	21	1	7	13.2	0.6	4.4		1	1					30	1								1			1						1	1		
24R-5, 30-32	696.11	M	A	189	140	41	0	8	21.7	0.0	4.2						2		25									3									5	1		
24R-5, 44-46	696.25	M	A	246	149	77	4	16	31.3	1.6	6.5						2		26						4			4									1			
24R-5, 77-79	696.58	M	A	183	103	68	1	12	37.2	0.5	6.6						1		25						3			4									1			
24R-5, 115-117	696.96	M	A	270	155	75	5	35	27.8	1.9	13.0						2		38						1			4									1			
24R-CC, 0-6	699.02	M	F	121	42	75	4	1	62.0	3.3	0.8								5						1			7												
25R-CC, 14-20	709.17	M	F	x	27																																			
31R-CC, 17-22	766.14	G	F	105	84	20	4	1	19.0	3.8	1.0	1																						1						

Notes: Preservation: G = good, M = moderate, P = poor. Indications of group abundance refer to abundance of dinocysts: A = abundant, C = common, F = few, R = rare, T = trace, B = barren. x = no representative count possible. G&F '83 = Goodman and Ford, 1983; B&B '93 = Brinkhuis and Biffi, 1993; C&H '96 = Crouch and Hollis, 1996.

Table T10 (continued).

Core, section, interval (cm)	Depth (mbsf)	*Glaphyrocysta ordinata*	*Glaphyrocysta retiintexta*	*Hemiplacophora semilunifera*	*Homotryblium tenuispinosum*	*Hystrichokolpoma rigaudiae*	*Hystrichokolpoma spinosum*	*Hystrichosphaeridium tubiferum*	*Hystrichostrogylon* spp.	*Impagidinium aculeatum*	*Impagidinium dispertitum*	*Impagidinium maculatum*	*Impagidinium paradoxum*	*Impagidinium patulum*	*Impagidinium* sp. (B&B '93)	*Impagidinium* sp. a (C&H '96)	*Impagidinium* spp. (pars)	*Impagidinium victorianum*	*Impagidinium waipawaensis*	*Isabelidinium* spp.	*Lejeunecysta* spp.	*Manumiella druggii*	*Multispinula quanta*	*Octodinium askiniae*	*Oligosphaeridium complex*	*Operculodinium centrocarpum*	*Operculodinium* sp. A	*Operculodinium* sp. B	*Palaeocystodinium* spp.	*Palaeoperidinium pyrophorum*	*Phthanoperidinium* spp.	*Pyxidinopsis waipawaensis*	*Pyxidinopsis* spp.	*Schematophora speciosa*	*Selenopemphix nephroides*	*Spinidinium luciae*	*Spinidinium macmurdoense*	*Spiniferites mirabilis*	*Spiniferites pseudofurcatus*	*Spiniferites ramosus*	*Spongodinium* sp.	*Stoveracysta kakanuiensis*	*Systematophora placacantha*	*Thalassiphora pelagica*	*Trithyrodinium evittii*	*Turbiosphaera filosa*	*Vozzhennikovia* spp.	*Wilsonidinium ornatum*
189-1172A-																																															
1H-CC, 10-15	6.24									1				1								1															5										
4H-CC, 12-17	35.11												1																																		
8H-CC, 15-20	73.22																																														
12H-CC, 10-15	110.05																																														
37X-CC, 38-43	345.10																																														
38X-CC, 24-29	353.76																																														
39X-2, 18-20	356.28																																														
39X-2, 135-137	357.45																																														
39X-3, 122-124	358.82														1										2	1					5						1									1	4
39X-5, 22-24	360.82			1					1	1					1			1			1				2	1				5				1	2			1	1			2	1			12
39X-6, 64-66	362.74										1					1		1			1				15	1	1			4					3	3	105			1				1			17
39X-CC, 27-33	364.34															1		1			1				1	6	1			17					1	1	19			1							11
40X-CC, 26-31	374.00														1			1			1				5	1				5							1			2						1	25
50X-CC, 0-8	460.20										1																			1										2				1			
51X-CC, 43-48	476.19										1														1	1				32										3				1			
53X-CC, 34-39	498.80																				1									25	1			1						2				1			
56X-CC, 23-33	518.23																									6				6	3									7							
189-1172D-																																															
12R-CC, 23-28	584.27				1	1	1	1			5								1		1				1	8		1			6								19			3				1	
13R-CC, 0-5	593.63							1																		1					1								1							
19R-CC, 23-28	645.91							1			1	1								3	1				1	3					1								1							
20R-CC, 7-12	660.85	50	17					2																	1													2			2					
21R-CC, 5-11	667.20	16	1					1				1									1							1											1							
22R-CC, 17-23	673.03	180	20					1																				1										1							
23R-CC, 28-33	682.06	30						3									1											1										3					1		
24R-5, 12-14	698.93																											5	79									4					1		
24R-5, 30-32	696.11							1																	2			10	74									9	1				4		
24R-5, 44-46	696.25							1														62		1				10	12									6	5				1		
24R-5, 77-79	696.58																					38			1			4									6	13						
24R-5, 115-117	696.96																					38			7			13				28					8							
24R-CC, 0-6	699.02							1									1				2	22						1									2							
25R-CC, 14-20	709.17																					25				1											1							
31R-CC, 17-22	766.14																15			10		50				6											1							1

Table T11. Selected dinocyst datums, Holes 1172A and 1172D.

Bioevent	Age (Ma)	Interval (cm) Top	Interval (cm) Bottom	Depth (mbsf) Top	Depth (mbsf) Bottom	Mean (mbsf)	Error (m)	Source
LO *Ennedocysta partridgei*	33.30	1172A-39X-2, 135.0–137.0	1172A-39X-3, 122.0–124.0	357.45	358.82	358.135	0.685	Williams et al., 1998a
LO *Schematophora speciosa*	35.50	1172A-39X-3, 122.0–124.0	1172A-39X-5, 22.0–24.0	358.82	360.82	359.820	1.000	Brinkhuis and Biffi, 1993
FO *Schematophora speciosa*	36.50	1172A-39X-5, 22.0–24.0	1172A-39X-6, 64.0–66.0	360.82	362.74	361.780	0.960	Brinkhuis and Biffi, 1993
FCO *Alterbidinium distinctum*	37.00	1172A-39X-CC	1172A-40X-CC	364.34	374.00	369.170	4.830	Raine et al., 1997
LO *Cerebrocysta bartonensis*	38.60	1172A-40X-CC	1172A-50X-CC	374.00	460.20	417.100	43.100	Williams et al., 1998a
LAO *Enneadocysta partridgei*	39.50	1172A-40X-CC	1172A-50X-CC	374.00	460.20	417.100	43.100	Raine et al., 1997
FAO *Enneadocysta partridgei*	43.00	1172A-50X-CC	1172A-51X-CC	460.20	476.19	468.195	7.995	Raine et al., 1997
LO *Hystrichokolpoma spinosa*	47.00	1172A-56X-CC	1172D-12R-CC	518.23	584.27	551.250	33.020	Wilson, 1988
LO *Wilsonidinium ornatum*	50.00	1172A-56X-CC	1172D-12R-CC	518.23	584.27	551.250	33.020	Wilson, 1988
FO *Wilsonidinium ornatum*	53.20	1172D-12R-CC	1172D-13R-CC	584.27	593.63	588.950	4.680	Wilson, 1988
FO *Hystrichokolpoma spinosa*	53.50	1172D-12R-CC	1172D-13R-CC	584.27	593.63	588.950	4.680	Wilson, 1988
FO *Deflandrea phosphoritica* cpx	55.00	1172D-13R-CC	1172D-19R-CC	593.63	645.91	619.770	26.140	Wilson, 1988
LO *Cerodinium boloniensis*	~58	1172D-19R-CC	1172D-20R-CC	645.91	660.85	653.380	7.470	Wrenn and Hart, 1988
LO *Alisocysta reticulata*	60.95	1172D-22R-CC	1172D-23R-CC	673.03	682.06	677.545	4.515	Williams et al., 1998a
FO *Alisocysta reticulata*	63.27	1172D-23R-CC	1172D-24R-CC	682.06	699.02	690.540	8.480	Williams et al., 1998a
FO *Trithyrodinium evittii*	64.90	1172D-24R-5, 44-46	1172D-24R-5, 77-79	696.25	696.58	696.415	0.165	Williams et al., 1998a
LAO *Manumiella druggii*	~63	1172D-23R-CC	1172D-24R-CC	682.06	699.02	690.540	8.480	Williams et al., 1998a
FAO *Manumiella druggii*	~69.0	1172D-31R-CC	1172D Bottom of hole	766.14	766.19	766.170	0.020	Raine et al., 1997

Notes: LO = last occurrence, FO = first occurrence, FCO = first consistent occurrence, LAO = last abundant occurrence, FAO = first abundant occurrence. This table is also available in **ASCII format.**

Table T12. Age-diagnostic biostratigraphic events, Site 1172. (**See table notes.** Continued on next page.)

Group	Hole	Bioevent	Age (Ma)	Interval (cm)		Depth (mbsf)		Mean (mbsf)	Error bar (m)
				Top	Bottom	Top	Bottom		
R	1172A	LO *Stylatractus universus*	0.45	1H-CC	2H-CC	6.24	16.15	11.20	4.96
N	1172A	LO *Pseudoemiliania lacunosa*	0.46	1H-CC	2H-CC	6.24	16.15	11.20	4.96
N	1172A	LO *Discoaster brouweri*	1.95	2H-CC	3H-CC	16.15	25.45	20.80	4.65
N	1172A	LO *Discoaster pentaradiatus*	2.40	3H-CC	4H-CC	25.45	35.11	30.28	4.83
N	1172A	LO *Discoaster surculus*	2.50	4H-CC	5H-CC	35.11	44.50	39.81	4.70
P	1172A	FO *Globorotalia inflata*	3.20	5H-CC	6H-CC	44.50	53.97	49.24	4.74
N	1172A	LO *Reticulofenestra pseudoumbilica*	3.75	5H-CC	6H-CC	44.50	53.97	49.24	4.74
N	1172A	LO *Amaurolithus primus*	4.60	6H-CC	7H-CC	53.97	63.79	58.88	4.91
P	1172A	LO *Globorotalia pliozea*	4.60	7H-CC	8H-CC	63.79	73.22	68.51	4.72
N	1172A	LO *Discoaster quinqueramus*	5.30	8H-CC	9H-CC	73.22	82.52	77.87	4.65
P	1172A	FO *Globorotalia puncticulata*	5.30	9H-CC	10H-CC	82.52	92.10	87.31	4.79
P	1172A	FO *Globorotalia conomiozea*	6.90	13H-CC	14H-CC	120.76	129.24	125.00	4.24
P	1172A	LO *Paragloborotalia continuosa*	8.00	15H-CC	16H-CC	139.79	149.22	144.51	4.72
P	1172A	LO *Paragloborotalia nympha*	10.10	17H-CC	18H-CC	158.27	167.85	163.06	4.79
D	1172A	LO *Denticulopsis dimorpha*	10.70	23H-CC	24H-CC	215.27	225.15	220.21	4.94
N	1172A	LO *Coccolithus miopelagicus*	11.00	25X-CC	26X-CC	228.01	235.84	231.93	3.91
P	1172A	LO *Paragloborotalia mayeri*	11.40	19H-CC	20H-CC	177.76	186.44	182.10	4.34
N	1172A	LO *Cyclicargolithus floridanus*	11.90	26X-CC	27X-CC	235.84	246.86	241.35	5.51
P	1172A	FO *Paragloborotalia mayeri*	12.10	27X-CC	28X-CC	246.86	255.65	251.26	4.40
R	1172A	LAO *Cyrtocapsella tetrapera*	12.50	26X-CC	27X-CC	235.84	246.86	241.35	5.51
N	1172A	LO *Sphenolithus heteromorphus*	13.60	32X-CC	33X-CC	295.79	306.37	301.08	5.29
P	1172A	FO *Orbulina suturalis*	15.10	28X-CC	29X-CC	255.65	266.27	260.96	5.31
P	1172A	FO *Praeorbulina curva*	16.30	33X-CC	34X-CC	306.37	316.34	311.36	4.98
N	1172A	LO *Calcidiscus premacintyrei*	17.40	34X-CC	35X-CC	316.14	324.92	320.53	4.39
P	1172A	FO *Globoturborotalita connecta*	20.90	35X-CC	36X-CC	324.92	335.08	330.00	5.08
P	1172A	FO *Globoquadrina dehiscens*	23.20	37X-CC	38X-CC	345.10	353.76	349.43	4.33
N	1172A	LO *Reticulofenestra bisecta*	23.90	36X-CC	37X-CC	335.08	345.10	340.09	5.01
N	1172A	LO *Chiasmolithus altus*	26.10	37X-CC	38X-CC	345.10	353.76	349.43	4.33
P	1172A	LO *Subbotina angiporoides*	30.00	38X-CC	39X, 2-5	353.76	356.15	354.96	1.19
D	1172A	FO *Rocella vigilans* (small)	30.24	39X-2, 3	39X-3, 61	356.14	358.22	357.18	1.04
D	1172A	FO *Cavitatus (Synedra) jouseanus*	30.62	39X-2, 3	39X-3, 61	356.14	358.22	357.18	1.04
N	1172A	LO *Reticulofenestra umbilica*	32.30	39X-2, 143	39X-5, 63	356.69	360.39	358.54	1.85
R	1172A	LO *Lychnocanoma amphitrite*	32.80	39X-CC	40X-CC	364.34	374.00	369.17	4.83
R	1172A	FO *Eucyrtidium antiquum*	32.96	40X-CC	41X-CC	374.00	383.60	378.80	4.80
C	1172A	LO *Ennedocysta partridgei*	33.30	39X-2, 135	39X-3, 122	357.45	358.82	358.14	0.69
N	1172A	LO *Reticulofenestra reticulata*	35.00	39X-2, 143	39X-5, 63	356.69	360.39	358.54	1.85
C	1172A	LO *Schematophora speciosa*	35.50	39X-3, 122	39X-5, 22	358.82	360.82	359.82	1.00
R	1172A	FO *Lychnocanoma amphitrite*	36.4-37.3	46X-CC	47X-CC	431.66	441.29	436.48	4.82
C	1172A	FO *Schematophora speciosa*	36.50	39X-5, 22	39X-6, 64	360.82	362.74	361.78	0.96
R	1172A	FO *Eucyrtidium spinosum*	37.00	41X-CC	42X-CC	383.60	393.18	388.39	4.79
C	1172A	FCO *Alterbidinium distinctum*	37.00	39X-CC	40X-CC	364.34	374.00	369.17	4.83
R	1172A	LO *Spongatractus pachystylus*	37.3-38.8	48X-CC	49X-CC	450.85	460.45	455.65	4.80
C	1172A	LO *Cerebrocysta bartonensis*	38.60	40X-CC	50X-CC	374.00	460.20	417.10	43.10
C	1172A	LAO *Enneadocysta partridgei*	39.50	40X-CC	50X-CC	374.00	460.20	417.10	43.10
N	1172A	LO *Chiasmolithus solitus*	40.40	42X-CC	43X-CC	393.18	402.83	398.01	4.82
N	1172A	FO *Reticulofenestra reticulata*	42.00	43X-CC	44X-CC	402.83	412.47	407.65	4.82
C	1172A	FAO *Enneadocysta partridgei*	43.00	50X-CC	51X-CC	460.20	476.19	468.20	8.00
N	1172A	FO *Reticulofenestra umbilica*	43.70	45X-CC	53X-CC	422.11	498.80	460.46	38.35
N	1172B	FO *Emiliania huxleyi*	0.26	Top of core	1H-CC	0.00	2.79	1.40	1.40
R	1172B	LO *Stylatractus universus*	0.45	1H-CC	2H-CC	2.79	12.73	7.76	4.97
N	1172B	LO *Pseudoemiliania lacunosa*	0.46	1H-CC	2H-CC	2.79	12.73	7.76	4.97
N	1172B	LO *Discoaster surculus*	2.50	3H-CC	4H-CC	22.10	31.77	26.94	4.84
N	1172B	LO *Reticulofenestra pseudoumbilica*	3.75	4H-CC	5H-CC	31.77	41.31	36.54	4.77
N	1172B	LO *Amaurolithus primus*	4.60	6H-CC	7H-CC	50.52	60.33	55.43	4.91
N	1172B	LO *Discoaster quinqueramus*	5.30	9H-CC	10H-CC	79.20	89.05	84.13	4.93
N	1172B	LO *Amaurolithus amplificus*	6.00	11H-CC	12H-CC	98.06	107.95	103.01	4.95
N	1172B	LO *Discoaster loeblichii*	7.40	14H-CC	15H-CC	126.46	136.11	131.29	4.83
N	1172C	LO *Pseudoemiliania lacunosa*	0.46	Top of core	1H-CC	0.00	9.47	4.74	4.74
N	1172C	LO *Discoaster brouweri*	1.95	2H-CC	3H-CC	19.06	28.40	23.73	4.67
N	1172C	LO *Discoaster surculus*	2.50	3H-CC	4H-CC	28.40	37.89	33.15	4.75
N	1172C	LO *Reticulofenestra pseudoumbilica*	3.75	4H-CC	5H-CC	37.89	47.36	42.63	4.74
N	1172C	LO *Amaurolithus primus*	4.60	6H-CC	7H-CC	56.94	66.14	61.54	4.60
N	1172C	LO *Discoaster quinqueramus*	5.30	8H-CC	9H-CC	76.22	85.81	81.02	4.80
N	1172C	LO *Amaurolithus amplificus*	6.00	10H-CC	11H-CC	94.45	104.90	99.68	5.22
N	1172C	LO *Discoaster loeblichii*	7.40	14H-CC	15H-CC	133.12	141.93	137.53	4.41
C	1172D	LO *Hystrichokolpoma spinosa*	47.00	56X-CC	12R-CC	518.23	584.27	551.25	33.02

Table T12 (continued).

Group	Hole	Bioevent	Age (Ma)	Interval (cm) Top	Interval (cm) Bottom	Depth (mbsf) Top	Depth (mbsf) Bottom	Mean (mbsf)	Error bar (m)
C	1172D	LO *Wilsonidinium ornatum*	50.00	56X-CC	12R-CC	518.23	584.27	551.25	33.02
C	1172D	FO *Wilsonidinium ornatum*	53.20	12R-CC	13R-CC	584.27	593.63	588.95	4.68
C	1172D	FO *Hystrichokolpoma spinosa*	53.50	12R-CC	13R-CC	584.27	593.63	588.95	4.68
C	1172D	FO *Deflandrea phosphoritica* cpx	55.00	13R-CC	19R-CC	593.63	645.91	619.77	26.14
C	1172D	LO *Cerodinium boloniensis*	~58	19R-CC	20R-CC	645.91	660.85	653.38	7.47
C	1172D	LO *Alisocysta reticulata*	60.95	22R-CC	23R-CC	673.03	682.06	677.55	4.51
C	1172D	LAO *Manumiella druggii*	~63	23R-CC	24R-CC	682.06	699.02	690.54	8.48
C	1172D	FO *Alisocysta reticulata*	63.27	23R-CC	24R-CC	682.06	699.02	690.54	8.48
C	1172D	FO *Trithyrodinium evittii*	64.90	24R-5, 44-46	24R-5, 77-79	696.25	696.58	696.42	0.17
N	1172D	LO *Arkhangelskiella cymbiformis*	65.00	24R-5, 41	25R-5, 40	696.11	705.70	700.91	4.80
N	1172D	LO *Eiffellithus turriseiffelii*	65.00	24R-5, 41	25R-5, 40	696.11	705.70	700.91	4.80

Notes: See individual microfossil sections this chapter for top and bottom samples of event interval. Mean depth is the midpoint between the top and bottom sample of the event interval. Group: R = radiolarian, N = nannofossil, P = planktonic foraminifer, D = diatom, C = dinocyst. LO = last occurrence, FO = first occurrence, LAO = last abundant occurrence, FAO = first abundant occurrence, FCO = first consistent occurrence.

Table T13. Magnetostratigraphic Results, Site 1172.

Chron/ Subchron	Age (Ma)	Depth (mbsf)
C1n	0.780	12.50
C2n	1.770	17.10
C2n	1.950	19.55
C2An.1n	2.581	30.90
C2An.1n	3.040	36.90
C2An.2n	3.110	38.60
C2An.2n	3.220	40.20
C2An.3n	3.330	41.70
C2An.3n	3.580	46.25
C3n.1n	4.180	57.80
C3n.1n	4.290	60.00
C3n.2n	4.480	63.40
C3n.2n	4.620	66.60
C3n.4n	5.230	78.90
C3An.1n	5.894	94.10
C3An.1n	6.137	100.70
C3An.2n	6.269	105.40
C3An.2n	6.567	107.40
C3Bn	6.935	121.50
C3Bn	7.091	124.20
C3Br.1n	7.135	125.40
C3Br.1n	7.170	126.80
C4n	8.072	146.90
C4r.1n	8.225	149.20
C4r.1n	8.257	150.30
C4An	8.669	154.20
C4An	9.025	167.00
C4Ar.1n	9.230	169.20
C4Ar.1n	9.308	169.80
C4Ar.2n	9.580	174.00
C4Ar.2n	9.642	175.00
C5n	9.740	176.70
C5n	10.949	215.00
C5An.1n	11.935	245.00
C5En	18.281	320.00
C5En	18.781	323.50
C6n.	19.048	326.00
C6n	20.131	337.00
C7n	24.730	346.00
C11n.1n	29.401	356.00
C11n.1n	29.662	356.80
C11n.2n	29.765	357.30
C11n.2n	30.098	358.60
C16n.1n	35.343	361.00
C16.1n	35.526	362.50
C16.2n	36.341	361.00
C17n.1n	36.618	362.80
C17n.1n	37.473	366.00
C17n.3n	37.920	367.20
C17n.3n	38.113	367.20
C18n.1n	38.426	368.00
C18n.2n	40.130	415.00
C19n	41.257	430.00
C19n	41.521	432.00
C20n	43.789	440.00
C23n.1n	50.778	555.00
C23n.2n	51.743	569.00
C24n.3n	53.347	594.00

Table T14. Composite depth section, Site 1172.

Hole, core	Depth (mbsf)	Offset (m)	Depth (mcd)
189-1172A-			
1H	0.00	0.32	0.32
2H	6.30	0.92	7.22
3H	15.80	2.22	18.02
4H	25.30	1.92	27.22
5H	34.80	2.94	37.74
6H	44.30	2.94	47.24
7H	53.80	2.94	56.74
8H	63.30	2.94	66.24
9H	72.80	2.94	75.74
10H	82.30	2.94	85.24
11H	91.80	9.92	101.72
12H	101.30	11.00	112.30
13H	110.80	11.12	121.92
14H	120.30	11.08	131.38
15H	129.80	11.08	140.88
16H	139.30	11.08	150.38
17H	148.80	11.08	159.88
18H	158.30	11.08	169.38
19H	167.80	11.08	178.88
20H	177.30	11.08	188.38
21H	186.80	11.08	197.88
22H	196.30	11.08	207.38
23H	205.80	11.08	216.88
24H	215.30	11.08	226.38
25X	224.80	11.08	235.88
26X	230.10	11.08	241.18
27X	239.70	11.08	250.78
28X	249.30	11.08	260.38
29X	258.90	11.08	269.98
30X	268.00	11.08	279.08
31X	277.60	11.08	288.68
32X	287.20	11.08	298.28
33X	296.80	11.08	307.88
34X	306.50	11.08	317.58
35X	316.10	11.08	327.18
36X	325.70	11.08	336.78
37X	335.30	11.08	346.38
38X	344.90	11.08	355.98
39X	354.60	11.84	366.44
40X	364.20	11.84	376.04
41X	373.80	11.84	385.64
42X	383.40	11.84	395.24
43X	393.00	11.84	404.84
44X	402.60	11.84	414.44
45X	412.20	11.84	424.04
46X	421.80	11.84	433.64
47X	431.40	11.84	443.24
48X	441.00	11.84	452.84
49X	450.60	11.84	462.44
51X	469.80	11.84	481.64
52X	479.40	11.84	491.24
53X	489.00	11.84	500.84
54X	498.60	11.84	510.44
55X	508.30	11.84	520.14
56X	518.00	11.84	529.84
189-1172B-			
1H	0.00	0.00	0.00
2H	2.90	1.32	4.22
3H	12.40	2.68	15.08
4H	21.90	2.40	24.30
5H	31.40	3.40	34.80
6H	40.90	4.10	45.00
7H	50.40	5.42	55.82
8H	59.90	6.30	66.20
9H	69.40	7.44	76.84
10H	78.90	9.20	88.10
11H	88.40	9.76	98.16
12H	97.90	10.68	108.58
13H	107.40	11.41	118.81
14H	116.90	11.46	128.36
15H	126.40	11.46	137.86
16H	135.90	11.46	147.36
17H	145.40	11.46	156.86
18H	154.90	11.46	166.36
19H	164.40	11.46	175.86
20H	173.90	11.46	185.36
21H	183.40	11.46	194.86
22H	192.90	11.46	204.36
189-1172C-			
1H	0.00	0.32	0.32
2H	9.50	0.64	10.14
3H	19.00	0.90	19.90
4H	28.50	2.38	30.88
5H	38.00	3.92	41.92
6H	47.50	4.24	51.74
7H	57.00	4.96	61.96
8H	66.50	6.82	73.32
9H	76.00	8.56	84.56
10H	85.50	9.66	95.16
11H	95.00	10.08	105.08
12H	104.50	10.22	114.72
13H	114.00	10.74	124.74
14H	123.50	12.02	135.52
15H	133.00	12.02	145.02
16H	142.50	12.02	154.52
17H	152.00	12.02	164.02
18H	161.50	12.02	173.52
189-1172D-			
2R	353.20	10.70	363.90
3R	362.80	10.83	373.63
4R	497.40	10.83	508.23
5R	507.00	10.83	517.83
6R	516.60	10.83	527.43
7R	526.20	10.83	537.03
8R	535.80	10.83	546.63
9R	545.40	10.83	556.23
10R	555.10	10.83	565.93
11R	564.70	10.83	575.53
12R	574.30	10.83	585.13
13R	583.90	10.83	594.73
14R	593.50	10.83	604.33
15R	603.10	10.83	613.93
16R	612.70	10.83	623.53
17R	622.30	10.83	633.13
18R	631.90	10.83	642.73
19R	641.50	10.83	652.33
20R	651.10	10.83	661.93
21R	660.70	10.83	671.53
22R	670.30	10.83	681.13
23R	680.00	10.83	690.83
24R	689.70	10.83	700.53
25R	699.30	10.83	710.13
26R	708.90	10.83	719.73
27R	718.50	10.83	729.33
28R	728.10	10.83	738.93
29R	737.70	10.83	748.53
30R	756.90	10.83	767.73

Table T15. Splice tie points, Site 1172.

Hole, core, section, interval (cm)	Depth (mbsf)	Depth (mcd)		Hole, core, section, interval (cm)	Depth (mbsf)	Depth (mcd)
189-				189-		
1172A-1H-5, 12	5.82	6.14	Tie to	1172B-2H-2, 42	4.82	6.14
1172B-2H-3, 88	6.78	8.10	Tie to	1172A-2H-1, 88	7.18	8.10
1172A-2H-6, 128	15.08	16.00	Tie to	1172C-2H-4, 136	15.36	16.00
1172C-2H-7, 8	18.58	19.22	Tie to	1172A-3H-1, 120	17.00	19.22
1172A-3H-6, 134	24.64	26.86	Tie to	1172B-4H-2, 106	24.46	26.86
1172B-4H-3, 100	25.90	28.30	Tie to	1172A-4H-1, 108	26.38	28.30
1172A-4H-7, 22	34.52	36.44	Tie to	1172C-4H-4, 106	34.06	36.44
1172C-4H-6, 18	36.18	38.56	Tie to	1172B-5H-3, 76	35.16	38.56
1172B-5H-6, 122	40.12	43.52	Tie to	1172C-5H-2, 10	39.60	43.52
1172C-5H-3, 138	42.38	46.30	Tie to	1172B-6H-1, 130	42.20	46.30
1172B-6H-6, 128	49.68	53.78	Tie to	1172C-6H-2, 54	49.54	53.78
1172C-6H-4, 24	52.24	56.48	Tie to	1172B-7H-1, 66	51.06	56.48
1172B-7H-6, 82	58.72	64.14	Tie to	1172C-7H-2, 68	59.18	64.14
1172C-7H-4, 76	62.26	67.22	Tie to	1172B-8H-1, 102	60.92	67.22
1172B-8H-6, 78	68.18	74.48	Tie to	1172C-8H-1, 116	67.66	74.48
1172C-8H-4, 40	71.40	78.22	Tie to	1172B-9H-1, 138	70.78	78.22
1172B-9H-6, 126	78.16	85.60	Tie to	1172C-9H-1, 104	77.04	85.60
1172C-9H-4, 80	81.30	89.86	Tie to	1172B-10H-2, 26	80.66	89.86
1172B-10H-6, 92	87.32	96.52	Tie to	1172C-10H-1, 136	86.86	96.52
1172C-10H-4, 74	90.74	100.40	Tie to	1172B-11H-2, 74	90.64	100.40
1172B-11H-5, 132	95.72	105.48	Tie to	1172A-11H-3, 76	95.56	105.48
1172A-11H-6, 96	100.26	110.18	Tie to	1172B-12H-2, 10	99.50	110.18
1172B-12H-3, 138	102.28	112.96	Tie to	1172A-12H-1, 66	101.96	112.96
1172A-12H-3, 140	105.70	116.70	Tie to	1172C-12H-2, 48	106.48	116.70
1172C-12H-6, 64	112.64	122.86	Tie to	1172A-13H-1, 93	111.74	122.86
1172A-13H-5, 90	117.70	128.82	Tie to	1172C-13H-3, 108	118.08	128.82
1172C-13H-6, 144	122.94	133.68	Tie to	1172A-14H-2, 79	122.60	133.68
1172A-14H-5, 10	126.40	137.48	Tie to	1172C-14H-2, 46	125.46	137.48
1172C-14H-CC, 8	133.08	145.10				

Table T16. Values for inorganic carbon, calcium carbonate, total carbon, total organic carbon, total nitrogen, total sulfur, and hydrogen in sediments, Hole 1172. (See table notes. Continued on next three pages.)

Hole, core, section	Depth (mbsf)	IC (wt%)	$CaCO_3$ (wt%)	TC (wt%)	TOC (wt%)	N (wt%)	S (wt%)	H (mg H/g)	C/N	C/S
189-1172A-										
1H-1	0.00	9.05	75.35	10.81	1.76	0.05	0.06	0.17	39.22	28.96
1H-3	3.00	10.14	84.50	NA	NA	NA	NA	NA	NA	NA
2H-2	7.80	10.10	84.14	NA	NA	NA	NA	NA	NA	NA
2H-3	9.30	9.33	77.73	10.21	0.88	0.05	0.07	0.24	19.53	13.50
2H-5	12.30	9.92	82.66	NA	NA	NA	NA	NA	NA	NA
3H-1	15.80	9.67	80.57	NA	NA	NA	NA	NA	NA	NA
3H-3	18.80	9.58	79.79	10.35	0.77	0.01	NA	0.15	124.48	NA
3H-5	21.80	3.64	30.32	NA	NA	NA	NA	NA	NA	NA
4H-1	25.30	7.05	58.69	NA	NA	NA	NA	NA	NA	NA
4H-3	28.30	9.58	79.78	10.03	0.45	0.00	0.10	0.18	452.30	4.67
4H-5	31.30	9.46	78.82	NA	NA	NA	NA	NA	NA	NA
5H-2	36.30	9.08	75.66	NA	NA	NA	NA	NA	NA	NA
5H-3	37.80	10.14	84.49	10.68	0.54	0.01	NA	0.16	59.62	NA
5H-5	40.80	9.91	82.58	NA	NA	NA	NA	NA	NA	NA
6H-1	44.30	10.27	85.54	NA	NA	NA	NA	NA	NA	NA
6H-3	47.30	10.33	86.04	10.84	0.51	0.01	0.01	0.15	56.79	61.18
6H-5	50.30	10.56	87.96	NA	NA	NA	NA	NA	NA	NA
7H-1	53.80	10.32	85.96	NA	NA	NA	NA	NA	NA	NA
7H-3	56.80	10.14	84.48	10.31	0.17	0.01	0.04	0.16	17.02	4.61
7H-5	59.80	9.79	81.52	NA	NA	NA	NA	NA	NA	NA
8H-1	63.30	9.79	81.55	NA	NA	NA	NA	NA	NA	NA
8H-3	66.30	10.44	86.96	10.54	0.10	0.01	NA	0.12	13.01	NA
8H-5	69.30	10.08	83.97	NA	NA	NA	NA	NA	NA	NA
10H-3	85.30	10.20	85.01	10.37	0.17	0.00	0.02	0.11	165.10	9.74
11H-1	91.80	10.73	89.40	NA	NA	NA	NA	NA	NA	NA
11H-3	94.80	9.78	81.46	10.25	0.47	0.00	0.01	0.16	NA	92.49
11H-5	97.80	10.92	91.00	NA	NA	NA	NA	NA	NA	NA
12H-1	101.30	9.86	82.17	NA	NA	NA	NA	NA	NA	NA
12H-3	104.30	10.92	90.99	11.33	0.41	0.00	0.00	0.07	NA	NA
12H-5	107.30	10.55	87.85	NA	NA	NA	NA	NA	NA	NA
13H-1	110.80	10.77	89.68	NA	NA	NA	NA	NA	NA	NA
13H-3	113.80	10.77	89.75	11.00	0.23	0.00	0.00	0.07	NA	NA
13H-5	116.80	10.82	90.15	NA	NA	NA	NA	NA	NA	NA
14H-1	120.30	10.58	88.11	NA	NA	NA	NA	NA	NA	NA
14H-3	123.30	10.30	85.81	10.76	0.46	0.00	0.00	0.12	NA	NA
14H-5	126.30	9.44	78.62	NA	NA	NA	NA	NA	NA	NA
15H-1	129.80	10.57	88.03	NA	NA	NA	NA	NA	NA	NA
15H-4	134.30	11.01	91.72	11.45	0.44	0.00	0.00	0.06	NA	NA
16H-2	140.80	10.11	84.25	NA	NA	NA	NA	NA	NA	NA
16H-4	143.80	10.21	85.04	10.21	0.00	0.00	0.00	0.11	NA	NA
17H-1	148.80	10.17	84.71	NA	NA	NA	NA	NA	NA	NA
17H-3	151.80	10.60	88.28	11.04	0.44	0.00	0.00	0.11	NA	NA
17H-5	154.80	10.92	90.95	NA	NA	NA	NA	NA	NA	NA
18H-1	158.30	10.60	88.29	NA	NA	NA	NA	NA	NA	NA
18H-3	161.30	9.79	81.59	10.04	0.25	0.00	0.00	0.15	NA	NA
18H-5	164.30	10.02	83.48	NA	NA	NA	NA	NA	NA	NA
19H-1	167.80	10.76	89.66	NA	NA	NA	NA	NA	NA	NA
19H-3	170.80	10.57	88.03	10.96	0.39	0.00	0.00	0.09	NA	NA
19H-5	173.80	10.90	90.78	NA	NA	NA	NA	NA	NA	NA
20H-1	177.30	11.18	93.15	NA	NA	NA	NA	NA	NA	NA
20H-3	180.30	11.15	92.84	11.62	0.47	0.00	0.00	0.04	NA	NA
20H-5	183.30	11.27	93.91	NA	NA	NA	NA	NA	NA	NA
21H-3	189.80	11.37	94.71	11.75	0.38	0.00	0.00	0.03	NA	NA
21H-5	192.80	11.33	94.38	NA	NA	NA	NA	NA	NA	NA
22H-1	196.30	11.48	95.62	NA	NA	NA	NA	NA	NA	NA
22H-3	199.30	11.46	95.49	11.29	0.00	0.00	0.00	0.03	NA	NA
22H-5	202.30	11.42	95.11	NA	NA	NA	NA	NA	NA	NA
23H-1	205.80	11.56	96.30	NA	NA	NA	NA	NA	NA	NA
23H-3	208.80	11.07	92.22	10.93	0.00	0.00	0.00	0.04	NA	NA
23H-5	211.80	11.69	97.34	NA	NA	NA	NA	NA	NA	NA
24H-1	215.30	11.41	95.02	NA	NA	NA	NA	NA	NA	NA
24H-3	218.30	11.53	96.03	11.54	0.01	0.00	0.00	0.02	NA	NA
25X-1	224.80	11.61	96.72	11.79	0.18	0.00	0.00	0.03	NA	NA
26X-1	230.10	11.45	95.38	NA	NA	NA	NA	NA	NA	NA
26X-3	233.10	11.43	95.21	11.69	0.26	0.00	0.00	0.04	NA	NA

Table T16 (continued).

Hole, core, section	Depth (mbsf)	IC (wt%)	$CaCO_3$ (wt%)	TC (wt%)	TOC (wt%)	N (wt%)	S (wt%)	H (mg H/g)	C/N	C/S
27X-1	239.70	11.28	93.98	NA	NA	NA	NA	NA	NA	NA
27X-3	242.70	10.95	91.22	11.05	0.10	0.00	0.00	0.05	NA	NA
27X-5	245.70	11.16	93.00	NA	NA	NA	NA	NA	NA	NA
28X-1	249.30	11.31	94.19	NA	NA	NA	NA	NA	NA	NA
28X-3	252.30	11.42	95.11	11.11	0.00	0.00	0.00	0.04	NA	NA
28X-5	255.00	11.14	92.78	NA	NA	NA	NA	NA	NA	NA
29X-1	258.90	11.33	94.34	NA	NA	NA	NA	NA	NA	NA
29X-3	261.90	11.23	93.52	11.67	0.44	0.00	0.00	0.04	NA	NA
29X-5	264.90	11.25	93.74	NA	NA	NA	NA	NA	NA	NA
30X-1	268.00	10.97	91.41	NA	NA	NA	NA	NA	NA	NA
30X-3	271.00	11.19	93.20	11.58	0.39	0.00	0.00	0.05	NA	NA
30X-5	274.00	10.79	89.90	NA	NA	NA	NA	NA	NA	NA
31X-1	277.60	11.05	92.04	NA	NA	NA	NA	NA	NA	NA
31X-3	280.60	10.98	91.48	11.48	0.50	0.00	0.00	0.08	NA	NA
31X-5	283.60	10.73	89.36	NA	NA	NA	NA	NA	NA	NA
32X-1	287.20	10.96	91.32	NA	NA	NA	NA	NA	NA	NA
32X-3	290.20	10.57	88.07	11.06	0.49	0.00	0.00	0.10	NA	NA
32X-5	293.20	10.70	89.13	NA	NA	NA	NA	NA	NA	NA
33X-1	296.80	11.18	93.15	NA	NA	NA	NA	NA	NA	NA
33X-3	299.80	10.44	87.00	10.96	0.52	0.00	0.00	0.09	NA	NA
33X-5	302.80	10.75	89.55	NA	NA	NA	NA	NA	NA	NA
34X-1	306.50	10.73	89.40	NA	NA	NA	NA	NA	NA	NA
34X-3	309.50	10.97	91.42	11.38	0.41	0.00	0.00	0.06	NA	NA
34X-5	312.50	10.68	88.95	NA	NA	NA	NA	NA	NA	NA
35X-1	316.10	10.85	90.36	NA	NA	NA	NA	NA	NA	NA
35X-3	319.10	10.56	87.99	11.03	0.47	0.00	0.00	0.08	NA	NA
35X-5	322.10	10.35	86.23	NA	NA	NA	NA	NA	NA	NA
36X-1	325.70	10.79	89.88	NA	NA	NA	NA	NA	NA	NA
36X-3	328.70	10.72	89.26	11.18	0.46	0.00	0.00	0.07	NA	NA
36X-5	331.70	10.47	87.23	NA	NA	NA	NA	NA	NA	NA
37X-1	335.30	10.00	83.29	NA	NA	NA	NA	NA	NA	NA
37X-3	338.30	9.41	78.41	9.30	0.00	0.01	0.00	0.18	0.00	NA
37X-5	341.30	9.78	81.49	NA	NA	NA	NA	NA	NA	NA
38X-1	344.90	9.36	77.96	NA	NA	NA	NA	NA	NA	NA
38X-3	347.90	7.74	64.48	7.32	0.00	0.01	0.00	0.34	0.00	NA
38X-5	350.90	8.26	68.84	NA	NA	NA	NA	NA	NA	NA
39X-1	354.60	6.43	53.58	NA	NA	NA	NA	NA	NA	NA
39X-1	354.60	4.88	40.69	NA	NA	NA	NA	NA	NA	NA
39X-2	356.10	2.39	19.95	NA	NA	NA	NA	NA	NA	NA
39X-2	356.10	0.54	4.52	NA	NA	NA	NA	NA	NA	NA
39X-3	357.60	0.04	0.29	0.10	0.06	0.02	0.00	1.02	3.04	NA
39X-3	357.60	0.04	0.33	NA	NA	NA	NA	NA	NA	NA
39X-4	359.10	0.18	1.51	NA	NA	NA	NA	NA	NA	NA
39X-4	359.10	0.04	0.34	NA	NA	NA	NA	NA	NA	NA
39X-5	360.60	0.39	3.25	NA	NA	NA	NA	NA	NA	NA
39X-5	360.60	0.59	4.95	NA	NA	NA	NA	NA	NA	NA
39X-6	362.10	0.91	7.58	NA	NA	NA	NA	NA	NA	NA
39X-6	362.10	1.32	11.02	NA	NA	NA	NA	NA	NA	NA
40X-1	364.20	1.26	10.48	NA	NA	NA	NA	NA	NA	NA
40X-3	367.20	2.19	18.25	2.71	0.52	0.04	0.34	0.79	13.02	1.51
40X-5	370.20	1.19	9.93	NA	NA	NA	NA	NA	NA	NA
41X-1	373.80	0.00	0.00	NA	NA	NA	NA	NA	NA	NA
41X-3	376.80	1.16	9.68	1.67	0.51	0.04	0.62	0.84	12.67	0.83
41X-5	379.80	1.09	9.11	NA	NA	NA	NA	NA	NA	NA
42X-1	383.40	0.33	2.77	NA	NA	NA	NA	NA	NA	NA
42X-3	386.40	1.67	13.89	2.16	0.49	0.02	0.34	0.80	28.01	1.43
42X-5	389.40	1.21	10.11	NA	NA	NA	NA	NA	NA	NA
43X-1	393.00	0.75	6.22	NA	NA	NA	NA	NA	NA	NA
43X-3	396.00	0.73	6.07	1.34	0.61	0.01	0.29	0.78	55.02	2.14
43X-5	399.00	1.79	14.91	NA	NA	NA	NA	NA	NA	NA
44X-1	402.60	1.83	15.27	NA	NA	NA	NA	NA	NA	NA
44X-3	405.60	0.55	4.57	1.05	0.50	0.03	0.25	0.80	19.80	2.01
44X-5	408.60	1.27	10.61	NA	NA	NA	NA	NA	NA	NA
45X-1	412.20	0.76	6.36	NA	NA	NA	NA	NA	NA	NA
45X-3	415.20	0.03	0.29	0.40	0.36	0.04	0.28	0.86	9.87	1.29
45X-5	418.20	0.09	0.72	NA	NA	NA	NA	NA	NA	NA
46X-1	421.80	0.66	5.54	NA	NA	NA	NA	NA	NA	NA
46X-3	424.80	0.33	2.74	0.74	0.41	0.03	0.36	0.79	12.59	1.14
46X-5	427.80	0.51	4.22	NA	NA	NA	NA	NA	NA	NA

Table T16 (continued).

Hole, core, section	Depth (mbsf)	IC (wt%)	$CaCO_3$ (wt%)	TC (wt%)	TOC (wt%)	N (wt%)	S (wt%)	H (mg H/g)	C/N	C/S
47X-1	431.40	0.23	1.95	NA	NA	NA	NA	NA	NA	NA
47X-3	434.40	0.06	0.51	0.51	0.45	0.01	0.22	0.81	54.44	2.04
47X-5	437.40	0.02	0.17	NA	NA	NA	NA	NA	NA	NA
48X-1	441.00	0.04	0.30	NA	NA	NA	NA	NA	NA	NA
48X-3	444.00	0.03	0.24	0.76	0.73	0.04	0.49	0.88	18.42	1.50
48X-5	447.00	0.02	0.16	NA	NA	NA	NA	NA	NA	NA
49X-1	450.60	0.03	0.23	NA	NA	NA	NA	NA	NA	NA
49X-3	453.60	0.03	0.21	0.79	0.77	0.05	1.08	1.02	15.84	0.71
49X-5	456.60	0.03	0.21	NA	NA	NA	NA	NA	NA	NA
51X-1	469.80	0.03	0.28	NA	NA	NA	NA	NA	NA	NA
51X-3	472.80	0.03	0.21	0.48	0.46	0.01	0.43	0.80	52.77	1.07
52X-1	479.40	0.04	0.32	NA	NA	NA	NA	NA	NA	NA
52X-3	482.40	0.03	0.23	0.99	0.97	0.04	0.61	0.91	22.74	1.58
52X-5	485.40	0.02	0.15	NA	NA	NA	NA	NA	NA	NA
53X-3	492.00	0.04	0.37	0.62	0.58	0.01	0.36	0.99	85.95	1.60
53X-5	495.00	0.14	1.16	NA	NA	NA	NA	NA	NA	NA
54X-1	498.60	1.00	8.31	NA	NA	NA	NA	NA	NA	NA
54X-3	501.60	0.77	6.37	1.15	0.39	0.03	0.33	0.81	14.91	1.15
189-1172D-										
3R-1	362.80	0.87	7.22	NA	NA	NA	NA	NA	NA	NA
3R-3	365.80	0.91	7.58	1.49	0.58	0.05	0.44	1.07	10.64	1.33
3R-5	368.80	0.62	5.17	NA	NA	NA	NA	NA	NA	NA
5R-1	507.00	0.08	0.69	NA	NA	NA	NA	NA	NA	NA
5R-3	510.00	NA	NA	0.64	NA	0.03	0.28	0.68	NA	NA
6R-1	516.60	0.38	3.20	NA	NA	NA	NA	NA	NA	NA
6R-3	519.60	0.26	2.16	0.67	0.41	0.03	0.45	0.52	12.94	0.91
7R-1	526.20	0.29	2.40	NA	NA	NA	NA	NA	NA	NA
7R-3	529.20	0.13	1.07	0.81	0.68	0.03	0.52	0.74	21.12	1.30
7R-5	532.20	0.22	1.85	NA	NA	NA	NA	NA	NA	NA
8R-1	535.80	0.67	5.61	NA	NA	NA	NA	NA	NA	NA
8R-3	538.80	0.87	7.21	1.48	0.61	0.03	0.29	0.51	18.05	2.13
8R-5	541.80	0.71	5.90	NA	NA	NA	NA	NA	NA	NA
9R-1	545.40	0.76	6.30	NA	NA	NA	NA	NA	NA	NA
9R-3	548.40	0.43	3.57	0.90	0.47	0.02	0.28	0.58	18.98	1.70
9R-5	551.40	0.09	0.77	NA	NA	NA	NA	NA	NA	NA
10R-1	555.10	0.60	5.00	NA	NA	NA	NA	NA	NA	NA
10R-3	558.10	0.22	1.83	0.49	0.27	0.00	0.26	0.47	81.83	1.06
10R-5	561.10	0.46	3.84	NA	NA	NA	NA	NA	NA	NA
11R-1	564.70	0.04	0.33	NA	NA	NA	NA	NA	NA	NA
11R-3	567.70	0.03	0.23	0.45	0.42	0.05	0.33	0.70	8.55	1.29
11R-5	570.70	0.04	0.30	NA	NA	NA	NA	NA	NA	NA
12R-1	574.30	0.03	0.26	NA	NA	NA	NA	NA	NA	NA
12R-3	577.30	0.03	0.29	0.36	0.32	0.03	0.12	0.71	10.26	2.61
12R-5	580.30	0.04	0.31	NA	NA	NA	NA	NA	NA	NA
13R-1	583.90	0.03	0.21	NA	NA	NA	NA	NA	NA	NA
13R-3	586.90	0.02	0.19	0.90	0.88	0.04	0.22	0.88	22.78	4.01
13R-5	589.90	0.01	0.08	NA	NA	NA	NA	NA	NA	NA
14R-1	593.50	0.02	0.20	NA	NA	NA	NA	NA	NA	NA
14R-3	596.50	0.02	0.20	0.59	0.56	0.05	0.41	0.69	11.04	1.38
14R-5	599.50	0.02	0.16	NA	NA	NA	NA	NA	NA	NA
15R-1	603.10	0.02	0.18	NA	NA	NA	NA	NA	NA	NA
15R-3	606.10	0.03	0.23	0.78	0.75	0.05	0.65	0.86	14.45	1.16
15R-5	609.10	0.02	0.17	NA	NA	NA	NA	NA	NA	NA
16R-1	612.70	0.03	0.23	NA	NA	NA	NA	NA	NA	NA
16R-3	615.70	0.02	0.16	0.54	0.52	0.03	0.41	0.75	16.79	1.26
17R-1	622.30	0.02	0.15	NA	NA	NA	NA	NA	NA	NA
17R-3	625.30	0.01	0.07	1.01	1.00	0.07	0.84	0.66	15.02	1.19
17R-5	628.30	0.01	0.09	NA	NA	NA	NA	NA	NA	NA
18R-1	631.90	0.01	0.12	NA	NA	NA	NA	NA	NA	NA
18R-3	634.90	0.02	0.15	0.88	0.86	0.05	1.10	0.68	16.35	0.79
18R-5	637.90	0.03	0.22	NA	NA	NA	NA	NA	NA	NA
19R-1	641.50	0.02	0.14	NA	NA	NA	NA	NA	NA	NA
19R-3	644.50	0.02	0.20	0.56	0.54	0.04	0.69	0.55	13.18	0.78
20R-1	651.10	0.05	0.41	NA	NA	NA	NA	NA	NA	NA
20R-3	654.10	0.03	0.23	1.20	1.17	0.06	0.41	0.76	18.54	2.88
20R-5	657.10	0.02	0.20	NA	NA	NA	NA	NA	NA	NA
21R-1	660.70	0.03	0.25	NA	NA	NA	NA	NA	NA	NA
21R-3	663.70	0.02	0.20	0.64	0.62	0.04	0.72	0.49	15.41	0.86
22R-1	670.30	0.03	0.25	0.61	0.58	0.06	0.79	0.55	9.96	0.73

Table T16 (continued).

Hole, core, section	Depth (mbsf)	IC (wt%)	$CaCO_3$ (wt%)	TC (wt%)	TOC (wt%)	N (wt%)	S (wt%)	H (mg H/g)	C/N	C/S
23R-1	680.00	0.02	0.19	0.69	0.67	0.05	0.62	0.60	14.08	1.07
26R-1	708.90	0.26	2.20	NA	NA	NA	NA	NA	NA	NA
26R-3	711.88	0.19	1.60	0.87	0.68	0.05	1.08	0.53	14.80	0.63
26R-5	714.63	0.12	0.99	NA	NA	NA	NA	NA	NA	NA
27R-1	718.50	0.25	2.08	NA	NA	NA	NA	NA	NA	NA
27R-3	721.26	0.14	1.15	0.81	0.67	0.05	1.40	0.60	14.61	0.48
28R-1	728.10	0.08	0.71	NA	NA	NA	NA	NA	NA	NA
28R-3	731.07	0.12	0.98	0.85	0.73	0.05	1.23	0.67	15.43	0.60
28R-5	733.93	0.08	0.63	NA	NA	NA	NA	NA	NA	NA
29R-1	737.70	0.02	0.13	NA	NA	NA	NA	NA	NA	NA
29R-3	740.70	0.07	0.58	0.75	0.68	0.06	1.15	0.62	11.28	0.60
29R-5	743.70	0.02	0.14	NA	NA	NA	NA	NA	NA	NA
31R-1	756.90	0.20	1.67	NA	NA	NA	NA	NA	NA	NA
31R-3	759.90	0.04	0.30	0.78	0.75	0.04	0.77	0.66	17.23	0.98
31R-5	762.90	0.78	6.48	NA	NA	NA	NA	NA	NA	NA

Notes: IC = inorganic carbon, $CaCO_3$ = calcium carbonate, TC = total carbon, TOC = total organic carbon, N = total nitrogen, S = total sulfur, H = hydrogen. C/N = carbon nitrogen ratio, C/S = carbon sulfur ratio. NA = not analyzed.

Table T17. Results of Rock-Eval analyses on sediments, Site 1172.

Hole, core, section	Depth (mbsf)	T_{max} (°C)	S_1	S_2	S_3	TOC (%)	HI	OI
189-1172A-								
43X-CC	397.50	598	0.03	0.40	1.09	0.14	285	778
45X-CC	416.70	597	0.01	0.74	0.65	0.21	352	309
46X-CC	426.30	505	0.14	1.73	0.45	0.36	480	125
49X-CC	455.10	588	0.05	1.70	0.29	0.32	531	90
51X-CC	474.30	402	0.06	2.55	0.42	0.48	531	87
52X-CC	484.00	597	0.20	2.30	0.25	0.37	621	67
53X-CC	493.50	418	0.03	0.48	0.58	0.22	218	263
54X-CC	503.10	599	0.04	0.41	0.39	0.10	410	390
55X-CC	508.30	594	0.03	0.31	0.69	0.16	193	431
56X-CC	518.00	406	0.03	0.11	0.63	0.16	68	393
189-1172D-								
4R-CC	501.90	598	0.05	1.42	0.95	0.61	232	155
5R-CC	511.50	596	0.02	0.79	0.88	0.30	263	293
6R-CC	521.10	407	0.02	1.27	0.24	0.46	276	52
7R-CC	530.70	598	0.03	0.57	0.81	0.44	129	184
8R-CC	540.30	500	0.05	1.74	0.50	0.43	404	116
9R-CC	549.90	481	0.09	2.22	0.34	0.50	444	68
10R-CC	559.60	469	0.06	1.92	0.41	0.16	1200	256
11R-CC	569.20	580	0.01	1.44	0.50	0.35	411	142
12R-CC	578.80	436	0.03	2.12	0.44	0.88	240	50
13R-CC	588.40	469	0.00	1.86	0.47	0.24	775	195
14R-CC	598.00	438	0.01	1.66	0.52	0.84	197	61
15R-CC	607.60	420	0.02	2.07	0.46	0.40	768	151
16R-CC	617.20	415	0.01	1.62	0.39	0.13	1246	300
17R-CC	626.80	414	0.13	2.98	0.75	1.53	194	49
18R-CC	636.40	444	0.02	1.94	0.15	0.48	404	31
19R-CC	644.50	NA	0.00	0.00	0.20	0.31	0	64
20R-CC	655.60	477	0.03	1.95	0.41	0.57	342	71
21R-CC	665.20	548	0.02	1.21	0.46	0.30	361	208
22R-CC	671.80	512	0.02	2.21	0.34	0.72	306	47
23R-CC	681.50	438	0.00	1.43	0.35	0.45	317	77
24R-CC	691.20	421	0.01	1.61	0.45	0.79	203	56
25R-CC	703.80	412	0.03	1.96	0.33	0.83	236	39
26R-CC	714.00	456	0.08	1.73	0.82	0.89	194	92
27R-CC	722.70	447	0.45	1.28	0.24	0.37	345	64
28R-CC	732.60	597	0.05	1.67	0.61	0.76	219	80
29R-CC	742.20	596	0.02	1.80	0.48	0.64	281	75
30R-CC	747.40	421	0.03	1.82	0.49	0.49	371	100
31R-CC	761.40	591	0.00	0.89	0.52	0.55	161	94

Notes: T_{max} = temperature (°C) of maximum hydrocarbon generation from kerogen. S_1 = volatile hydrocarbons, S_2 = kerogen-derived hydrocarbons, S_3 = organic CO_2 from kerogen. All S values are measured in milligrams hydrocarbon. TOC = total organic carbon obtained by Rock-Eval analysis. HI = hydrogen index, OI = oxygen index. NA = not analyzed.

Table T18. Headspace gas composition, Site 1172.

Hole, core, section	Depth (mbsf)	C_1 (ppmv)	C_2 (ppmv)	C_3 (ppmv)
189-1172A-				
1H-4	4.50	2	0	0
2H-4	10.80	2	0	0
3H-4	20.30	2	0	0
4H-4	29.80	3	0	0
5H-4	39.30	3	0	0
6H-4	48.80	2	0	0
7H-4	58.30	2	0	0
8H-4	67.80	3	0	0
9H-4	77.30	2	0	0
10H-4	86.80	3	0	0
11H-4	96.30	4	0	0
12H-4	105.80	4	0	0
13H-4	115.30	3	0	0
14H-4	124.80	4	0	0
15H-4	134.30	2	0	0
16H-4	143.80	2	0	0
17H-4	153.30	2	0	0
18H-4	162.80	2	0	0
19H-4	172.30	2	0	0
20H-4	181.80	2	0	0
21H-4	191.30	12	0	0
22H-4	200.80	2	0	0
23H-4	210.30	3	0	0
24H-4	219.80	3	0	0
25X-2	226.30	2	0	0
26X-3	233.10	2	0	0
27X-4	244.20	3	0	0
28X-3	252.30	5	0	0
29X-4	263.40	4	0	0
30X-4	272.50	3	0	0
31X-4	282.10	3	0	0
32X-4	291.70	2	0	0
33X-4	301.30	3	0	0
34X-4	311.00	2	0	0
35X-4	320.60	4	0	0
36X-4	330.20	4	0	0
37X-4	339.80	2	0	0
38X-4	349.40	2	0	0
39X-4	359.10	10	0	0
40X-4	368.70	2	0	0
41X-4	378.30	2	0	0
42X-4	387.90	2	0	0
43X-4	397.50	2	0	0
44X-4	407.10	2	0	0
45X-4	416.70	2	0	0
46X-4	426.30	2	0	0
47X-4	435.90	2	0	0
48X-4	445.50	9	0	0
49X-4	455.10	2	0	0
51X-4	474.30	4	0	0
53X-4	493.50	5	0	0
54X-4	503.10	21	15	14
55X-1	508.30	5	0	0
56X-CC	518.00	4	0	0
189-1172D-				
4R-4	501.90	3	0	0
5R-4	511.50	3	0	0
6R-4	521.10	4	0	0
7R-4	530.70	5	0	0
8R-4	540.30	11	0	0
9R-4	549.90	10	0	0
10R-4	559.60	10	0	0
11R-4	569.20	24	0	0
12R-4	578.80	24	0	0
13R-4	588.40	24	0	0
14R-4	598.00	31	0	0
15R-4	607.60	28	1	0
16R-4	617.20	31	1	0
17R-4	626.80	33	2	0
18R-4	636.40	17	0	0
19R-3	644.50	19	1	0
20R-4	655.60	34	1	0
21R-4	665.20	44	2	0
22R-2	671.80	51	2	0
23R-2	681.50	36	1	0
24R-2	691.20	19	1	0
25R-4	703.80	91	3	0
27R-4	722.70	91	3	0
28R-4	732.60	129	4	0
29R-4	742.20	84	2	0
30R-CC	747.40	135	3	0
31R-4	761.40	185	4	0

Notes: C_1 = methane, C_2 = ethane, C_3 = propane. ppmv = parts per million by volume.

Table T19. Interstitial water data, Site 1172.

Core, section, interval (cm)	Depth (mbsf)	pH	Alkalinity (mM)	Salinity	Cl^- (mM)	SO_4^{2-} (mM)	Na^+ (mM)	Mg^{2+} (mM)	Ca^{2+} (mM)	K^+ (mM)	$H_4SiO_4^0$ (µM)	NH_4^+ (µM)	Sr^{2+} (µM)	Li^+ (µM)
189-1172A-														
1H-3, 145-150	4.45	7.56	3.84	35.0	557	27.7	468	54.1	11.1	11.5	401	69	112	20
2H-3, 145-150	10.75	7.50	4.58	35.0	559	27.3	474	53.7	11.1	11.5	505	130	151	20
3H-3, 145-150	20.25	7.47	5.35	35.0	566	26.6	478	52.6	11.3	12.0	541	198	202	23
4H-3, 145-150	29.75	7.40	5.37	35.0	563	26.0	477	51.4	11.6	11.9	579	220	253	26
5H-3, 145-150	39.25	7.42	6.08	35.0	563	25.1	477	51.0	13.0	12.1	568	248	296	29
6H-3, 145-150	48.75	7.30	6.35	35.0	563	24.5	473	49.7	11.9	11.5	421	266	355	34
7H-3, 145-150	58.25	7.32	6.42	35.0	562	24.5	478	49.7	12.6	11.5	391	319	392	36
8H-3, 145-150	67.75	7.26	6.85	35.0	561	24.1	477	48.5	12.2	11.2	439	321	460	42
9H-3, 145-150	77.25	7.24	7.21	35.0	562	23.2	476	47.9	12.5	11.2	489	379	498	45
10H-3, 145-150	86.75	7.07	7.33	35.0	560	22.9	474	46.8	13.2	10.8	559	370	546	50
11H-3, 145-150	96.25	7.18	7.87	35.0	561	22.6	476	46.5	13.9	11.0	595	416	613	55
14H-3, 140-150	124.70	7.11	7.80	35.0	561	22.4	477	44.9	15.0	10.7	801	452	737	72
17H-3, 140-150	153.20	7.05	NM	35.0	562	21.3	479	42.6	15.9	10.6	897	505	818	99
20H-3, 140-150	181.70	6.97	8.76	35.0	563	20.6	475	41.1	18.4	10.0	921	481	914	124
23H-3, 140-150	210.20	6.96	9.49	35.0	565	20.4	477	39.9	19.1	10.8	999	551	910	151
26X-2, 140-150	233.00	6.98	9.70	36.0	570	20.7	482	39.2	19.6	10.4	961	567	884	176
29X-3, 135-150	263.25	7.00	9.52	37.0	569	19.4	482	37.3	20.6	10.4	1039	636	877	221
32X-3, 140-150	291.60	6.94	9.04	36.0	568	18.9	484	36.2	21.1	10.2	887	667	853	267
35X-3, 138-150	320.48	7.03	8.40	35.0	570	18.1	475	34.5	22.6	9.8	615	711	793	310
38X-3, 135-150	349.25	7.01	8.12	35.0	571	17.7	477	32.7	23.9	9.5	923	795	734	363
41X-3, 135-150	378.15	7.12	9.63	35.0	573	17.0	477	31.5	25.5	9.5	1079	825	666	409
44X-3, 135-150	406.95	7.31	8.42	35.0	569	16.3	478	29.9	26.7	8.7	919	868	598	435
47X-3, 135-150	435.75	7.31	10.76	35.0	563	15.3	471	29.7	28.5	7.3	877	815	551	454
51X-3, 135-150	474.15	7.11	11.00	35.0	569	13.6	475	27.8	28.4	7.4	1013	826	452	484
54X-3, 135-150	502.95	7.02	9.98	35.0	574	12.9	479	27.2	27.6	7.4	1149	946	398	475
189-1172D-														
4R-3, 135-150	501.75	7.10	8.70	35.0	570	13.1	480	26.1	25.0	7.5	924	984	399	469
7R-3, 135-150	530.55	NM	NM	30.0	503	9.8	415	24.2	22.3	4.6	425	638	314	415
10R-3, 135-150	559.45	NM	NM	30.0	551	8.1	414	23.2	23.5	4.3	353	676	276	400
13R-3, 135-150	588.25	7.76	4.62	32.0	506	8.3	458	23.5	24.3	5.0	297	974	287	416
16R-3, 135-150	617.05	NM	NM	28.0	476	5.7	396	21.2	20.8	3.6	285	542	234	362
24R-1, 138-150	691.08	8.64	1.15	33.0	567	5.1	474	19.5	25.2	4.8	45	1277	272	382
27R-3, 125-140	722.51	8.07	2.17	32.0	548	5.3	454	21.6	25.0	3.5	121	963	272	373
31R-3, 135-150	761.25	NM	NM	34.0	552	4.6	462	21.3	26.4	3.3	73	1032	274	389

Note: NM = not measured.

Table T20. *P*-wave velocities measured at discrete intervals, Site 1172. (**See table notes.** Continued on next three pages.)

Core, section, interval (cm)	Depth (mbsf)	PWS1 (km/s)	PWS2 (km/s)	PWS3 (km/s)
189-1172A-				
1H-1, 62.90	0.63			1.610
1H-1, 108.00	1.08			1.587
1H-2, 48.50	1.99	1.570		1.594
1H-3, 49.40	3.49	1.527		
1H-3, 49.60	3.50			1.552
1H-4, 49.50	4.99	1.517		1.533
2H-2, 43.90	8.24	1.522		1.541
2H-3, 51.90	9.82	1.567	1.556	1.596
2H-4, 55.60	11.36	1.574	1.551	1.593
2H-5, 48.20	12.78	1.549	1.532	1.580
2H-6, 40.30	14.20	1.555	1.524	1.584
2H-7, 42.60	15.73	1.544	1.532	1.581
3H-1, 95.00	16.75	1.550	1.480	1.625
3H-2, 49.90	17.80	1.549	1.561	1.582
3H-3, 49.90	19.30	1.566	1.547	1.591
3H-4, 50.00	20.80	1.535	1.529	1.580
3H-5, 50.10	22.30	1.545	1.544	
3H-5, 50.50	22.31			1.569
3H-6, 50.00	23.80	1.542	1.543	
3H-6, 51.10	23.81			1.578
4H-1, 47.10	25.77	1.536	1.523	1.558
4H-2, 49.90	27.30	1.536	1.534	1.554
4H-3, 49.30	28.79		1.566	
4H-3, 49.50	28.80	1.571		1.573
4H-4, 49.90	30.30	1.531	1.534	1.553
4H-5, 50.60	31.81	1.522	1.528	1.545
4H-6, 49.90	33.30	1.531	1.540	
4H-6, 50.80	33.31			1.547
5H-2, 49.40	36.79		1.541	
5H-2, 50.00	36.80	1.532		
5H-2, 50.70	36.81			1.554
5H-5, 49.00	41.29		1.525	
5H-5, 49.90	41.30	1.526		1.539
6H-3, 113.70	48.44	1.579		
6H-3, 115.20	48.45		1.561	1.607
6H-5, 49.70	50.80	1.586	1.602	1.613
6H-6, 85.00	52.65	1.598	1.597	1.611
7H-4, 49.80	58.80	1.560		
7H-4, 50.80	58.81			1.572
8H-2, 46.30	65.26	1.551		
8H-2, 47.10	65.27			1.574
8H-3, 39.20	66.69	1.538	1.571	1.555
9H-4, 42.50	77.72	1.540	1.568	
9H-4, 43.10	77.73			1.569
9H-6, 43.40	80.73	1.543		1.560
10H-3, 48.30	85.78	1.531		1.557
11H-1, 47.40	92.27	1.534	1.532	
11H-1, 63.30	92.43			1.570
11H-2, 55.70	93.86	1.548		1.568
11H-3, 48.50	95.29	1.532		1.556
11H-4, 44.30	96.74	1.521		1.536
11H-5, 49.40	98.29	1.530		1.565
11H-6, 48.60	99.79	1.536		1.563
12H-2, 51.00	103.31	1.528		1.561
12H-3, 48.40	104.78	1.538		
12H-3, 48.50	104.79			1.566
12H-4, 49.60	106.30	1.539		1.558
12H-5, 49.70	107.80	1.547		1.577
12H-6, 49.10	109.29	1.535		
12H-6, 49.10	109.29			1.571
13H-1, 48.30	111.28			1.573
13H-1, 48.70	111.29	1.534		
13H-2, 53.70	112.84	1.520		1.548
13H-3, 46.40	114.26	1.534		1.560
13H-4, 49.70	115.80	1.539		1.571
13H-5,58.3	117.38			1.583
13H-6, 55.1	118.85			1.569
14H-1, 49.20	120.79	1.546		1.573
14H-2, 48.30	122.28	1.549		1.566
14H-3, 48.50	123.79	1.552		1.578
14H-4, 48.10	125.28	1.554		1.583
14H-5, 42.90	126.73	1.560		1.583
14H-6, 46.10	128.26	1.548		1.578
15H-1, 110.90	130.91	1.530		1.561
16H-2, 52.20	141.32			1.619
16H-2, 52.80	141.33	1.565		
16H-4, 48.90	144.29	1.546		1.583
16H-6, 50.60	147.31	1.538		1.577
17H-1, 50.50	149.30	1.519		1.578
17H-2, 61.30	150.91			1.572
17H-3, 34.60	152.15			1.585
17H-4, 59.40	153.89			1.590
17H-5, 51.50	155.32			1.586
17H-6, 52.40	156.82			1.595
18H-1, 50.00	158.80			1.575
18H-2, 49.40	160.29			1.572
18H-3, 50.30	161.80			1.603
18H-4, 50.50	163.30			1.587
18H-5, 50.00	164.80			1.572
18H-6, 49.70	166.30			1.573
19H-3, 50.50	171.30			1.571
19H-4, 50.30	172.80			1.595
19H-5, 49.60	174.30			1.592
19H-6, 50.00	175.80			1.605
20H-1, 48.40	177.78			1.590
20H-2, 50.00	179.30			1.577
20H-3, 48.90	180.79			1.569
20H-4, 46.10	182.26			1.570
20H-5, 43.40	183.73			1.564
20H-6, 50.90	185.31			1.570
21H-1, 49.60	187.30			1.591
21H-4, 56.70	191.87			1.590
21H-5, 53.90	193.34			1.555
21H-6, 54.00	194.84			1.590
22H-1, 50.50	196.80			1.602
22H-2, 97.90	198.78			1.584
22H-3, 79.20	200.09			1.605
22H-4, 49.00	201.29			1.614
22H-5, 51.50	202.82			1.613
22H-6, 61.90	204.42			1.603
23H-1, 48.10	206.28			1.606
23H-2, 49.40	207.79			1.592
23H-3, 53.60	209.34			1.584
23H-4, 49.90	210.80			1.598
23H-5, 59.70	212.40			1.578
23H-6, 46.50	213.76			1.583
24H-1, 49.60	215.80			1.629
24H-2, 50.00	217.30			1.584
24H-3, 49.40	218.79			1.590
24H-4, 50.20	220.30			1.586
25X-1, 48.70	225.29			1.584
25X-2, 49.00	226.79			1.576
26X-1, 52.00	230.62			1.577
26X-2, 49.10	232.09			1.579
26X-3, 55.00	233.65			1.563
26X-4, 32.70	234.93			1.577
27X-1, 56.40	240.26			1.597
27X-2, 56.70	241.77			1.620
27X-3, 48.80	243.19			1.595
27X-4, 58.00	244.78			1.586
27X-5, 39.80	246.10			1.602
28X-1, 136.70	250.67			1.651
28X-2, 49.90	251.30			1.589
28X-3, 49.60	252.80			1.568
28X-4, 50.10	254.30			1.566

Table T20 (continued).

Core, section, interval (cm)	Depth (mbsf)	PWS1 (km/s)	PWS2 (km/s)	PWS3 (km/s)
29X-1, 27.20	259.17			1.657
29X-2, 34.50	260.74			1.671
29X-3, 79.50	262.70			1.608
29X-3, 102.70	262.93			1.599
29X-4, 37.50	263.77			1.596
29X-5, 45.00	265.35			1.663
30X-1, 45.10	268.45			1.603
30X-2, 69.40	270.19			1.581
30X-3, 58.30	271.58			1.676
30X-4, 62.10	273.12			1.663
30X-5, 35.30	274.35			1.643
30X-6, 24.20	275.74			1.762
31X-1, 25.00	277.85			1.735
31X-1, 61.60	278.22			1.642
31X-3, 50.90	281.11			1.850
31X-4, 35.40	282.45			1.797
31X-4, 41.70	282.52			1.724
32X-1, 49.90	287.70			1.755
32X-2, 50.70	289.21			1.866
32X-3, 49.30	290.69			1.898
32X-4, 50.30	292.20			1.996
32X-5, 52.00	293.72			1.743
32X-6, 39.50	295.10			1.925
33X-1, 25.30	297.05			1.754
33X-2, 22.50	298.52			1.716
33X-2, 94.50	299.24			2.067
33X-3, 46.60	300.27			1.863
33X-4, 51.60	301.82			1.857
33X-5, 50.00	303.30			1.743
33X-6, 57.90	304.88			1.951
34X-1, 54.00	307.04			1.822
34X-2, 116.30	309.16			1.835
34X-3, 44.90	309.95			1.721
34X-3, 106.00	310.56			1.750
34X-4, 80.00	311.80			1.902
34X-5, 49.30	312.99			1.608
34X-5, 80.30	313.30			1.733
34X-6, 39.60	314.40			1.676
35X-1, 50.80	316.61			1.932
35X-2, 53.00	318.13			1.725
35X-3, 47.80	319.58			1.831
35X-4, 51.10	321.11			1.689
35X-5, 53.30	322.63			1.829
35X-6, 46.00	324.06			1.892
36X-1, 62.50	326.33			1.739
36X-2, 57.70	327.78			1.651
36X-2, 82.90	328.03			1.856
36X-3, 37.30	329.07			1.721
36X-4, 57.20	330.77			1.937
36X-5, 46.30	332.16			1.892
36X-5, 49.30	332.19			1.784
37X-1, 63.30	335.93			1.841
37X-2, 44.00	337.24			2.070
37X-3, 61.30	338.91			2.113
37X-4, 31.70	340.12			2.041
37X-4, 92.40	340.72			1.868
37X-5, 45.90	341.76			2.021
37X-5, 62.20	341.92			2.169
37X-7, 32.50	344.33			2.087
37X-7, 62.50	344.64			2.042
38X-1, 45.60	345.36			2.164
38X-2, 50.30	346.90			2.104
38X-3, 58.20	348.48			2.047
38X-4-6.20	349.46			1.875
38X-4, 55.50	349.95			1.795
38X-4, 120.00	350.60			1.830
38X-5, 47.10	351.37			1.945
38X-6, 21.70	352.62			1.835
39X-1, 35.80	354.96			1.742
39X-2, 54.30	356.64			1.688
39X-3, 29.00	357.89			1.777
39X-3, 125.90	358.86			2.057
39X-4, 31.40	359.41			1.777
39X-4, 110.70	360.21			1.814
39X-5, 39.80	361.00			1.754
39X-6, 89.00	362.99			1.715
40X-1, 63.70	364.84			1.669
40X-2, 39.50	366.10			1.659
40X-3, 87.90	368.08			1.703
40X-4, 33.50	369.04			1.689
40X-5, 60.50	370.80			1.697
40X-6, 39.40	372.09			1.748
41X-1, 56.30	374.36			1.766
41X-2, 63.20	375.93			1.721
41X-3, 58.40	377.38			1.720
41X-4, 78.00	379.08			1.747
41X-5, 44.00	380.24			1.755
41X-6, 46.90	381.77			1.796
42X-1, 3.90	383.44			1.908
42X-1, 46.80	383.87			1.777
42X-2, 55.30	385.45			1.776
42X-3, 31.30	386.71			1.995
42X-3, 58.30	386.98			1.822
42X-4, 40.70	388.31			1.799
42X-5, 51.70	389.92			1.785
42X-6, 30.90	391.21			1.787
43X-1, 41.50	393.42			1.769
43X-2, 51.70	395.02			1.780
43X-3, 58.00	396.58			1.763
43X-4, 55.30	398.05			1.784
43X-5, 54.20	399.54			1.813
43X-6, 50.00	401.00			1.762
44X-1, 33.40	402.93			1.745
44X-2, 57.00	404.67			1.782
44X-3, 33.10	405.93			1.772
44X-4, 40.60	407.51			1.771
44X-5, 56.20	409.16			1.772
44X-6, 29.50	410.39			1.721
45X-1, 35.20	412.55			1.801
45X-2, 72.30	414.42			1.810
45X-3, 42.20	415.62			1.726
45X-4, 65.80	417.36			1.772
45X-5, 36.00	418.56			1.772
46X-1, 15.70	421.96			1.766
46X-2, 23.70	423.54			1.746
46X-3, 32.60	425.13			1.781
46X-4, 43.00	426.73			1.748
46X-5, 49.20	428.29			1.783
46X-6, 33.40	429.63			1.696
46X-6, 46.40	429.76			1.788
47X-1, 36.50	431.77			1.811
47X-2, 75.40	433.65			1.783
47X-3, 59.00	434.99			1.723
47X-4, 57.00	436.47			1.788
47X-5, 53.00	437.93			1.824
47X-5, 75.70	438.16			1.805
48X-1, 39.30	441.39			1.784
48X-2, 44.90	442.95			1.735
48X-3, 44.30	444.44			1.757
48X-4, 75.70	446.26			1.790
48X-5, 64.90	447.65			1.763
48X-6, 45.30	448.95			1.777
49X-1, 33.30	450.93			1.784
49X-2, 58.20	452.68			1.772
49X-3, 45.30	454.05			1.789
49X-4, 82.70	455.93			1.759
49X-5, 54.30	457.14			1.808

Table T20 (continued).

Core, section, interval (cm)	Depth (mbsf)	PWS1 (km/s)	PWS2 (km/s)	PWS3 (km/s)
49X-6, 56.00	458.66			1.778
51X-1, 41.20	470.21			1.768
51X-2, 48.70	471.79			1.772
51X-3, 53.20	473.33			1.783
51X-4, 85.30	475.15			1.783
52X-1, 54.50	479.95			1.785
52X-2, 69.80	481.60			1.774
52X-3, 54.80	482.95			1.793
52X-4, 31.90	484.22			1.785
52X-5, 52.60	485.93			1.778
52X-6, 63.60	487.54			1.771
53X-1, 63.70	489.64			1.755
53X-2, 48.20	490.98			1.738
53X-3, 40.30	492.40			1.726
53X-4, 28.20	493.78			1.721
53X-5, 52.00	495.52			1.737
53X-6, 56.90	497.07			1.664
54X-1, 58.30	499.18			1.749
54X-2, 64.70	500.75			1.729
54X-3, 53.10	502.13			1.711
54X-4, 47.60	503.58			1.767
55X-1, 32.30	508.62			2.446
189-1172D-				
4R-1, 62.00	498.02			1.801
4R-2, 58.00	499.48			1.761
4R-3, 59.00	500.99			1.780
4R-4, 50.00	502.40			1.904
4R-4, 57.00	502.47			2.409
5R-1, 54.00	507.54			2.121
5R-2, 63.00	509.13			2.039
5R-3, 53.00	510.53			2.213
5R-4, 36.00	511.86			2.055
6R-1, 119.00	517.79			2.012
7R-1, 58.00	526.78			1.938
7R-2, 46.00	528.16			1.940
7R-3, 18.00	529.38			1.927
7R-4, 86.00	531.56			1.892
7R-5, 67.00	532.87			1.877
7R-6, 40.00	534.10			1.897
8R-1, 56.00	536.36			1.886
8R-2, 22.20	537.52			1.844
8R-3, 51.30	539.31			1.924
8R-4, 48.10	540.78			1.912
8R-5, 58.10	542.38			1.896
8R-6, 26.30	543.56			1.944
9R-1, 52.50	545.92			1.926
9R-2, 36.00	547.26			1.858
9R-3, 48.60	548.89			1.879
9R-4, 65.60	550.56			1.906
9R-5, 59.60	552.00			1.875
9R-6, 54.20	553.44			1.892
10R-1, 35.50	555.46			1.874
10R-2, 73.80	557.34			1.912
10R-3, 43.00	558.53			1.908
10R-4, 53.70	560.14			1.945
10R-5, 60.30	561.70			1.945
10R-5, 62.00	561.72			1.884
11R-1, 50.90	565.21			1.861
11R-2, 44.40	566.64			1.866
11R-3, 52.20	568.22			1.857
11R-4, 53.70	569.74			1.899
11R-5, 61.00	571.31			1.942
11R-6, 52.70	572.73			1.996
12R-2, 46.30	576.26			1.907
12R-3, 40.20	577.70			1.931
12R-4, 44.80	579.25			1.878
12R-5, 59.20	580.89			1.974
12R-6, 42.90	582.23			1.954
13R-1, 56.40	584.46			1.878
13R-2, 58.20	585.98			2.351
13R-3, 25.50	587.16			1.888
13R-4, 59.50	588.99			1.947
13R-5, 40.00	590.30			1.923
13R-5, 51.40	590.41			1.915
14R-1, 29.90	593.80			1.760
14R-1, 107.50	594.58			1.758
14R-2, 30.20	595.30			1.831
14R-3, 59.10	597.09			1.800
14R-4, 64.60	598.65			1.768
14R-5, 61.70	600.12			1.752
14R-6, 45.60	601.46			1.797
15R-1, 52.50	603.62			1.763
15R-2, 57.50	605.17			1.808
15R-3, 62.20	606.72			1.744
15R-4, 67.80	608.28			1.758
15R-5, 44.40	609.54			1.771
15R-6, 45.10	611.05			1.736
16R-2, 82.20	615.02			1.733
16R-3, 45.20	616.15			1.748
16R-4, 67.60	617.88			1.788
17R-1, 60.70	622.91			1.764
17R-2, 35.30	624.15			1.755
17R-3, 44.00	625.74			1.819
17R-4, 75.00	627.55			1.797
17R-5, 25.00	628.55			1.761
17R-6, 33.00	630.13			1.826
18R-1, 64.00	632.54			1.738
18R-2, 58.00	633.98			1.766
18R-4, 23.00	636.63			1.814
18R-5, 33.00	638.23			1.852
19R-1, 55.00	642.05			1.840
20R-1, 54.00	651.64			1.822
20R-2, 89.00	653.49			1.805
20R-3, 52.00	654.62			1.830
20R-4, 64.00	656.24			1.839
20R-5, 44.00	657.54			1.832
20R-6, 82.00	659.42			1.832
21R-1, 140.00	662.10			1.838
21R-2, 140.00	663.60			1.883
21R-3, 135.00	665.05			1.831
21R-4, 135.00	666.55			1.894
22R-1, 8.00	670.38			1.904
23R-1, 38.00	680.38			1.863
24R-1, 94.00	690.64			1.982
24R-2, 147.00	692.67			1.923
24R-3, 140.00	694.10			1.863
24R-4, 140.00	695.60			1.955
24R-5, 145.00	697.15			1.978
24R-6, 147.00	698.67			1.897
26R-1, 95.00	709.85			1.872
26R-2, 23.00	710.61			1.974
26R-3, 103.00	712.91			1.823
26R-4, 50.00	713.88			1.914
26R-6, 17.00	716.30			1.946
27R-1, 120.00	719.70			1.971
27R-2, 144.00	721.20			1.952
27R-3, 90.00	722.16			1.915
27R-4, 114.00	723.80			1.968
27R-5, 117.00	725.33			1.940
27R-6, 107.00	726.73			2.124
27R-6, 113.00	726.79			1.976
27R-7, 94.00	727.94			2.032
28R-1, 56.00	728.66			1.985
28R-2, 38.00	729.95			1.896
28R-3, 104.00	732.11			1.924
28R-4, 88.00	733.45			1.949
28R-5, 45.00	734.38			1.984
28R-6, 92.00	736.29			1.983

Table T20 (continued).

Core, section, interval (cm)	Depth (mbsf)	PWS1 (km/s)	PWS2 (km/s)	PWS3 (km/s)
29R-1, 34.00	738.04			1.868
29R-3, 37.00	741.07			2.053
29R-4, 102.00	743.22			1.983
29R-5, 86.00	744.56			2.075
31R-1, 55.00	757.45			1.938
31R-2, 57.00	758.97			1.952
31R-3, 51.00	760.41			1.945
31R-4, 56.00	761.96			1.999
31R-5, 85.00	763.75			1.934
31R-6, 50.00	764.90			1.902
31R-7, 15.00	765.55			2.065

Notes: All *P*-wave velocities measured at discrete intervals. PSW1 = measured along the core, PSW2 = measured perpendicular to the core, PSW3 = measured across the core (Hamilton frame). Blank = no data.

Table T21. Thermal conductivity measured on whole-core sections, Hole 1172A.

Core, section, interval (cm)	Depth (mbsf)	Thermal conductivity (W/[m·K])
189-1172A-		
1H-2, 75	2.25	0.95
2H-3, 75	10.05	1.12
3H-3, 75	19.55	0.97
4H-3, 75	29.05	1.19
5H-3, 75	38.55	1.19
6H-3, 75	48.05	1.16
7H-3, 75	57.55	1.26
8H-3, 75	67.05	1.21
9H-3, 75	76.55	1.23
10H-3, 75	86.05	1.20
11H-3, 75	95.55	1.23
12H-3, 75	105.05	1.13
13H-3, 75	114.55	1.26
14H-3, 75	124.05	0.86
15H-3, 75	133.55	1.22
16H-3, 75	143.05	1.23
17H-3, 75	152.55	1.25
18H-3, 75	162.05	1.21
19H-3, 75	171.55	1.24
20H-3, 75	181.05	1.20
21H-3, 75	190.55	1.26
22H-3, 75	200.05	1.26
23H-3, 75	209.55	1.26
24H-3, 75	219.05	1.30

Table T22. Undrained shear strength from miniature vane-shear measurements, Hole 1172A.

Core, section, interval (cm)	Depth (mbsf)	Undrained shear strength (kPa)
189-1172A-		
1H-1, 112.0	1.12	4.435
1H-2, 97.8	2.48	13.528
1H-3, 109.3	4.09	5.101
1H-4, 98.6	5.49	6.764
2H-2, 98.3	8.78	7.984
2H-3, 99.9	10.30	7.984
2H-4, 105.1	11.85	8.538
2H-5, 86.9	13.17	13.306
2H-6, 107.9	14.88	11.310
2H-7, 60.2	15.90	10.423
3H-1, 95.0	16.75	17.853
3H-2, 99.2	18.29	9.869
3H-3, 99.1	19.79	11.643
3H-4, 99.1	21.29	17.187
3H-5, 99.6	22.80	25.282
3H-6, 100.1	24.30	14.304
4H-1, 96.3	26.26	26.834
4H-2, 99.0	27.79	17.520
4H-3, 98.9	29.29	14.526
4H-4, 99.0	30.79	20.514
4H-5, 99.8	32.30	23.175
4H-6, 99.9	33.80	17.409
5H-2, 99.8	37.30	14.083
6H-3, 102.6	48.33	9.758
6H-5, 99.1	51.29	7.762
6H-6, 134.9	53.15	15.967
7H-4, 99.9	59.30	18.407
8H-2, 96.2	65.76	13.085
8H-3, 53.1	66.83	12.197
9H-6, 89.2	81.19	13.085
10H-3, 98.8	86.29	35.927
11H-1, 99.7	92.80	23.619
11H-2, 100.6	94.31	22.953
11H-3, 101.3	95.81	22.066
11H-4, 100.1	97.30	30.383
11H-5, 89.3	98.69	33.044
11H-6, 107.0	100.37	48.679
12H-2, 100.4	103.80	21.733
12H-3, 100.6	105.31	27.278
12H-4, 94.1	106.74	36.149
12H-5, 101.9	108.32	27.167
12H-6, 98.4	109.78	24.506
13H-1, 97.6	111.78	57.993
13H-2, 112.0	113.42	32.711
13H-3, 108.7	114.89	28.941
13H-4, 110.7	116.41	35.262
13H-6, 106.9	119.37	38.921
14H-1, 98.5	121.29	45.463
14H-2, 103.4	122.83	33.598
14H-3, 97.8	124.28	27.721
14H-4, 90.3	125.70	26.612
14H-5, 112.9	127.43	25.171
14H-6, 100.6	128.81	40.362
15H-1, 109.8	130.90	13.195
16H-4, 98.5	144.79	39.032
17H-1, 99.6	149.80	38.366
17H-3, 84.0	152.64	34.375
17H-5, 100.9	155.81	37.590
18H-1, 99.4	159.29	20.957
18H-3, 99.6	162.30	57.439
18H-5, 99.3	165.29	57.217
19H-3, 99.9	171.80	17.631
19H-5, 98.9	174.79	14.083
20H-1, 101.0	178.31	19.072
20H-2, 99.3	179.79	15.746
20H-3, 98.3	181.28	11.643
20H-5, 92.7	184.23	16.411
21H-6, 111.9	195.42	19.183
22H-1, 99.8	197.30	9.869
22H-3, 108.9	200.39	18.629
22H-5, 100.8	203.31	16.744
23H-1, 99.2	206.79	23.508
23H-3, 108.1	209.88	17.076
23H-5, 99.8	212.80	18.407
24H-1, 117.5	216.48	23.729
24H-3, 101.2	219.31	18.851
26X-1, 101.3	231.11	18.518
26X-3, 112.2	234.22	11.532
27X-1, 108.4	240.78	8.316
27X-3, 102.3	243.72	17.076
28X-1, 102.1	250.32	15.191
28X-1, 99.2	250.29	9.980
28X-3, 99.0	253.29	7.762

Table T23. Index properties measured at discrete intervals, Hole 1172A. (Continued on next two pages.)

Core, section, interval (cm)	Depth (mbsf)	Water content (wt%)		Density (g/cm^3)			Porosity (%)	Void ratio
		Bulk	Dry	Bulk	Dry	Grain		
189-1172A-								
1H-1, 70.0-72.0	0.7	43.8	78.0	1.570	0.882	2.691	67.2	2.051
1H-2, 70.0-72.0	2.2	46.2	86.0	1.540	0.828	2.719	69.5	2.283
1H-3, 70.0-72.0	3.7	43.8	78.1	1.582	0.889	2.755	67.7	2.100
1H-4, 70.0-72.0	5.2	45.0	81.9	1.561	0.858	2.735	68.6	2.186
2H-2, 70.0-72.0	8.5	44.5	80.3	1.573	0.872	2.758	68.4	2.162
2H-3, 70.0-72.0	10.0	43.7	77.7	1.574	0.886	2.702	67.2	2.050
2H-4, 70.0-72.0	11.5	42.2	73.0	1.596	0.923	2.696	65.8	1.922
2H-5, 70.0-72.0	13.0	43.1	75.9	1.586	0.902	2.717	66.8	2.013
2H-6, 70.0-72.0	14.5	42.4	73.6	1.595	0.919	2.706	66.0	1.945
3H-1, 70.0-72.0	16.5	42.1	72.6	1.602	0.928	2.714	65.8	1.925
3H-2, 70.0-72.0	18.0	44.5	80.3	1.563	0.867	2.709	68.0	2.125
3H-3, 70.0-72.0	19.5	42.7	74.5	1.599	0.916	2.746	66.6	1.996
3H-4, 70.0-72.0	21.0	39.0	63.9	1.645	1.003	2.685	62.6	1.677
3H-5, 70.0-72.0	22.5	47.0	88.7	1.525	0.808	2.694	70.0	2.333
3H-6, 70.0-72.0	24.0	41.6	71.3	1.617	0.944	2.756	65.7	1.919
4H-1, 70.0-72.0	26.0	39.7	65.8	1.636	0.987	2.695	63.4	1.731
4H-2, 70.0-72.0	27.5	37.4	59.8	1.674	1.048	2.701	61.2	1.578
4H-3, 70.0-72.0	29.0	38.5	62.7	1.653	1.016	2.687	62.2	1.644
4H-4, 70.0-72.0	30.5	41.3	70.5	1.613	0.946	2.713	65.1	1.868
4H-5, 70.0-72.0	32.0	38.4	62.2	1.675	1.033	2.773	62.7	1.684
4H-6, 70.0-72.0	33.5	45.0	81.7	1.563	0.860	2.742	68.6	2.189
5H-2, 70.0-72.0	37.0	38.8	63.4	1.654	1.012	2.710	62.7	1.678
5H-3, 70.0-72.0	38.5	37.8	60.8	1.671	1.040	2.714	61.7	1.610
5H-4, 70.0-72.0	40.0	35.8	55.7	1.706	1.096	2.710	59.6	1.473
6H-1, 70.0-72.0	45.0	35.7	55.5	1.705	1.096	2.705	59.5	1.467
6H-3, 70.0-72.0	48.0	35.4	54.8	1.720	1.111	2.741	59.5	1.466
6H-5, 70.0-72.0	51.0	35.4	54.9	1.712	1.105	2.712	59.2	1.453
7H-3, 70.0-72.0	57.5	36.7	58.0	1.695	1.072	2.735	60.8	1.551
7H-4, 70.0-72.0	59.0	36.1	56.4	1.717	1.098	2.775	60.4	1.528
7H-5, 70.0-72.0	60.5	36.5	57.5	1.693	1.075	2.710	60.3	1.522
7H-6, 70.0-72.0	62.0	35.5	55.0	1.705	1.100	2.690	59.1	1.446
8H-2, 70.0-72.0	65.5	36.1	56.5	1.709	1.092	2.748	60.3	1.517
8H-3, 70.0-72.0	67.0	36.4	57.1	1.707	1.087	2.760	60.6	1.540
8H-4, 70.0-72.0	68.5	35.9	56.1	1.710	1.096	2.740	60.0	1.500
8H-5, 70.0-72.0	70.0	35.6	55.3	1.721	1.108	2.761	59.9	1.492
9H-4, 70.0-72.0	78.0	35.0	53.7	1.721	1.119	2.713	58.7	1.424
9H-5, 48.0-50.0	79.3	33.9	51.2	1.739	1.150	2.709	57.5	1.355
9H-6, 70.0-72.0	81.0	34.6	53.0	1.735	1.134	2.744	58.7	1.420
10H-3, 58.0-60.0	85.9	36.4	57.1	1.692	1.077	2.699	60.1	1.506
11H-1, 70.0-72.0	92.5	34.7	53.1	1.723	1.125	2.705	58.4	1.403
11H-3, 73.0-75.0	95.5	35.6	55.3	1.710	1.101	2.717	59.5	1.468
11H-5, 70.0-72.0	98.5	34.5	52.7	1.729	1.132	2.714	58.3	1.398
12H-1, 70.0-72.0	102.0	35.8	55.8	1.704	1.094	2.708	59.6	1.476
12H-3, 70.0-72.0	105.0	34.7	53.2	1.723	1.125	2.705	58.4	1.404
12H-5, 70.0-72.0	108.0	34.8	53.3	1.714	1.118	2.673	58.2	1.391
13H-1, 70.0-72.0	111.5	35.9	55.9	1.700	1.090	2.696	59.6	1.472
13H-3, 70.0-72.0	114.5	34.9	53.7	1.713	1.115	2.683	58.4	1.407
13H-5, 70.0-72.0	117.5	33.7	50.9	1.731	1.147	2.669	57.0	1.328
14H-1, 70.0-72.0	121.0	32.5	48.1	1.752	1.183	2.665	55.6	1.253
14H-3, 70.0-72.0	124.0	32.7	48.7	1.744	1.173	2.650	55.7	1.260
14H-5, 70.0-72.0	127.0	32.9	48.9	1.749	1.174	2.675	56.1	1.278
15H-1, 70.0-72.0	130.5	34.5	52.8	1.734	1.135	2.736	58.5	1.410
15H-3, 70.0-72.0	133.5	33.4	50.2	1.743	1.161	2.690	56.8	1.317
15H-5, 70.0-72.0	136.5	31.9	46.9	1.773	1.207	2.700	55.3	1.237
16H-2, 70.0-72.0	141.5	36.8	58.2	1.691	1.069	2.723	60.7	1.547
16H-4, 70.0-72.0	144.5	37.1	59.0	1.680	1.056	2.700	60.9	1.557
16H-6, 70.0-72.0	147.5	34.4	52.5	1.724	1.130	2.690	58.0	1.380
17H-1, 70.0-72.0	149.5	36.4	57.3	1.689	1.074	2.689	60.1	1.504
17H-3, 70.0-72.0	152.5	25.7	34.5	1.890	1.405	2.670	47.4	0.900
17H-5, 70.0-72.0	155.5	33.0	49.3	1.753	1.174	2.698	56.5	1.298
18H-1, 70.0-72.0	159.0	34.7	53.1	1.728	1.129	2.722	58.5	1.411
18H-3, 70.0-72.0	162.0	36.1	56.6	1.699	1.085	2.709	60.0	1.498
18H-5, 70.0-72.0	165.0	35.3	54.6	1.707	1.104	2.685	58.9	1.432
19H-1, 70.0-72.0	168.5	36.3	57.0	1.699	1.082	2.720	60.2	1.513
19H-3, 70.0-72.0	171.5	35.3	54.6	1.711	1.107	2.701	59.0	1.441
19H-5, 70.0-72.0	174.5	34.4	52.3	1.738	1.141	2.738	58.3	1.399

Table T23 (continued).

Core, section, interval (cm)	Depth (mbsf)	Water content (wt%)		Density (g/cm^3)			Porosity (%)	Void ratio
		Bulk	Dry	Bulk	Dry	Grain		
20H-1, 70.0-72.0	178.0	33.9	51.2	1.747	1.156	2.738	57.8	1.370
20H-3, 70.0-72.0	181.0	34.4	52.5	1.721	1.128	2.678	57.9	1.373
20H-5, 70.0-72.0	184.0	33.8	51.0	1.752	1.160	2.749	57.8	1.370
21H-1, 70.0-72.0	187.5	35.0	53.8	1.721	1.119	2.717	58.8	1.428
21H-5, 70.0-72.0	193.5	34.5	52.7	1.723	1.128	2.691	58.1	1.385
22H-1, 67.0-69.0	197.0	33.4	50.2	1.750	1.165	2.717	57.1	1.332
22H-3, 71.0-73.0	200.0	33.4	50.3	1.756	1.169	2.742	57.4	1.346
22H-5, 70.0-72.0	203.0	34.2	51.9	1.729	1.138	2.691	57.7	1.364
23H-1, 70.0-72.0	206.5	33.3	49.9	1.753	1.169	2.721	57.0	1.327
23H-3, 70.0-72.0	209.5	34.1	51.8	1.733	1.142	2.703	57.8	1.367
23H-5, 70.0-72.0	212.5	32.8	48.9	1.759	1.181	2.710	56.4	1.294
24H-1, 70.0-72.0	216.0	34.0	51.5	1.732	1.143	2.690	57.5	1.354
24H-3, 70.0-72.0	219.0	33.2	49.6	1.760	1.177	2.736	57.0	1.325
25X-1, 70.0-72.0	225.5	35.2	54.3	1.721	1.115	2.727	59.1	1.445
26X-1, 70.0-72.0	230.8	35.4	54.7	1.714	1.107	2.714	59.2	1.450
26X-3, 70.0-72.0	233.8	36.6	57.8	1.700	1.078	2.751	60.8	1.552
27X-1, 70.0-72.0	240.4	34.7	53.1	1.731	1.131	2.731	58.6	1.415
27X-3, 70.0-72.0	243.4	33.2	49.6	1.759	1.175	2.731	57.0	1.323
27X-5, 70.0-72.0	246.4	31.7	46.5	1.779	1.214	2.707	55.1	1.229
28X-1, 70.0-72.0	250.0	33.3	49.9	1.748	1.166	2.700	56.8	1.316
28X-3, 70.0-72.0	253.0	35.2	54.3	1.715	1.112	2.710	59.0	1.438
29X-1, 70.0-72.0	259.6	33.7	50.8	1.739	1.153	2.696	57.2	1.338
29X-3, 70.0-72.0	262.6	34.6	52.9	1.729	1.131	2.721	58.4	1.406
29X-5, 70.0-72.0	265.6	33.4	50.1	1.740	1.159	2.678	56.7	1.311
30X-1, 70.0-72.0	268.7	33.6	50.6	1.755	1.165	2.747	57.6	1.357
30X-3, 71.0-73.0	271.7	32.8	48.7	1.767	1.188	2.732	56.5	1.300
30X-5, 70.0-72.0	274.7	32.3	47.7	1.759	1.191	2.676	55.5	1.247
31X-1, 70.0-72.0	278.3	33.3	50.0	1.741	1.161	2.678	56.7	1.307
31X-3, 70.0-72.0	281.3	31.6	46.1	1.790	1.225	2.733	55.2	1.231
31X-5, 70.0-72.0	284.3	31.9	46.7	1.776	1.210	2.705	55.3	1.235
32X-1, 70.0-72.0	287.9	27.8	38.6	1.878	1.355	2.768	51.1	1.043
32X-3, 70.0-72.0	290.9	27.6	38.1	1.881	1.362	2.760	50.7	1.027
32X-5, 70.0-72.0	293.9	26.3	35.8	1.910	1.407	2.767	49.2	0.967
33X-1, 70.0-72.0	297.5	30.5	44.0	1.828	1.270	2.793	54.5	1.199
33X-3, 70.0-72.0	300.5	29.4	41.6	1.843	1.302	2.762	52.9	1.121
33X-5, 70.0-72.0	303.5	31.8	46.7	1.785	1.217	2.735	55.5	1.248
34X-1, 70.0-72.0	307.2	31.2	45.3	1.796	1.236	2.726	54.7	1.206
34X-3, 70.0-72.0	310.2	34.5	52.6	1.736	1.138	2.738	58.4	1.406
34X-5, 70.0-72.0	313.2	30.9	44.6	1.802	1.246	2.728	54.3	1.189
35X-1, 70.0-72.0	316.8	30.8	44.5	1.809	1.251	2.746	54.4	1.194
35X-3, 70.0-72.0	319.8	28.6	40.1	1.856	1.325	2.756	51.9	1.080
35X-5, 70.0-72.0	322.8	28.6	40.1	1.865	1.332	2.780	52.1	1.088
36X-1, 70.0-72.0	326.4	28.3	39.5	1.845	1.323	2.701	51.0	1.042
36X-3, 70.0-72.0	329.4	29.4	41.6	1.822	1.286	2.697	52.3	1.097
36X-5, 79.0-81.0	332.5	28.4	39.7	1.854	1.328	2.734	51.4	1.059
37X-1, 73.0-75.0	336.0	23.3	30.4	1.963	1.506	2.723	44.7	0.808
37X-3, 70.0-72.0	339.0	27.4	37.7	1.869	1.357	2.716	50.0	1.001
37X-5, 70.0-72.0	342.0	27.5	37.9	1.854	1.344	2.674	49.7	0.989
38X-1, 70.0-72.0	345.6	27.1	37.2	1.873	1.365	2.708	49.6	0.985
38X-3, 70.0-72.0	348.6	27.7	38.2	1.865	1.349	2.720	50.4	1.016
38X-5, 71.0-73.0	351.6	29.0	40.9	1.824	1.294	2.681	51.7	1.072
39X-1, 70.0-72.0	355.3	30.4	43.7	1.786	1.243	2.645	53.0	1.128
39X-2, 70.0-72.0	356.8	31.9	46.7	1.759	1.199	2.648	54.7	1.208
39X-3, 70.0-72.0	358.3	40.5	68.2	1.644	0.978	2.802	65.1	1.867
39X-4, 70.0-72.0	359.8	31.8	46.7	1.786	1.217	2.735	55.5	1.246
39X-5, 70.0-72.0	361.3	42.1	72.6	1.589	0.921	2.650	65.3	1.879
39X-6, 70.0-72.0	362.8	41.6	71.2	1.570	0.917	2.533	63.8	1.762
40X-1, 70.0-72.0	364.9	39.8	66.0	1.613	0.972	2.598	62.6	1.674
40X-3, 70.0-72.0	367.9	44.5	80.2	1.537	0.853	2.568	66.8	2.010
40X-5, 70.0-72.0	370.9	39.5	65.3	1.614	0.977	2.586	62.2	1.648
41X-1, 70.0-72.0	374.5	37.9	61.0	1.650	1.025	2.630	61.0	1.566
41X-3, 70.0-72.0	377.5	38.2	61.7	1.659	1.026	2.686	61.8	1.619
41X-5, 70.0-72.0	380.5	41.1	69.8	1.597	0.940	2.620	64.1	1.786
42X-1, 70.0-72.0	384.1	34.0	51.6	1.714	1.131	2.626	56.9	1.323
42X-3, 70.0-72.0	387.1	35.1	54.2	1.703	1.104	2.657	58.4	1.406
42X-5, 70.0-72.0	390.1	38.4	62.3	1.630	1.004	2.580	61.1	1.569
43X-1, 70.0-72.0	393.7	37.5	60.1	1.643	1.027	2.581	60.2	1.514
43X-3, 70.0-72.0	396.7	34.9	53.6	1.696	1.104	2.615	57.8	1.369

Table T23 (continued).

Core, section, interval (cm)	Depth (mbsf)	Water content (wt%)		Density (g/cm^3)			Porosity (%)	Void ratio
		Bulk	Dry	Bulk	Dry	Grain		
43X-5, 70.0-72.0	399.7	35.3	54.5	1.679	1.086	2.576	57.8	1.371
44X-1, 70.0-72.0	403.3	36.8	58.3	1.658	1.047	2.595	59.7	1.478
44X-3, 70.0-72.0	406.3	40.2	67.1	1.597	0.956	2.558	62.6	1.677
44X-5, 70.0-72.0	409.3	36.9	58.4	1.637	1.034	2.518	58.9	1.436
45X-1, 70.0-72.0	412.9	34.4	52.4	1.695	1.112	2.580	56.9	1.319
45X-3, 70.0-72.0	415.9	39.0	64.0	1.606	0.979	2.526	61.2	1.579
45X-5, 70.0-72.0	418.9	42.3	73.3	1.554	0.897	2.505	64.2	1.792
46X-1, 70.0-72.0	422.5	42.6	74.1	1.562	0.897	2.556	64.9	1.849
46X-3, 70.0-72.0	425.5	37.5	60.1	1.646	1.028	2.593	60.3	1.522
46X-5, 70.0-72.0	428.5	39.4	65.0	1.612	0.977	2.572	62.0	1.633
47X-1, 70.0-72.0	432.1	36.3	57.0	1.669	1.063	2.603	59.2	1.449
47X-3, 73.0-75.0	435.1	35.9	55.9	1.673	1.073	2.591	58.6	1.415
47X-5, 70.0-72.0	438.1	33.6	50.6	1.696	1.126	2.539	55.6	1.255
48X-1, 71.0-73.0	441.7	34.5	52.7	1.707	1.118	2.632	57.5	1.354
48X-3, 70.0-72.0	444.7	41.2	70.1	1.558	0.916	2.459	62.7	1.684
48X-5, 70.0-72.0	447.7	41.1	69.7	1.581	0.931	2.544	63.4	1.731
49X-1, 70.0-72.0	451.3	44.1	78.8	1.543	0.863	2.569	66.4	1.978
49X-3, 70.0-72.0	454.3	41.0	69.5	1.585	0.935	2.560	63.5	1.739
49X-5, 70.0-72.0	457.3	40.4	67.8	1.576	0.939	2.483	62.2	1.644
51X-1, 70.0-72.0	470.5	44.1	78.7	1.515	0.848	2.435	65.2	1.872
51X-3, 70.0-72.0	473.5	39.1	64.2	1.614	0.983	2.561	61.6	1.605
52X-1, 70.0-72.0	480.1	38.7	63.2	1.628	0.998	2.595	61.6	1.602
52X-3, 70.0-72.0	483.1	36.8	58.3	1.640	1.036	2.526	59.0	1.438
52X-5, 70.0-72.0	486.1	41.4	70.5	1.578	0.926	2.553	63.7	1.758
53X-1, 70.0-72.0	489.7	43.0	75.5	1.541	0.878	2.489	64.7	1.834
53X-3, 70.0-72.0	492.7	47.9	92.1	1.460	0.760	2.404	68.4	2.161
53X-5, 70.0-72.0	495.7	44.8	81.3	1.510	0.833	2.456	66.1	1.949
54X-1, 70.0-72.0	499.3	48.4	93.7	1.460	0.754	2.430	69.0	2.225
54X-3, 70.0-72.0	502.3	46.5	86.8	1.480	0.793	2.414	67.2	2.046